POLLEN-BASED RECONSTRUCTION OF THE VEGETATION AND CLIMATE OF THE EASTERN MEDITERRANEAN REGION DURING THE HOLOCENE

A thesis submitted for the degree of

DOCTOR OF PHILOSOPHY

School of Archaeology, Geography and Environmental Science

University of Reading

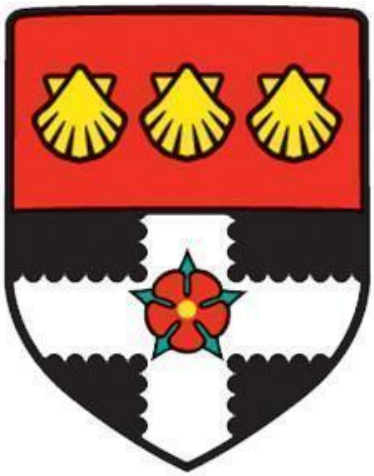

Esmeralda Cruz Silva

Main supervisor: Dr. Sandy P. Harrison

Co-supervisor: Dr. Elena Marinova

Date: June 2023

Declaration

I confirm that this is my own work and the use of all material from the other sources has been properly and fully acknowledged

_____

Esmeralda Cruz Silva

Acknowledgments

First and foremost, I want to express my gratitude to Sandy P. Harrison, my PhD supervisor. Sandy, thank you for your guidance and uninterrupted support during the entire PhD journey, these have not only helped me to reach this point but also have motivated me to push the boundaries and embrace more ambitious scientific perspectives and objectives. Your active scientific engagement has had a profound impact on enhancing the quality of my work. Thank you for the priceless gift: the fire of Prometheus.

I thank Colin I. Prentice, whose scientific advances and knowledge have greatly allowed the development of this work. Thank you, Colin, for your substantial contributions to this thesis and your willingness to share your knowledge.

I also thank Elena Marinova, my co-supervisor. Elena, despite we primarily interacted through video conferences, your scientific expertise in the social and environmental history of the Eastern Mediterranean was instrumental in providing valuable revisions to my work.

I acknowledge the funding from the European Research Council grant "Global Change 2.0: Unlocking the past for a clearer future"

I would also want to thank the members of the SPECIAL research team, full of brilliant people from whom I have never stopped learning. Particularly I would like to thank Roberto Villegas-Diaz, for his willingness to help me solve data science issues and for showing me the way to unlock new levels in the programming world. Roberto, also thank you for your friendship.

Thank you to my mom, for being a large driving force of this journey. Mom, although we lived these years of the PhD separated by an ocean, our hearts were always close.

Thank you to Benjamin, for being a solidary partner at all times. Benjamin, thank you for being my home and for filling every moment of this journey with plenty of love and joy. Love with love is paid!

Thank you to my family, Deya, Juve, Paty, Cecilia, Sebastian, Perla, Enrique, Francisco, Azucena, Lulu, Luna and Benito, for always expressing their support and love to me. You are my assigned companions on this journey called life.

To the memory of my father

Agradecimientos

Primero quiero expresar mi agradecimiento a Sandy P. Harrison, mi supervisora de doctorado. Sandy, gracias por tu guía e ininterrumpido apoyo durante todo el proceso del doctorado, estos no solo me ha servido para alcanzar este punto, sino que tambien me ha motivado a empujar los límites y a adoptar perspectivas y objetivos científicos mas ambiciosos. Tu compromiso activo ha tenido un profundo impacto en mejorar la calidad de mi trabajo. Gracias por el regalo mas grande: El fuego de Prometeo.

Agradezco a Colin I. Prentice, cuyos desarrollos científicos y conocimiento han permitido grandemente el desarrollo de este trabajo. Gracias Colin, por tus contribucions sustanciales en esta tesis y por tu disposicion para compartir tu conocimiento.

También quiero agradecer a Elena Marinova, mi co-supervisora. Elena, a pesar de que interactuamos mayoritatiametne por videoconferencias, tu experiencia científica en la historia ambiental y social del Mediterraneo Oeste, fue crucial para proveer valiosas revisiones.

Agradezco la financiación de la subvención del Consejo Europeo de Investigación “Global Change 2.0: Unlocking the past for a clearer future”

También quiero agradecer a los miembros del equipo de investigación de SPECIAL, lleno de gente brillante de la que nunca he dejado de aprender. En particular, me gustaría agradecer a Roberto Villegas-Diaz por su disposición para ayudarme a resolver problemas de ciencia de datos y por mostrarme el camino para desbloquear nuevos niveles en el mundo de la programación. Roberto, también gracias por tu amistad.

Gracias a mi mamá, que ha sido la gran fuerza impulsora de este viaje. Mamá, aunque vivimos estos años de doctorado separados por un océano, nuestro corazón siempre estuvo unido.

Gracias a mi pareja Benjamín, por ser un compañero solidario en todo momento. Benjamín, gracias por ser mi hogar y por llenar cada momento de esta aventura con mucho amor y alegría. ¡Amor con amor se paga!

Gracias a mi familia, Deya, Juve, Paty, Cecilia, Sebastián, Perla, Enrique, Francisco, Azucena, Lulu, Luna y Benito, por expresarme siempre su apoyo y cariño. Ustedes son mis compañeros asignados en este viaje llamado vida.

A la memoria de mi padre

Impact statement

- The three chapters of this thesis are already published:

Cruz-Silva, E., Harrison, S. P., Marinova, E., & Prentice, I. C. (2022). A new method based on surface-sample pollen data for reconstructing palaeovegetation patterns. Journal of Biogeography, 49(7), 1381–1396. https://doi.org/10.1111/jbi.14448

Cruz-Silva, E., Harrison, S. P., Prentice, I. C. & Marinova, E.,. (2023). Holocene vegetation dynamics of the Eastern Mediterranean region: Old controversies addressed by a new analysis. Journal of Biogeography, 00, 1–17. https://doi.org/10.1111/jbi.14749 . It has been written according to the guidelines of the journal.

Cruz-Silva, E., Harrison, S. P., Prentice, I. C., Marinova, E., Bartlein, P. J., Renssen, H., and Zhang, Y. (2023). Pollen-based reconstructions of Holocene climate trends in the eastern Mediterranean region. Clim. Past, 19, 2093–2108, https://doi.org/10.5194/cp-19-2093-2023, 2023. It has been written according to the guidelines of the journal

- Part of this research led to the publication of an open-access database:

Harrison, S. P., Marinova, E., & **Cruz-Silva, E.** (2021). EMBSeCBIO pollen database [Data set]. University of Reading. https://doi.org/10.17864/1947.309

- An R package was constructed for this research: Villegas-Diaz, R., **Cruz-Silva, E.**, & Harrison, S. P. (2021). ageR: Supervised Age Models [R]. Zenodo. https://doi.org/10.5281/zenodo.4636716

Authors contributions

For published and submitted manuscripts, author contributions are detailed below.

Chapter 2 - A new method based on surface-sample pollen data for reconstructing palaeovegetation patterns

SPH, ICP, ECS and EM devised this study. ICP, SPH and ECS developed the reconstruction technique. SPH, EM and ECS expanded and revised the EMBSeCBIO database, including the construction of new age models. ECS and SPH were responsible for the analysis. ECS and SPH wrote the first draft of the paper, and all authors contributed to the final version

Chapter 3 - Holocene vegetation dynamics of the Eastern Mediterranean region: old controversies addressed by a new analysis

SPH, ECS, ICP and EM devised the study. SPH, ECS and ICP designed the analyses. ECS performed the analyses. ECS and SPH wrote the first draft of the paper, and all authors contributed to the final version.

Chapter 4 - Pollen-based reconstructions of long-term regional climate trends of the eastern Mediterranean during the Holocene

ECS, SPH, ICP designed the study; ECS performed the analyses; PJB, HR and YZ provided climate model output; SPH and ECS wrote the first draft of the paper; all authors contributed to the final version.

Abstract

This thesis presents reconstructions of the vegetation and climate history of the Eastern Mediterranean region during the Holocene, based on a comprehensive pollen data set, the development and application of new reconstruction techniques, and rigorous statistical analyses. The Eastern Mediterranean is of interest because it experienced one of the earliest transitions to permanent agriculture, facilitating the expansion of human populations in the region. Nevertheless, there were significant changes in population across the region during the Holocene, as witnessed by rise and often abrupt decline of specific ancient civilizations. There is an ongoing debate about whether climate changes influenced vegetation, which in turn affected the availability of resources for ancient societies, or if human activities altered vegetation and subsequently those changes impacted the climate. The current uncertainty arises from a focus on records from individual sites and the lack of a comprehensive regional understanding of vegetation and climate history. Understanding historical events in the Eastern Mediterranean region necessitates robust reconstructions of the vegetation and climate in the region during the last 12000 years in order to disentangle the causal factors underpinning observed changes in vegetation and societal events in the region.

The thesis leverages the Eastern Mediterranean-Black Sea-Caspian Corridor (EMBSeCBIO) project, which collected modern and fossil pollen data for the Eastern Mediterranean region, to develop or apply statistically based predictive models for vegetation and climate reconstruction. Standardized data syntheses, when analysed using statistical techniques, are an effective tool for generating objective regional environmental reconstructions, addressing uncertainties and reducing analytical biases.

In this thesis, a new technique for reconstructing vegetation is developed and calibrated by using a modern pollen training dataset to characterize the composition and variability in the abundance of pollen taxa within different biomes. The new technique performs better than existing vegetation reconstruction methods, is more robust when applied to pollen time series, and allows the explicit recognition of assemblages that have no analogue in the modern vegetation. This new method was then applied to fossil pollen data from the Eastern Mediterranean region to predict changes in vegetation types through the Holocene. These reconstructions were used to address several controversies about the regional vegetation history. These analyses showed that the greatest extent of non-analogue vegetation occurred during the early Holocene, the timing of re-afforestation was broadly synchronous across the region, that the maximum expansion of temperate deciduous forest occurred between 5.5 and 5 ka, and that the increase in drought-adapted vegetation in the late Holocene was regionally heterogeneous.

The thesis addresses climate changes during the Holocene by applying a recently developed method, frequency-weighted (fx) Tolerance-weighted Weighted Averaging Partial Least Squares (fxTWA-PLS) to the EMBSeCBIO database in order to reconstruct four climate variables crucial to vegetation growth and relevant to human well-being. Reconstructions were obtained for the

mean temperature of the coldest month (MTCO), mean temperature of the warmest month (MTWA), growing degree days above a threshold of 0° C (GDD_0) and plant-available moisture, represented by the ratio of actual to equilibrium evapotranspiration (α), for 71 individual pollen records. The reconstructions were compared with independent evidence for climate changes and with climate model simulations in order to identify the drivers of observed changes. The glacial-Holocene transition and the early part of the Holocene were characterised by conditions colder and drier than present. Rapid increases in temperature and moisture occurred between ca 10.3 and 9.3 ka, which is considerably after the end of the Younger Dryas. MTCO showed a gradual increase from 9 ka to the present, indicating that winter temperatures were forced by orbitally induced increases in insolation during the Holocene. MTWA also showed an increasing trend from 9 ka to 5 ka, followed by a gradual decline towards present-day conditions. The initial increase in summer temperature is not consistent with a response to orbital forcing, but comparison with climate model simulations suggests that a delayed response to summer insolation changes is likely a reflection of the persistence of the Laurentide and Fennoscandian ice sheets; summer cooling post-5 ka is consistent with the expected response to insolation changes. After the initial rapid increase in plant-available moisture between 11 and 9.3 ka, subsequent changes were small.

This thesis represents the first effort to obtain a comprehensive and quantitative reconstruction of regional vegetation and climate changes in the Eastern Mediterranean. In addition to providing a secure foundation for documenting the environmental history of the region through the Holocene, it also provides the necessary basis for understanding historical events and their potential impact on the regional vegetation. It has resolved a number of persistent controversies about the nature of regional vegetation changes and provides a resource to explore the remaining controversies about the interaction between climate, vegetation and human activities in a region that is of great interest to multiple scientific communities.

Contents

Chapter 1. Introduction

1.1 Relevance of vegetation and climate reconstructions for the Eastern Mediterranean

Reconstructing vegetation and climate changes in the Eastern Mediterranean over the past 12,000 years is crucial as a foundation for understanding the natural and social events that have shaped the history of the region. The Eastern Mediterranean has been the scene of significant historical occurrences, including the adoption of agriculture as the primary form of subsistence during the Pleistocene-Holocene transition. The region has also witnessed the development and decline of several major civilisations. For example, there was a major cultural discontinuity between the Neolithic and the Bronze Age (between ca. 6300 and 5000 cal. yr. BP) in the southeastern part of the Balkans and the Aegean regions (Tsirtsoni, 2014; Lespez et al., 2016; Rascovan et al., 2019), the Akkadian empire in Mesopotamia terminated abruptly at ca. 4200 yrs. BP (Weiss, 1982; Szczęsny, 2016) and many cities from Greece to Egypt were abandoned during the Late Bronze Age ca. 3200 BP (Dickinson, 2012; Drake, 2012). It has been argued that environmental factors played a primary role in driving these cultural events (Weiss, 2012; Bar-Yosef et al., 2017; Kaniewski & Van Campo, 2017; Weiss, 2017; Sinha et al., 2019) as human subsistence is closely tied to climate because agricultural productivity relies on suitable environmental conditions. There have been significant fluctuations in climate during the Holocene (Wanner et al., 2008; Wanner, 2021) which could have impacted subsistence systems sufficiently to lead to societal destabilization. However, it has also been argued that socio-political, economic, or technological changes may have been more important than climate change. Examples of these factors include increased social inequalities, concentration of power, economic consequences of heavy irrigation leading to soil salinization and reduced production, and advancements in irrigation systems (Carozza et al., 2015; Middleton, 2018; Sołtysiak & Fernandes, 2021; Groucutt et al., 2022). It has also been emphasised that the ability of a society to respond and adapt to climatic stresses may vary and will affect the apparent response to climate changes (Degroot et al., 2021).

The fall of the Akkadian Empire is one of the best-documented examples of social changes and serves as an example of the ongoing debate about the role of climate and cultural factors. The collapse of the Akkadian Empire at ca. 4200 years BP lead to the abandonment of urban settlements in northern Mesopotamia and the shift from agriculture to pastoralism as the main subsistence strategy (Weiss et al., 1993; Weiss, 2017). The scarcity of resources, particularly grains, lead to stresses on the population and political instability and ultimately the collapse of the Akkadian Empire. This, in turn, led to increasing pressure on Third Dynasty of Ur civilization from refugees from the north moving southward and, coupled with grain shortages, led to the subsequent collapse of that civilisation. Some paleoclimatic records indicate that this interval was characterised by drought conditions in the eastern Mediterranean region (Cullen et al., 2000; Drysdale et al., 2006; Bar-Matthews et al., 1999; Sinha et al., 2019), which would certainly have led

to conditions unfavourable for the growth of crops. However, the magnitude of this drought is rarely quantifiable and the signal is difficult to compare both between palaeoclimate records and with societal evidence because of differences in the temporal resolution of the records. Furthermore, not all regional climate records show a signal of drought (McMahon, 2006; Ön et al., 2021). Indeed, there are uncertainties about the chronology of the Akkadian Empire, including the possibility that the empire emerged during the drought rather than before it (Zettler, 2003; Sallaberger, 2007; Riehl et al., 2014). Critics of the drought-driven collapse model have argued that complex societies continued to exist uninterrupted in the region even after the collapse of Akkadian elite palace structures (Zettler, 2003; Wossink, 2009) and have questioned whether alternative factors, such as the desire for independence among Mesopotamian city-states, might have been more important in explaining the observed societal changes (Middleton, 2018).

Investigating what factors constrained population growth, why agricultural economies emerged, spread, declined, or intensified, and how humans responded to abrupt environmental changes are regarded as priority questions for archaeology (Kintigh et al., 2014). However, an understanding of past climate-society dynamics is not possible without robust reconstructions of regional climate and climate-induced vegetation changes (Degroot et al., 2021). This involves environmental reconstructions based on appropriate data, with appropriate temporal resolution and spatial coverage, and performed using adequate statistical methods that allow the identification of genuine trends or anomalies, the cause of which can be explored in a way that allows the influence of climate and human activities on the environment to be disentangled (Degroot et al., 2021).

Much of the uncertainty around the question of whether climate influenced vegetation, and hence the resources available to people, or whether people altered the vegetation and hence impacted climate, reflects the focus on evidence from individual sites and a largely subjective interpretation of the data for reconstructing vegetation and climate changes. Relying on the interpretation of individual sites to obtain a regional picture is challenging because of the potential for idiosyncrasies between individual records due to site-specific differences. Comparing individual records can be hindered by variations in the quality of the age models, or differences in temporal resolution and reconstruction methods (Sadori et al., 2011; Bini et al., 2019). Regional paleoenvironmental data compilations offer an alternative because they necessarily imply standardising the data and the age models, which facilitates comparison across records but, more importantly, enables the application of uniform statistical analyses to tackle uncertainties in environmental reconstruction (Harrison, 2017) and minimizing subjective interpretation (e.g. Parker et al., 2021; Parker & Harrison, 2022).

The goal of my thesis is to exploit the advantages of large-scale pollen data compilations, specifically drawing on the Eastern Mediterranean-Black Sea-Caspian Corridor (EMBSeCBIO) database (Cordova et al., 2009; Marinova et al., 2018; Harrison, Marinova, et al., 2021). I first improved the EMBSeCBIO database by incorporating new sites and constructing new age models. I then used these data to develop statistically-based reconstructions of vegetation and climate

changes in the Eastern Mediterranean during the past 12,000 years. These reconstructions, in turn, will make it possible to examine whether societal changes were a response to climate and environmental changes or whether societal changes contributed to changing the environment and climate.

1.2 Reconstructing vegetation from pollen

1.2.1 Overview of the pollen-vegetation relationship for reconstructing vegetation

A vegetation type, or biome, is defined as a collection of plant taxa that occur within a specific bioclimatic range. While individual plant species may have unique responses to climate, species within a biome generally share similar climatic preferences and can coexist and interact with each other (Fig. 1.1) (Pausas & Bond, 2021). The interactions between species are particularly important for plant assemblages in water-stressed environments (Figure 1.1 b) such as those typical of the Eastern Mediterranean (Michalet et al., 2006; Valiente-Banuet et al., 2006; Verdú et al., 2021). Climate plays a predominant role in determining the distribution of plant species, and various approaches have been used to define biomes based solely on climate. Some examples of vegetation classifications based on this approach are Schimper et al. (1903), Whittaker, (1970) and Walter (1973). Alternatively, biomes can be defined based on plant physiognomy, which considers the dominant or mixed growth forms of plants (Woodward et al., 2004). This approach takes climate into account as a principal driver but also considers other factors such as soil type, interactions among species, and fire regimes that are also important in shaping plant communities (Pausas & Bond, 2021). One advantage of using the plant physiognomy approach is that it allows vegetation to be classified at different resolution levels, ranging from fine-scale classifications (e.g. sclerophyllous shrublands or heathlands) to intermediate-scale classifications (e.g. shrublands), and coarse-scale classifications (e.g. open vegetation) depending on the purposes of the classification (Pausas & Bond, 2021). In contrast, defining biomes solely based on climatic distribution can blur the distinction between vegetation and climate and overlook the underlying processes that shape vegetation patterns (Woodward et al., 2004). The way a vegetation type (or biome) is defined is important for palaeovegetation reconstruction because it determines the target for palaeovegetation reconstruction and the assumptions incorporated in the method for reconstructing vegetation from pollen.

There are several possible sources of information about past vegetation, including plant macrofossils, pollen, ancient DNA, and biomarkers. However, pollen is the most abundant source of past terrestrial environmental conditions and has been widely used to reconstruct past vegetation and climate changes (see Prentice, 1988; Prentice et al., 2000; Bartlein et al., 2011). Pollen grains are highly resistant to decay because their outer wall or exine is made of sporopollenin biopolymer, which is extremely tough (Mackenzie et al., 2015). The shapes, sizes, and surface characteristics of pollen grains allow identification of individual plant taxa,

sometimes to species level. Pollen assemblages, preserved in anoxic sediments that have been dated, provide a record of changing vegetation composition through time.

There is a relationship between the regional vegetation cover and the abundance of taxa in modern pollen assemblages that have been extensively studied to reconstruct past vegetation dynamics and understand changes in plant communities over time (e.g. Davis, 1963; Livingstone, 1968; Webb, 1974; Prentice, 1983; Broström et al. 2008; Li et al., 2011; Dawson et al., 2016). These studies have shown that pollen samples can be used to represent the source vegetation, but there are considerations to take into account. The sampling area of the pollen record, which is related to the type of record (e.g., lake core, moss polster) and the size of the basin, is a crucial factor in representing the regional vegetation. This concept is known as the pollen source area theory (Tauber, 1965; Janssen, 1973; Prentice, 1985; Sugita, 1993). The size and characteristics of the sampling area can influence the composition of the pollen assemblage and its representation of the vegetation. However, there are factors that complicate the direct interpretation of pollen taxa abundances as a reflection of vegetation plant abundances because they influence the composition of the pollen record (Prentice, 1988 provides a comprehensive review of these factors). One important consideration is the pollen productivity of different plant taxa. Some plant taxa produce a large amount of pollen, such as Poaceae (grasses), while others produce less, such as *Larix* (larch), or rely on insect pollination, like *Acer* (maple). These differences in pollen productivity can skew the representation of plant abundances in the pollen record. Another factor to consider is the transportability of pollen grains. Some plants have pollen grains that are easily dispersed by wind (e.g. *Pinus*), while others have heavier or less aerodynamic pollen grains that are less easily transported (e.g. Malvaceae) (Dyakowska, 1936).

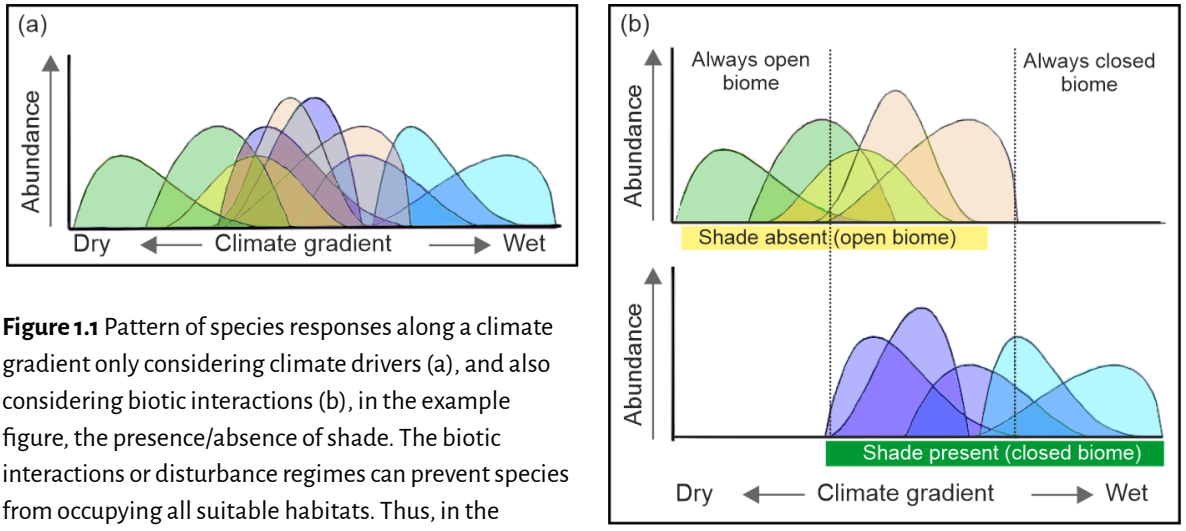

Figure 1.1 Pattern of species responses along a climate gradient only considering climate drivers (a), and also considering biotic interactions (b), in the example figure, the presence/absence of shade. The biotic interactions or disturbance regimes can prevent species from occupying all suitable habitats. Thus, in the intermediate levels of the gradient, species that may coexist when considering climate only (a) are not really coexisting. Redrawn from Pausas and Bond (2021).

Pollen records can vary in the level of taxonomic identification, often chosen based on research purposes or available resources. The level of taxonomic identification impacts the precision and

detail at which vegetation can be reconstructed, as different species within a genus or family may have different life forms and phenologies. For example, in the Mediterranean region, *Pinus* can be both an arctic dwarf shrub (e.g. dwarf mountain pine: *Pinus mugo*) or a warm-temperate sclerophyll tree (e.g. Aleppo pine: *Pinus halepensis*; stone (or umbrella) pine: *Pinus pinea*). The Malvaceae family includes both warm-temperate low-to-high shrubs/small trees (e.g. tree mallow: *Malva eriocalyx*) and a drought tolerant forb (e.g. *Malva cretica*). The genus Erica genus can be both a xerophytic shrub (e.g. *Erica multiflora*) and warm-temperate low-to-high shrub/small tree (e.g. *Erica arborea*).

The information carried by pollen to reconstruct the vegetation can be analyzed through several methods. The simplest method for reconstructing vegetation from pollen involves qualitatively interpreting pollen percentages. This method implicitly deals with differences in pollen productivity by excluding taxa with high pollen productivity (e.g., Cyperaceae) from the total pollen sum and upweighting taxa with low pollen production that nevertheless represent a significant component of the vegetation assemblage (e.g. *Larix*). These diagrams are then interpreted in terms of climate based on expert knowledge of the regional vegetation and the characteristics of the pollen record. While this subjective interpretation has proven valuable for characterizing broadscale vegetation changes, for example, changes in the abundance of forest taxa, is highly dependent on the analyst and thus difficult the comparisons between records. Alternative methods have been developed, including biomisation, modern analogue reconstructions, and explicit modelling of pollen production and dispersion that are base on taking into account the relationship between pollen and vegetation.

The following section provides a brief overview of the main quantitative methods, and their respective advantages and disadvantages. This assessment underpins my research to utilize the strengths of two different methods to develop a novel technique for reconstructing vegetation that mitigates the weaknesses associated with existing approaches.

1.2.2 Methods for palaeovegetation reconstruction

Biomisation technique

The concept of using Plant Functional Types (PFTs) to define biomes in pollen analysis for vegetation reconstruction was introduced by Prentice et al. (1996). This approach involves categorizing biomes based on plant physiognomy, i.e. on the mixture of dominant growth forms of plants within a given area. The concept of PFTs captures the influence of various environmental factors on the formation and characteristics of different biomes (e.g. climate, fire regimes, soil type and herbivory) (Prentice et al., 1992; Woodward et al., 2004; Pausas & Bond, 2021). In the approach proposed by Prentice et al. (1996), biomes are defined as a combination of PFTs that are themselves defined based on specific plant traits. These traits include growth form (e.g., tree, shrub, herb), leaf form (broad-leaved, needle-leaved), phenology (evergreen, deciduous), and bioclimatic limits (e.g. cold-tolerant, drought-adapted). Prentice et al. (1996) defined the

temperate deciduous forest biome, for example, as a combination of the boreal summer green tree, cool-temperate needle-leaved tree, eurythermic needle-leaved tree, temperate summer green tree, and cool-temperate summer green tree PFTs. Similarly, they defined the xerophytic woods/scrub biomes as consisting of the warm-temperate sclerophyll shrub, warm-temperate broad-leaved evergreen tree/shrub, and eurythermic needle-leaved tree PFTs.

The biomisation technique is based on the assignment of pollen taxa into PFTs (expressed in a PFT - taxon matrix) and the subsequent definition of biomes as a mixture of dominant PFTs (expressed in a biome - PFT matrix). This allows pollen taxa to be transferred into biomes (expressed in a 0 - 1, absence-presence, biome-taxon matrix). The allocation of pollen taxa to PFTs and of PFTs to biomes is made on the basis of expert knowledge of the flora of a specific region. A similarity index (Equation 1.1) is used to estimate the affinity of a given pollen sample for each of the defined biomes, taking into account the abundance of each taxon in the sample. A square root transformation of the pollen abundances is used to reduce the effect of variability in pollen production, bringing the extreme values closer to the mean. A threshold value (usually 0.5%) is used to remove the noise caused by taxa that are present in low abundance on the assignments. The pollen sample is then assigned to the biome with the highest affinity score.

$$A_{ik} = \Sigma_j \, \delta_{ij} \sqrt{\left\{ max\left[0, \left(p_{jk} - \theta_j\right)\right]\right\}}$$

Equation 1.1. Biomisation similarity index. A_{ik} is the affinity of pollen sample *k* for biome *i*; summation is over all taxa *j*; δ_{ij} is the entry in the biome - taxon matrix for biome *i* and taxon *j*; p_{jk} are the pollen percentages, and θ_j is a threshold pollen percentage (usually set at 0.5% abundance). The square-root operation stabilizes variance and increases the sensitivity of the method to less abundant taxa.

The accuracy of biomisation is assessed by comparing biome predictions based on modern samples against a target vegetation map, either visually or through a comparison (confusion) matrix. Biomisation is an iterative process: depending on the accuracy of the initial reconstructions, the taxa-PFT and the PFT-biome matrices are adjusted to reduce misclassifications. This is necessary, in part, because some taxa could be assigned to multiple PFTs and it is necessary to determine which PFTs they are most likely to represent in a given region. Similarly, there is some uncertainty caused by including all constituent PFTs and in some cases a better prediction is obtained by only using PFTs that are dominant or highly characteristic of a given biome.

Biomisation is the most widely used method to reconstruct past vegetation based on pollen records (Prentice et al., 1996; Prentice & Webb, 1998; Jolly et al., 1998; Tarasov et al., 1998; Williams et al., 1998; Yu, 1998; Allen et al., 2000; Edwards et al., 2000; Elenga et al., 2000; Takahara & Takeoka, 1992; Thompson & Anderson, 2000; Williams et al., 2000; Yu et al., 2000; Harrison et al., 2001; Marchant et al., 2001; Bigelow et al., 2003; Pickett et al., 2004; Allen & Huntley, 2009; Marchant et al., 2009; Tarasov et al., 2013) because it provides good reconstructions of vegetation at the sub-continental scale, has the advantage of being simple and does not require an extensive

modern training data set. However, the subjective classification of taxa to PFTs and PFTs to biomes can cause problems given the limited taxonomic resolution of most pollen assemblages. Taxa identified at genus or family level can frequently be assigned to more than one PFT, and therefore contribute to the similarity score for multiple biomes where these PFTs are present, and similarly PFTs may be present in multiple biomes but not characteristic of every biome. Grasses (Poaceae), for example, are present in practically all vegetation types, although they are most characteristic of open vegetation, such as woodlands, shrublands or steppe. The inclusion of the grass PFT in every biome could therefore make it difficult to discriminate between forests and open vegetation. One solution to this problem is to define biomes in terms of characteristic PFTs. However, this could make it difficult to account for within-biome variability in the abundance of characteristics PFTs. For example, shrubs are characteristic of the warmer/wetter end of the tundra biome but become less abundant as conditions become colder or drier, resulting in considerable variability in the proportion of shrubs present in samples assigned to this biome (see e.g. Edwards et al., 2000). One approach to solving this problem has been the introduction of additional biome types, for example distinguishing shrub tundra from graminoid and forb tundra as was done by Bigelow et al. (2003), but clearly this proliferation would make large-scale mapping of vegetation changes problematic (Prentice et al., 2000). A further problem with the biomisation approach is that taxa that are present in low abundances can introduce confusion in the assignment to biomes. The introduction of a threshold value for including taxa was designed to minimise this problem, but can be counterproductive when there are characteristic taxa that produce little pollen (e.g. *Larix* in the cold deciduous forest) and, even if they are not removed by the threshold, would be given very little weight in the biome assignment. One solution to this problem has been up-weighting the abundances of such taxa (see e.g. Edwards et al., 2000; Bigelow et al., 2003) but this necessitates making a subjective and largely arbitrary decision about the weighting to apply. Another possible solution is to apply specific thresholds for different taxa, a higher value for species that produce a large amount of pollen, and a lower threshold for taxa that produce little pollen (Williams et al., 2000), but this assignment is also subjective and can vary between regions.

Even when defining biomes in terms of their most characteristic PFTs, there is still a problem in that some PFTs can be dominant in several different biomes and that some biomes are effectively characterised by a sub-set of PFTs present in a related biome. For example, the temperate deciduous forest is characterised by the dominance of a subset of PFTs that also characterise cool mixed forest. Prentice et al. (1996) defined a rule for allocating assemblages to a biome where the affinity score is the same between two biomes, specifically giving preference to the biome with the greatest number of PFTs included. However, even when applying this rule, the existence of biomes that are represented by a subset of the PFTs in a closely related biome can result in the calculation of similarity scores for the two biomes, so-called ties. In the downcore application of biomisation this can lead to instability, where relatively small changes in pollen abundance of a taxon in a non-shared PFT can lead to switches between biomes (often called the flickering switch problem: Allen & Huntley, 2009).

However, perhaps the most important limitation of the biomisation technique is the reliance on expert knowledge and the necessity for an iterative approach to optimise the allocation of taxa to PFTs and PFTs to biomes. This subjectivity has led to the creation of different schemes for different regions, which in turn makes comparisons of regional reconstructions difficult (Williams et al., 1998; Prentice et al., 2000).

The Landscape Reconstruction Algorithm (LRA)

The Landscape Reconstruction Algorithm (LRA) is an approach that tries to account for the complexities that influence the pollen rain sample. LRA is a mathematical method that involves modelling the relative contributions of different pollen sources to the pollen signal observed in sedimentary deposits, considering the factors involved in this process including specific-taxon pollen productivity (RPPs: Relative Pollen Productivity Estimates), modes of dispersal dependent on pollen grain physical properties and local geophysical factors, and the abundance of source vegetation types in the study area. The model is used to estimate the proportion of each type of vegetation in the landscape, which can be reconstructed at two different scales by using the two models (Sugita et al. 2007), first at a regional scale with the Regional Estimates of VEgetation Abundance from Large Sites (REVEALS: Sugita, 2007a) model that uses pollen from multiple sites (≥104 km2), and then at a local scale (relevant source area of pollen) with the Local Vegetation Estimates (LOVE: Sugita, 2007b) model that uses pollen from smaller sites (≥ca. 1-5 km radius, relevant source of pollen sensu Sugita, 1993) (Githumbi et al., 2022).

The REVEALS model has been widely employed to produce reconstructions of the regional changes in vegetation abundance and land use in large parts of the North Hemisphere. This model has found application in various regions, including Sweden (Hellman et al., 2008b, 2008a; Mazier et al., 2008; Cui et al., 2014), the Swiss plateau (Soepboer et al., 2010), parts of USA (Sugita et al., 2010), northern Asia (Cao et al., 2019), northern subtropical China (Li et al. 2020, 2023) and Europe as a whole (Trondman et al.,2015, Githumbi et al., 2022; Serge et al.,2023). However, a major limitation of REVEALS is that is data demanding as the inputs of REVEALS model are original pollen counts, relative pollen productivity estimates (RPPs) and their standard deviation, the fall speed of pollen grains (FSP), basin type (lake or bog), size of basin (radius), maximum extent of regional vegetation, atmospheric conditions and wind speed (m s–1). The FSP can be calculated using measurements of the pollen grains and Stokes' law (Gregory, 1973) and the wind speed, atmospheric conditions, and maximum extent of regional vegetation are generally assumed and input as constant values.

The RPP is a crucial parameter to obtaining a good accuracy of the REVEALS model (Sugita, 2007a; Broström et al., 2008). RPPs are derived from modern pollen rain studies, where the amount of pollen produced by different plant species is measured in relation to their abundance in the local vegetation assessed by extensive fieldwork to characterise vegetation around each site. Thus, RPPs are coefficients that represent the relationship between pollen production by a plant taxon and its abundance in the vegetation. These estimates are then used in the LRA to model the

dispersal of pollen from source vegetation to the sedimentary deposits, taking into account the relative productivity of different plant species. Despite its significance, obtaining RPPs poses several challenges. RPPs rely on the comparison of modern pollen assemblages with vegetation composition. Obtaining representative modern reference data for all plant taxa in a given region requires extensive field surveys and pollen sampling across various vegetation types, which may not be feasible or logistically possible in some areas. though RPPs have been estimated for a reasonable number of European plant taxa. Githumbi et al. (2022) synthesized 39 plant taxa from boreal and temperate Europe, including 22 herbs or low shrubs. They also examined 22 plant taxa from Mediterranean Europe, with seven taxa in common with the first region. Serge et al. (2023) expanded Githumbi et al. (2022) synthesis by adding RPP values for 13 more additional entomophilous taxa. However, RPPs have only been collected for 18 taxa in the Eastern Mediterranean region. Filipova-Marinova et al. (2010) obtained RPPs for 5 Tertiary-relict species, while Grindean et al. (2019) obtained them RPPs for 13 taxa (6 families, 5 genus and 2 species) of the Romanian forest steppe. The scarcity of RPPs from the region is a limitation for the application of the REVEALS approach to the Eastern Mediterranean region, given the extensive taxonomic diversity represented by the EMBSeCBIO fossil dataset, which includes over 200 taxa.

One approach to address the scarcity of RPPs for certain regions is to use REVEALS without pollen productivity estimates (PPE) (ROPES: REVEALS without PPEs) (Theuerkauf & Couwenberg, 2018). This approach consists of assessing how appropriate is to use PPEs values obtained from another region (or a random value) in the REVEALS model to reconstruct the abundance of plants by assessing how constant the ratio between the pollen accumulation rate of a taxa (PAR) and the plant abundance reconstructed by REVEALS along a pollen record. If the PPE used is correct and appropriate for the interest region, this ratio will be constant over time otherwise, the ratio will instead vary. This is under the assumption that the changes in plant abundance are linearly represented in the observed pollen accumulation rate (PAR). ROPES preserves all the other assumptions of the REVEALS model and still needs information on parameters such as speed of pollen grains (FSP), basin type (lake or bog), size of the basin (radius), the maximum extent of regional vegetation, atmospheric conditions and wind speed (m s–1). However, the most important limitation of this method is that it can only be applied in well-dated, high-resolution pollen records with substantial variation present in each pollen type and low noise in the PAR data (Theuerkauf & Couwenberg, 2018, 2022). This means that it would be unsuitable, for example, for application in the eastern Mediterranean region, where most of the records are of moderate resolution, or indeed for many other regions of the world.

The modern analogue technique (MAT)

The Modern Analog Technique (MAT) is a statistical method that is based on measuring the degree of similarity or distance between fossil pollen samples and a collection of modern pollen samples to attribute the properties of the modern assemblages to the fossil assemblage with the highest similarity (or the highest analogy). The technique has been applied both to reconstruct vegetation types (Overpeck et al., 1985; Jackson & Overpeck, 2000; Janská et al., 2017; Chytrý et al.,

2019; S. Liu et al., 2021; Jackson & Williams, 2004; Correa-Metrio et al., 2012; Caballero-Rodríguez et al., 2017; Zanon et al., 2018) and climate parameters (Prentice, 1980; Prentice et al., 1991; Bartlein & Whitlock, 1993; Gaillard et al., 1994; Davis, 1995; Zhang et al., 2022). For vegetation reconstruction, MAT is based on the rationale that similar pollen assemblages originate from the same type of vegetation. While for climate reconstruction, MAT assumes that pollen assemblages formed under similar climate conditions. MAT has the advantages of being conceptually simple, the distances are straightforward to calculate and as it does not explicitly model the pollen-climate relationship, these relationships is not required to be either linear or unimodal. However, applying MAT requires making several decisions that can impact the reconstruction accuracy (Lytle & Wahl, 2005; Williams & Shuman, 2008).

Metric	Type	Formula
Canberra distance	Equal-weight metrics	$D_{ij} = \Sigma_k \frac{\lvert p_{ik} - p_{jk} \rvert}{p_{ik} + p_{jk}}$
Standardized Euclidean distance		$D_{ij} = \sqrt{\Sigma_k \frac{(p_{ik} - p_{jk})^2}{s_k}}$
Gower's distance		$D_{ij} = \sqrt{2\Sigma_k \frac{\lvert p_{ik} - p_{jk} \rvert^2}{R_k}}$
Manhatan distnace	Unweighted metrics	$D_{ij} = \Sigma_K \lvert p_{ik} - p_{jk} \rvert$
Euclidean distance		$D_{ij} = \sqrt{\Sigma_K (p_{ik} - p_{jk})^2}$
Squares cos-θ distance		$D_{ij} = \Sigma_k \left(\frac{p_{ik}}{\sqrt{\Sigma_k p_{ik}^2}} - \frac{p_{jk}}{\sqrt{\Sigma_k p_{jk}^2}} \right)^2$
Squared-chord distance	Signal-to-noise metrics	$D_{ij} = \Sigma_k (p_{ik} - p_{jk})^2$
Squared χ^2 distance		$D_{ij} = \Sigma_k \frac{(p_{ik} - p_{jk})^2}{p_{ik} + p_{jk}}$
Information statistic		$D_{ij} = \Sigma_k \left(p_{jk} ln \frac{2p_{ik}}{p_{ik} + p_{jk}} + p_{jk} ln \frac{2p_{jk}}{p_{ik} + p_{jk}} \right)$

p_{ik} = the proportion of pollen type k in sample i, R_k = the range of proportions for pollen type k over all samples, and s_k = the standar deviation of proportions of pollen type k over all samples

Table 1.1 Nine distance metrics for determining dissimilarity between two pollen assemblages (Prentice, 1980; Overpeck et al., 1985). Equal-weight metrics standardize the pollen types so that each affects the distance value

equally. Unweighted metrics do not scale pollen abundance in any way. Signal-to-noise metrics moderately increase the contribution of rare pollen types (Prentice, 1980). After Gavin et al., (2003).

One decision is the choice of distance metric to measure the similarity between fossil and modern pollen samples. Several metrics to measure the distance between two samples have been proposed (Prentice, 1980; Overpeck et al., 1985). There are three types (Table 1.1) differing in how much weight is applied to rare pollen types. Although there are metrics that perform better for certain types of vegetation (e.g. Oswald et al., 2003) or that perform similarly well (see Gavin et al., 2003), the squared chord distance (SCD) is routinely chosen in MAT, as it performs well across different pollen assemblages (Overpeck et al., 1985; Gavin et al., 2003).

One crucial decision is the selection of the geographical and taxonomic extent of the modern dataset. In MAT each modern sample represents a unique example of vegetation with a unique combination of taxa and taxon abundances. However, the information content of an analogue is typically carried by the more dominant pollen taxa, particularly when signal-to-noise metrics such as SCD are used. Thus, rare taxa can introduce noise into the analysis (the shared dominant species will reduce the dissimilarity, but the presence of less abundant species will increase this distance). Strategies such as restricting comparisons to the most common pollen types (Overpeck et al., 1985; Calcote, 1995; Zanon et al., 2018) or using PFTs instead of taxa to reconstruct either vegetation (Zanon et al., 2018) or climate (Davis et al., 2003; Mauri et al., 2015; Zhang et al., 2022) have been implemented to reduce this problem. However, as described above in the context of biomisation, the allocation of taxa to PFTs is affected by the taxonomic resolution of the pollen samples and this means that some taxa could represent multiple PFTs. As in the case of the allocation of taxa to PFTs in the biomisation approach, the assignment to PFTs is based on expert knowledge and this introduces a degree of subjectivity into the method. Moreover, comparisons of the performance of different distance metrics including some that focus on poorly represented taxa by equal weighting between taxa, such as Canberra distance, have shown that rare species are important to differentiate between biomes, especially between those that are similar (Overpeck et al., 1985; Oswald et al., 2003). In theory, the noise introduced by rare taxa should be mitigated by enlarging the pool of potential analogues to a wider variety of plant communities. Recent applications of MAT have focused on expanding modern datasets to include more climatic and ecological variation and thus improve analogue selection. However, expanding the geographic range of the modern data set often leads to an effective decrease in the taxonomic resolution of pollen data, because the number of species contributing to each pollen morphotype increases. As a result, there is a higher risk of inappropriate matches between apparently analogous pollen samples (Williams & Shuman, 2008). Splitting taxa based on regional variation has been proposed as a way to reduce the risk of false positives (Williams & Shuman, 2008), but this means the selection of the pool of modern analogues would be scale-dependent and dependent on the analyst. Additionally, an extensive pollen modern dataset that could allow taxonomic regional subgrouping is not available in many regions of the world, including the Eastern Mediterranean region, which would preclude the wider application of such an approach.

Another limitation of MAT is the choice of an appropriate threshold for the distances between modern and fossil samples to define the degree of similarity required for a modern sample to be considered an analogue of a fossil sample. The threshold can be defined a priori based on expert knowledge or by choosing a cut-off point on the statistical distribution of the distances, for example, e.g. by using the distribution quantiles (Simpson, 2012). This selection should take into account the number and geographical or climatic spatial coverage of the modern samples, the taxonomic diversity of the samples, and the scale of the study (Gavin et al., 2003; Jackson & Williams, 2004; Overpeck et al., 1992). The routine practice is to use a single threshold, the on-off scheme, to determine whether a sample is similar enough to be considered an analogue. However, more flexible schemes such as two-tier schemes, where the first tier (threshold) represents a likely analogy of vegetation and the second tier defines a potential although less certain analogue (Davis et al., 1999; Lytle & Wahl, 2005) and the reconstruction is based either on a single first-tier analogue or two second-tier analogues, have shown better performance. The conservative criteria of restricting analyses to the "best" analogues, removes from consideration "good" analogues that also carry useful information (Lytle & Wahl, 2005). Additionally, pairwise comparison of dissimilarity scores for biomes (through the ROC curve) has shown that threshold values are different between biomes (Gavin et al., 2003). When fossil assemblages do not pass the threshold for having an acceptable modern analogue, this may reflect the selected threshold, the use of a restricted collection of modern samples or because past environmental conditions were completely different from the conditions typified by the modern spectra and the fossil assemblage is indeed a "no-analogue" assemblage.

There may be several potential best analogues, and in such cases, it is general practice to assign an averaged value of all the analogues to the fossil sample. Averaging can reduce the impact of any single modern assemblage that might not fully represent the conditions of the fossil sample. However, how many analogues to take is a subjective decision. When MAT is used for climate reconstruction, it is possible to average several best analogues. However, when applied to vegetation reconstruction, this averaging process is not straightforward, and the use of MAT for combining multiple analogues has remained qualitative or has necessitated refinement through the use of extra information, such as ratios of pollen types. MAT is sensitive to small changes in pollen abundance, which can lead to rapid and unrealistic shifts in biome assignments downcore, known as the "flickering switch" problem.

In summary, while MAT offers a simple and flexible approach for reconstructing vegetation and climate based on fossil pollen samples, it requires careful decision-making by the analyst, particularly regarding the geographical and taxonomic extension of the modern dataset, the type of metric to use and how much weight to give to rare taxa, the choice of threshold for analogues, and the appropriateness of averaging across multiple analogues.

Overall

In this thesis, I have taken advantage of different existing approaches to design a new method for reconstructing vegetation (Chapter 2). The new method adopts a similar approach to biomisation in terms of the classification of vegetation types and uses a similar distance index to estimate the distance between a fossil sample and the samples from the training dataset. However, similar to MAT, it uses an extensive modern training data set, as to MAT approaches, to minimise the subjective decisions inherent in biomisation. The new approach also makes use of the ROC curve to estimate a unique threshold for each biome, allowing the identification of fossil assemblages that are not analogous to any modern biome.

1.3 Reconstructing climate from pollen

1.3.1 Overview of the plants-climate relationship for reconstructing climate

The different methods for reconstructing climate from pollen all rely on the fact that the geographic range and abundance of species are largely determined by aspects of climate (e.g. seasonal temperatures or moisture availability). There are two main sources of evidence supporting climate as the main determinant of species distributions (Araújo & Peterson, 2012). Firstly, the geographic distributional limits of species are often found to correspond to specific combinations of several climate variables (e.g. Woodward & Williams, 1987; Walther et al., 2005; Harrison et al., 2009), and this is also true for altitudinal ranges (e.g. Wilson et al., 2005; Lenoir et al., 2008). Secondly, these limits have been shown to change in response to changes in climate, demonstrated by ongoing climate changes (e.g. with biomes in Gonzalez et al. (2010), with species in Lenoir et al. (2007), and with ecosystems in Higgins et al. (2023) and to past climate changes (e.g. Dobrowski et al., 2011). However, it is not always straightforward to model the vegetation response to climate changes because different plant species are sensitive to different climate variables (Figure 1.2).

The distribution of some species, for example, is controlled primarily by winter temperature while other species reflect growing season temperatures or the availability of water during the thermal growing season (Harrison et al., 2010). If a species is controlled by winter temperature, then it could display a multimodal response to some other aspect of the climate. The perfect equilibrium between species and climate, where a certain combination of climate variables will determine the presence and abundance of a given species, is thought to be unrealistic as other factors including biotic interactions or dispersal constraints may prevent or facilitate species from occupying all suitable habitats (Beale et al., 2008; Huntley, 2012; Araújo & Peterson, 2012).

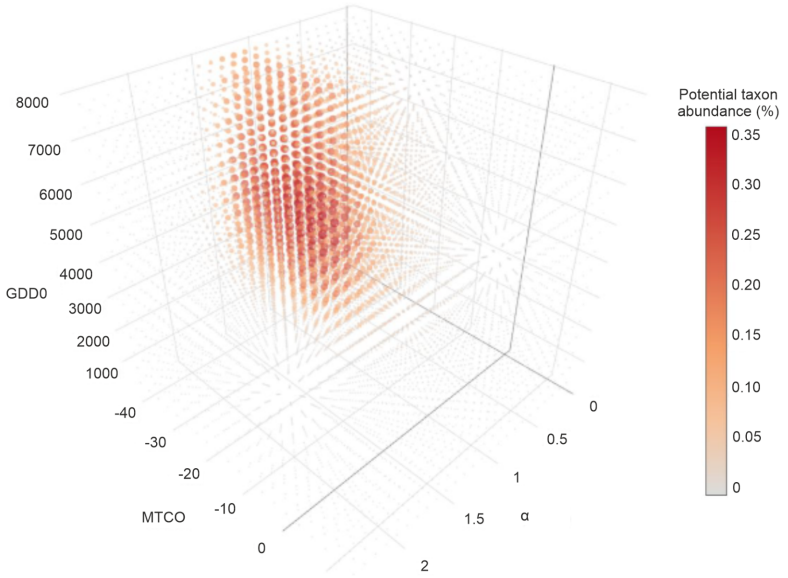

Figure 1.2 Potential taxon abundance of *Abies* in a climatic space defined by growing degree days above a base level of 0°C (GDD0), the mean temperature of the coldest month (MTCO), and a plant available moisture index calculated as the ratio of annual precipitation to annual potential evapotranspiration (MI). Modified from Wei et al. (2020).

There are several indicators that have been used to infer past climates including δ_{18}O and δ_{13}C from speleothems (e.g. Bar-Matthews & Ayalon, 2004; Göktürk et al., 2011) or shells (e.g. Dean et al., 2015), inorganic (e.g. Ti, Mg, Ca, Si) elemental composition of sediments (e.g. Bliedtner et al., 2020) u organic elements (e.g. alkenones) (Marriner et al., 2022). However, in general, they only provide inferences about trends in specific climatic variables, such as temperature or precipitation, and cannot provide information about the seasonality of the climate, which is probably more important for human well-being because it is related to the productivity of agricultural crops. Pollen data are therefore still the most widely used source of climate reconstructions, particularly quantitative climate reconstructions (Bartlein et al., 2011; Chevalier et al., 2020), at regional to continental scales.

1.3.2 Methods for palaeoclimate reconstruction

Process-based methods

In this approach, the outputs from the process-based vegetation models that predict the distribution and properties of plant functional types (PFTs) including, for example, net primary production and leaf area index, as a function of climate, soil properties, and atmospheric CO2 content are inverted to infer past climate conditions from fossil pollen samples (Wu et al., 2007; Garreta et al., 2010; Izumi & Bartlein, 2016). Pollen taxa are assigned to PFTs using standard tables developed for vegetation reconstruction (Prentice et al., 2000; Pickett et al., 2004; Marchant et al., 2009) in order to characterise the fossil pollen assemblages. A climate space is then constructed by systematically varying the input variables of the model. The inversion method then identifies the point in this climate space that provides the best match between the

PFT profile of the fossil pollen sample (in terms of abundance) and the PFT profiles generated by the model. To accelerate the search and make the approach computationally tractable, a Monte Carlo Markov Chain algorithm is often used.

Model inversion could be a valuable tool for reconstructing the past climate because it takes into account all the factors that could influence species distribution, including the impact of changes in CO_2 on photosynthesis and water use efficiency and competition. However, the quality of the model used is critical (Harrison et al., 2023). Model inversion has generally been performed using relatively simple biogeography models, particularly models from the BIOME family (Haxeltine & Prentice, 1996; Kaplan et al., 2003). These models do not include, for example, the impact of fire or biotic interactions (including human activities) on vegetation (Harrison et al., 2023). Thus, they may not capture all the complexities involved in the processes that govern species distribution. More complex or more realistic vegetation models require the specification of a large number of PFT-specific parameters and therefore tend to simulate vegetation as a function of only a limited number of PFTs (Fisher et al., 2018). Furthermore, inverting such complex models is computationally very intensive.

Statistical tools

Modern Analogue Technique (MAT)

The MAT technique, when applied to climate reconstruction, works under the same principles and assumptions described in section 1.2 and has the same limitations. When MAT is applied to reconstruct climate, rather than vegetation, there is the possibility of averaging climate values from several analogues (usually between 5 and 10 analogues). Although the number of analogues to average is a subjective decision, averaging is considered to provide a more robust estimate of the actual climate of a fossil sample than using only a single best analogue. MAT has been used with extensive fossil pollen datasets to provide continental-scale climate reconstructions, including gridded maps created by interpolation of the site-based reconstructions (e.g. Davis et al., 2003; Gajewski et al., 2000; Ladd et al., 2018; Mauri et al., 2015; Sawada et al., 2004). It has also been used to provide time-series climate reconstructions (e.g. Marsicek et al., 2018; Viau & Gajewski, 2009).

Artificial neural networks

Artificial neural networks (ANN) are a type of machine learning algorithm that consists of interconnected nodes or "neurons" organized into layers. Each node takes input data, applies a mathematical function to it, and produces an output. These outputs are then fed into the next layer of nodes until a final output is produced (Warner & Misra, 1996). The network learns by adjusting the weights between nodes through a process called backpropagation (Kubat, 2021). During training, the network is shown examples of inputs and their corresponding desired

outputs, and the weights are adjusted to minimize the difference between the predicted output and the desired output. Once the network has been trained, it can be used to make predictions on new input data that has not been seen before. Peyron et al. (1998) were the first to apply ANN for reconstructing climate variables, specifically using a modern pollen data set for training and then applying the model to reconstruct climate at 18000 yr B.P. in Europe. The technique has subsequently been applied several times, particularly for reconstructing sea surface temperature (e.g. Peyron & Vernal, 2001; Malmgren et al., 2001; de Vernal et al., 2005; Kucera et al., 2005).

One advantage of ANN is that it performs very well for non-linear relationships between pollen abundances and climate variables, which is something that can be difficult to model using traditional statistical techniques (Bartlein et al., 2011; Chevalier et al., 2020). However, ANN has a tendency to overfit the training data, which means that the method may not generalize well to new data. This problem is exacerbated when using small datasets (Kubat, 2021), so ANN works best when trained using an extensive modern pollen dataset, which is not available in many parts of the world, including the eastern Mediterranean. Also, since the ANN algorithm is complex, it is challenging to improve the model if the predictions or reconstructions are poor. Furthermore, despite the sophistication of ANN technique, it does not consistently outperform simpler climate reconstruction techniques (Salonen et al., 2019).

The response surface technique

The response surface technique (Bartlein et al., 1986; Prentice et al., 1991; Huntley et al., 1993) involves fitting a smooth surface to pollen taxon abundances in a climate space defined by two (or more) climatic variables such as temperature (e.g. Anderson et al., 1991), and precipitation. The surfaces are fitted using a flexible surface-fitting procedure that allows for complicated shapes and some extrapolation of the values of the pollen percentages as a function of these variables. The climate conditions at the time the fossil pollen sample was deposited are identified by finding the point on the response surface space where the sample shows the lowest dissimilarity to the assemblage constructed from the fitted values of all the taxa. The climate at this point is then attributed to the fossil pollen sample.

One advantage of the response surface approach is that it provides a continuous estimation of the climate space through interpolation. Thus, unlike MAT, it can provide an estimate for the climate of the fossil sample that is not observed in the training data set. It also filters out non-climatic noise in the pollen data and only retains primary pollen-climate signals (Chevalier et al., 2020). However, an issue with the application of response surfaces to reconstruct past climates is the necessity for the analyst to define *a priori* the fitting procedure and the degree of smoothness for describing the taxon abundances. The most commonly used approach has been to use second or third order polynomial curves for fitting (Bartlein et al., 1986) and locally weighted smoothing (e.g. LOWESS; Prentice et al., 1991; Huntley et al., 1989). However, there is a risk of excessive smoothing which will increase the area of climate that is considered to be the best match (Bartlein et al., 1986).

Regression-based techniques: inverse regression and weighted averaging partial least squares

Inverse regression

Inverse regression is a statistical method used to estimate the input parameters of a model given the output or response variables. In the context of palaeoclimate reconstructions, inverse regression was developed and used by Huntley & Prentice (1988) to create a transfer function for reconstructing summer temperature. The first step is to derive transfer functions (regression equations) to relate the pollen abundances of different taxa to the climate variables of interest using a modern calibration pollen dataset and corresponding climate variables. The statistical model is then inverted, where each climate variable is treated as a dependent variable in a multiple regression with the taxon abundances as the predictors. The transfer function is then used to estimate the past climate variables from the fossil pollen data. The inverse regression method is used to estimate the most likely values of the climate variables that would have produced the observed plant species distribution in the fossil pollen record. Improved fit can be obtained by Box-Cox transformation of the taxon abundances (Bartlein et al., 1984). This approach is particularly useful because multiple types of data can be used, when available, for a given time period. Inverse regression does not account for the non-linear or non-monotonic responses of pollen taxa to climate, but this can be solved by using multiple transfer functions for different subsets of the data. However, using multiple transfer functions for each region or sub-region makes the method complicated. It also means that the best-fitting equation for a given point under modern conditions may not be the most suitable when applied to the same point in the past (Bartlein et al., 2011).

Weighted averaging partial least squares regression

Weighted averaging partial least squares (WA-PLS) regression is a variant of partial least squares (PLS) regression (Wold, 1966; Wold et al., 2001) that places more emphasis on important variables by assigning weights. It is particularly useful in situations where there are more predictor variables than observations and where the predictor variables are highly correlated and therefore difficult to interpret individually. The method was first introduced for reconstructing climate by ter Braak & Juggins (1993). WA-PLS involves transforming the pollen abundances into predictor variables using a weighted averaging procedure based on the degree of correlation between each taxon and the response variables (in this case climate variables). The PLS regression method is then used to find a linear combination of the predictor variables that is most strongly related to the response variables, and this linear combination is called the first PLS component.

The weighting scheme in WA-PLS assigns weights to each taxon based on their sensitivity to the different environmental variables and their reliability. Taxa that are strongly correlated with the climate variable of interest are given higher weights, while taxa with weaker correlations may receive lower weights or be excluded altogether. The weights can be estimated from the data

using a variance-covariance matrix, where taxa with higher covariance with the response variable receive higher weights. These weights are then used to scale the predictor variables before applying the PLS regression. PLS regression is a multivariate statistical technique that finds a linear combination of the predictor variables that is most strongly related to the response variables, this combination is also called the latent variable or component (H. Birks, 2003). In the context of WA-PLS, PLS regression is performed after the predictor variables have been transformed and weighted. The first PLS component is calculated by maximizing the covariance between the linear combination of the predictors and the response variables. This component represents the most important pattern of variation in the predictors related to the response. After calculating the first PLS component, the residuals (the part of the data not explained by the first component) are computed, and the process is repeated to find subsequent PLS components. This

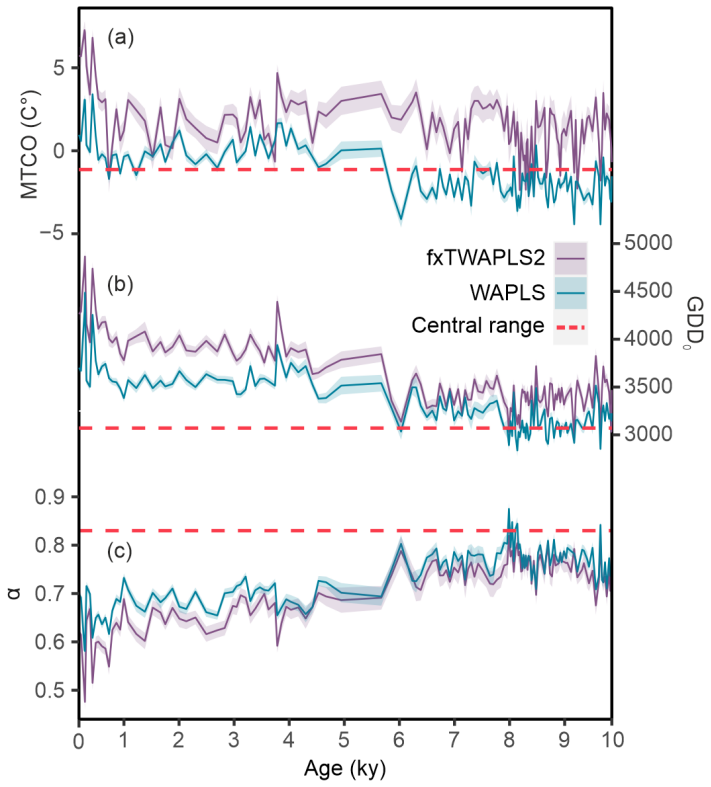

Figure 1. 3 Comparison of climate variables reconstructions under WA-PLS and xfTWA-PLS2 approaches, based on the Holocene pollen record from Basa de la Mora in the Iberian Peninsula. Redrawn from Liu et al. (2020)

iterative process continues until a predetermined number of components are calculated or until the amount of variance explained by the components reaches a certain threshold. The components are ordered based on their ability to explain the variance in the response variables, with the first component explaining the most variance, and the model is fitted using the first few components. The determination of the number of components to use in the WA-PLS model is a crucial step. Using too few components may result in an inadequate representation of the relationship between predictors and response while using too many components can lead to overfitting, where the model captures noise rather than meaningful patterns. The optimal number of components depends on the complexity of the relationship between the observations

and the climate variables. Various statistical criteria, such as cross-validation or information criteria, can be employed to select the appropriate number of components. These methods assess the predictive performance of the model using a subset of the data that was not used in model building and selects the number of components that yield the best performance. The performance of the model can be evaluated using statistical measures, and the weights can be optimized iteratively to enhance the reconstruction quality.

One limitation of WA-PLS regression is that it assumes that the relationship between the environmental variables and the pollen abundances is linear and that the relationship can be approximated by a set of partial least squares (PLS) components, implying that the changes in the pollen abundances are linear to the changes in the climate variables, and also, it assumes the variance of the proxy data to be constant over time. WA-PLS is specifically designed to deal with unimodal responses of taxa to environmental gradients, it has difficulty in handling more complex responses such as bimodal or multimodal distributions (Liu et al., 2020). In common with inverse regression, it always gives an answer, which could be the wrong answer in no-analogue situations (Bartlein et al., 2011).

A further issue that affects the accuracy of climate reconstructions using all regression-based techniques, including WA-PLS, is the tendency for the reconstruction to be compressed towards the center of the sampled climate range (Seppä et al., 2004; Shen et al., 2006; Salonen et al., 2012). This leads to an overestimation of values at the high end and an underestimation of values at the low end of the range of the climate variable. A modified approach that takes into account the climatic tolerance of individual taxa and the frequency of sampled climate (fx) in the training dataset has been developed to reduce this compression bias. Tolerance weighted average partial least-square considering fx (fxTWA-PLS2) has been described and tested in two consecutive works (Liu et al., 2020, 2023) and has been shown both to considerably reduce the compression bias and to perform better than other reconstruction approaches. One consequence of the reduction of the compression bias is that the method produces a greater amplitude of changes through time (Fig. 1.3), and thus is likely to provide a more realistic reconstruction of climate variability.

Overall

In this thesis, I use the fxTWA-PLS technique to make climate reconstructions because it is a relatively simple statistical technique but at the same time appears to provide a significant improvement on other available statistical techniques, in particular through minimising the compression bias that is characteristic of other regression-based approaches.

1.4 Paleoenvironmental controversies in the Eastern Mediterranean

Palynological studies have been conducted in the eastern Mediterranean region since the 1970s to address a variety of research questions, including tracing the origin of agriculture (e.g. van Zeist et

al., 1970) or documenting the impact of climate changes known from the high latitudes (e.g. Turner & Greig, 1975; van Zeist & Woldring, 1980). Efforts were made quite early on to summarize the existing data to document the environmental history of the region (e.g. van Zeist et al., 1975; van Zeist & Bottema, 1977; Bottema & Woldring, 1984; van Zeist & Bottema, 1991; Bozilova & Tonkov, 1995). Although the number of sites records continued to increase, there was no attempt to produce new regional compilations until the creation of the Eastern Mediterranean-Black Sea-Caspian Corridor (EMBSeCBIO) database (Cordova et al., 2009; Marinova et al., 2018; Harrison, Prentice, et al., 2021). In the absence of a large-scale synthesis, analysis has focused on comparing individual pollen records from the eastern Mediterranean and this has led to a number of unresolved debates about the Holocene climate and vegetation history in the region (Sadori et al., 2011; Roberts et al., 2011; Messager et al., 2017).

One significant factor contributing to the persistence of these controversies is that many climate or vegetation reconstructions are based on the subjective interpretation of individual records (Sadori et al., 2011; Bini et al., 2019). Differences between records may reflect the importance of local factors at a given site compared to the regional signal. Cross-comparison may also be hampered by data gaps in a particular record. A major challenge in interpreting individual records is the variability in chronologies and resolutions across different sources, which limits the comparison of specific environmental periods or events between records. Further uncertainties can be introduced by the subjective selection of particular records for comparison, which can result in an incomplete representation of the processes being studied.

The use of large-scale data syntheses to examine regional signals through the statistical analysis of standardized data in a uniform manner has proved to be a powerful tool for analysing many types of data (Prentice & Webb, 1998; Prentice et al., 2000; Power et al., 2008; Davis et al., 2003, 2013; Parker et al., 2021; Parker & Harrison, 2022; M. Liu et al., 2023). The Eastern Mediterranean was included in the BIOME 6000 Palaeovegetation Mapping Project, but it was not treated as a separate region because there was no specific regional data synthesis available. Instead, some sites from the region were included in the European biomisation (Prentice et al., 1996; Elenga et al., 2000), some in the African and Middle Eastern biomisation (Jolly et al., 1998; Elenga et al., 2000) and some in the biomisation of the Former Soviet Union (Tarasov et al., 1998, 2000). This resulted in differences in the methodological decisions made, for example in the classification of taxa to PFTs, which in turn impacted the reconstructions. Given the long history of human occupation of the eastern Mediterranean stretching back to the Pleistocene, and the highly heterogeneous nature of the regional climate, topography, and vegetation cover, it is important to treat the region in a consistent manner to determine whether differences between sites are a reflection of the methodology or a real feature reflecting the complexity of the climate and vegetation history.

The production of new records from the eastern Mediterranean (e.g. Vermoere et al., 2001; M. Filipova-Marinova, 2003; Wick et al., 2003; Atanassova & Stefanova, 2005; Atanassova, 2005; Leroy et al., 2006), not included in any of the BIOME6000 regional biomisations, was a motivation for

the EMBSeCBIO project (Cordova et al., 2009), which sought to create a regional database including records that were not part of any existing dataset. The resultant EMBSeBIO database was subsequently used to test the biomisation approach for mapping modern vegetation in the eastern Meditteranean region (Marinova et al., 2018). The database has not been exploited beyond this.

This thesis exploits the EMBSeCBIO database analysis to tackle uncertainties in reconstructing climate and vegetation from pollen data by developing or using predictive models and applying different statistical methods. The relatively poor performance of the biomisation technique in the eastern Mediterranean, as shown by Marinova et al., (2018), was one motivation for developing a new approach to reconstruct vegetation in this thesis.

1.5 Overall purposes and thesis outline

The overall goal of my thesis is to provide reconstructions of vegetation and climate changes for the eastern Mediterranean region that can ultimately be used to explore the relationships between climate, vegetation and human activities during the Holocene using the most up-to-date and robust tools possible.

Although I capitalised on the existence of the EMBSeCBIO pollen database (Cordova et al., 2009; Marinova et al., 2018), it was necessary to extend the site coverage and to create new age models for all the sites, benefitting from the most recent radiocarbon calibration (IntCal20: Reimer et al., 2020) and Bayesian age modelling tools (Blaauw et al., 2021; Villegas-Diaz et al., 2021). Given the limitations of existing vegetation reconstruction techniques, as summarised above, I developed a new method that combines the strengths of biomisation and the MAT approach. This work is presented in Chapter 2. Having demonstrated that this new technique produced reliable vegetation reconstructions and allowed the identification of non-analogue samples, I used these reconstructions to resolve some of the persistent controversies about the vegetation history of the region, including examining the potential relationship between reconstructed vegetation changes and human population changes. This work is presented in Chapter 3. Finally, I used the new reconstruction method developed by Liu et al. (2020, 2023) to provide reconstructions of bioclimatic variables, including measures of season temperature and plant-available water, at sites across the region and used these to create composite curves of regional climate evolution through the Holocene. In reconstructing plant-available water, I made use of the recent modelling work that allows the physiological effects of changing CO_2 on water-use efficiency (Prentice et al., 2022), to provide a correction for the reconstructed plant-available water which therefore provides a more realistic estimate of changes in moisture through time than previous approaches. The climate reconstructions are presented in Chapter 4. I address the implications of these new reconstructions in my final chapter (Chapter 5).

1.6. References

Allen, J. R. M., & Huntley, B. (2009). Last Interglacial palaeovegetation, palaeoenvironments and chronology: A new record from Lago Grande di Monticchio, southern Italy. Quaternary Science Reviews, 28(15), Article 15. https://doi.org/10.1016/j.quascirev.2009.02.013

Allen, J. R. M., Watts, W. A., & Huntley, B. (2000). Weichselian palynostratigraphy, palaeovegetation and palaeoenvironment; the record from Lago Grande di Monticchio, southern Italy. Quaternary International, 73–74, 91–110. https://doi.org/10.1016/S1040-6182(00)00067-7

Anderson, P. M., Bartlein, P. J., Brubaker, L. B., Gajewski, K., & Ritchie, J. C. (1991). Vegetation-Pollen-Climate Relationships for the Arcto-Boreal Region of North America and Greenland. Journal of Biogeography, 18(5), 565–582. https://doi.org/10.2307/2845692

Araújo, M. B., & Peterson, A. T. (2012). Uses and misuses of bioclimatic envelope modeling. Ecology, 93(7), 1527–1539. https://doi.org/10.1890/11-1930.1

Atanassova, J. (2005). Palaeoecological setting of the western Black Sea area during the last 15000 years. The Holocene, 15(4), 576–584. https://doi.org/10.1191/0959683605hl832rp

Atanassova, J., & Stefanova, V. (2005). Late Holocene vegetation changes in the Northern Pirin Mountains (southwestern Bulgaria). Palynological data from Lake Suho Breznishko and Lake Okadensko. Geologica Carpathica, 56, 447–453.

Bar-Matthews, M., & Ayalon, A. (2004). Speleothems as palaeoclimate indicators, a case study from Soreq Cave located in the Eastern Mediterranean Region, Israel. In R. W. Battarbee, F. Gasse, & C. E. Stickley (Eds.), Past Climate Variability through Europe and Africa (pp. 363–391). Springer Netherlands. https://doi.org/10.1007/978-1-4020-2121-3_18

Bar-Matthews, M., Ayalon, A., Kaufman, A., & Wasserburg, G. J. (1999). The Eastern Mediterranean paleoclimate as a reflection of regional events: Soreq cave, Israel. Earth and Planetary Science Letters, 166(1), 85–95. https://doi.org/10.1016/S0012-821X(98)00275-1

Bartlein, P. J., Harrison, S. P., Brewer, S., Connor, S., Davis, B. A. S., Gajewski, K., Guiot, J., Harrison-Prentice, T. I., Henderson, A., Peyron, O., Prentice, I. C., Scholze, M., Seppä, H., Shuman, B., Sugita, S., Thompson, R. S., Viau, A. E., Williams, J., & Wu, H. (2011). Pollen-based continental climate reconstructions at 6 and 21 ka: A global synthesis. Climate Dynamics, 37(3), Article 3. https://doi.org/10.1007/s00382-010-0904-1

Bartlein, P. J., Prentice, I. C., & Webb, T. (1986). Climatic Response Surfaces from Pollen Data for Some Eastern North American Taxa. Journal of Biogeography, 13(1), 35–57. https://doi.org/10.2307/2844848

Bartlein, P. J., Webb, T., & Fleri, E. (1984). Holocene Climatic Change in the Northern Midwest: Pollen-Derived Estimates. Quaternary Research, 22(3), 361–374. https://doi.org/10.1016/0033-5894(84)90029-2

Bartlein, P. J., & Whitlock, C. (1993). Paleoclimatic interpretation of the Elk Lake pollen record. In J. P. Bradbury & W. E. Dean (Eds.), Elk Lake, Minnesota: Evidence for Rapid Climate Change in the North-Central United States (Vol. 276, p. 0). Geological Society of America. https://doi.org/10.1130/SPE276-p275

Bar-Yosef, O., Bar-Matthews, M., & Ayalon, A. (2017). 12,000–11,700 cal BP: The Collapse of Foraging and Origins of Cultivation in Western Asia. In H. Weiss (Ed.), Megadrought and Collapse: From Early Agriculture to Angkor (p. 0). Oxford University Press. https://doi.org/10.1093/oso/9780199329199.003.0002

Beale, C. M., Lennon, J. J., & Gimona, A. (2008). Opening the climate envelope reveals no macroscale associations with climate in European birds. Proceedings of the National Academy of Sciences, 105(39), 14908–14912. https://doi.org/10.1073/pnas.0803506105

Bigelow, N. H., Brubaker, L. B., Edwards, M. E., Harrison, S. P., Prentice, I. C., Anderson, P. M., Andreev, A. A., Bartlein, P. J., Christensen, T. R., Cramer, W., Kaplan, J. O., Lozhkin, A. V., Matveyeva, N. V., Murray, D. F., McGuire, A. D., Razzhivin, V. Y., Ritchie, J. C., Smith, B., Walker, D. A., … Volkova, V. S. (2003). Climate change and Arctic ecosystems: 1. Vegetation changes north of 55°N between the last glacial maximum, mid-Holocene, and present. Journal of Geophysical Research: Atmospheres, 108(D19), Article D19. https://doi.org/10.1029/2002JD002558

Bini, M., Zanchetta, G., Perşoiu, A., Cartier, R., Català, A., Cacho, I., Dean, J. R., Di Rita, F., Drysdale, R. N., Finnè, M., Isola, I., Jalali, B., Lirer, F., Magri, D., Masi, A., Marks, L., Mercuri, A. M., Peyron, O., Sadori, L., … Brisset, E. (2019). The 4.2 ka BP Event in the Mediterranean region: An overview. Climate of the Past, 15(2), 555–577. https://doi.org/10.5194/cp-15-555-2019

Birks, H. (2003). Quantitative palaeoenvironmental reconstructions from Holocene biological data. Global Change in the Holocene, 342–357.

Blaauw, M., Christen, J. A., Lopez, M. A. A., Vazquez, J. E., V, O. M. G., Belding, T., Theiler, J., Gough, B., & Karney, C. (2021). rbacon: Age-Depth Modelling using Bayesian Statistics (2.5.6) [R]. https://CRAN.R-project.org/package=rbacon

Bliedtner, M., Zech, R., Zech, J., Schäfer, I., & von Suchodoletz, H. (2020). A first Holocene leaf wax isotope-based paleoclimate record from the semi-humid to semi-arid south-eastern Caucasian lowlands. Journal of Quaternary Science, 35(5), 625–633. https://doi.org/10.1002/jqs.3210

Bottema, S., & Woldring, H. (1984). Late Quaternary vegetation and climate of Southwestern Turkey. Part II. Palaeohistoria, 123–149.

Bozilova, E., & Tonkov, S. (Eds.). (1995). Advances in Holocene Palaeoecology in Bulgaria. Pensoft Publishers. https://doi.org/10.1177/095968369600600317

Broström, A., Nielsen, A. B., Gaillard, M.-J., Hjelle, K., Mazier, F., Binney, H., Bunting, J., Fyfe, R., Meltsov, V., Poska, A., Räsänen, S., Soepboer, W., von Stedingk, H., Suutari, H., & Sugita, S. (2008). Pollen productivity estimates of key European plant taxa for quantitative reconstruction of past

vegetation: A review. Vegetation History and Archaeobotany, 17(5), Article 5. https://doi.org/10.1007/s00334-008-0148-8

Caballero-Rodríguez, D., Lozano-García, S., & Correa-Metrio, A. (2017). Vegetation assemblages of central Mexico through the late Quaternary: Modern analogs and compositional turnover. Journal of Vegetation Science. https://doi.org/10.1111/jvs.12515

Calcote, R. (1995). Pollen Source Area and Pollen Productivity: Evidence from Forest Hollows. Journal of Ecology, 83(4), 591–602. https://doi.org/10.2307/2261627

Cao, X., Tian, F., Li, F., Gaillard, M.-J., Rudaya, N., Xu, Q., & Herzschuh, U. (2019). Pollen-based quantitative land-cover reconstruction for northern Asia covering the last 40 ka cal BP. Climate of the Past, 15(4), 1503–1536. https://doi.org/10.5194/cp-15-1503-2019

Carozza, L., Berger, J. F., Burens-Carozza, A., & Cyril, M. (2015). Society and environment in Southern France from the 3rd millennium BC to the beginning of the 2nd millennium BC: 2200 BC a tipping point? In H. Meller, H. W. Arz, R. Jung, & R. Risch (Eds.), 2200 BC – A climatic breakdown as a cause for the collapse of the old world? Löhner - Druck.

Chevalier, M., Davis, B. A. S., Heiri, O., Seppä, H., Chase, B. M., Gajewski, K., Lacourse, T., Telford, R. J., Finsinger, W., Guiot, J., Kühl, N., Maezumi, S. Y., Tipton, J. R., Carter, V. A., Brussel, T., Phelps, L. N., Dawson, A., Zanon, M., Vallé, F., … Kupriyanov, D. (2020). Pollen-based climate reconstruction techniques for late Quaternary studies. Earth-Science Reviews, 210, 103384. https://doi.org/10.1016/j.earscirev.2020.103384

Chytrý, M., Horsák, M., Danihelka, J., Ermakov, N., German, D. A., Hájek, M., Hájková, P., Kočí, M., Kubešová, S., Lustyk, P., Nekola, J. C., Pavelková Řičánková, V., Preislerová, Z., Resl, P., & Valachovič, M. (2019). A modern analogue of the Pleistocene steppe-tundra ecosystem in southern Siberia. Boreas, 48(1), 36–56. https://doi.org/10.1111/bor.12338

Cordova, C. E., Harrison, S. P., Mudie, P. J., Riehl, S., Leroy, S. A. G., & Ortiz, N. (2009). Pollen, plant macrofossil and charcoal records for palaeovegetation reconstruction in the Mediterranean-Black Sea Corridor since the Last Glacial Maximum. Quaternary International, 197(1–2), 12–26. https://doi.org/10.1016/j.quaint.2007.06.015

Correa-Metrio, A., Lozano-García, S., Xelhuantzi-López, S., Sosa-Nájera, S., & Metcalfe, S. E. (2012). Vegetation in western Central Mexico during the last 50 000 years: Modern analogs and climate in the Zacapu Basin. Journal of Quaternary Science, 27(5), 509–518. https://doi.org/10.1002/jqs.2540

Cui, Q.-Y., Gaillard, M.-J., Lemdahl, G., Stenberg, L., Sugita, S., & Zernova, G. (2014). Historical land-use and landscape change in southern Sweden and implications for present and future biodiversity. Ecology and Evolution, 4(18), Article 18. https://doi.org/10.1002/ece3.1198

Cullen, H. M., deMenocal, P. B., Hemming, S., Hemming, G., Brown, F. H., Guilderson, T., & Sirocko, F. (2000). Climate change and the collapse of the Akkadian empire: Evidence from the deep sea. Geology, 28(4), 379–382. https://doi.org/10.1130/0091-7613(2000)28<379:CCATCO>2.0.CO;2

Davis, B. A. S., Brewer, S., Stevenson, A. C., & Guiot, J. (2003). The temperature of Europe during the Holocene reconstructed from pollen data. Quaternary Science Reviews, 22(15), Article 15. https://doi.org/10.1016/S0277-3791(03)00173-2

Davis, B. A. S., Zanon, M., Collins, P., Mauri, A., Bakker, J., Barboni, D., Barthelmes, A., Beaudouin, C., Bjune, A. E., Bozilova, E., Bradshaw, R. H. W., Brayshay, B. A., Brewer, S., Brugiapaglia, E., Bunting, J., Connor, S., de Beaulieu, J.-L., Edwards, K., Ejarque, A., … Kaplan, J. O. (2013). The European Modern Pollen Database (EMPD) project. Vegetation History and Archaeobotany, 22(6), Article 6. https://doi.org/10.1007/s00334-012-0388-5

Davis, M. B. (1963). On the theory of pollen analysis. American Journal of Science, 261(10), 897–912. https://doi.org/Retrieved from the University of Minnesota Digital Conservancy, https://hdl.handle.net/11299/178665.

Davis, M., Douglas, C., Calcote, R., Cole, K. L., Winkler, M. G., & Flakne, R. (1999). Holocene Climate in the Western Great Lakes National Parks and Lakeshores: Implications for Future Climate Change. Conservation Biology, 14(4), 968–983.

Davis, O. K. (1995). Climate and Vegetation Patterns in Surface Samples from Arid Western U.S.A.: Application to Holocene Climatic Reconstructions. Palynology, 19, 95–117.

Dawson, A., Paciorek, C. J., McLachlan, J. S., Goring, S., Williams, J. W., & Jackson, S. T. (2016). Quantifying pollen-vegetation relationships to reconstruct ancient forests using 19th-century forest composition and pollen data. Quaternary Science Reviews, 137, 156–175. https://doi.org/10.1016/j.quascirev.2016.01.012

de Vernal, A., Eynaud, F., Henry, M., Hillaire-Marcel, C., Londeix, L., Mangin, S., Matthiessen, J., Marret, F., Radi, T., Rochon, A., Solignac, S., & Turon, J.-L. (2005). Reconstruction of sea-surface conditions at middle to high latitudes of the Northern Hemisphere during the Last Glacial Maximum (LGM) based on dinoflagellate cyst assemblages. Quaternary Science Reviews, 24(7), 897–924. https://doi.org/10.1016/j.quascirev.2004.06.014

Dean, J. R., Jones, M. D., Leng, M. J., Noble, S. R., Metcalfe, S. E., Sloane, H. J., Sahy, D., Eastwood, W. J., & Roberts, C. N. (2015). Eastern Mediterranean hydroclimate over the late glacial and Holocene, reconstructed from the sediments of Nar lake, central Turkey, using stable isotopes and carbonate mineralogy. Quaternary Science Reviews, 124, 162–174. https://doi.org/10.1016/j.quascirev.2015.07.023

Degroot, D., Anchukaitis, K., Bauch, M., Burnham, J., Carnegy, F., Cui, J., de Luna, K., Guzowski, P., Hambrecht, G., Huhtamaa, H., Izdebski, A., Kleemann, K., Moesswilde, E., Neupane, N., Newfield, T., Pei, Q., Xoplaki, E., & Zappia, N. (2021). Towards a rigorous understanding of societal responses to climate change. Nature, 591(7851), Article 7851. https://doi.org/10.1038/s41586-021-03190-2

Dobrowski, S. Z., Thorne, J. H., Greenberg, J. A., Safford, H. D., Mynsberge, A. R., Crimmins, S. M., & Swanson, A. K. (2011). Modeling plant ranges over 75 years of climate change in California, USA:

Temporal transferability and species traits. Ecological Monographs, 81(2), 241–257. https://doi.org/10.1890/10-1325.1

Drysdale, R., Zanchetta, G., Hellstrom, J., Maas, R., Fallick, A., Pickett, M., Cartwright, I., & Piccini, L. (2006). Late Holocene drought responsible for the collapse of Old World civilizations is recorded in an Italian cave flowstone. Geology, 34(2), 101–104. https://doi.org/10.1130/G22103.1

Dyakowska, J. (1936). Researches on the rapidity of the falling down of pollen of some trees. Bulletin International de l'Academie Des Sciences de Cracovie, B1, 155–168.

Edwards, M. E., Anderson, P. M., Brubaker, L. B., Ager, T. A., Andreev, A. A., Bigelow, N. H., Cwynar, L. C., Eisner, W. R., Harrison, S. P., Hu, F.-S., Jolly, D., Lozhkin, A. V., MacDonald, G. M., Mock, C. J., Ritchie, J. C., Sher, A. V., Spear, R. W., Williams, J. W., & Yu, G. (2000). Pollen-based biomes for Beringia 18,000, 6000 and 0 14C yr bp. Journal of Biogeography, 27(3), Article 3. https://doi.org/10.1046/j.1365-2699.2000.00426.x

Elenga, H., Peyron, O., Bonnefille, R., Jolly, D., Cheddadi, R., Guiot, J., Andrieu, V., Bottema, S., Buchet, G., Beaulieu, J.-L. D., Hamilton, A. C., Maley, J., Marchant, R., Perez-Obiol, R., Reille, M., Riollet, G., Scott, L., Straka, H., Taylor, D., … Jonson, H. (2000). Pollen-based biome reconstruction for southern Europe and Africa 18,000 yr bp. Journal of Biogeography, 27(3), 621–634. https://doi.org/10.1046/j.1365-2699.2000.00430.x

Filipova-Marinova, M. (2003). Postglacial vegetation dynamics in the coastal part of the Strandza Mountains, southeastern Bulgaria. In S. Tonkov (Ed.), Aspects of palynology and palaeoecology. (pp. 213–231). Pensoft Publishers.

Filipova-Marinova, M. V., Kvavadze, E. V., Connor, S. E., & Sjögren, P. (2010). Estimating absolute pollen productivity for some European Tertiary-relict taxa. Vegetation History and Archaeobotany, 19(4), 351–364. https://doi.org/10.1007/s00334-010-0257-z

Fisher, R. A., Koven, C. D., Anderegg, W. R. L., Christoffersen, B. O., Dietze, M. C., Farrior, C. E., Holm, J. A., Hurtt, G. C., Knox, R. G., Lawrence, P. J., Lichstein, J. W., Longo, M., Matheny, A. M., Medvigy, D., Muller-Landau, H. C., Powell, T. L., Serbin, S. P., Sato, H., Shuman, J. K., … Moorcroft, P. R. (2018). Vegetation demographics in Earth System Models: A review of progress and priorities. Global Change Biology, 24(1), 35–54. https://doi.org/10.1111/gcb.13910

Gaillard, M.-J., Birks, H. J. B., Emanuelsson, U., Karlsson, S., Lagerås, P., & Olausson, D. (1994). Application of modern pollen/land-use relationships to the interpretation of pollen diagrams—Reconstructions of land-use history in south Sweden, 3000-0 BP. Review of Palaeobotany and Palynology, 82(1), Article 1. https://doi.org/10.1016/0034-6667(94)90019-1

Gajewski, K., Vance, R., Sawada, M., Fung, I., Gignac, L. D., Halsey, L., John, J., Maisongrande, P., Mandell, P., Mudie, P. J., Richard, P. J., Sherin, A. G., Soroko, J., & Vitt, D. H. (2000). The climate of North America and adjacent ocean waters ca. 6 ka. Canadian Journal of Earth Sciences, 37(5), 661–681. https://doi.org/10.1139/e99-065

Garreta, V., Miller, P. A., Guiot, J., Hély, C., Brewer, S., Sykes, M. T., & Litt, T. (2010). A method for climate and vegetation reconstruction through the inversion of a dynamic vegetation model. Climate Dynamics, 35(2), 371–389. https://doi.org/10.1007/s00382-009-0629-1

Gavin, D. G., Oswald, W. W., Wahl, E. R., & Williams, J. W. (2003). A statistical approach to evaluating distance metrics and analog assignments for pollen records. Quaternary Research, 60(3), 356–367. https://doi.org/10.1016/S0033-5894(03)00088-7

Githumbi, E., Fyfe, R., Gaillard, M.-J., Trondman, A.-K., Mazier, F., Nielsen, A.-B., Poska, A., Sugita, S., Woodbridge, J., Azuara, J., Feurdean, A., Grindean, R., Lebreton, V., Marquer, L., Nebout-Combourieu, N., Stančikaitė, M., Tanţău, I., Tonkov, S., Shumilovskikh, L., & LandClimII data contributors. (2022). European pollen-based REVEALS land-cover reconstructions for the Holocene: Methodology, mapping and potentials. Earth System Science Data, 14(4), 1581–1619. https://doi.org/10.5194/essd-14-1581-2022

Göktürk, O. M., Fleitmann, D., Badertscher, S., Cheng, H., Edwards, R. L., Leuenberger, M., Fankhauser, A., Tüysüz, O., & Kramers, J. (2011). Climate on the southern Black Sea coast during the Holocene: Implications from the Sofular Cave record. Quaternary Science Reviews, 30(19), 2433–2445. https://doi.org/10.1016/j.quascirev.2011.05.007

Gonzalez, P., Neilson, R. P., Lenihan, J. M., & Drapek, R. J. (2010). Global patterns in the vulnerability of ecosystems to vegetation shifts due to climate change. Global Ecology and Biogeography, 19(6), 755–768. https://doi.org/10.1111/j.1466-8238.2010.00558.x

Gregory, P. H. (1973). The microbiology of the atmosphere (2nd ed). L. Hill.

Grindean, R., Nielsen, A. B., Tanţău, I., & Feurdean, A. (2019). Relative pollen productivity estimates in the forest steppe landscape of southeastern Romania. Review of Palaeobotany and Palynology, 264, 54–63. https://doi.org/10.1016/j.revpalbo.2019.02.007

Groucutt, H. S., Carleton, W. C., Fenech, K., Gauci, R., Grima, R., Scerri, E. M. L., Stewart, M., & Vella, N. C. (2022). The 4.2 ka Event and the End of the Maltese "Temple Period". Frontiers in Earth Science, 9, 771683. https://doi.org/10.3389/feart.2021.771683

Harrison, S. P. (2017). The big data revolution and paleoecology. Past Global Changes Magazine, 25(2), 96–97. https://doi.org/10.22498/pages.25.2.96

Harrison, S. P., Cruz-Silva, E., Haas, O., Liu, M., Parker, S. E., Qiao, S., Shen, Y., & Sweeney, L. (2023). Tools and approaches to addressing the climate-humans nexus during the Holocene. In N. Marchetti, M. Campeggi, F. Cavaliere, C. D'Orazio, G. Giacosa, & E. Mariani (Eds.), Proceedings of the 12th International Congress on the Archaeology of the Ancient Near East. Harrassowitz Verlag. https://doi.org/10.13173/9783447118736

Harrison, S. P., Marinova, E., & Cruz-Silva, E. (2021). EMBSeCBIO pollen database [Data set]. University of Reading. https://doi.org/10.17864/1947.309

Harrison, S. P., Prentice, I. C., Barboni, D., Kohfeld, K. E., Ni, J., & Sutra, J.-P. (2010). Ecophysiological and bioclimatic foundations for a global plant functional classification. Journal of Vegetation Science, 21(2), 300–317. https://doi.org/10.1111/j.1654-1103.2009.01144.x

Harrison, S. P., Prentice, I. C., Bloomfield, K. J., Dong, N., Forkel, M., Forrest, M., Ningthoujam, R. K., Pellegrini, A., Shen, Y., Baudena, M., Cardoso, A. W., Huss, J. C., Joshi, J., Oliveras, I., Pausas, J. G., & Simpson, K. J. (2021). Understanding and modelling wildfire regimes: An ecological perspective. Environmental Research Letters, 16(12), 125008. https://doi.org/10.1088/1748-9326/ac39be

Harrison, S. P., Prentice, I. C., Sutra, J.-P., Barboni, D., Kohfeld, K., & Ni, J. (2009). Towards a global scheme of plant functional types for ecosystem modelling, palaeoecology and climate impact research. Journal of Vegetation Science, 21, 300–317.

Harrison, S. P., Yu, G., Takahara, H., & Prentice, I. C. (2001). Diversity of temperate plants in east Asia. Nature, 413(6852), 129–130. https://doi.org/10.1038/35093166

Haxeltine, A., & Prentice, I. C. (1996). BIOME3: An equilibrium terrestrial biosphere model based on ecophysiological constraints, resource availability, and competition among plant functional types. Global Biogeochemical Cycles, 10(4), 693–709. https://doi.org/10.1029/96GB02344

Hellman, S., Gaillard, M.-J., Broström, A., & Sugita, S. (2008a). Effects of the sampling design and selection of parameter values on pollen-based quantitative reconstructions of regional vegetation: A case study in southern Sweden using the REVEALS model. Vegetation History and Archaeobotany, 17(5), Article 5. https://doi.org/10.1007/s00334-008-0149-7

Hellman, S., Gaillard, M.-J., Broström, A., & Sugita, S. (2008b). The REVEALS model, a new tool to estimate past regional plant abundance from pollen data in large lakes: Validation in southern Sweden. Journal of Quaternary Science, 23(1), Article 1. https://doi.org/10.1002/jqs.1126

Higgins, S. I., Conradi, T., & Muhoko, E. (2023). Shifts in vegetation activity of terrestrial ecosystems attributable to climate trends. Nature Geoscience, 16(2), Article 2. https://doi.org/10.1038/s41561-022-01114-x

Huntley, B. (2012). Reconstructing palaeoclimates from biological proxies: Some often overlooked sources of uncertainty. Quaternary Science Reviews, 31, 1–16. https://doi.org/10.1016/j.quascirev.2011.11.006

Huntley, B., Bartlein, P. J., & Prentice, I. C. (1989). Climatic Control of the Distribution and Abundance of Beech (Fagus L.) in Europe and North America. Journal of Biogeography, 16(6), 551–560. https://doi.org/10.2307/2845210

Huntley, B., & Prentice, I. C. (1988). July Temperatures in Europe from Pollen Data, 6000 Years Before Present. Science, 241(4866), 687–690. https://doi.org/10.1126/science.241.4866.687

Huntley, B., Spicer, R. A., Chaloner, W. G., Jarzembowski, E. A., Allen, J. R. L., Hoskins, B. J., Sellwood, B. W., Spicer, R. A., & Valdes, P. J. (1993). The use of climate response surfaces to

reconstruct palaeoclimate from Quaternary pollen and plant macrofossil data. Philosophical Transactions of the Royal Society of London. Series B: Biological Sciences, 341(1297), 215–224. https://doi.org/10.1098/rstb.1993.0106

Izumi, K., & Bartlein, P. J. (2016). North American paleoclimate reconstructions for the Last Glacial Maximum using an inverse modeling through iterative forward modeling approach applied to pollen data. Geophysical Research Letters, 43(20), 10,965-10,972. https://doi.org/10.1002/2016GL070152

Jackson, S. T., & Overpeck, J. T. (2000). Responses of Plant Populations and Communities to Environmental Changes of the Late Quaternary. Paleobiology, 26(4), 194–220.

Jackson, S. T., & Williams, J. W. (2004). Modern analogs in Quaternary paleoecology: Here today, gone yesterday, gone tomorrow? Annual Review of Earth and Planetary Sciences, 32, 495–537. https://doi.org/10.1146/annurev.earth.32.101802.120435

Janská, V., Jiménez-Alfaro, B., Chytrý, M., Divíšek, J., Anenkhonov, O., Korolyuk, A., Lashchinskyi, N., & Culek, M. (2017). Palaeodistribution modelling of European vegetation types at the Last Glacial Maximum using modern analogues from Siberia: Prospects and limitations. Quaternary Science Reviews, 159, 103–115. https://doi.org/10.1016/j.quascirev.2017.01.011

Janssen, C. R. (1973). Local and regional pollen deposition. In H. J. B. Birks & R. G. West (Eds.), Quaternary Plant Ecology (pp. 31–42). Blackwell. https://scholar.google.com/scholar_lookup?title=Local+and+regional+pollen+deposition&author=Janssen%2C+C.R.&publication_year=1973

Jolly, D., Prentice, I. C., Bonnefille, R., Ballouche, A., Bengo, M., Brenac, P., Buchet, G., Burney, D., Cazet, J.-P., Cheddadi, R., Edorh, T., Elenga, H., Elmoutaki, S., Guiot, J., Laarif, F., Lamb, H., Lezine, A.-M., Maley, J., Mbenza, M., … Waller, M. (1998). Biome reconstruction from pollen and plant macrofossil data for Africa and the Arabian peninsula at 0 and 6000 years. Journal of Biogeography, 25(6), 1007–1027. https://doi.org/10.1046/j.1365-2699.1998.00238.x

Kaniewski, D., & Van Campo, E. (2017). 3.2 ka BP Megadrought and the Late Bronze Age Collapse. In H. Weiss (Ed.), Megadrought and Collapse: From Early Agriculture to Angkor (p. 0). Oxford University Press. https://doi.org/10.1093/oso/9780199329199.003.0005

Kaplan, J. O., Bigelow, N. H., Prentice, I. C., Harrison, S. P., Bartlein, P. J., Christensen, T. R., Cramer, W., Matveyeva, N. V., McGuire, A. D., Murray, D. F., Razzhivin, V. Y., Smith, B., Walker, D. A., Anderson, P. M., Andreev, A. A., Brubaker, L. B., Edwards, M. E., & Lozhkin, A. V. (2003). Climate change and Arctic ecosystems: 2. Modeling, paleodata-model comparisons, and future projections. Journal of Geophysical Research: Atmospheres, 108(D19). https://doi.org/10.1029/2002JD002559

Kintigh, K. W., Altschul, J. H., Beaudry, M. C., Drennan, R. D., Kinzig, A. P., Kohler, T. A., Limp, W. F., Maschner, H. D. G., Michener, W. K., Pauketat, T. R., Peregrine, P., Sabloff, J. A., Wilkinson, T. J.,

Wright, H. T., & Zeder, M. A. (2014). Grand Challenges for Archaeology. American Antiquity, 79(1), 5–24. https://doi.org/10.7183/0002-7316.79.1.5

Kubat, M. (2021). An Introduction to Machine Learning. Springer Nature.

Kucera, M., Weinelt, M., Kiefer, T., Pflaumann, U., Hayes, A., Weinelt, M., Chen, M.-T., Mix, A. C., Barrows, T. T., Cortijo, E., Duprat, J., Juggins, S., & Waelbroeck, C. (2005). Reconstruction of sea-surface temperatures from assemblages of planktonic foraminifera: Multi-technique approach based on geographically constrained calibration data sets and its application to glacial Atlantic and Pacific Oceans. Quaternary Science Reviews, 24(7), 951–998. https://doi.org/10.1016/j.quascirev.2004.07.014

Ladd, M., Viau, A., Way, R., Gajewski, K., & Sawada, M. (2018). Variations in precipitation in North America during the past 2000 years. The Holocene, 28(4), 667–675. https://doi.org/10.1177/0959683617735583

Lenoir, J., Gégout, J. C., Marquet, P. A., de Ruffray, P., & Brisse, H. (2008). A Significant Upward Shift in Plant Species Optimum Elevation During the 20th Century. Science, 320(5884), 1768–1771. https://doi.org/10.1126/science.1156831

Leroy, S., Marret, F., Giralt, S., & Bulatov, S. A. (2006). Natural and anthropogenic rapid changes in the Kara-Bogaz Gol over the last two centuries by palynological analyses. Quaternary International, 55. https://www.academia.edu/210872/Leroy_S_A_G_Marret_F_Giralt_S_and_Bulatov_S_A_2006_Natural_and_anthropogenic_rapid_changes_in_the_Kara_Bogaz_Gol_over_the_last_two_centuries_by_palynological_analyses

Lespez, L., Glais, A., Lopez-Saez, J.-A., Drezen, Y. L., Tsirtsoni, Z., Davidson, R., Biree, L., & Malamidou, D. (2016). Middle Holocene rapid environmental changes and human adaptation in Greece. Quaternary Research, 85(2), 227–244. https://doi.org/10.1016/j.yqres.2016.02.002

Li, F., Gaillard, M.-J., Cao, X., Herzschuh, U., Sugita, S., Ni, J., Zhao, Y., An, C., Huang, X., Li, Y., Liu, H., Sun, A., & Yao, Y. (2023). Gridded pollen-based Holocene regional plant cover in temperate and northern subtropical China suitable for climate modelling. Earth System Science Data, 15(1), 95–112. https://doi.org/10.5194/essd-15-95-2023

Li, F., Gaillard, M.-J., Cao, X., Herzschuh, U., Sugita, S., Tarasov, P. E., Wagner, M., Xu, Q., Ni, J., Wang, W., Zhao, Y., An, C., Beusen, A. H. W., Chen, F., Feng, Z., Goldewijk, C. G. M. K., Huang, X., Li, Y., Li, Y., … Jia, X. (2020). Towards quantification of Holocene anthropogenic land-cover change in temperate China: A review in the light of pollen-based REVEALS reconstructions of regional plant cover. Earth-Science Reviews, 203, 103119. https://doi.org/10.1016/j.earscirev.2020.103119

Li, Y., Bunting, M. J., Xu, Q., Jiang, S., Ding, W., & Hun, L. (2011). Pollen–vegetation–climate relationships in some desert and desert-steppe communities in northern China. The Holocene, 21(6), 997–1010. https://doi.org/10.1177/0959683611400202

Liu, M., Prentice, I. C., ter Braak, C. J. F., & Harrison, S. P. (2020). An improved statistical approach for reconstructing past climates from biotic assemblages. Proceedings of the Royal Society A: Mathematical, Physical and Engineering Sciences, 476(2243), 20200346. https://doi.org/10.1098/rspa.2020.0346

Liu, M., Shen, Y., González-Sampériz, P., Gil-Romera, G., ter Braak, C. J. F., Prentice, I. C., & Harrison, S. P. (2023). Holocene climates of the Iberian Peninsula: Pollen-based reconstructions of changes in the west–east gradient of temperature and moisture. Climate of the Past, 19(4), 803–834. https://doi.org/10.5194/cp-19-803-2023

Liu, S., Li, K., Jia, W., Stoof-Leichsenring, K. R., Liu, X., Cao, X., & Herzschuh, U. (2021). Vegetation Reconstruction From Siberia and the Tibetan Plateau Using Modern Analogue Technique–Comparing Sedimentary (Ancient) DNA and Pollen Data. Frontiers in Ecology and Evolution, 9. https://www.frontiersin.org/articles/10.3389/fevo.2021.668611

Livingstone, D. A. (1968). Some Interstadial and Postglacial Pollen Diagrams from Eastern Canada. Ecological Monographs, 38(2), 87–125. https://doi.org/10.2307/1942289

Lytle, D. E., & Wahl, E. R. (2005). Palaeoenvironmental reconstructions using the modern analogue technique: The effects of sample size and decision rules. The Holocene, 15(4), 554–566. https://doi.org/10.1191/0959683605hl830rp

Mackenzie, G., Boa, A. N., Diego-Taboada, A., Atkin, S. L., & Sathyapalan, T. (2015). Sporopollenin, The Least Known Yet Toughest Natural Biopolymer. Frontiers in Materials, 2. https://www.frontiersin.org/articles/10.3389/fmats.2015.00066

Malmgren, B. A., Kucera, M., Nyberg, J., & Waelbroeck, C. (2001). Comparison of statistical and artificial neural network techniques for estimating past sea surface temperatures from planktonic foraminifer census data. Paleoceanography, 16(5), 520–530. https://doi.org/10.1029/2000PA000562

Marchant, R., Behling, H., Berrio, J. C., Cleef, A., Duivenvoorden, J., Hooghiemstra, H., Kuhry, P., Melief, B., Geel, B. V., Hammen, T. V. der, Reenen, G. V., & Wille, M. (2001). Mid- to Late-Holocene pollen-based biome reconstructions for Colombia. Quaternary Science Reviews, 20(12), Article 12. https://doi.org/10.1016/S0277-3791(00)00182-7

Marchant, R., Cleef, A., Harrison, S. P., Hooghiemstra, H., Markgraf, V., van Boxel, J., Ager, T., Almeida, L., Anderson, R., Baied, C., Behling, H., Berrio, J. C., Burbridge, R., Björck, S., Byrne, R., Bush, M., Duivenvoorden, J., Flenley, J., De Oliveira, P., … Wille, M. (2009). Pollen-based biome reconstructions for Latin America at 0, 6000 and 18 000 radiocarbon years ago. Climate of the Past, 5, 725–767. https://doi.org/10.5194/cp-5-725-2009

Marinova, E., Harrison, S. P., Bragg, F., Connor, S., Laet, V. de, Leroy, S. A. G., Mudie, P., Atanassova, J., Bozilova, E., Caner, H., Cordova, C., Djamali, M., Filipova-Marinova, M., Gerasimenko, N., Jahns, S., Kouli, K., Kotthoff, U., Kvavadze, E., Lazarova, M., … Tonkov, S. (2018). Pollen-derived biomes in the Eastern Mediterranean–Black Sea–Caspian-Corridor. Journal of Biogeography, 45(2), 484–499. https://doi.org/10.1111/jbi.13128

Marriner, N., Kaniewski, D., Pourkerman, M., & Devillers, B. (2022). Anthropocene tipping point reverses long-term Holocene cooling of the Mediterranean Sea: A meta-analysis of the basin's Sea Surface Temperature records. Earth-Science Reviews, 227, 103986. https://doi.org/10.1016/j.earscirev.2022.103986

Marsicek, J., Shuman, B. N., Bartlein, P. J., Shafer, S. L., & Brewer, S. (2018). Reconciling divergent trends and millennial variations in Holocene temperatures. Nature, 554(7690), Article 7690. https://doi.org/10.1038/nature25464

Mauri, A., Davis, B. A. S., Collins, P. M., & Kaplan, J. O. (2015). The climate of Europe during the Holocene: A gridded pollen-based reconstruction and its multi-proxy evaluation. Quaternary Science Reviews, 112, 109–127. https://doi.org/10.1016/j.quascirev.2015.01.013

Mazier, F., Broström, A., Gaillard, M.-J., Sugita, S., Vittoz, P., & Buttler, A. (2008). Pollen productivity estimates and relevant source area of pollen for selected plant taxa in a pasture woodland landscape of the Jura Mountains (Switzerland). Vegetation History and Archaeobotany, 17(5), 479–495. https://doi.org/10.1007/s00334-008-0143-0

Mazier, F., Gaillard, M.-J., Kuneš, P., Sugita, S., Trondman, A.-K., & Broström, A. (2012). Testing the effect of site selection and parameter setting on REVEALS-model estimates of plant abundance using the Czech Quaternary Palynological Database. Review of Palaeobotany and Palynology, 187, 38–49. https://doi.org/10.1016/j.revpalbo.2012.07.017

McMahon, A. (2006). Nippur V. The early dynastic to Akkadian transition: the area WF sounding at Nippur. Oriental Institute of the University of Chicago.

Messager, E., Nomade, S., Wilhelm, B., Joannin, S., Scao, V., Grafenstein, U. von, Martkoplishvili, I., Ollivier, V., Mgeladze, A., Dumoulin, J., Mazuy, A., Belmecheri, S., & Lordkipanidze, D. (2017). New pollen evidence from Nariani (Georgia) for delayed postglacial forest expansion in the South Caucasus. Quaternary Research, 87(1), 121–132. https://doi.org/10.1017/qua.2016.3

Michalet, R., Brooker, R. W., Cavieres, L. A., Kikvidze, Z., Lortie, C. J., Pugnaire, F. I., Valiente-Banuet, A., & Callaway, R. M. (2006). Do biotic interactions shape both sides of the humped-back model of species richness in plant communities? Ecology Letters, 9(7), 767–773. https://doi.org/10.1111/j.1461-0248.2006.00935.x

Middleton, G. D. (2018). Bang or whimper? Science, 361(6408), 1204–1205. https://doi.org/10.1126/science.aau8834

Ön, Z. B., Greaves, A. M., Akçer-Ön, S., & Özeren, M. S. (2021). A Bayesian test for the 4.2 ka BP abrupt climatic change event in southeast Europe and southwest Asia using structural time series analysis of paleoclimate data. Climatic Change, 165(1), 7. https://doi.org/10.1007/s10584-021-03010-6

Oswald, W. W., Brubaker, L. B., Hu, F. S., & Gavin, D. G. (2003). Pollen-vegetation calibration for tundra communities in the Arctic Foothills, northern Alaska. Journal of Ecology, 91(6), 1022–1033. https://doi.org/10.1046/j.1365-2745.2003.00823.x

Overpeck, J. T., Webb, R. S., & Webb, T., III. (1992). Mapping eastern North American vegetation change of the past 18 ka: No-analogs and the future. Geology, 20(12), 1071–1074. https://doi.org/10.1130/0091-7613(1992)020<1071:MENAVC>2.3.CO;2

Overpeck, J. T., Webb, T., & Prentice, I. C. (1985). Quantitative interpretation of fossil pollen spectra: Dissimilarity coefficients and the method of modern analogs. Quaternary Research, 23(01), Article 01. https://doi.org/10.1016/0033-5894(85)90074-2

Parker, S. E., & Harrison, S. P. (2022). The timing, duration and magnitude of the 8.2 ka event in global speleothem records. Scientific Reports, 12(1), Article 1. https://doi.org/10.1038/s41598-022-14684-y

Parker, S. E., Harrison, S. P., Comas-Bru, L., Kaushal, N., LeGrande, A. N., & Werner, M. (2021). A data–model approach to interpreting speleothem oxygen isotope records from monsoon regions. Climate of the Past, 17(3), 1119–1138. https://doi.org/10.5194/cp-17-1119-2021

Pausas, J. G., & Bond, W. J. (2021). Alternative biome states challenge the modelling of species' niche shifts under climate change. Journal of Ecology, 109(12), 3962–3971. https://doi.org/10.1111/1365-2745.13781

Peyron, O., Guiot, J., Cheddadi, R., Tarasov, P., Reille, M., Beaulieu, J.-L. de, Bottema, S., & Andrieu, V. (1998). Climatic reconstruction in Europe for 18,000 YR B.P. from pollen data. Quaternary Research, 49(2), 183–196. https://doi.org/10.1006/qres.1997.1961

Peyron, O., & Vernal, A. de. (2001). Application of artificial neural networks (ANN) to high-latitude dinocyst assemblages for the reconstruction of past sea-surface conditions in Arctic and sub-Arctic seas. Journal of Quaternary Science, 16(7), 699–709. https://doi.org/10.1002/jqs.651

Pickett, E. J., Harrison, S. P., Hope, G., Harle, K., Dodson, J. R., Peter Kershaw, A., Prentice, I. C., Backhouse, J., Colhoun, E. A., D'Costa, D., Flenley, J., Grindrod, J., Haberle, S., Hassell, C., Kenyon, C., Macphail, M., Martin, H., Martin, A. H., McKenzie, M., … Ward, J. (2004). Pollen-based reconstructions of biome distributions for Australia, Southeast Asia and the Pacific (SEAPAC region) at 0, 6000 and 18,000 14C yr BP. Journal of Biogeography, 31(9), Article 9. https://doi.org/10.1111/j.1365-2699.2004.01001.x

Power, M. J., Marlon, J., Ortiz, N., Bartlein, P. J., Harrison, S. P., Mayle, F. E., Ballouche, A., Bradshaw, R. H. W., Carcaillet, C., Cordova, C., Mooney, S., Moreno, P. I., Prentice, I. C., Thonicke, K., Tinner, W.,

Whitlock, C., Zhang, Y., Zhao, Y., Ali, A. A., … Zhang, J. H. (2008). Changes in fire regimes since the Last Glacial Maximum: An assessment based on a global synthesis and analysis of charcoal data. Climate Dynamics, 30(7), 887–907. https://doi.org/10.1007/s00382-007-0334-x

Prentice, I. C. (1980). Multidimensional scaling as a research tool in quaternary palynology: A review of theory and methods. Review of Palaeobotany and Palynology, 31, 71–104. https://doi.org/10.1016/0034-6667(80)90023-8

Prentice, I. C. (1983). Pollen mapping of regional forest patterns in south and central Sweden. Journal of Biogeography, 10, 441–454.

Prentice, I. C. (1985). Pollen representation, source area, and basin size: Toward a unified theory of pollen analysis. Quaternary Research, 23(1), 76–86. https://doi.org/10.1016/0033-5894(85)90073-0

Prentice, I. C. (1988). Records of vegetation in time and space: The principles of pollen analysis. In B. Huntley & T. Webb (Eds.), Vegetation history (pp. 17–42). Springer Netherlands. https://doi.org/10.1007/978-94-009-3081-0_2

Prentice, I. C., Bartlein, P. J., & Webb, T. (1991). Vegetation and Climate Change in Eastern North America Since the Last Glacial Maximum. Ecology, 72(6), 2038–2056. https://doi.org/10.2307/1941558

Prentice, I. C., Cramer, W., Harrison, S. P., Leemans, R., Monserud, R. A., & Solomon, A. M. (1992). Special Paper: A Global Biome Model Based on Plant Physiology and Dominance, Soil Properties and Climate. Journal of Biogeography, 19(2), Article 2. https://doi.org/10.2307/2845499

Prentice, I. C., Guiot, J., Huntley, B., Jolly, D., & Cheddadi, R. (1996). Reconstructing biomes from palaeoecological data: A general method and its application to European pollen data at 0 and 6 ka. Climate Dynamics, 12, 185–194. https://doi.org/10.1007/BF00211617

Prentice, I. C., Jolly, D., & BIOME 6000 Participants. (2000). Mid-Holocene and glacial-maximum vegetation geography of the northern continents and Africa. Journal of Biogeography, 27(3), Article 3. https://doi.org/10.1046/j.1365-2699.2000.00425.x

Prentice, I. C., Villegas-Diaz, R., & Harrison, S. P. (2022). Accounting for atmospheric carbon dioxide variations in pollen-based reconstruction of past hydroclimates. Global and Planetary Change, 211, 103790. https://doi.org/10.1016/j.gloplacha.2022.103790

Prentice, I. C., & Webb, T. (1998). BIOME 6000: Reconstructing global mid-Holocene vegetation patterns from palaeoecological records. Journal of Biogeography, 25(6), Article 6.

Rascovan, N., Sjögren, K.-G., Kristiansen, K., Nielsen, R., Willerslev, E., Desnues, C., & Rasmussen, S. (2019). Emergence and Spread of Basal Lineages of Yersinia pestis during the Neolithic Decline. Cell, 176(1), 295-305.e10. https://doi.org/10.1016/j.cell.2018.11.005

Reimer, P., Austin, W. E. N., Bard, E., Bayliss, A., Blackwell, P. G., Ramsey, C. B., Butzin, M., Cheng, H., Edwards, R. L., Friedrich, M., Grootes, P. M., Guilderson, T. P., Hajdas, I., Heaton, T. J., Hogg, A.

G., Hughen, K. A., Kromer, B., Manning, S. W., Muscheler, R., … Talamo, S. (2020). The IntCal20 Northern Hemisphere radiocarbon age calibration curve (0-55 cal kBP). Radiocarbon, 62(4). https://doi.org/10.1017/RDC.2020.41

Riehl, S., Pustovoytov, K. E., Weippert, H., Klett, S., & Hole, F. (2014). Drought stress variability in ancient Near Eastern agricultural systems evidenced by δ13C in barley grain. Proceedings of the National Academy of Sciences, 111(34), 12348–12353. https://doi.org/10.1073/pnas.1409516111

Roberts, N., Brayshaw, D., Kuzucuoğlu, C., Perez, R., & Sadori, L. (2011). The mid-Holocene climatic transition in the Mediterranean: Causes and consequences. The Holocene, 21(1), 3–13. https://doi.org/10.1177/0959683610388058

Sadori, L., Jahns, S., & Peyron, O. (2011). Mid-Holocene vegetation history of the central Mediterranean. The Holocene, 21(1), Article 1. https://doi.org/10.1177/0959683610377530

Sallaberger, W. (2007). From Urban Culture to Nomadism: A History of Upper Mesopotamia in the Late Third Millennium. Publications de l'Institut Français d'Études Anatoliennes, 19(1), 417–456.

Salonen, J. S., Ilvonen, L., Seppä, H., Holmström, L., Telford, R. J., Gaidamavičius, A., Stančikaitė, M., & Subetto, D. (2012). Comparing different calibration methods (WA/WA-PLS regression and Bayesian modelling) and different-sized calibration sets in pollen-based quantitative climate reconstruction. The Holocene, 22(4), 413–424. https://doi.org/10.1177/0959683611425548

Salonen, J. S., Korpela, M., Williams, J. W., & Luoto, M. (2019). Machine-learning based reconstructions of primary and secondary climate variables from North American and European fossil pollen data. Scientific Reports, 9(1), Article 1. https://doi.org/10.1038/s41598-019-52293-4

Sawada, M., Viau, A. E., Vettoretti, G., Peltier, W. R., & Gajewski, K. (2004). Comparison of North-American pollen-based temperature and global lake-status with CCCma AGCM2 output at 6ka. Quaternary Science Reviews, 23(3), 225–244. https://doi.org/10.1016/j.quascirev.2003.08.005

Schimper, A. F. W., Fisher, W. R., Groom, P., & Balfour, I. B. (1903). Plant-geography upon a physiological basis (Rev. and ed., pp. 1–1024). Clarendon Press. https://doi.org/10.5962/bhl.title.8099

Seppä, H., Birks, H. J. B., Odland, A., Poska, A., & Veski, S. (2004). A modern pollen–climate calibration set from northern Europe: Developing and testing a tool for palaeoclimatological reconstructions. Journal of Biogeography, 31(2), 251–267. https://doi.org/10.1111/j.1365-2699.2004.00923.x

Serge, M. A., Mazier, F., Fyfe, R., Gaillard, M.-J., Klein, T., Lagnoux, A., Galop, D., Githumbi, E., Mindrescu, M., Nielsen, A. B., Trondman, A.-K., Poska, A., Sugita, S., Woodbridge, J., Abel-Schaad, D., Åkesson, C., Alenius, T., Ammann, B., Andersen, S. T., … Zernitskaya, V. P. (2023). Testing the Effect of Relative Pollen Productivity on the REVEALS Model: A Validated Reconstruction of Europe-Wide Holocene Vegetation. Land, 12(5), Article 5. https://doi.org/10.3390/land12050986

Shen, C., Liu, K., Tang, L., & Overpeck, J. T. (2006). Quantitative relationships between modern pollen rain and climate in the Tibetan Plateau. Review of Palaeobotany and Palynology, 140(1), 61–77. https://doi.org/10.1016/j.revpalbo.2006.03.001

Simpson, G. L. (2012). Analogue Methods in Palaeolimnology. In H. J. B. Birks, A. F. Lotter, S. Juggins, & J. P. Smol (Eds.), Tracking Environmental Change Using Lake Sediments: Data Handling and Numerical Techniques (pp. 495–522). Springer Netherlands. https://doi.org/10.1007/978-94-007-2745-8_15

Sinha, A., Kathayat, G., Weiss, H., Li, H., Cheng, H., Reuter, J., Schneider, A. W., Berkelhammer, M., Adalı, S. F., Stott, L. D., & Edwards, R. L. (2019). Role of climate in the rise and fall of the Neo-Assyrian Empire. Science Advances, 5(11), eaax6656. https://doi.org/10.1126/sciadv.aax6656

Soepboer, W., Sugita, S., & Lotter, A. F. (2010). Regional vegetation-cover changes on the Swiss Plateau during the past two millennia: A pollen-based reconstruction using the REVEALS model. Quaternary Science Reviews, 29(3), 472–483. https://doi.org/10.1016/j.quascirev.2009.09.027

Sołtysiak, A., & Fernandes, R. (2021). Much ado about nothing: Assessing the impact of the 4.2 kya event on human subsistence patterns in northern Mesopotamia using stable isotope analysis. Antiquity, 95(383), 1145–1160. https://doi.org/10.15184/aqy.2021.117

Sugita, S. (1993). A model of pollen source area for an entire lake surface. Quaternary Research, 39(2), Article 2. https://doi.org/10.1006/qres.1993.1027

Sugita, S. (2007a). Theory of quantitative reconstruction of vegetation I: Pollen from large sites REVEALS regional vegetation composition. The Holocene, 17(2), Article 2. https://doi.org/10.1177/0959683607075837

Sugita, S. (2007b). Theory of quantitative reconstruction of vegetation II: all you need is LOVE. The Holocene, 17(2), Article 2. https://doi.org/10.1177/0959683607075838

Sugita, S., Gaillard, M.-J., Hellman, S., & Broström, A. (2007). Model-based reconstruction of vegetation and landscape using fossil pollen. In A. Posluschny, K. Lambers, & I. Herzog (Eds.), Proceedings of the 35th International Conference on Computer Applications and Quantitative Methods in Archaeology (CAA) (p. 428). Kolloquien zur Vor- und Frühgeschichte.

Sugita, S., Parshall, T., Calcote, R., & Walker, K. (2010). Testing the Landscape Reconstruction Algorithm for spatially explicit reconstruction of vegetation in northern Michigan and Wisconsin. Quaternary Research, 74(2), 289–300. https://doi.org/10.1016/j.yqres.2010.07.008

Takahara, H., & Takeoka, M. (1992). Vegetation history since the last glacial period in the Mikata lowland, the Sea of Japan area, western Japan. Ecological Research, 7(3), 371–386. https://doi.org/10.1007/BF02347104

Tarasov, P. E., Andreev, A. A., Anderson, P. M., Lozhkin, A. V., Leipe, C., Haltia, E., Nowaczyk, N. R., Wennrich, V., Brigham-Grette, J., & Melles, M. (2013). A pollen-based biome reconstruction over

the last 3.562 million years in the Far East Russian Arctic—New insights into climate-vegetation relationships at the regional scale. Climate of the Past, 9(6), Article 6. https://doi.org/10.5194/cp-9-2759-2013

Tarasov, P. E., Volkova, V. S., Webb III, T., Guiot, J., Andreev, A. A., Bezusko, L. G., Bezusko, T. V., Bykova, G. V., Dorofeyuk, N. I., Kvavadze, E. V., Osipova, I. M., Panova, N. K., & Sevastyanov, D. V. (2000). Last glacial maximum biomes reconstructed from pollen and plant macrofossil data from northern Eurasia. Journal of Biogeography, 27(3), 609–620. https://doi.org/10.1046/j.1365-2699.2000.00429.x

Tarasov, P. E., Webb III, T., Andreev, A. A., Afanas'eva, N. B., Berezina, N. A., Bezusko, L. G., Blyakharchuk, T. A., Bolikhovskaya, N. S., Cheddadi, R., Chernavskaya, M. M., Chernova, G. M., Dorofeyuk, N. I., Dirksen, V. G., Elina, G. A., Filimonova, L. V., Glebov, F. Z., Guiot, J., Gunova, V. S., Harrison, S. P., … Zernitskaya, V. P. (1998). Present-day and mid-Holocene biomes reconstructed from pollen and plant macrofossil data from the former Soviet Union and Mongolia. Journal of Biogeography, 25(6), 1029–1053. https://doi.org/10.1046/j.1365-2699.1998.00236.x

Tauber, H. (1965). Differential pollen dispersion and the interpretation of pollen diagrams. With a contribution to the interpretation of the elm fall. Danmarks Geologiske Undersøgelse II. Række, 89, 1–69. https://doi.org/10.34194/raekke2.v89.6880

ter Braak, C. J. F., & Juggins, S. (1993). Weighted averaging partial least squares regression (WA-PLS): An improved method for reconstructing environmental variables from species assemblages. Hydrobiologia, 269(1), 485–502. https://doi.org/10.1007/BF00028046

Theuerkauf, M., & Couwenberg, J. (2018). ROPES reveals past land cover and PPEs from single pollen records. Frontiers in Earth Science, 6. https://doi.org/10.3389/feart.2018.00014

Theuerkauf, M., & Couwenberg, J. (2022). Pollen productivity estimates strongly depend on assumed pollen dispersal II: Extending the ERV model. The Holocene, 32(11), 1233–1250. https://doi.org/10.1177/09596836211041729

Thompson, R. S., & Anderson, K. H. (2000). Biomes of western North America at 18,000, 6000 and 0 14C yr bp reconstructed from pollen and packrat midden data. Journal of Biogeography, 27(3), Article 3. https://doi.org/10.1046/j.1365-2699.2000.00427.x

Trondman, A.-K., Gaillard, M.-J., Mazier, F., Sugita, S., Fyfe, R., Nielsen, A. B., Twiddle, C., Barratt, P., Birks, H. J. B., Bjune, A. E., Björkman, L., Broström, A., Caseldine, C., David, R., Dodson, J., Dörfler, W., Fischer, E., van Geel, B., Giesecke, T., … Wick, L. (2015). Pollen-based quantitative reconstructions of Holocene regional vegetation cover (plant-functional types and land-cover types) in Europe suitable for climate modelling. Global Change Biology, 21(2), 676–697. https://doi.org/10.1111/gcb.12737

Tsirtsoni, Z. (2014). Formation or transformation? The 4th millennium BC in the Aegean and the Balkans. In B. Horejs & M. Mehofer (Eds.), Western Anatolia before Troy. Proto-Urbanisation in the 4th Millennium BC?: Proceedings of the International Symposium held at the Kunsthistorisces Museum Wien (pp. 275–304). Austrian Academy of Sciences Press.

Turner, J., & Greig, J. R. A. (1975). Some Holocene pollen diagrams from Greece. Review of Palaeobotany and Palynology, 20(3), Article 3. https://doi.org/10.1016/0034-6667(75)90020-2

Valiente-Banuet, A., Rumebe, A. V., Verdú, M., & Callaway, R. M. (2006). Modern Quaternary plant lineages promote diversity through facilitation of ancient Tertiary lineages. Proceedings of the National Academy of Sciences, 103(45), 16812–16817. https://doi.org/10.1073/pnas.0604933103

van Zeist, W., & Bottema, S. (1977). Palynological investigations in Western Iran. Palaeohistoria, 19, Article 19.

van Zeist, W., & Bottema, S. (1991). Late Quaternary Vegetation of the Near East. Dr Ludwig Reichert Verlag.

van Zeist, W., Timmers, R. W., & Bottema, S. (1970). Studies of Modern and Holocene Pollen Precipitation in Southeastern Turkey. Palaeohistoria, 19–39.

van Zeist, W., & Woldring, H. (1980). Holocene vegetation and climate of Northwestern Syria. Palaeohistoria, 111–125.

van Zeist, W., Woldring, H., & Stapert, D. (1975). Late Quaternary vegetation and climate of southwestern Turkey. Palaeohistoria, 17, Article 17.

Verdú, M., Gómez, J. M., Valiente-Banuet, A., & Schöb, C. (2021). Facilitation and plant phenotypic evolution. Trends in Plant Science, 26(9), 913–923. https://doi.org/10.1016/j.tplants.2021.04.005

Vermoere, M., Vanhecke, L., Waelkens, M., & Smets, E. (2001). Modern pollen studies in the territory of Sagalassos (Southwest Turkey) and their use in the interpretation of a Late Holocene pollen diagram. Review of Palaeobotany and Palynology, 114(1–2), 29–52. https://doi.org/10.1016/s0034-6667(00)00072-5

Viau, A. E., & Gajewski, K. (2009). Reconstructing Millennial-Scale, Regional Paleoclimates of Boreal Canada during the Holocene. Journal of Climate, 22(2), 316–330.

Villegas-Diaz, R., Cruz-Silva, E., & Harrison, S. P. (2021). ageR: Supervised Age Models [R]. Zenodo. https://doi.org/10.5281/zenodo.4636716

Walter, H. (1973). Vegetation of the earth in relation to climate and the eco-physiological conditions / translated [from the 2nd German ed.] by Joy Wieser. English Universities Press.

Walther, G.-R., Berger, S., & Sykes, M. T. (2005). An ecological 'footprint' of climate change. Proceedings of the Royal Society B: Biological Sciences, 272(1571), 1427–1432. https://doi.org/10.1098/rspb.2005.3119

Wanner, H. (2021). Late-Holocene: Cooler or warmer? The Holocene, 31(9), 1501–1506. https://doi.org/10.1177/09596836211019106

Wanner, H., Beer, J., Bütikofer, J., Crowley, T. J., Cubasch, U., Flückiger, J., Goosse, H., Grosjean, M., Joos, F., Kaplan, J. O., Küttel, M., Müller, S. A., Prentice, I. C., Solomina, O., Stocker, T. F., Tarasov, P., Wagner, M., & Widmann, M. (2008). Mid- to Late Holocene climate change: An overview. Quaternary Science Reviews, 27(19), 1791–1828. https://doi.org/10.1016/j.quascirev.2008.06.013

Warner, B., & Misra, M. (1996). Understanding Neural Networks as Statistical Tools. The American Statistician, 50(4), 284–293. https://doi.org/10.1080/00031305.1996.10473554

Webb, T. (1974). Corresponding Patterns of Pollen and Vegetation in Lower Michigan: A Comparison of Quantitative Data. Ecology, 55(1), 17–28. https://doi.org/10.2307/1934614

Wei, D., Prentice, I. C., & Harrison, S. P. (2020). The climatic space of European pollen taxa. Ecology, 101(8), Article 8. https://doi.org/10.1002/ecy.3055

Weiss, H. (2012). Quantifying Collapse: The Late Third Millennium Khabur Plains. In Seven Generations since the Fall of Akkad. (Vol. 3, pp. vii–24). Harrassowitz Verlag. https://www.academia.edu/2465773/Quantifying_Collapse_The_Late_Third_Millennium_Khabur_Plains

Weiss, H. (2017). 4.2 ka BP Megadrought and the Akkadian Collapse. In H. Weiss (Ed.), Megadrought and Collapse: From Early Agriculture to Angkor (p. 0). Oxford University Press. https://doi.org/10.1093/oso/9780199329199.003.0004

Weiss, H., Courty, M.-A., Wetterstrom, W., Guichard, F., Senior, L., Meadow, R., & Curnow, A. (1993). The Genesis and Collapse of Third Millennium North Mesopotamian Civilization. Science, 261(5124), 995–1004. https://doi.org/10.1126/science.261.5124.995

Whittaker, R. H. (1970). Communities and ecosystems. Communities and Ecosystems. https://www.cabdirect.org/cabdirect/abstract/19740615709

Wick, L., Lemcke, G., & Sturm, M. (2003). Evidence of Lateglacial and Holocene climatic change and human impact in eastern Anatolia: High-resolution pollen, charcoal, isotopic and geochemical records from the laminated sediments of Lake Van, Turkey. The Holocene, 13(5), Article 5. https://doi.org/10.1191/0959683603hl653rp

Wieczorek, M., & Herzschuh, U. (2020). Compilation of relative pollen productivity (RPP) estimates and taxonomically harmonised RPP datasets for single continents and Northern Hemisphere extratropics. Earth System Science Data, 12(4), 3515–3528. https://doi.org/10.5194/essd-12-3515-2020

Williams, J. W., & Shuman, B. (2008). Obtaining accurate and precise environmental reconstructions from the modern analog technique and North American surface pollen dataset. Quaternary Science Reviews, 27(7), 669–687. https://doi.org/10.1016/j.quascirev.2008.01.004

Williams, J. W., Summers, R. L., & Webb III, T. (1998). Applying plant functional types to construct biome maps from eastern North American pollen data: Comparisons with model results. Quaternary Science Reviews, 17(6), Article 6. https://doi.org/10.1016/S0277-3791(98)00014-6

Williams, J. W., Webb, T., Richard, P. H., & Newby, P. (2000). Late Quaternary biomes of Canada and the eastern United States. Journal of Biogeography, 27(3), Article 3. https://doi.org/10.1046/j.1365-2699.2000.00428.x

Wilson, R. J., Gutiérrez, D., Gutiérrez, J., Martínez, D., Agudo, R., & Monserrat, V. J. (2005). Changes to the elevational limits and extent of species ranges associated with climate change. Ecology Letters, 8(11), 1138–1146. https://doi.org/10.1111/j.1461-0248.2005.00824.x

Wold, H. O. A. (1966). Nonlinear estimation by iterative least squares procedures. In F. N. David (Ed.), Research Papers in Statistics (pp. 411–444). Wiley.

Wold, S., Sjöström, M., & Eriksson, L. (2001). PLS-regression: A basic tool of chemometrics. Chemometrics and Intelligent Laboratory Systems, 58(2), 109–130. https://doi.org/10.1016/S0169-7439(01)00155-1

Woodward, F. I., Lomas, M. R., & Kelly, C. K. (2004). Global climate and the distribution of plant biomes. Philosophical Transactions of the Royal Society of London. Series B: Biological Sciences, 359(1450), 1465–1476. https://doi.org/10.1098/rstb.2004.1525

Woodward, F. I., & Williams, B. G. (1987). Climate and plant distribution at global and local scales. Vegetatio, 69(1), 189–197. https://doi.org/10.1007/BF00038700

Wossink, A. (2009). Challenging climate change. Competition and cooperation among pastoralists and agriculturalists in northern Mesopotamia (c. 3000-1600 BC). Sidestone press. https://www.sidestone.com/books/challenging-climate-change

Wu, H., Guiot, J., Brewer, S., & Guo, Z. (2007). Climatic changes in Eurasia and Africa at the last glacial maximum and mid-Holocene: Reconstruction from pollen data using inverse vegetation modelling. Climate Dynamics, 29(2), 211–229. https://doi.org/10.1007/s00382-007-0231-3

Yu. (1998). Pollen-based biome reconstructions for China at 0 and 6000 years. Journal of Biogeography. https://onlinelibrary.wiley.com/doi/abs/10.1046/j.1365-2699.1998.00237.x

Yu, G., Chen, X., Ni, J., Cheddadi, R., Guiot, J., Han, H., Harrison, S. P., Huang, C., Ke, M., Kong, Z., Li, S., Li, W., Liew, P., Liu, G., Liu, J., Liu, Q., Liu, K.-B., Prentice, I. C., Qui, W., … Zheng, Z. (2000). Palaeovegetation of China: A pollen data-based synthesis for the mid-Holocene and last glacial maximum. Journal of Biogeography, 27(3), Article 3. https://doi.org/10.1046/j.1365-2699.2000.00431.x

Zanon, M., Davis, B. A. S., Marquer, L., Brewer, S., & Kaplan, J. O. (2018). European forest cover during the past 12,000 years: A palynological reconstruction based on modern analogs and remote sensing. Frontiers in Plant Science, 9, 253. https://doi.org/10.3389/fpls.2018.00253

Zettler, R. L. (2003). Reconstructing the World of Ancient Mesopotamia: Divided Beginnings and Holistic History. Journal of the Economic and Social History of the Orient, 46(1), 3–45.

Zhang, W., Wu, H., Cheng, J., Geng, J., Li, Q., Sun, Y., Yu, Y., Lu, H., & Guo, Z. (2022). Holocene seasonal temperature evolution and spatial variability over the Northern Hemisphere landmass. Nature Communications, 13(1), Article 1. https://doi.org/10.1038/s41467-022-33107-0

Chapter 2. A new method based on surface-sample pollen data for reconstructing palaeovegetation patterns

This chapter has been published as: **Cruz-Silva, E.**, Harrison, S. P., Marinova, E., & Prentice, I. C. (2022). A new method based on surface-sample pollen data for reconstructing palaeovegetation patterns. Journal of Biogeography, 49(7), 1381–1396. https://doi.org/10.1111/jbi.14448. It has been written according to the guidelines of the journal

2.1 Abstract

Aim: Biomisation has been the most widely used technique to reconstruct past regional vegetation patterns because it does not require an extensive modern pollen dataset. However, it has well-known limitations including its dependence on expert judgement for the assignment of pollen taxa to plant functional types (PFTs) and PFTs to biomes. Here we present a new method that combines the strengths of biomisation with those of the alternative dissimilarity-based techniques.

Location: The Eastern Mediterranean-Black Sea Caspian Corridor (EMBSeCBIO).

Taxon: Plants

Methods: Modern pollen samples, assigned to biomes based on potential natural vegetation data, are used to characterize the within-biome means and standard deviations of the abundances of each taxon. These values are used to calculate a dissimilarity index between any pollen sample and every biome, and thus assign the sample to the most likely biome. We calculate a threshold value for each modern biome; fossil samples with scores below the threshold for all modern biomes are thus identified as non-analogue vegetation. We applied the new method to the EMBSeCBIO region to compare its performance with existing reconstructions.

Results: The method captured changes in the importance of individual taxa along environmental gradients. The balanced accuracy obtained for the EMBSeCBIO region using the new method was better than that obtained using biomisation (77% vs. 65%). When the method was applied to high-resolution fossil records, 70% of the entities showed more temporally stable biome assignments than obtained using biomisation. The technique also identified likely non-analogue assemblages in a synthetic modern dataset and in fossil records.

Main conclusions: The new method yields more accurate and stable reconstructions of vegetation than biomisation. It requires an extensive modern pollen dataset, but is conceptually simple, and avoids subjective choices about taxon allocations to PFTs and PFTs to biomes.

2.2 Introduction

Pollen evidence has been widely used to reconstruct Holocene changes in vegetation, both at individual sites and at a regional scale (e.g. Bozilova & Tonkov, 1995; Edwards et al., 2017; Huntley & Birks, 1983). These reconstructions provide insights into how vegetation responds to climate changes and human activities (Gaillard et al., 2010; Prentice, 1986), relevant for understanding how vegetation patterns and biodiversity may respond to future climate changes (Bradshaw et al., 2015; Cole, 2010). They also provide information about the resource base for human societies, relevant for understanding how cultural changes such as the adoption of agriculture affected the natural environment, and documenting the sensitivity of human societies to environmental change and degradation (Leroy et al., 2010; Turner & Sabloff, 2012). Vegetation reconstructions have also been widely used to test the performance of Earth System models (Foley et al., 2013; Kaplan et al., 2003; Song et al., 2021).

Available methods use modern pollen–vegetation relationships to reconstruct regional vegetation changes. Semi-quantitative approaches, including biomisation (Prentice et al.,1996, 2000), distinguish between vegetation types by grouping individual taxa into plant functional types (PFTs) and PFTs into biomes or Land Cover Classes (LCC) (pseudobiomisation: Fyfe et al., 2010). Quantitative approaches, based on pollen source area theory (Prentice, 1985; Prentice & Parsons, 1983; Sugita, 1993), include the Landscape Reconstruction Algorithms (Sugita, 2007a, 2007b) that accounts for pollen dispersal dynamics using region-specific pollen productivity estimates (PPEs) and pollen size and deposition velocities, or the Regional Estimates of VEgetation Abundance from Large Sites (REVEALS) without PPEs method (ROPES: Theuerkauf & Couwenberg,2018), which derives PPEs and mean plant abun-dances from single pollen records. The lack of information on PPEs and deposition velocities means these model-based reconstructions have only been applied in limited regions and for limited vegetation classes (Gaillard et al., 2010; Harrison et al., 2020). Statistical approaches including the Modern Analogue Technique (MAT; Gaillard et al., 1994; Jackson & Williams, 2004; Overpeck et al., 1985, 1992; Wang et al., 2020; Williams & Jackson, 2007) use modern training datasets to establish relationships between pollen assemblages and biomes, and then use these relationships to reconstruct biomes for fossil pollen assemblages. The accuracy of statistical reconstructions depends on the representativeness of the training dataset (Turner et al., 2021); the lack of sufficiently extensive modern training data precludes MAT reconstructions for many regions.

Biomisation has been one of the most widely used vegetation-reconstruction methods (Allen & Huntley, 2009; Allen et al., 2000; Bigelow et al., 2003; Edwards et al., 2000; Elenga et al., 2000; Harrison et al., 2001; Jolly et al., 1998; Marchant et al., 2001, 2009; Pickett et al., 2004; Prentice & Webb, 1998; Prentice et al., 1996; Takahara et al., 2000; Tarasov et al., 1998, 2013; Thompson & Anderson, 2000; Williams et al., 1998, 2000; Yu et al., 1998, 2000), in large part because of its conceptual simplicity and minimal data requirements. Although modern pollen samples are used to test the method, biomisation does not require the extensive modern calibration datasets

needed for statistical approaches, nor does it require regional information about pollen productivity and deposition velocities.

The principle of the biomisation method is to assign pollen taxa to PFTs defined based on life form, leaf type, phenology and climate tolerance, where taxa within a PFT are assumed to have similar responses to physical and biotic environmental factors. Major vegetation types (biomes) are then characterized as assemblages of PFTs, where the PFTs included represent either the dominant taxa or taxa that are characteristic of the biome. The allocation of pollen taxa into PFTs and PFTs into biomes is initially determined by knowledge of the regional vegetation and subsequently optimized, after comparison of reconstructions to observed vegetation, by re-moving non-diagnostic taxa or PFTs. The assignment of individual pollen samples to biomes is made by calculating an affinity score for the similarity of the pollen assemblage to every biome, based on the weighted average of the square root of the pollen abundances of taxa that could be present in each biome.

Biomisation has been shown to produce robust reconstructions of vegetation patterns at key times in the past. However, it has some well-known limitations. These include the fact that there is no direct relationship between pollen abundance and plant abun-dance such that the dominant taxa in the regional vegetation may be under-represented in the pollen assemblages. For example, Larixis the dominant genus in the boreal cold-deciduous forest of Eurasia but produces little pollen and is systematically under-represented in pollen samples (Bigelow et al.,2003). In contrast, Pinus produces abundant and easily dispersed pollen and is often over-represented in pollen samples, both in biomes where it actually occurs and as a result of long-distance transport into biomes representing open vegetation types (Bigelow et al., 2003; Edwards et al., 2000). The use of the square root of pollen abundance in the biomisation formula decreases the weight of over-represented taxa, but they still contribute to biomes that contain the PFT to which they belong. An alternative method of down-weighting over-represented taxa is to set a universal threshold of abundance for inclusion in the analysis higher than the 0.5% default value (Williams et al., 2000), but this eliminates a large number of under-represented taxa that might be diagnostic.

The definition of biomes in terms of diagnostic or dominant PFTs emphasizes the most characteristic expression of a biome but does not account for the fact that there is variability in the abundance of these PFTs within a biome and considerable differences between PFT abundance at, for example, the northern and southern limits of the biome (Edwards et al., 2000). This issue has been solved by creating additional PFTs or biomes. For example, the temperate summer green PFT in the eastern United States and Canada was split into intermediate and warm variants to separate out taxa with different climatic tolerances (Williams et al., 2000). Similarly, the tundra (TUND) biome has been split into multiple sub-biomes which are differentiated by the presence/absence of different categories of shrubs (Bigelow et al., 2003). However, these approaches still only consider part of the within-biome variability.

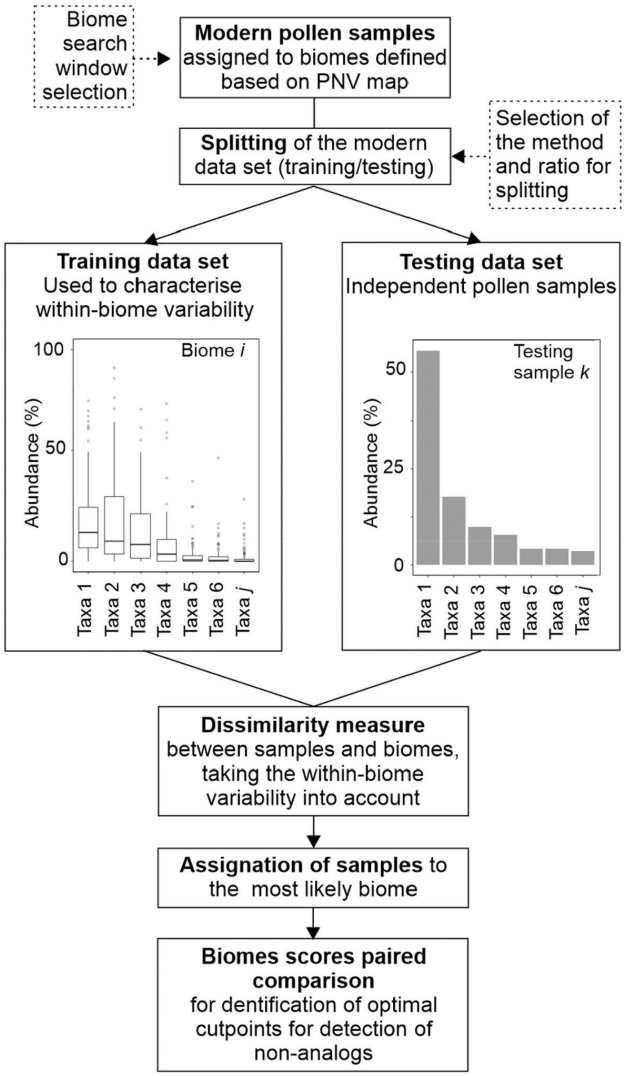

Figure 2.1 Overview of the approach for pollen-based vegetation reconstruction accounting for within-biome variability. PNV, potential natural vegetation.

A further problem is associated with the fact that some biomes are characterized by a subset of the PFTs present in another biome. For example, the PFTs defining deciduous forest types are often a subset of those defining equivalent mixed forest types, creating a situation where identical affinity scores are obtained for the two biomes. The biomisation approach solves this through a tie-break rule that favours the less PFT-rich biome. However, the presence of a small amount of pollen from a PFT that is not shared would be sufficient to change the affinity score and hence the biome allocation, meaning that the biome assignments can be sensitive to small changes in pollen abundance and may not be stable. Small changes in pollen abundance can also result in shifts towards biomes that are not characterized by a subset of the PFTs representative of another biome, for example in the case where taxa are assigned to more than one PFT. The problem referred to as the 'flickering switch' problem, is most noticeable when biomisation is used to reconstruct changes in vegetation through time using down-core pollen samples at a single site (Allen et al., 2000; Fyfe et al., 2018). The flickering switch problem has been observed to be acute in high-resolution records where one might expect greater similarity in biome allocation

between adjacent samples (see e.g. Allen & Huntley, 2009; Marchant et al., 2001). One final issue poorly addressed by the biomisation technique is the existence of palaeovegetation communities with non-analogue in the present-day vegetation because they consist of extant species but in combinations not found at present (Jackson & Overpeck,2000; Overpeck et al., 1992; Williams & Jackson, 2007). Statistical dissimilarity approaches have addressed this by establishing thresholds for detecting such assemblages, but it is important then to establish criteria to avoid ad hoc choices of such thresholds (Gavin et al., 2003).

In this study, we have derived a method that overcomes these problems and extends existing dissimilarity-based approaches by accounting explicitly for within-biome variability. We calculated a dissimilarity index (which takes account of this variability) between a given pollen sample and every biome, and thereby assess the likelihood that a sample belongs to a particular biome. We applied this method to reconstruct the modern vegetation of the Eastern Mediterranean- Black Sea Caspian Corridor (EMBSeCBIO) region (33°– 49°N, 20°–60°E), where the performance of the new approach can be compared to reconstructions made using biomisation (Marinova et al., 2018). The EMBSeCBIO region is characterized by strong temperature and precipitation gradients and topographic heterogeneity, resulting in clear patterns in biome distribution within a relatively limited geographical space and thus provides an excellent case to test how well the different methods capture spatially complex vegetation patterns.

2.3 Materials and Methods

The workflow is summarized in Figure 2.1. We first assigned modern pollen samples to biomes, where the biomes are defined using a recently developed global modern potential vegetation map. Since the modern samples were derived from different settings and basins of different sizes, we tested what would be an appropriate search window for determining the biome for each sample. We then divided the modern pollen samples into training and testing datasets. The training dataset was used to characterize the within-biome variability of the pollen assemblages assigned to a given biome, in terms of the mean, range and standard deviation of each pollen taxon. We then calculated the dissimilarity index between every sample in the test dataset and every biome. This index provides an approximation of the probability that a given pollen assemblage would be produced by a particular biome such that samples can be allocated to the biome with the highest likelihood. We tested the robustness of these assignments using different training and testing data, since the selection and size of the training and testing datasets could influence the within-biome variability and hence the dissimilarity calculation.

We then compared the reconstructions based on this new approach to previous vegetation reconstructions for the EMBSeCBIO region. Finally, we estimated optimal threshold values for the biome scores by pairwise comparison of every biome, using the receiver operating characteristic (ROC) curve as a performance metric, to determine whether assemblages were characteristic of an

observed modern biome or could represent a non-analogue vegetation type. We tested this procedure using a synthetic modern dataset and also applied it to fossil pollen assemblages from the EMBSeCBIO region.

2.3.1 Pollen and vegetation data

The modern pollen dataset was derived from the SPECIAL Modern Pollen Data Set (SMPDS: Harrison, 2019) and the EMBSeCBIO pollen database (Harrison & Marinova, 2017; Harrison et al., 2021). The SMPDS consists of relative abundance records of 247 pollen taxa from 6459 terrestrial sites from Europe, the Middle East and northern Eurasia. These taxa result from taxonomic harmonization of the individual records and amalgamation of rare taxa into higher taxonomic groups, after ensuring that this was consistent with their distribution in climate space (Harrison, 2020; Wei et al., 2020). To avoid duplication, we removed all SMPDS samples from the EMBSeCBIO region (28° to 49°N, 20° to 62°E). We did not use SMPDS sites from east of 62°E, where the sampling is limited and likely not representative of the diversity of the vegetation. Most of the pollen assemblages in the SMPDS (94%) are from lake or bog environments where sediments are currently accumulating, have been dated to the last 50 years, or are modern samples from moss polsters, litter or pollen traps. For comparability, we only used sites from the EMBSeCBIO database with ages <150 calibrated years before present (cal BP). This resulted in the selection of 1356 samples from the EMBSeCBIO database and 4409 samples from the SMPDS (Figure 2.2). Pollen counts in the EMBSeCBIO database were amalgamated into higher taxon groupings consistent with the SMPDS (Supplementary Table 2.1).

Since our goal was to develop a method to reconstruct vegetation changes through time, we used potential natural vegetation (PNV) as a target for the modern reconstructions. Maps of PNV have been widely used in this way to test regional vegetation reconstructions (e.g. Bigelow et al., 2003; Marchant et al., 2009; Marinova et al., 2018). The modern vegetation data were extracted from an updated version of the Global PNV map produced by Hengl et al. (2018). The original version of this map had a resolution of 1 km; the updated version (https://github.com/Envirometrix/PNVmaps) has a resolution of 250 m. The PNV map was produced using pollen-based vegetation reconstructions as a target, a large set of spatially explicit covariate datasets representing the potential climatic, topographic, geologic and hydrological controls on plant growth, and an ensemble of five machine-learning approaches (neural networks, random forest, gradient boosting, K-nearest neighbourhoods, Cubist) to account for the relationships between vegetation and these covariates. Different machine-learning approaches vary in terms of computational requirements, predictive power and interpretability; the use of an ensemble of machine-learning tools allows an assessment to be made of the robustness of the predictions (Hengl et al., 2018; Heung et al., 2016). The prediction accuracy of this dataset at 1 km is ca 70% globally. The PNV map has 13 biomes in the area covered by the SMPDS and EMBSeCBIO databases. We amalgamated biomes that covered a limited area or occurred as disjunct patches (e.g. erect dwarf shrub tundra, cool evergreen needleaf forest) because they do not sample

within-biome pollen variability adequately. As a result, we defined nine biomes (Table 2.1) that are structurally distinctive and represent distinct parts of the climate space of the region: tundra (TUND), desert (DESE), graminoids with forbs (GRAM), evergreen needleleaf woodland (ENWD), xeric shrubland (XSHB), cold evergreen needleleaf forest (CENF), temperate malacophyll broadleaf forest (TEDE), cool mixed evergreen needleleaf and deciduous broadleaf forest (CMIX), warm-temperate evergreen needleleaf and sclerophyll broadleaf forest (WTFS). Thus, graminoid and forb tundra, erect dwarf shrub tundra, low and high shrub tundra, and prostrate dwarf shrub tundra were amalgamated into a single tundra biome (TUND in Table 2.1) and the cool evergreen needleleaf forest was amalgamated into the cool mixed evergreen needleleaf and deciduous broadleaf forest (CMIX in Table 2.1).

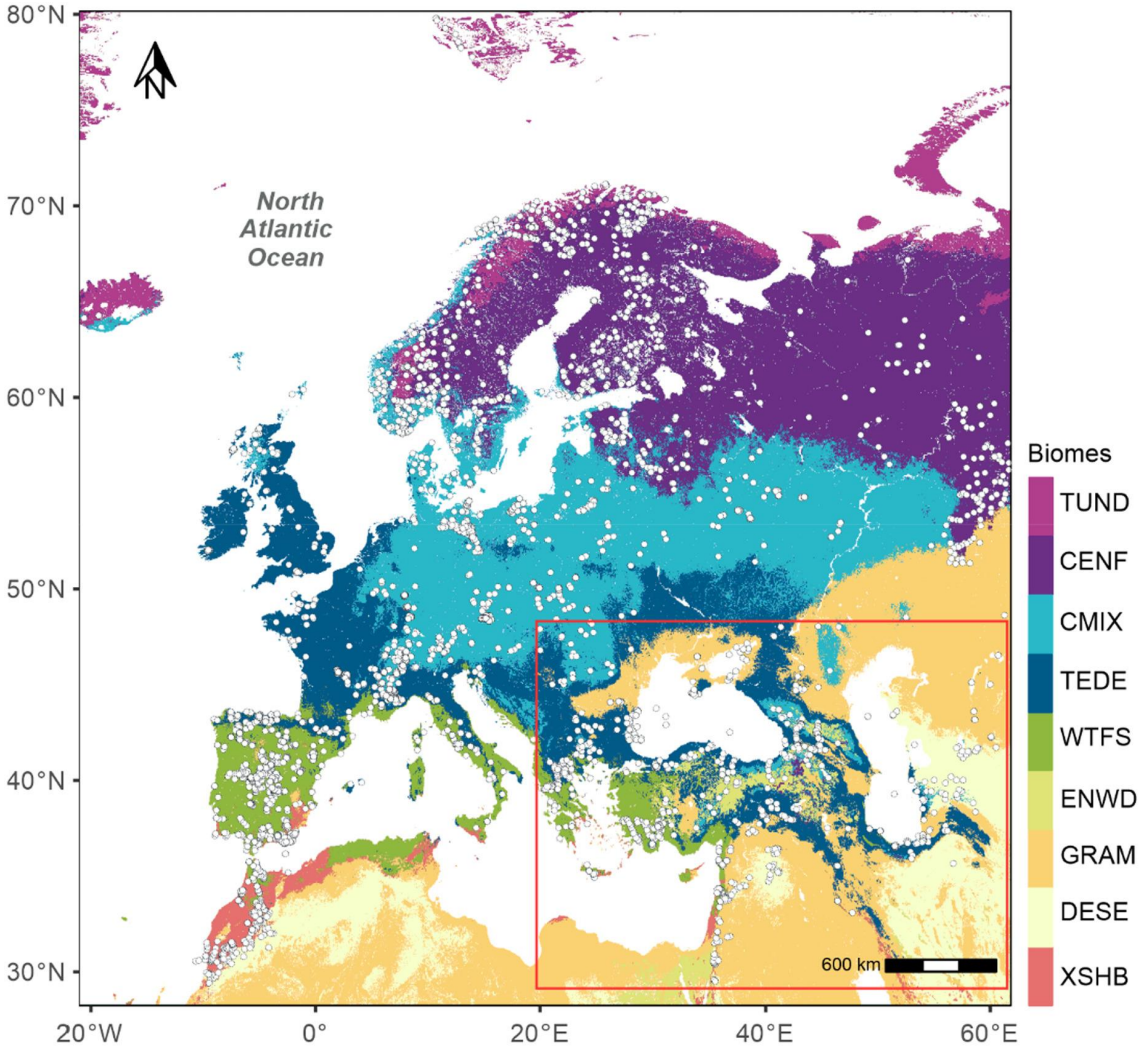

Figure 2.2 Map of the distribution of modern pollen samples from the SPECIAL modern pollen dataset (SMPDS) and the eastern Mediterranean-Black Sea Caspian corridor (EMBSeCBIO) database used for the training and testing datasets. The red box delineates the area covered by the EMBSeCBIO database; samples outside the red box were obtained from the SMPDS dataset. The background map shows the distribution of major biomes derived from the Hengl et al. (2018) reconstruction of potential natural vegetation. The biome codes are: CENF, cold evergreen needleleaf forest; CMIX, cool mixed evergreen needleleaf and deciduous broadleaf forest; DESE, desert; ENWD, evergreen needleleaf woodland; GRAM, graminoids with forbs; TEDE, temperate deciduous malacophyll broadleaf forest; TUND, tundra; WTFS, warm-temperate evergreen needleleaf and sclerophyll broadleaf forest; XSHB, xeric shrubland.

2.3.2 Biome characterization

The training and testing datasets were created by sub-sampling the modern pollen samples using the PNV map to assign samples to biomes. We used samples from this larger area to sample the whole of the realized range of each biome and to include biomes that are not currently represented in the EMBSeCBIO region but may have occurred there under different climate conditions in the past. This 'space-for-time' substitution is warranted because the climatic drivers of plant compositional turnover across space are similar to those that drive compositional turnover through time during the Late Quaternary (Blois et al., 2013).

There are some locations with multiple modern samples in a very small area, for example, multiple moss polsters within a catchment of a few square kilometres. This could lead to the over-representation of some localities in the training dataset and therefore an apparent reduction in the variability of assemblages from the biome(s) involved. Similarly, there are some regions where there are modern pollen samples from sites that are geographically close together and have similar vegetation, resulting in over-sampling of that biome in the training dataset (Supplementary Figure 2.1) and consequently overfitting to the better sampled biome. To limit redundancy in such cases, a single modern sample at each point (defined by latitude and longitude coordinates) was randomly selected for the analyses. We tested different ways of subsampling the data to reduce the biome oversampling bias. The best performance was obtained by down-sampling biomes with a large number of samples to create a dataset with a similar number of samples from each biome. The down-sampled data were then split into training and test datasets.

Code	Biome name	Definition
TUND	Tundra	Open vegetation characterized by cold-adapted forbs, sedges, graminoids and shrubs found in arctic and high alpine regions
DESE	Desert	Open or non-vegetated landscape characterized by sporadic occurrence of drought-adapted vegetation including succulents, graminoids, forbs and shrubs
GRAM	Graminoids with forbs	Grasslands dominated by graminoids and forbs
ENWD	Evergreen needleleaf woodland	Semi-open vegetation characterized by evergreen conifer trees, with an understorey of graminoids, forbs and sedges

XSHB	Xeric shrubland	Vegetation dominated by tall drought-tolerant or sclerophyll shrubs.
CENF	Cold evergreen needleleaf forest	Forest vegetation dominated by cold-tolerant conifers
TEDE	Temperate deciduous malacophyll broadleaf forest	Forest vegetation dominated by summer green trees
CMIX	Cool mixed evergreen needle leaf and deciduous broadleaf forest	Forest vegetation characterized by a mix of temperate summer green trees and conifers
WTFS	Warm-temperate evergreen needleleaf and sclerophyll broadleaf forest	Forest vegetation dominated by broad-leaved and needle-leaved evergreen trees, characteristic of Mediterranean-type climates with summer drought

Table 2.1 Description of the nine biomes used in the analyses. The table gives the code, the full biome name and a brief definition of the vegetation

The observed PNV biome for each pollen sample in the modern training dataset was derived using different search windows (from 12 × 12 km up to 50 × 50 km) around the location of the sample point. We determined both the dominant and subdominant biome in each search window for subsequent evaluation, based on which biomes occupied the largest (dominant) and second largest (sub-dominant) number of 1 km2 pixels within the search window. We also tested the impact of using different proportions of sites for the training set and the test set for each of these search windows, splitting using ratios of 50:50, 60:40, 70:30, 75:25 and 80:20. We tested how well each of these combinations predicted the modern vegetation of the EMBSeCBIO region using only modern samples from this region in the test set. The best performance, based on the balanced accuracy, was obtained using a search window of 20 × 20 km centred on the sample location, with a training/test data partitioning ratio of 70:30 (Supplementary Tables 2.2 and 2.3).

The training samples were grouped according to the dominant biome observed in the PNV map. Each modern biome was then characterized by the relative abundance (expressed in terms of the mean, and standard deviation) of all taxa present to account for variability in pollen abundances within each biome.

2.3.3 Calculation of the dissimilarity and similarity scores

We calculated the following coefficient of dissimilarity between the pollen assemblage of a sample from the test dataset and each biome:

$$D_{ik} = \sqrt{\Sigma_{jk} \frac{\left(p_{jk} - \mu_{jk}\right)^2}{\left(s_{ji} - \varepsilon\right)^2}} \quad (2.1)$$

where D_{ik} is the dissimilarity of pollen sample k from biome i; p_{jk} is the pollen percentage of taxon j in sample k; μ_{ji} is the mean of taxon j in biome i, s_{ji} is the sample standard deviation of taxon j in biome i and ε is a parameter. Summation is over all taxa in sample k.

Equation (2.1) is based on the idea that each taxon has a certain distribution of values within a biome, and more weight is assigned to those taxa for which this distribution is narrow. For each taxon, Dik is related inversely to the log-likelihood that a pollen sample is drawn from the population represented by the abundance of that taxon among the modern pollen samples in each biome. The term ε has two functions. First, it decreases the weight of characteristic taxa with low values of s (e.g. due to limited sampling) in the calculation of the dissimilarity measure. Second, it allows the absence of taxa from a fossil sample (s = 0) to be informative, with ε = 0 they could not be considered in the calculation. The choice of the value of ε represents a balance between accuracy and sensitivity, since small values of ε could result in more accurate predictions of well-sampled biomes but increase the sensitivity such that poorly sampled biomes are less well predicted. Values between 0% and 1% were tried, and good results obtained with a value of 0.5% (Supplementary Table 2.4) which was therefore used for the subsequent calculations.

The dissimilarity values were converted to similarities by:

$$S_{ik} = e^{-D_{ik}/100} \quad (2.2)$$

where S_{ik} is an approximation of the likelihood of biome i given pollen sample k. By the nature of the dissimilarity index, these similarity scores quantify how close a pollen sample is to the mean abundance values in the biome, accounting for within-biome variability. Samples that represent vegetation closer to the ecotonal boundary of a biome will necessarily have a lower similarity score, although this score will still be higher than the score for other biomes.

2.3.4 Evaluation of the modern biome reconstructions

The biome reconstructions were evaluated quantitatively using a matrix of predicted versus observed vegetation at each site ('confusion matrix': e.g. Bigelow et al., 2003). We constructed confusion matrices for the test dataset and the EMBSeCBIO dataset, based on both the dominant

and subdominant biome registered in the search window around the sample. The confusion matrix provides an assessment of the accuracy of the reconstructions, but is strongly influenced by imbalances in the sampling of different classes (Carrillo et al., 2014; Grandini et al., 2020). Some biomes are less well represented in the training dataset even after down-sampling to reduce differences in sample numbers between biomes. Under these circumstances, the 'balanced accuracy' metric, defined as the average accuracy obtained on all classes (Carrillo et al., 2014), provides a better performance metric. The balanced accuracy metric is given by:

$$BA = \frac{1}{l}\sum_{i=1}^{l}\frac{k_i}{n_i} \quad (2.3)$$

where k_i is the number of sites correctly predicted for biome i, l is the number of biomes and n_i is the number of sites in biome i. The evaluation was performed both on the testing dataset and on samples only from the EMBSeCBIO region. The reconstructed modern biome distribution for the EMBSeCBIO region was mapped.

We compared the performance of the new method to a reconstruction made using the biomisation method (Marinova et al., 2018). We reclassified the 13 biomes used by Marinova et al. (2018) to match the set of nine biomes (Table 2.1) used here, by considering the three types of warm-temperate vegetation they recognized as equivalent to our WTFS biome, combining cool and cold evergreen needleleaf forest, and combining deciduous broadleaf woodland with evergreen needleleaf woodland. However, the allocations of taxa to PFTs and PFTs to these biomes were entirely based on Marinova et al. (2018) (Supplementary Tables 2.5 and 2.6). We then applied the biomisation technique to samples from the EMBSeCBIO region. The accuracy of the reconstructed biomes was evaluated against the PNV map based on the dominant and subdominant biome in the search window.

2.3.5 Impact on the flickering switch problem

We used fossil pollen data from the EMBSeCBIO database to assess the impact of the new method on the stability of biome reconstructions through time. The EMBSeCBIO database contains 187 records covering some part of the Holocene. New age-depth models have been produced for 149 of these records using the IntCal20 calibration curve (Reimer et al., 2020) and the 'rbacon' R package (Blaauw et al., 2021) in the framework of the 'AgeR' R package (Villegas-Diaz et al., 2021), which automates the supervised creation of multiple age models for multiple cores. Optimum age modelling scenarios were initially selected from multiple 'rbacon' age models run using different prior accumulation rate and thickness values, using the lowest quantified area between the prior and posterior accumulation rate distribution curves; the optimum model was verified by comparing the distance of the estimated ages and the dating control points to check the accuracy

of the model interpolation and through visual inspection to ensure that changes in accumulation rate were independent of the control points. We extracted 30 fossil pollen records with a temporal resolution <100 years and covering an interval of at least 1000 years, on the assumption that it is unlikely that there will be multiple biome changes within a specific interval between samples that are <100 years apart and that large numbers of such changes would indicate instability due to the flickering switch problem. We applied the biomisation technique and our new method to these 30 records and counted the number of biome changes that occurred between adjacent samples. This number was standardized for differing lengths of record by dividing by the total number of samples in the record minus one.

2.3.6 Estimation and evaluation of biome analogue thresholds

We used the similarity scores obtained from the pollen samples in the modern testing dataset for each biome (Supplementary Figure 2.3) and made pairwise comparisons between biomes. We obtained the optimal threshold value differentiating each pair of biomes by calculating specificity and sensitivity metrics (Supplementary Figure 2.4) and plotting these on a ROC curve (Supplementary Figure 2.5) using the 'cutpoint' R package (Thiele, 2021), where the point with the maximum balance (sensitivity + specificity) was selected as the optimal threshold between two biomes. The ROC curve has been used previously in MAT-based vegetation reconstructions to assess the ability of different distance metrics to distinguish between groups and to avoid ad hoc interpretations of dissimilarity scores and thresholds (Gavin et al., 2003). We derived a single threshold value per biome, as the lowest value obtained in comparisons of that biome against all other biomes. If a pollen sample has a similarity score below the lowest threshold value for all biomes, it is assumed to represent a non-analogue assemblage. We tested this approach using (1) the 3650 modern samples in the testing dataset, and (2) a synthetic dataset of 70 samples, using pollen abundances from actual samples and removing taxa or assigning abundances to different taxa randomly. We then applied this approach to fossil samples to determine if it identified non-analogue samples in these records and summarized these analyses by quantifying the proportion of records with at least one non-analogue sample in specific time periods, defined as 200-year windows with 50% overlap.

2.4 Results

2.4.1 Within-biome variability in the training dataset

Most biomes show considerable within-biome variability in taxon abundances, reflecting changes in the importance of individual taxa along climate and environmental gradients (Figure 2.3; Supplementary Figure 2.2). The most abundant taxa in every biome of the training dataset correspond to PFTs characteristic of that vegetation type (Figure 2.3). For example, open-vegetation types such as GRAM (Figure 2.3 b) are characterized by high abundances of Poaceae ($\mu \approx 20\%$), Amaranthaceae ($\mu \approx 20\%$), *Artemisia* ($\mu \approx 15\%$), Asteroideae ($\mu \approx 3\%$) and

Cyperaceae (μ ≈3%). Similarly, CMIX (Figure 2.3 f) is characterized by high abundances of *Pinus* (diploxylon) (μ ≈25%), *Betula* (μ ≈10%), *Alnus* (μ ≈5%), *Picea* (μ ≈4%), *Fagus* (μ ≈4%) and deciduous *Quercus* (μ ≈4%). Each biome has less characteristic taxa that represent understorey vegetation (e.g. Poaceae in CMIX, μ ≈11%), indicates azonal vegetation (e.g. Cyperaceae in CMIX, μ ≈5%) or (e.g. *Pinus* diploxylon in GRAM, μ ≈9%).

Differences in composition along the climate gradients covered by a specific biome are reflected in the abundance of the dominant taxa (Figures 2.3 a,e). For example, Poaceae, *Artemisia* and Amaranthaceae are the three most important taxa in GRAM (Figure 2.3 b) but their relative importance changes between cold and warm ends (here distinguished by the MTCO value that represents the mid-point of the sample range, < or > 2°C for GRAM and < or > –3°C for CMIX) of the climate range occupied by the biome. Differences can be even more extreme for subordinate taxa. *Picea* and *Fagus* are present in GRAM in low abundances when MTCO <2°C (Figure 2.3 c) but are absent when winter temperatures are higher, where the subordinate taxa include *Olea* and *Argania* in low abundance (Figure 2.3 d). Similar shifts in composition can be seen in other biomes, for example CMIX (Figure 2.3 f), where *Pinus* (Diploxylon) and Poaceae are the dominant taxa throughout the range, but *Betula* and *Picea* are important at the cold (Figure 2.3 g) and *Quercus* and *Alnus* are important at the warm (Figure 2.3 h) end.

2.4.2 Assessment of the modern reconstructions

The modern reconstruction using the training dataset reached a balanced accuracy of 66%, which improved to 76% when both dominant and subdominant biomes were considered (Table 2.2). The best predictions, considering both dominant and subdominant biomes (Table 2.2), were for CMIX (89%), TUND (83%), XSHB (82%), GRAM (76%), TEDE (74%), ENWD (72%), CENF (71%), DESE (70%). The least well-predicted biome was WTFS (65%). Persistent mismatches can occur between closely related biomes: DESE samples were allocated to xerophytic shrublands in 13% of the cases, while samples from GRAM were allocated to DESE in 11% of the cases. Similarly, CENF samples were allocated to CMIX in 11% of cases.

The modern reconstruction using the EMBSeCBIO dataset (Table 2.3) (excluding CENF and TUND which had too few samples for useful evaluation) reached a balanced accuracy of 64%, which improved to 77% when both the dominant and subdominant biomes were considered. The best predictions, considering both dominant and subdominant biomes (Table 2.3), were for DESE (89%), XSHB and ENWD (85%), GRAM (75%), TEDE (74%), and CMIX (67%). The least well-predicted biome was WTFS (64%). GRAM samples were allocated to DESE in 12% of the cases, and CMIX samples were allocated to TEDE in 15% of the cases.

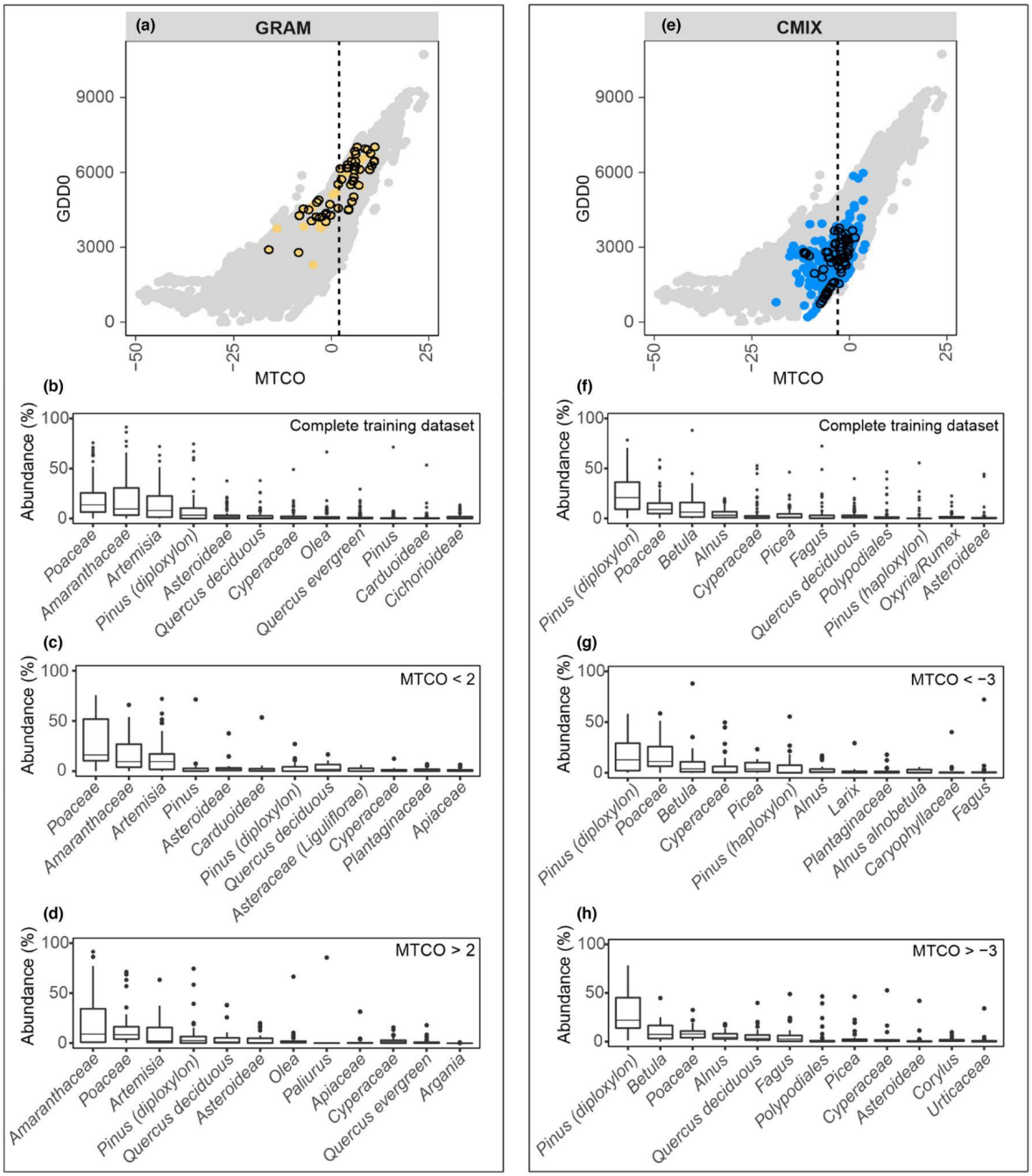

Figure 2.3 Examples of the characterization of individual biomes in terms of their pollen assemblages and the distribution of the pollen sites belonging to these biomes in bioclimatic space. The bioclimatic space is defined in terms of the mean temperature of the coldest month (MTCO) and growing degree days above a base level of 0°C (GDD0). The climate data at each pollen site were derived from Harrison (2020). Plot (a) shows the bioclimatic space occupied by graminoids with forbs (GRAM, yellow dots) and plot (e) the space occupied by cool mixed evergreen needle-leaf and deciduous broadleaf forest (CMIX, blue dots) in the context of the bioclimatic space of the whole Europe and middle eastern region (grey dots). Dashed lines indicate MTCO mid-point values for each biome. The box plots show the median and standard deviation of the abundance of the 12 most abundant individual taxa in GRAM and CMIX, where (b, f) show samples from the complete training dataset, (c, g) show samples from the training set with MTCO values lower than the mid-point values and (d, h) show samples from the training set with MTCO values higher than the mid-point value. Box plots for the other biomes are given in supplementary.

Biomes	Predicted									
	DESE	XSHB	WTFS	GRAM	ENWD	TEDE	CMIX	CENF	TUND	Σ
Observed										
DESE	16[0]	3	1	2	1	0	0	0	0	23
XSHB	2	27[4]	1	4	0	0	0	0	0	38
WTFS	0	4	16[6]	4	0	3	1	0	0	34
GRAM	4	1	1	23[5]	1	1	1	0	0	37
ENWD	1	3	2	3	21[2]	0	0	0	0	32
TEDE	0	1	4	1	1	19[6]	2	0	0	34
CMIX	0	0	0	1	2	1	28[3]	0	0	35
CENF	0	0	0	1	1	2	4	23[2]	2	35
TUND	0	0	0	1	0	0	3	0	19[1]	24
Σ	23	43	31	45	29	32	42	25	22	292

Table 2.2 Quantitative comparison of predicted and observed dominant and sub-dominant (in brackets) biomes across the whole testing dataset. The observed dominant and sub-dominant biomes are taken from the Hengl et al. (2018) potential natural vegetation map. The biome codes are: CENF, cold evergreen needleleaf forest; CMIX, cool mixed evergreen needleleaf and deciduous broadleaf forest; DESE, desert; ENWD, evergreen needleleaf woodland; GRAM, graminoids with forbs; TEDE, temperate deciduous malacophyll broadleaf forest; TUND, tundra; WTFS, warm-temperate evergreen needleleaf and sclerophyll broadleaf forest; XSHB, xeric shrubland. The total number of predicted and observed records for each biome are also shown (Σ). The grey diagonal shows the number of correctly predicted samples, while off-diagonal elements are those incorrectly predicted.

The method correctly predicted modern vegetation patterns across the EMBSeCBIO region (Figure 2.4), including the distribution of WTFS along the coastal plains around the Mediterranean and the transitions from forest through woodland to open vegetation in the Middle East and to the east of the Caspian Sea. The distribution of CMIX and TEDE in the Carpathian Mountains and the Balkans were also correctly predicted. In regions of complex topography, such as the Caucasus (Figure 2.4 c), the method successfully captured the transition from forest to more open vegetation with elevation.

2.4.3 Impact of choice of training dataset

The construction of the training dataset had only a minor impact on the overall accuracy of the reconstructions: the average balanced accuracy was 76±1.87% (Supplementary Table 2.2). In evaluation of different biome search windows with different training/test splits, the average

balanced accuracy was 76±0.96% (Supplementary Table 2.3). The prediction accuracy in the EMBSeCBIO region was similar (average balanced accuracy 76±0.77%) to that for datasets covering all of the SMPDS region (Supplementary Table 2.3). The removal of lakes larger than 50 km2, which have a larger pollen source area than the area used to allocate dominant and sub-dominant biomes for each sample (Prentice, 1985; Sugita, 1993), improved the prediction, but only marginally from a balanced accuracy of 76% to 77%.

Biomes	Predicted									Σ
	DESE	XSHB	WTFS	GRAM	ENWD	TEDE	CMIX	CENF	TUND	
Observed										
DESE	44[7]	1	0	4	1	0	0	0	0	57
XSHB	1	7[10]	0	0	0	2	0	0	0	20
WTFS	0	22	137[14]	24	3	35	0	0	0	235
GRAM	12	3	0	61[12]	4	4	1	0	0	97
ENWD	1	3	5	8	87[28]	2	1	0	0	135
TEDE	12	10	15	11	24	199[29]	6	0	0	306
CMIX	0	0	1	1	9	10	36[9]	1	0	66
CENF	0	0	0	0	1	0	0	0	0	1
TUND	0	0	0	0	0	0	0	0	0	0
Σ	77	56	172	121	157	281	52	1	0	917

Table 2.3 Quantitative comparison of predicted and observed dominant and sub-dominant (in brackets) biomes in the eastern Mediterranean-Black Sea Caspian corridor region. The observed dominant and sub-dominant biomes are taken from the Hengl et al. (2018) potential natural vegetation map. The biome codes are as follows: CENF, cold evergreen needleleaf forest; CMIX, cool mixed evergreen needleleaf and deciduous broadleaf forest; DESE, desert; ENWD, evergreen needleleaf woodland; GRAM, graminoids with forbs; TEDE, temperate deciduous malacophyll broadleaf forest; TUND, tundra; WTFS, warm-temperate evergreen needleleaf and sclerophyll broadleaf forest; XSHB, xeric shrubland. The total number of predicted and observed records for each biome are also shown (Σ). The grey diagonal shows the number of correctly predicted samples, while off-diagonal elements are those incorrectly predicted.

2.4.4 Comparison with reconstructions using the biomisation method

The balanced accuracy obtained for the EMBSeCBIO region using the new method was better than that obtained using the biomisation method (excluding CENF and TUND) (Table 2.4), with a value of 64% (compared to 49%) when considering only the dominant biome, and 76% (compared to 65%) when considering both dominant and sub-dominant biomes. Both methods produced better predictions for open vegetation types than forests: DESE (89%), XSHB (85%) and ENWD

(85%) are the best predicted biomes with the new method, and ENWD (89%), DESE (83%) and GRAM (73%) with biomisation. However, there is a considerably larger range of prediction accuracy with the biomisation approach. Thus, the worst predicted biome using the new method

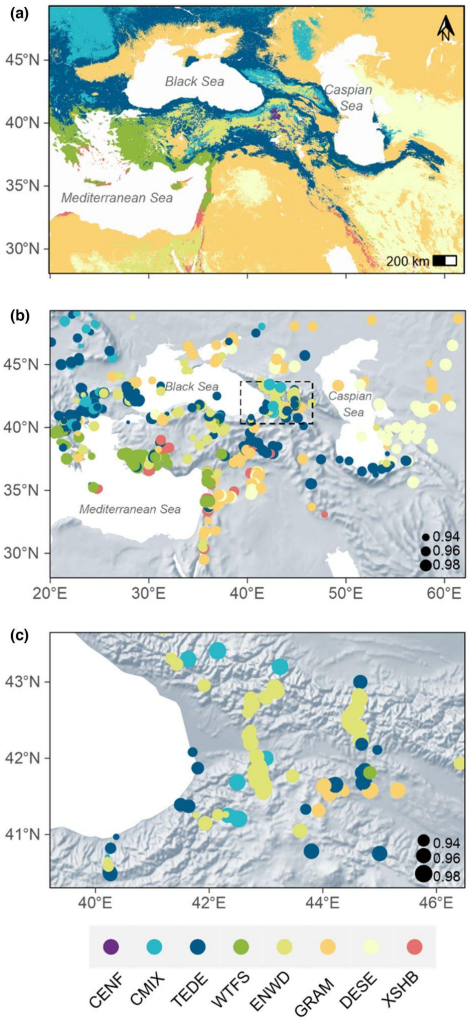

Figure 2.4 Maps showing (a) observed and (b) reconstructed biomes using the modern records across the eastern Mediterranean-Black Sea Caspian corridor region. The colours show the observed or reconstructed biome. The biome codes are: CENF, cold evergreen needleleaf forest; CMIX, cool mixed evergreen needleleaf and deciduous broadleaf forest; DESE, desert; ENWD, evergreen needleleaf woodland; GRAM, graminoids with forbs; TEDE, temperate deciduous malacophyll broadleaf forest; TUND, tundra; WTFS, warm-temperate evergreen needleleaf and sclerophyll broadleaf forest; XSHB, xeric shrubland. The size of the dots in (b) provides an indication of the similarity score obtained, where the larger dots mean higher similarities. Plot (c) shows an enlargement of the map of reconstructed biomes in the Caucasus region, where the distribution is strongly controlled by elevational gradients.

had an accuracy of 64% (WTFS), whereas the worst predicted biome using biomisation had an accuracy of only 37% (TEDE). Mismatches occur between similar biomes in both methods. Some GRAM samples, for example, were allocated to DESE in 12% of cases under the new method, and 15% of cases in biomisation. Similarly, CMIX samples were allocated to TEDE in 15% of cases using the new method and to CENF in 26% of cases using biomisation. Some TEDE samples were wrongly allocated either to ENWD (8% in the new method, 20% in biomisation) or WTFS (5% in the new method, 22% in biomisation).

2.4.5 Reconstruction stability

Down-core reconstructions for high-resolution records using the new method showed generally greater stability than was obtained using the biomisation approach. There was no difference in the range of the proportion of changes between contiguous samples per thousand years (0%–77%), but the new method reduced the proportion of changes in 70% of the records, and produced a similar number of changes in 7% of the records (Supplementary Table 2.7). Thus, the new method provides more stable reconstructions and reduces the tendency for small variations in taxon abundance to cause unrealistic temporal shifts between biomes.

Biomes	Predicted									
	DESE	XSHB	WTFS	GRAM	ENWD	TEDE	CMIX	CENF	TUND	Σ
Observed										
DESE	43[15]	2	8	1	1	0	0	0	0	70
XSHB	1	4[3]	1	0	2	0	0	0	0	11
WTFS	1	0	127[29]	27	9	3	3	28	3	230
GRAM	14	1	5	47[19]	3	0	1	0	0	90
ENWD	1	0	3	10	90[80]	2	1	3	0	190
TEDE	9	0	55	31	50	81[12]	4	10	0	252
CMIX	2	0	3	10	6	0	21[10]	19	2	73
CENF	0	0	0	1	0	0	0	0	0	1
TUND	0	0	0	0	0	0	0	0	0	0
Σ	86	10	231	146	241	98	40	60	5	917

Table 2.4 Quantitative comparison of predicted and observed dominant and sub-dominant (in brackets) biomes in the eastern Mediterranean-Black Sea Caspian corridor region. The predicted dominant and sub-dominant biomes were obtained using the biomisation method as described by Marinova et al. (2018); the observed dominant and sub-dominant biomes are taken from the Hengl et al. (2018) potential natural vegetation map. The biome codes are as follows: CENF, cold evergreen needleleaf forest; CMIX, cool mixed evergreen needleleaf and deciduous broadleaf forest; DESE, desert; ENWD, evergreen needleleaf woodland; GRAM, graminoids with forbs; TEDE, temperate deciduous malacophyll broadleaf forest; TUND, tundra; WTFS, warm-temperate evergreen needleleaf and sclerophyll broadleaf forest; XSHB, xeric shrubland. The total number of predicted and observed records for each biome are also shown (Σ). The grey diagonal shows the number of correctly predicted samples, while off-diagonal elements are those incorrectly predicted.

2.4.6 Assessment of the approach for non-analogue detection

A threshold value for identifying analogue and non-analogue samples was estimated for each biome (Supplementary Table 2.8). Only 4.5% of the modern samples were identified as non-analogue, a value that is reasonable for false positives. However, 100% of the synthetic dataset were identified as non-analogue. Application of this approach to the fossil dataset showed an abrupt increase in the proportion of non-analogues at the transition between the late-glacial and early Holocene (~11 ky), where the number of entities identified as having non-analogue assemblages exceeds 20% (Figure 2.5). After ~4 ky, the proportion of entities identified as having non-analogue samples is around 5% and taken to indicate the presence of false positives.

2.5 Discussion

We have devised a method to reconstruct vegetation that is conceptually simple and uses the observed within-biome variability in taxon abundances explicitly. Exploiting information about within-biome variability avoids subjective choices about taxon allocations to PFTs and biomes inherent in biomisation. It also circumvents issues associated with the under- or over-representation of some species in pollen assemblages. The new method produced a more accurate reconstruction of modern vegetation patterns in the EMBSeCBIO region than biomisation (77% vs. 65%) because it preserves the observed community properties acquired from all taxa across all samples. The substantial increase in balanced accuracy (64%–77%) when both dominant biome and subdominant biomes were considered shows, moreover, that many of

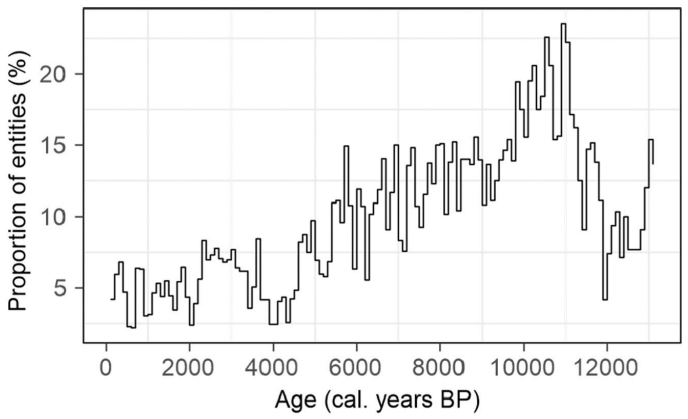

Figure 2.5 Proportion of high-resolution pollen records (entities) having at least one sample identified as non-analogue in a 200-year time-window over the past 12,000 years, where the time windows were constructed with 50% overlap. Values <5% are generally assumed to be false positives, but values above this are thought to indicate genuine non-analogue vegetation assemblages.

the remaining misallocations occurred between climatically related biomes, a feature that is common to biomisation reconstructions (Prentice et al., 1996, 2000). The method identifies even poorly sampled biomes successfully: DESE is represented by far fewer samples than forest biomes

in the training set, for example, but is predicted with 70% accuracy whereas scarcity of samples led to a very low probability of reconstructing DESE using biomisation, for example in Africa and the Arabian Peninsula (Jolly et al., 1998).

Our approach exploits a large modern pollen dataset to characterize biomes. This is important because previous research (Turner et al., 2021) has shown that the accuracy of pollen-based climate reconstructions is contingent on maximizing the sampled environmental space and is unaffected by the inclusion of climatically insensitive or systematically overrepresented taxa. Turner et al. (2021) also showed that the range and continuity of sampling along an environmental gradient is more important than the sampling density, consistent with our decision to reduce over-sampling of some biomes and eliminate redundant samples from the modern samples prior to model development. However, subsequent methodological decisions, such as the size of the search window or the partitioning of the data for testing and training, had very little impact and changed the overall accuracy of the reconstructions by less than ±2%.

The new method provides more stable reconstructions of past vegetation than the biomisation approach. Given that multiple switches between biomes within a limited period of time in high-resolution pollen records are more likely a reflection of the over-sensitivity of the reconstruction technique to minor fluctuations in taxon abundances rather than multiple changes in vegetation on decadal to sub-centennial timescales, this suggests that the new method largely overcomes the so-called flickering switch problem. Previous attempts to reconstruct vegetation patterns through time (e.g. Williams et al., 2000, 2011; Zanon et al., 2018) have minimized the flickering switch problem by focusing on reconstructions for widely spaced time periods. Our new approach opens up the possibility of making robust reconstructions at higher temporal resolution.

We have demonstrated how the similarity scores for individual biomes can be used to determine whether a given vegetation assemblage is present in the modern vegetation. We show that this approach identifies synthetic samples composed of extant taxa in combinations not seen in the modern dataset as non-analogue. If we assume a 5% cut-off for false positives based on the assignments of the modern testing dataset, there are analogues for late Holocene vegetation records from the EMBSeCBIO region but the number of non-analogues samples during the late glacial and early Holocene exceeds 20%. This is consistent with other studies that have identified late glacial and early Holocene non-analogue pollen assemblages in many regions (Caballero-Rodríguez et al., 2017; Correa-Metrio et al., 2012; Jones et al., 2017; Williams & Jackson, 2007), including the EMBSeCBIO region (Connor & Kvavadze, 2009).

Pseudobiomisation has been used to reconstruct LCCs for the Anatolian and Balkan parts of the EMBSeCBIO region (Fyfe et al., 2015; Woodbridge et al., 2014). The main focus of this work was to identify different degrees of anthropogenic modification of the vegetation (Fyfe et al., 2010), and most of the LCCs specifically include agricultural cover (e.g. mixed open vegetation, LCC8 which is defined as a combination of heath/scrubland, pastures/natural grassland and arable land). Although three LCCs are primarily natural vegetation, and are broadly equivalent to the biomes

used in this analysis, they represent only ≲25 sites and this precludes a direct comparison between the new method and the pseudobiomisation approach. Nevertheless, the overall accuracy of the pseudobiomisation for the whole of Europe was only 50%, and predictions for the Mediterranean region were recognized as being poor (Fyfe et al., 2015; Woodbridge et al., 2014), suggesting that the new method is likely to be more accurate.

We have evaluated our reconstructions using a PNV map created using a machine-learning approach with pollen-based biome reconstructions to infer the vegetation that should be present as a function of climate and other environmental factors from the evidence available about the (relict) natural vegetation. Although this map is reasonably accurate globally, it is nevertheless most reliable where there are abundant data for training and less reliable where data are scarce (Hengl et al., 2018). However, the stability of our reconstructions using different modern sub-samples drawn from different locations suggests that uncertainties in the PNV mapping have had little influence on our reconstructions.

Although we have focused on the reconstruction of natural vegetation, the new method could be applied to reconstruct actual vegetation cover including land use. This would be useful to quantify the magnitude of human impact on vegetation through time and the effect of such changes on biodiversity, landscape degradation, carbon storage and climate. However, while there are many satellite-based sources of high-resolution land-cover data (Buchhorn et al., 2020; CCI Land Cover, 2017; Gong et al., 2013; Sulla-Menashe et al., 2019), they focus on vegetation properties that impact land-surface feedbacks rather than biomes. Thus, for example, they make no distinction between the broadleaved evergreen tree cover characteristic of tropical environments and the sclerophyll broadleaved evergreen trees of the Mediterranean. Furthermore, since the amount of bare ground is important for water-exchange with the atmosphere, they distinguish low cover areas regardless of whether this cover is herbs, shrubs or trees. Finally, field validation of these maps has been limited, where it has been done the accuracy is only about 80% (Tsendbazar et al., 2021). Nevertheless, although there would be a considerable amount of work involved in creating more accurate biome descriptions from existing land cover datasets, it could be a useful to explore this in future.

A more important limitation of our method may be the use of a universal search window (20 × 20 km) to determine the biome for each modern site, selected by comparison of performance scores for different windows. The increase in balanced accuracy from 66% to 76% when both the dominant and subdominant biomes are considered suggests a greater degree of precision to take account of the pollen source area of each site could be beneficial. A fifth of the modern samples are from lakes or bogs (19%), and 68% of these records are from basins <1 km2 in area. The selected search window is close to the theoretical pollen source area for small (<1 km2) basins (Prentice, 1988; Sugita, 1993). Of the remaining modern samples, 33% are from moss polsters and 16% are from soil or other surface materials, both categories that record an even more local signal than small lakes or bogs, although the area sampled depends on vegetation openness and may be comparable with small lakes in some settings (Beer et al., 2007; Bunting et al., 2004; Jackson & Wong, 1994; Prentice, 1988). This again suggests that the choice of a 20 × 20 km search window is

reasonable. Improvements to prediction accuracy could be achieved using a search window appropriate to the pollen source of each site. However, the EMBSeCBIO database lacks information about site type for 27% and about basin size for 14% of the sample records. Furthermore, basin size is only recorded categorically, so the quantitative information required to allow us to test this idea still needs to be collected.

Our new method combines the relative simplicity of the biomisation approach with the more rigorous statistical basis of dissimilarity-based reconstruction techniques. One major advantage of the current approach compared to existing dissimilarity-based reconstruction techniques is that it explicitly takes account of within-biome variability. Samples that represent ecotonal transitions between biomes can therefore be assigned to a biome and the nature of the ecotone represented can be determined by comparing the scores for other biomes, providing a more nuanced way of examining past vegetation changes and transitions.

2.6 Conclusions

Our new approach provides a promising way of reconstructing past vegetation taking account of the non-proportionality in the relationship between vegetation cover and pollen abundances. There are alternative approaches to doing this, but their accuracy is tempered by very high data demands. Our new method requires an extensive modern pollen dataset but is less data-demanding than other approaches and yields robust results. Biomisation depends on expert judgement for the assignment of taxa to PFTs and PFTs to biomes; our method avoids this limitation, while producing more accurate and temporally stable reconstructions.

2.7 References

Allen, J. R. M., & Huntley, B. (2009). Last interglacial palaeovegetation, palaeoenvironments and chronology: A new record from Lago Grande di Monticchio, southern Italy. Quaternary Science Reviews, 28(15), 1521–1538. https://doi.org/10.1016/j.quascirev.2009.02.013.

Allen, J. R. M., Watts, W. A., & Huntley, B. (2000). Weichselian palynostratigraphy, palaeovegetation and palaeoenvironment; the record from Lago Grande di Monticchio, southern Italy. Quaternary International, 73–74, 91–110. https://doi.org/10.1016/S1040-6182(00)00067-7.

Beer, R., Tinner, W., Carraro, G., & Grisa, E. (2007). Pollen representation in surface samples of the Juniperus, Picea and Juglans forest belts of Kyrgyzstan, Central Asia. The Holocene, 17(5), 599–611. https://doi.org/10.1177/0959683607078984.

Bigelow, N. H., Brubaker, L. B., Edwards, M. E., Harrison, S. P., Prentice, I. C., Anderson, P. M., Andreev, A. A., Bartlein, P. J., Christensen, T. R., Cramer, W., Kaplan, J. O., Lozhkin, A. V., Matveyeva,

N. V., Murray, D. F., McGuire, A. D., Razzhivin, V. Y., Ritchie, J. C., Smith, B., Walker, D. A., … Volkova, V. S. (2003). Climate change and Arctic ecosystems: 1. Vegetation changes north of 55°N between the last glacial maximum, mid-Holocene, and present. Journal of Geophysical Research: Atmospheres, 108(D19). https://doi.org/10.1029/2002JD002558.

Blaauw, M., Christen, J. A., Lopez, M. A. A., Vazquez, J. E. Gonzalez O. M. V. Belding, T., Theiler, J, Gough, B., & Karney, C. (2021). rbacon: Age-depth modelling using Bayesian statistics (2.5.6) [R]. https://CRAN.R-project.org/package=rbacon.

Blois, J. L., Williams, J. W., Fitzpatrick, M. C., Jackson, S. T., & Ferrier, S. (2013). Space can substitute for time in predicting climate-change effects on biodiversity. Proceedings of the National Academy of Sciences of the United States of America, 110(23), 9374– 9379. https://doi.org/10.1073/pnas.1220228110.

Bozilova, E., & Tonkov, S. (1995). Advances in Holocene palaeoecology in Bulgaria. Pensoft Publishers. https://doi.org/10.1177/095968369600600317.

Bradshaw, R. H., Jones, C. S., Edwards, S. J., & Hannon, G. E. (2015). Forest continuity and conservation value in Western Europe. The Holocene, 25(1), 194– 202. https://doi.org/10.1177/0959683614556378.

Buchhorn, M., Lesiv, M., Tsendbazar, N.-E., Herold, M., Bertels, L., & Smets, B. (2020). Copernicus global land cover layers—Collection 2. Remote Sensing, 12(6), 1044. https://doi.org/10.3390/rs12061044.

Bunting, M. J., Gaillard, M.-J., Sugita, S., Middleton, R., & Broström, A. (2004). Vegetation structure and pollen source area. The Holocene, 14(5), 651– 660. https://doi.org/10.1191/0959683604hl744rp

Caballero-Rodríguez, D., Lozano-García, S., & Correa-Metrio, A. (2017). Vegetation assemblages of Central Mexico through the late quaternary: Modern analogs and compositional turnover. Journal of Vegetation Science. https://doi.org/10.1111/jvs.12515.

Carrillo, H., Brodersen, K. H., & Castellanos, J. A. (2014). Probabilistic performance evaluation for multiclass classification using the posterior balanced accuracy. In M. A. Armada, A. Sanfeliu, & M. Ferre (Eds.), ROBOT2013: First Iberian robotics conference: Advances in robotics (Vol. 252, pp. 347–361). Springer International Publishing. https://doi.org/10.1007/978-3-319-03413-3_25.

CCI Land Cover. (2017). Release of a 1992–2015 time series of annual global land cover maps at 300 M. https://www.esa-landcover-cci.org/index.php?q=webfm_send/88.

Cole, K. L. (2010). Vegetation response to early Holocene warming as an analog for current and future changes. Conservation Biology, 24(1), 29– 37. https://doi.org/10.1111/j.1523-1739.2009.01406.x.

Connor, S., & Kvavadze, E. V. (2009). Modelling late Quaternary changes in plant distribution, vegetation and climate using pollen data from Georgia, Caucasus. Journal of Biogeography, 36(3), 529– 545. https://doi.org/10.1111/j.1365-2699.2008.02019.x.

Correa-Metrio, A., Bush, M. B., Cabrera, K. R., Sully, S., Brenner, M., Hodell, D. A., Escobar, J., & Guilderson, T. (2012). Rapid climate change and no-analog vegetation in lowland Central America during the last 86,000 years. Quaternary Science Reviews, 38, 63– 75. https://doi.org/10.1016/j.quascirev.2012.01.025.

Edwards, K. J., Fyfe, R. M., & Jackson, S. T. (2017). The first 100 years of pollen analysis. Nature Plants, 3(2), 1– 4. https://doi.org/10.1038/nplants.2017.1.

Edwards, M. E., Anderson, P. M., Brubaker, L. B., Ager, T. A., Andreev, A. A., Bigelow, N. H., Cwynar, L. C., Eisner, W. R., Harrison, S. P., Hu, F.-S., Jolly, D., Lozhkin, A. V., MacDonald, G. M., Mock, C. J., Ritchie, J. C., Sher, A. V., Spear, R. W., Williams, J. W., & Yu, G. (2000). Pollen-based biomes for Beringia 18,000, 6000 and 0 14C yr bp. Journal of Biogeography, 27(3), 521– 554. https://doi.org/10.1046/j.1365-2699.2000.00426.x.

Elenga, H., Peyron, O., Bonnefille, R., Jolly, D., Cheddadi, R., Guiot, J., Andrieu, V., Bottema, S., Buchet, G., Beaulieu, J.-L. D., Hamilton, A. C., Maley, J., Marchant, R., Perez-Obiol, R., Reille, M., Riollet, G., Scott, L., Straka, H., Taylor, D., … Jonson, H. (2000). Pollen-based biome reconstruction for southern Europe and Africa 18,000 yr bp. Journal of Biogeography, 27(3), 621– 634. https://doi.org/10.1046/j.1365-2699.2000.00430.x.

Foley, A. M., Dalmonech, D., Friend, A. D., Aires, F., Archibald, A. T., Bartlein, P., Bopp, L., Chappellaz, J., Cox, P., Edwards, N. R., Feulner, G., Friedlingstein, P., Harrison, S. P., Hopcroft, P. O., Jones, C. D., Kolassa, J., Levine, J. G., Prentice, I. C., Pyle, J., … Zaehle, S. (2013). Evaluation of biospheric components in earth system models using modern and palaeo-observations: The state-of-the-art. Biogeosciences, 10(12), 8305– 8328. https://doi.org/10.5194/bg-10-8305-2013.

Fyfe, R., Roberts, N., & Woodbridge, J. (2010). A pollen-based pseudobiomisation approach to anthropogenic land-cover change. The Holocene, 20(7), 1165– 1171. https://doi.org/10.1177/0959683610369509.

Fyfe, R., Woodbridge, J., & Roberts, N. (2015). From forest to farmland: Pollen-inferred land cover change across Europe using the pseudobiomization approach. Global Change Biology, 21(3), 1197– 1212. https://doi.org/10.1111/gcb.12776.

Fyfe, R. M., Woodbridge, J., & Roberts, C. N. (2018). Trajectories of change in Mediterranean Holocene vegetation through classification of pollen data. Vegetation History and Archaeobotany, 27(2), 351– 364. https://doi.org/10.1007/s00334-017-0657-4.

Gaillard, M.-J., Birks, H. J. B., Emanuelsson, U., Karlsson, S., Lagerås, P., & Olausson, D. (1994). Application of modern pollen/land-use relationships to the interpretation of pollen

diagrams—Reconstructions of land-use history in South Sweden, 3000-0 BP. Review of Palaeobotany and Palynology, 82(1), 47–73. https://doi.org/10.1016/0034-6667(94)90019-1.

Gaillard, M.-J., Sugita, S., Mazier, F., Trondman, A.-K., Broström, A., Hickler, T., Kaplan, J. O., Kjellström, E., Kokfelt, U., Kuneš, P., Lemmen, C., Miller, P., Olofsson, J., Poska, A., Rundgren, M., Smith, B., Strandberg, G., Fyfe, R., Nielsen, A. B., … Seppä, H. (2010). Holocene land-cover reconstructions for studies on land cover-climate feedbacks. Climate of the Past, 6(4), 483–499. https://doi.org/10.5194/cp-6-483-2010.

Gavin, D. G., Oswald, W. W., Wahl, E. R., & Williams, J. W. (2003). A statistical approach to evaluating distance metrics and analog assignments for pollen records. Quaternary Research, 60(3), 356–367. https://doi.org/10.1016/S0033-5894(03)00088-7.

Gong, P., Wang, J., Yu, L., Zhao, Y., Zhao, Y., Liang, L., Niu, Z., Huang, X., Fu, H., Liu, S., Li, C., Li, X., Fu, W., Liu, C., Xu, Y., Wang, X., Cheng, Q., Hu, L., Yao, W., … Chen, J. (2013). Finer resolution observation and monitoring of global land cover: First mapping results with Landsat TM and ETM+ data. International Journal of Remote Sensing, 34(7), 2607–2654. https://doi.org/10.1080/01431161.2012.748992.

Grandini, M., Bagli, E., & Visani, G. (2020). Metrics for multi-class classification: An overview. ArXiv: 2008.05756.

Harrison, S. P. (2019). Modern pollen data for climate reconstructions, version 1 (SMPDS) [data set]. University of Reading. https://doi.org/10.17864/1947.194.

Harrison, S. P. (2020). Climate reconstructions for the SMPDSv1 modern pollen data set [data set]. Zenodo. https://doi.org/10.5281/zenodo.3605003.

Harrison, S. P., Gaillard, M.-J., Stocker, B. D., Vander Linden, M., Klein Goldewijk, K., Boles, O., Braconnot, P., Dawson, A., Fluet-Chouinard, E., Kaplan, J. O., Kastner, T., Pausata, F. S. R., Robinson, E., Whitehouse, N. J., Madella, M., & Morrison, K. D. (2020). Development and testing scenarios for implementing land use and land cover changes during the Holocene in earth system model experiments. Geoscientific Model Development, 13(2), 805–824. https://doi.org/10.5194/gmd-13-805-2020.

Harrison, S. P., & Marinova, E. (2017). EMBSeCBIO modern pollen biomisation [data set]. University of Reading. https://doi.org/10.17864/1947.109.

Harrison, S. P., Marinova, E., & Cruz-Silva, E. (2021). EMBSeCBIO pollen database [data set]. University of Reading. https://doi.org/10.17864/1947.309.

Harrison, S. P., Yu, G., Takahara, H., & Prentice, I. C. (2001). Diversity of temperate plants in East Asia. Nature, 413(6852), 129–130. https://doi.org/10.1038/35093166.

Hengl, T., Walsh, M. G., Sanderman, J., Wheeler, I., Harrison, S. P., & Prentice, I. C. (2018). Global mapping of potential natural vegetation: An assessment of machine learning algorithms for estimating land potential. PeerJ, 6, e5457. https://doi.org/10.7717/peerj.5457.

Heung, B., Ho (Derrick), H. C., Zhang, J., Knudby, A., Bulmer, C., & Schmidt, M. (2016). An overview and comparison of machine-learning techniques for classification purposes in digital soil mapping. Geoderma, 265, 62–77. https://doi.org/10.1016/j.geoderma.2015.11.014.

Huntley, B., & Birks, H. J. B. (1983). An atlas of past and present pollen maps of Europe: 0–13,000 years ago. Cambridge University Press. https://doi.org/10.1016/0034-6667(86)90044-8

Jackson, S. T., & Overpeck, J. T. (2000). Responses of plant populations and communities to environmental changes of the late Quaternary. Paleobiology, 26(4), 194–220.

Jackson, S. T., & Williams, J. W. (2004). Modern analogs in Quaternary paleoecology: Here today, gone yesterday, gone tomorrow? Annual Review of Earth and Planetary Sciences, 32, 495– 537. https://doi.org/10.1146/annurev.earth.32.101802.120435.

Jackson, S. T., & Wong, A. (1994). Using forest patchiness to determine pollen source areas of closed-canopy pollen assemblages. Journal of Ecology, 82(1), 89– 99. https://doi.org/10.2307/2261389.

Jolly, D., Prentice, I. C., Bonnefille, R., Ballouche, A., Bengo, M., Brenac, P., Buchet, G., Burney, D., Cazet, J.-P., Cheddadi, R., Edorh, T., Elenga, H., Elmoutaki, S., Guiot, J., Laarif, F., Lamb, H., Lezine, A.-M., Maley, J., Mbenza, M., … Waller, M. (1998). Biome reconstruction from pollen and plant macrofossil data for Africa and the Arabian peninsula at 0 and 6000 years. Journal of Biogeography, 25(6), 1007–1027. https://doi.org/10.1046/j.1365-2699.1998.00238.x.

Jones, R. A., Williams, J. W., & Jackson, S. T. (2017). Vegetation history since the last glacial maximum in the Ozark highlands (USA): A new record from Cupola Pond, Missouri. Quaternary Science Reviews, 170, 174–187. https://doi.org/10.1016/j.quascirev.2017.06.024.

Kaplan, J. O., Bigelow, N. H., Prentice, I. C., Harrison, S. P., Bartlein, P. J., Christensen, T. R., Cramer, W., Matveyeva, N. V., McGuire, A. D., Murray, D. F., Razzhivin, V. Y., Smith, B., Walker, D. A., Anderson, P. M., Andreev, A. A., Brubaker, L. B., Edwards, M. E., & Lozhkin, A. V. (2003). Climate change and Arctic ecosystems: 2. Modeling, paleodata-model comparisons, and future projections. Journal of Geophysical Research: Atmospheres, 108(D19). https://doi.org/10.1029/2002JD002559.

Leroy, S. A. G., Marco, S., Bookman, R., & Miller, C. S. (2010). Impact of earthquakes on agriculture during the Roman–Byzantine period from pollen records of the Dead Sea laminated sediment. Quaternary Research, 73(2), 191– 200. https://doi.org/10.1016/j.yqres.2009.10.003.

Marchant, R., Behling, H., Berrio, J. C., Cleef, A., Duivenvoorden, J., Hooghiemstra, H., Kuhry, P., Melief, B., Geel, B. V., der Hammen, T. V., Reenen, G. V., & Wille, M. (2001). Mid- to late-Holocene

pollen-based biome reconstructions for Colombia. Quaternary Science Reviews, 20(12), 1289–1308. https://doi.org/10.1016/S0277-3791(00)00182-7.

Marchant, R., Cleef, A., Harrison, S. P., Hooghiemstra, H., Markgraf, V., van Boxel, J., Ager, T., Almeida, L., Anderson, R., Baied, C., Behling, H., Berrio, J. C., Burbridge, R., Björck, S., Byrne, R., Bush, M., Duivenvoorden, J., Flenley, J., De Oliveira, P., … Wille, M. (2009). Pollen-based biome reconstructions for Latin America at 0, 6000 and 18 000 radiocarbon years ago. Climate of the Past, 5, 725–767. https://doi.org/10.5194/cp-5-725-2009.

Marinova, E., Harrison, S. P., Bragg, F., Connor, S., de Laet, V., Leroy, S. A. G., Mudie, P., Atanassova, J., Bozilova, E., Caner, H., Cordova, C., Djamali, M., Filipova-Marinova, M., Gerasimenko, N., Jahns, S., Kouli, K., Kotthoff, U., Kvavadze, E., Lazarova, M., … Tonkov, S. (2018). Pollen-derived biomes in the eastern Mediterranean–Black Sea–Caspian-corridor. Journal of Biogeography, 45(2), 484–499. https://doi.org/10.1111/jbi.13128.

Overpeck, J. T., Webb, R. S., & Webb, T., III. (1992). Mapping eastern North American vegetation change of the past 18 ka: No-analogs and the future. Geology, 20(12), 1071–1074. https://doi.org/10.1130/0091-7613(1992)020<1071:MENAVC>2.3.CO;2.

Overpeck, J. T., Webb, T., & Prentice, I. C. (1985). Quantitative interpretation of fossil pollen spectra: Dissimilarity coefficients and the method of modern analogs. Quaternary Research, 23(01), 87–108. https://doi.org/10.1016/0033-5894(85)90074-2.

Pickett, E. J., Harrison, S. P., Hope, G., Harle, K., Dodson, J. R., Peter Kershaw, A., Prentice, I. C., Backhouse, J., Colhoun, E. A., D'Costa, D., Flenley, J., Grindrod, J., Haberle, S., Hassell, C., Kenyon, C., Macphail, M., Martin, H., Martin, A. H., McKenzie, M., … Ward, J. (2004). Pollen-based reconstructions of biome distributions for Australia, Southeast Asia and the Pacific (SEAPAC region) at 0, 6000 and 18,000 14C yr BP. Journal of Biogeography, 31(9), 1381–1444. https://doi.org/10.1111/j.1365-2699.2004.01001.x.

Prentice, I. C. (1985). Pollen representation, source area, and basin size: Toward a unified theory of pollen analysis. Quaternary Research, 23(1), 76–86. https://doi.org/10.1016/0033-5894(85)90073-0

Prentice, I. C. (1986). Vegetation responses to past climatic variation. Vegetatio, 67(2), 131–141. https://doi.org/10.1007/BF00037363.

Prentice, I. C. (1988). Records of vegetation in time and space: The principles of pollen analysis. In B. Huntley & T. Webb (Eds.), Vegetation History (pp. 17–42). Springer. https://doi.org/10.1007/978-94-009-3081-0_2.

Prentice, I. C., Guiot, J., Huntley, B., Jolly, D., & Cheddadi, R. (1996). Reconstructing biomes from palaeoecological data: A general method and its application to European pollen data at 0 and 6 ka. Climate Dynamics, 12, 185–194. https://doi.org/10.1007/BF00211617.

Prentice, I. C., Jolly, D., & BIOME 6000 Participants. (2000). Mid-Holocene and glacial-maximum vegetation geography of the northern continents and Africa. Journal of Biogeography, 27(3), 507–519. https://doi.org/10.1046/j.1365-2699.2000.00425.x.

Prentice, I. C., & Parsons, R. W. (1983). Maximum likelihood linear calibration of pollen spectra in terms of forest composition. Biometrics, 39(4), 1051–1057. https://doi.org/10.2307/2531338.

Prentice, I. C., & Webb, T. (1998). BIOME 6000: Reconstructing global mid-Holocene vegetation patterns from palaeoecological records. Journal of Biogeography, 25(6), 997–1005.

Reimer, P., Austin, W. E. N., Bard, E., Bayliss, A., Blackwell, P. G., Ramsey, C. B., Butzin, M., Cheng, H., Edwards, R. L., Friedrich, M., Grootes, P. M., Guilderson, T. P., Hajdas, I., Heaton, T. J., Hogg, A. G., Hughen, K. A., Kromer, B., Manning, S. W., Muscheler, R., … Talamo, S. (2020). The IntCal20 northern hemisphere radiocarbon age calibration curve (0–55 cal kBP). Radiocarbon, 62(4). https://doi.org/10.1017/RDC.2020.41.

Song, J.-N., Fu, G., Xu, Y., Han, Z.-Y., Sun, Q.-Z., & Wang, H. (2021). Assessment of the capability of CMIP6 global climate models to simulate Arctic cyclones. Advances in Climate Change Research, 12(5), 660–676. https://doi.org/10.1016/j.accre.2021.07.007.

Sugita, S. (1993). A model of pollen source area for an entire lake surface. Quaternary Research, 39(2), 239–244. https://doi.org/10.1006/qres.1993.1027.

Sugita, S. (2007a). Theory of quantitative reconstruction of vegetation II: All you need is LOVE. The Holocene, 17(2), 243–257. https://doi.org/10.1177/0959683607075838.

Sugita, S. (2007b). Theory of quantitative reconstruction of vegetation I: Pollen from large sites REVEALS regional vegetation composition. The Holocene, 17(2), 229–241. https://doi.org/10.1177/0959683607075837.

Sulla-Menashe, D., Gray, J. M., Abercrombie, S. P., & Friedl, M. A. (2019). Hierarchical mapping of annual global land cover 2001 to present: The MODIS collection 6 land cover product. Remote Sensing of Environment, 222, 183–194. https://doi.org/10.1016/j.rse.2018.12.013.

Takahara, H., Sugita, S., Harrison, S. P., Miyoshi, N., Morita, Y., & Uchiyama, T. (2000). Pollen-based reconstructions of Japanese biomes at 0, 6000 and 18,000 14C yr bp. Journal of Biogeography, 27(3), 665–683. https://doi.org/10.1046/j.1365-2699.2000.00432.x.

Tarasov, P. E., Andreev, A. A., Anderson, P. M., Lozhkin, A. V., Leipe, C., Haltia, E., Nowaczyk, N. R., Wennrich, V., Brigham-Grette, J., & Melles, M. (2013). A pollen-based biome reconstruction over the last 3.562 million years in the Far East Russian Arctic—New insights into climate-vegetation relationships at the regional scale. Climate of the Past, 9(6), 2759–2775. https://doi.org/10.5194/cp-9-2759-2013.

Tarasov, P. E., Webb, T., III, Andreev, A. A., Afanas'eva, N. B., Berezina, N. A., Bezusko, L. G., Blyakharchuk, T. A., Bolikhovskaya, N. S., Cheddadi, R., Chernavskaya, M. M., Chernova, G. M.,

Dorofeyuk, N. I., Dirksen, V. G., Elina, G. A., Filimonova, L. V., Glebov, F. Z., Guiot, J., Gunova, V. S., Harrison, S. P., … Zernitskaya, V. P. (1998). Present-day and mid-Holocene biomes reconstructed from pollen and plant macrofossil data from the former Soviet Union and Mongolia. Journal of Biogeography, 25(6), 1029–1053. https://doi.org/10.1046/j.1365-2699.1998.00236.x.

Theuerkauf, M., & Couwenberg, J. (2018). ROPES reveals past land cover and PPEs from single pollen records. Frontiers in Earth Science, 6. https://doi.org/10.3389/feart.2018.00014.

Thiele, C. (2021). Cutpointr: Determine and evaluate optimal Cutpoints in binary classification task (1.1.1) [Computer software]. https://cran.r-project.org/web/packages/cutpointr/vignettes/cutpointr.html.

Thompson, R. S., & Anderson, K. H. (2000). Biomes of western North America at 18,000, 6000 and 0 14C yr bp reconstructed from pollen and packrat midden data. Journal of Biogeography, 27(3), 555– 584. https://doi.org/10.1046/j.1365-2699.2000.00427.x.

Tsendbazar, N., Herold, M., Li, L., Tarko, A., de Bruin, S., Masiliunas, D., Lesiv, M., Fritz, S., Buchhorn, M., Smets, B., Van De Kerchove, R., & Duerauer, M. (2021). Towards operational validation of annual global land cover maps. Remote Sensing of Environment, 266, 112686. https://doi.org/10.1016/j.rse.2021.112686.

Turner, B. L., & Sabloff, J. A. (2012). Classic period collapse of the central Maya lowlands: Insights about human-environment relationships for sustainability. Proceedings of the National Academy of Sciences of the United States of America, 109(35), 13908– 13914. https://doi.org/10.1073/pnas.1210106109.

Turner, M. G., Wei, D., Prentice, I. C., & Harrison, S. P. (2021). The impact of methodological decisions on climate reconstructions using WA-PLS. Quaternary Research, 99, 341– 356. https://doi.org/10.1017/qua.2020.44.

Villegas-Diaz, R., Cruz-Silva, E., & Harrison, S. P. (2021). ageR: Supervised age models [R]. Zenodo. https://doi.org/10.5281/zenodo.4636716.

Wang, Y., Shipley, B. R., Lauer, D. A., Pineau, R. M., & McGuire, J. L. (2020). Plant biomes demonstrate that landscape resilience today is the lowest it has been since end-Pleistocene megafaunal extinctions. Global Change Biology, 26(10), 5914– 5927. https://doi.org/10.1111/gcb.15299.

Wei, D., Prentice, I. C., & Harrison, S. P. (2020). The climatic space of European pollen taxa. Ecology, 101(8), e03055. https://doi.org/10.1002/ecy.3055.

Williams, J. W., & Jackson, S. T. (2007). Novel climates, no-analog communities, and ecological surprises. Frontiers in Ecology and the Environment, 5(9), 475– 482. https://doi.org/10.1890/070037.

Williams, J. W., Summers, R. L., & Webb, T., III. (1998). Applying plant functional types to construct biome maps from eastern North American pollen data: Comparisons with model results. Quaternary Science Reviews, 17(6), 607– 627. https://doi.org/10.1016/S0277-3791(98)00014-6.

Williams, J. W., Tarasov, P., Brewer, S., & Notaro, M. (2011). Late Quaternary variations in tree cover at the northern forest-tundra ecotone. Journal of Geophysical Research Biogeosciences, 116(G1). https://doi.org/10.1029/2010JG001458.

Williams, J. W., Webb, T., Richard, P. H., & Newby, P. (2000). Late Quaternary biomes of Canada and the eastern United States. Journal of Biogeography, 27(3), 585– 607. https://doi.org/10.1046/j.1365-2699.2000.00428.x.

Woodbridge, J., Fyfe, R. M., & Roberts, N. (2014). A comparison of remotely sensed and pollen-based approaches to mapping Europe's land cover. Journal of Biogeography, 41(11), 2080– 2092. https://doi.org/10.1111/jbi.12353.

Yu, G., Chen, X., Ni, J., Cheddadi, R., Guiot, J., Han, H., Harrison, S. P., Huang, C., Ke, M., Kong, Z., Li, S., Li, W., Liew, P., Liu, G., Liu, J., Liu, Q., Liu, K.-B., Prentice, I. C., Qui, W., … Zheng, Z. (2000). Palaeovegetation of China: A pollen data-based synthesis for the mid-Holocene and Last Glacial Maximum. Journal of Biogeography, 27(3), 635– 664. https://doi.org/10.1046/j.1365-2699.2000.00431.x.

Yu, G., Prentice, I. C., Harrison, S. P., & Sun, X. (1998). Pollen-based biome reconstructions for China at 0 and 6000 years. Journal of Biogeography, 25(6), 1055– 1069. https://doi.org/10.1046/j.1365-2699.1998.00237.x.

Zanon, M., Davis, B. A. S., Marquer, L., Brewer, S., & Kaplan, J. O. (2018). European forest cover during the past 12,000 years: A palynological reconstruction based on modern analogs and remote sensing. Frontiers in Plant Science, 9, 253. https://doi.org/10.3389/fpls.2018.00253.

2.8 Supplement

Supplementary Figure 2.1: Number of modern pollen samples allocated to each biome. The biomes were derived from the Potential Natural Vegetation (PNV) Map of Hengl et al. (2018) using a search window of 20 km x 20 km. This figure illustrates the extremely uneven nature of the sampling of biomes in the combined SPECIAL Modern Pollen Data Set (SMPDS) and the Eastern Mediterranean-Black Sea Caspian Corridor (EMBSeCBIO) database used for the training and testing datasets, and hence the necessity for down-weighting the representation of some biomes. The biome codes are: WTFS: warm-temperate evergreen needleleaf and sclerophyll broadleaf forest, CMIX: cool mixed evergreen needleleaf and deciduous broadleaf forest, TEDE: temperate deciduous malacophyll broadleaf forest, CENF: cold evergreen needleleaf forest, XSHB: xeric shrubland, ENWD: evergreen needleleaf woodland, GRAM: graminoids with forbs, DESE: desert, TUND: tundra.

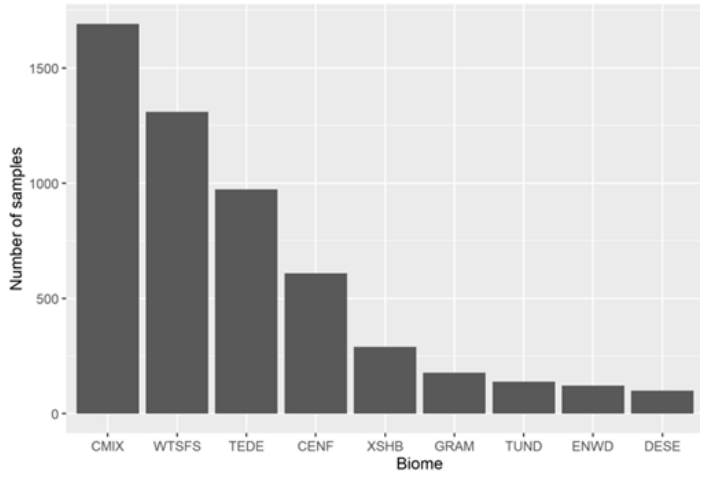

Supplementary Figure 2.2: Box and whisker plots showing the 25 most abundant taxa in each biome. The boxes show the median and standard deviation of the abundance of individual taxa, the whiskers show the 85% confidence interval, and the open circles show outliers. The biomes are: tundra (TUND), desert (DESE), graminoids with forbs (GRAM), evergreen needleleaf woodland (ENWD), xeric shrubland (XSHB), cold evergreen needleleaf forest (CENF), temperate malacophyll broadleaf forest (TEDE), cool mixed evergreen needleleaf and deciduous broadleaf forest (CMIX), warm-temperate evergreen needleleaf and sclerophyll broadleaf forest (WTFS).

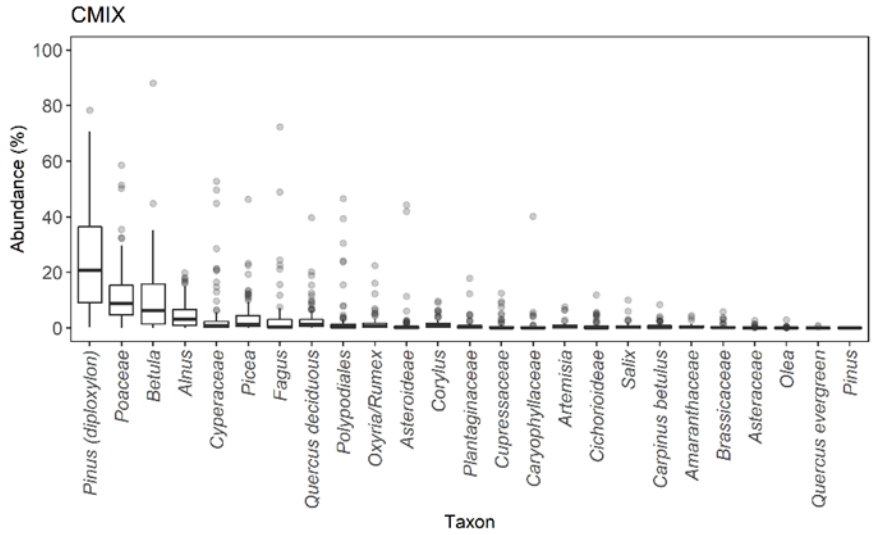

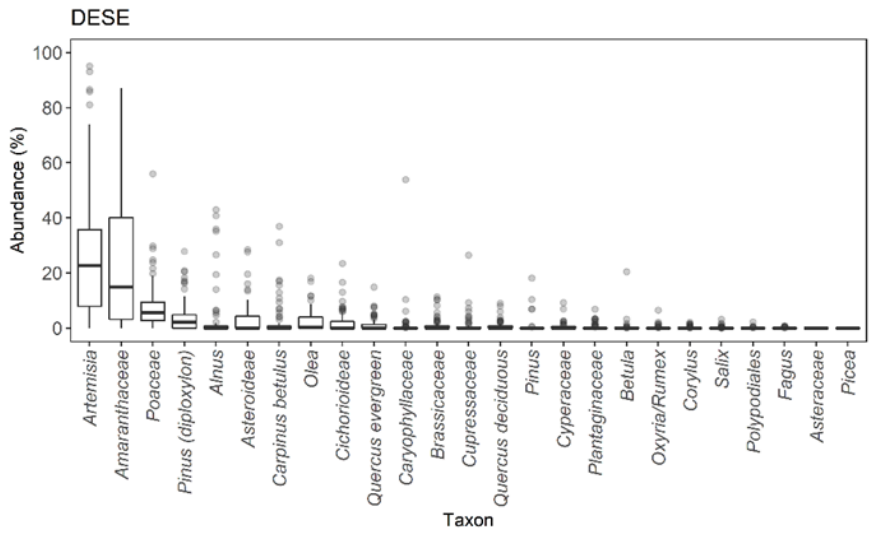

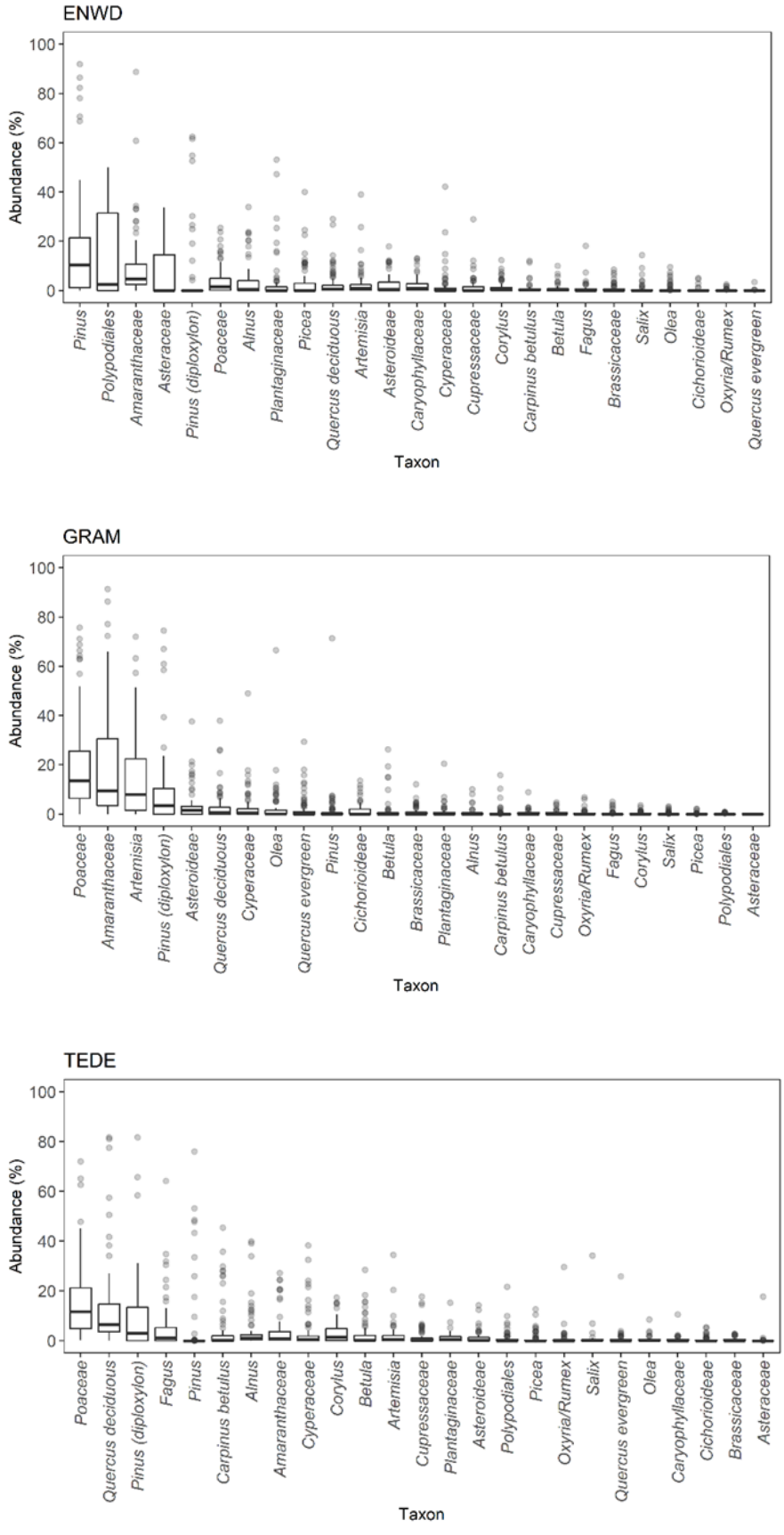
ENWD
Abundance (%)
100
80
60
40
20
0
Pinus
Polypodiales
Amaranthaceae
Asteraceae
Pinus (diploxylon)
Poaceae
Alnus
Plantaginaceae
Picea
Quercus deciduous
Artemisia
Asteroideae
Caryophyllaceae
Cyperaceae
Cupressaceae
Corylus
Carpinus betulus
Betula
Fagus
Brassicaceae
Salix
Olea
Cichorioideae
Oxyria/Rumex
Quercus evergreen
Taxon
GRAM
Abundance (%)
100
80
60
40
20
0
Poaceae
Amaranthaceae
Artemisia
Pinus (diploxylon)
Asteroideae
Quercus deciduous
Cyperaceae
Olea
Quercus evergreen
Pinus
Cichorioideae
Betula
Brassicaceae
Plantaginaceae
Alnus
Carpinus betulus
Caryophyllaceae
Cupressaceae
Oxyria/Rumex
Fagus
Corylus
Salix
Picea
Polypodiales
Asteraceae
Taxon
TEDE
Abundance (%)
100
80
60
40
20
0
Poaceae
Quercus deciduous
Pinus (diploxylon)
Fagus
Pinus
Carpinus betulus
Alnus
Amaranthaceae
Cyperaceae
Corylus
Betula
Artemisia
Cupressaceae
Plantaginaceae
Asteroideae
Polypodiales
Picea
Oxyria/Rumex
Salix
Quercus evergreen
Olea
Caryophyllaceae
Cichorioideae
Brassicaceae
Asteraceae
Taxon

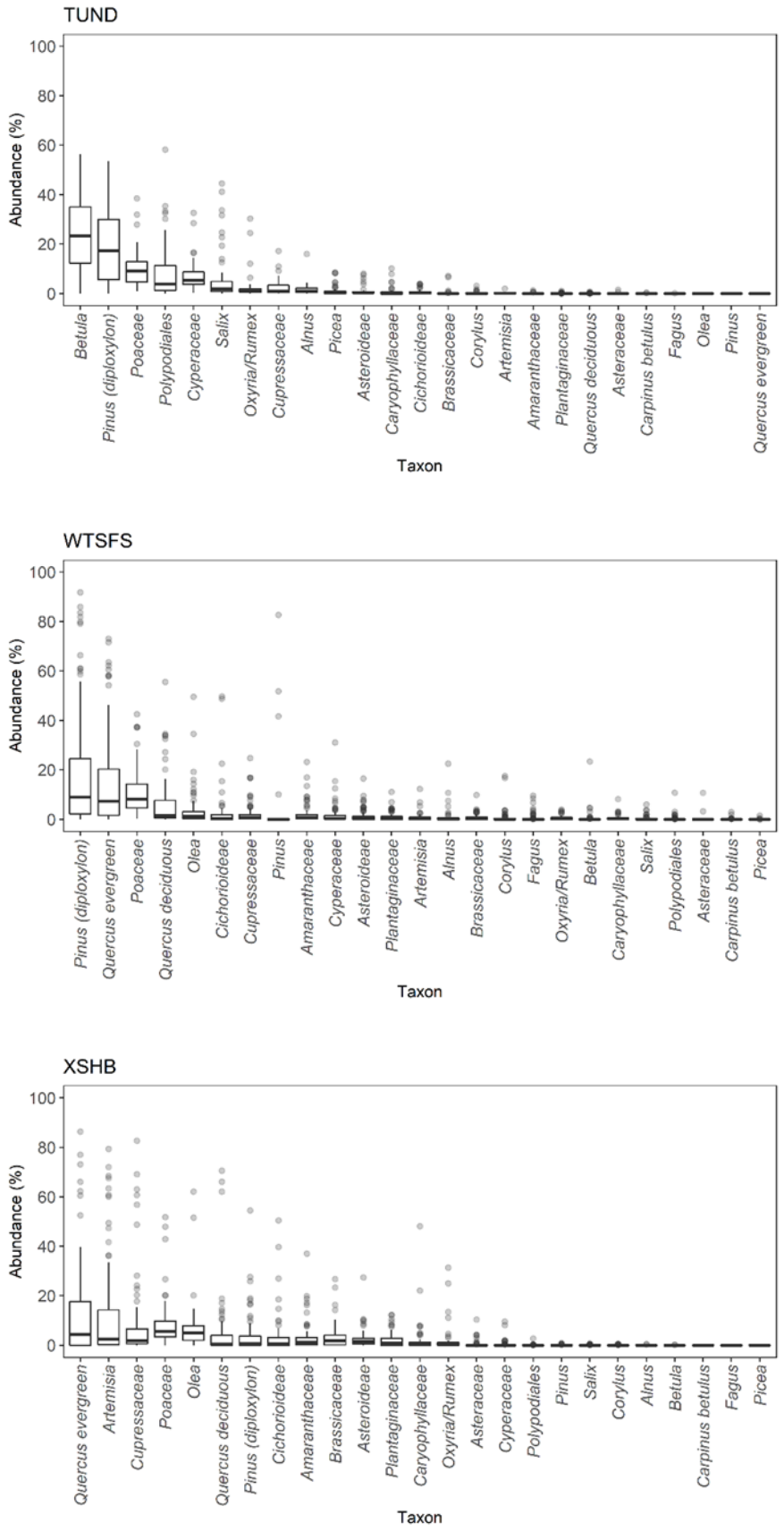
TUND
Abundance (%)
100
80
60
40
20
0
Betula
Pinus (diploxylon)
Poaceae
Polypodiales
Cyperaceae
Salix
Oxyria/Rumex
Cupressaceae
Alnus
Picea
Asteroideae
Caryophyllaceae
Cichorioideae
Brassicaceae
Corylus
Artemisia
Amaranthaceae
Plantaginaceae
Quercus deciduous
Asteraceae
Carpinus betulus
Fagus
Olea
Pinus
Quercus evergreen
Taxon
WTSFS
Abundance (%)
100
80
60
40
20
0
Pinus (diploxylon)
Quercus evergreen
Poaceae
Quercus deciduous
Olea
Cichorioideae
Cupressaceae
Pinus
Amaranthaceae
Cyperaceae
Asteroideae
Plantaginaceae
Artemisia
Alnus
Brassicaceae
Corylus
Fagus
Oxyria/Rumex
Betula
Caryophyllaceae
Salix
Polypodiales
Asteraceae
Carpinus betulus
Picea
Taxon
XSHB
Abundance (%)
100
80
60
40
20
0
Quercus evergreen
Artemisia
Cupressaceae
Poaceae
Olea
Quercus deciduous
Pinus (diploxylon)
Cichorioideae
Amaranthaceae
Brassicaceae
Asteroideae
Plantaginaceae
Caryophyllaceae
Oxyria/Rumex
Asteraceae
Cyperaceae
Polypodiales
Pinus
Salix
Corylus
Alnus
Betula
Carpinus betulus
Fagus
Picea
Taxon

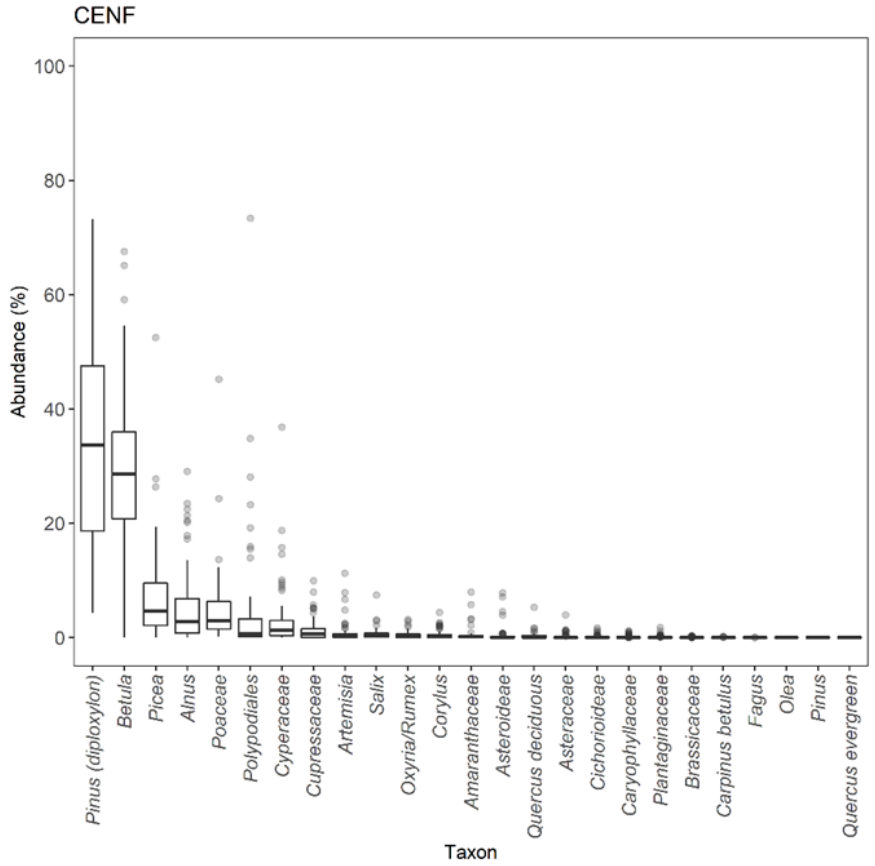
CENF
Abundance (%)
100
80
60
40
20
0
Pinus (diploxylon)
Betula
Picea
Alnus
Poaceae
Polypodiales
Cyperaceae
Cupressaceae
Artemisia
Salix
Oxyria/Rumex
Corylus
Amaranthaceae
Asteroideae
Quercus deciduous
Asteraceae
Cichorioideae
Caryophyllaceae
Plantaginaceae
Brassicaceae
Carpinus betulus
Fagus
Olea
Pinus
Quercus evergreen
Taxon

Supplementary Figure 2.3: Density distribution of similarity scores to every biome for samples assigned graminoids with forbs (GRAM) and cool mixed evergreen needleleaf and deciduous broadleaf forest (CMIX) according to the Potential Natural Vegetation (PNV) Map of Hengl et al. (2018). The biomes are: tundra (TUND), desert (DESE), graminoids with forbs (GRAM), evergreen needleleaf woodland (ENWD), xeric shrubland (XSHB), cold evergreen needleleaf forest (CENF), temperate malacophyll broadleaf forest (TEDE), cool mixed evergreen needleleaf and deciduous broadleaf forest (CMIX), warm-temperate evergreen needleleaf and sclerophyll broadleaf forest (WTFS). These plots are used to derive similarity score thresholds to determine samples with potential non-analogue vegetation types.

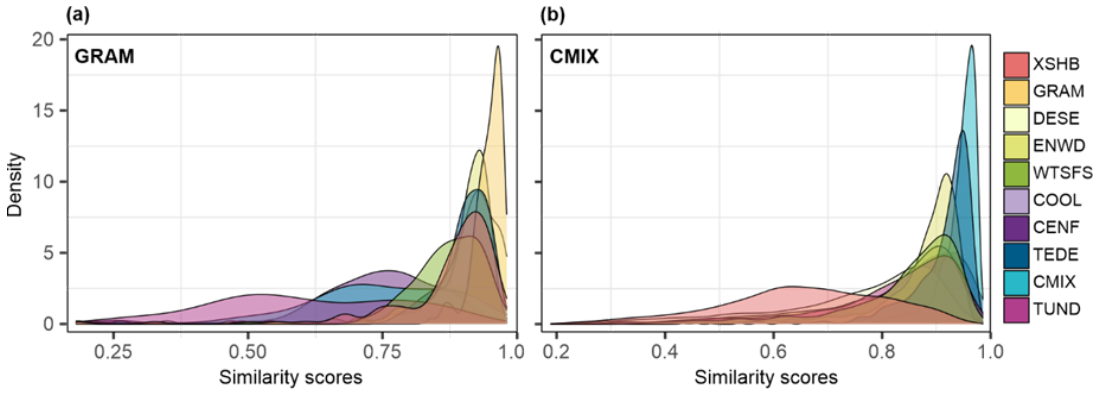

Supplementary Figure 2.4: Measurement of the balance between sensitivity and specificity in the evaluation of possible cut-off points between two biomes for samples assigned to graminoids with forbs (GRAM) and cool mixed evergreen needleleaf and deciduous broadleaf forest (CMIX) according to the Potential Natural Vegetation (PNV) Map of Hengl et al. (2018). The similarity score comparisons are made between GRAM and tundra (TUND) and between CMIX and xeric shrubland (XSHB). The dotted lines show the cut-off point above which the sample would be allocated to GRAM and CMIX respectively.

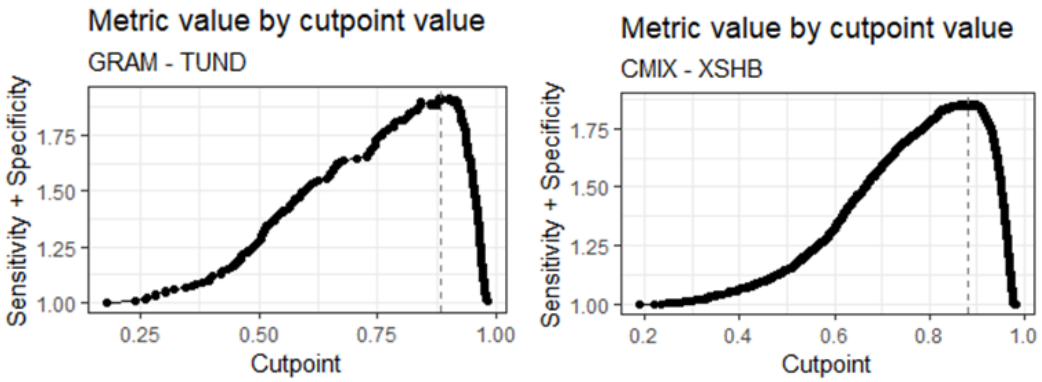

Supplementary Figure 2.5: Optimal threshold detection. Comparison of the distribution of similarity scores for samples allocated to (a) graminoids with forbs (GRAM) and (c) cool mixed evergreen needleleaf and deciduous broadleaf forest (CMIX) according to the Potential Natural Vegetation (PNV) Map of Hengl et al. (2018). The scores for GRAM are compared to scores obtained on these samples for tundra (TUND) and the scores for CMIX are compared to scores obtained on these samples for xeric shrubland (XSHB). The Receiver Operating Characteristic (ROC) curve for (b) the GRAM/TUND and (d) the CMIX/XSHB paired comparisons show the optimal threshold (black dot) in the ROC curve and as a dashed line in the density curves. The area under the ROC curve (AUC) is a measure of the overall ability of the optimal threshold to differentiate between the two biomes being compared. The AUC ranges between 0.5 (ROC curve is a diagonal line – no discrimination between categories as both density distributions are identical) and 1 (ROC curve follow left and upper borders of the ROC graph – perfect discrimination as the density distributions are completely separated).

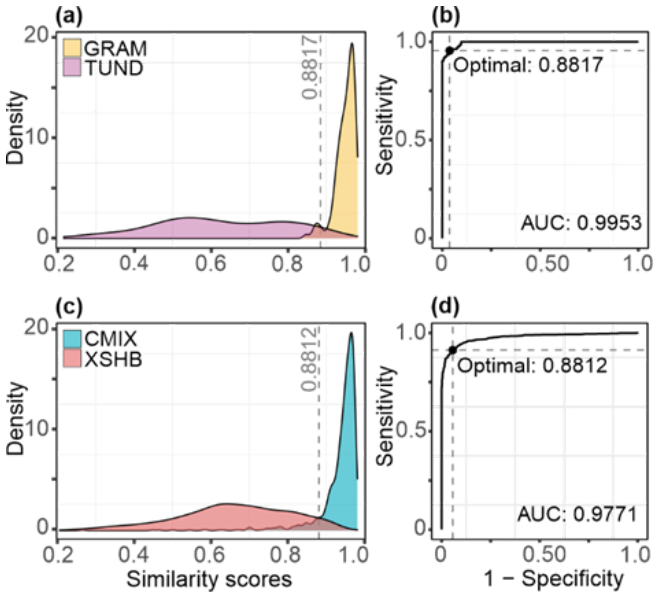

Supplementary Table 2.1: Allocation of pollen taxa found in samples of the Eastern Mediterranean-Black Sea Caspian Corridor (EMBSeCBIO) pollen database into the 247 types represented in the SPECIAL Modern Pollen Data Set (SMPDS) (Harrison, 2019; Wei et al., 2020). The table indicates the taxonomic level of aggregation, the name used for the amalgamated taxon, and the component species or genera included in this taxon.

Taxonomic level	Amalgamated taxon name	Individual taxa included
Genus	*Abies*	*Abies, Abies alba, Abies cilicica, Abies nordmanniana, Abies pinsapo subsp marocana*
Family	Acanthaceae	*Acanthus mollis*
Genus	*Acer*	*Acer, Acer campestre, Acer campestre* type, *Acer pseudoplatanus, Acer* type
Genus	*Aconitum*	*Aconitum, Aconitum group, Aconitum napellus* type, *Aconitum septentrionale, Aconitum* type
Family	Actinidiaceae	*Actinidia*
Genus	*Adonis*	*Adonis, Adonis aestivalis* type, *Adonis* type
Family	Adoxaceae	*Adoxa, Adoxa moschatellina, Adoxa* type
Genus	*Aesculus*	*Aesculus, Aesculus hippocastanum*
Genus	*Ailanthus*	*Ailanthus*
Family	Aizoaceae	*Carpobrotus*
Genus sub-group	*Alnus*	*Alnus, Alnus glutinosa, Alnus glutinosa* type, *Alnus glutinosa/Alnus incana, Alnus incana, Alnus incana* type, *Alnus incana/Alnus cordata* type, *Alnus non-viridis, Alnus* type
Genus sub-group	*Alnus alnobetula*	*Alnus viridis*
Family	Amaranthaceae	*Aellenia* type, Amaranthaceae, *Amaranthus, Atriplex nudicaulis, Chenopodium, Chenopodium album, Halothamnus* type, *Noaea* type

Family	Amaryllidaceae	Amaryllidaceae, *Narcissus*
Family	Anacardiaceae	Anacardiaceae
Genus	*Andromeda*	*Andromeda*
Family	Apiaceae	*Aegopodium, Anthriscus sylvestris* type, *Anthriscus* type, Apiaceae, *Apium, Apium* type, *Astrantia, Astrantia* type, *Athamanta cretensis, Berula erecta* type, *Bunium* type, *Aegopodium podagraria, Bupleurum, Bupleurum* type, *Carum carvi, Chaerophyllum, Chaerophyllum hirsutum* type, *Chaerophyllum* type, *Conopodium, Conopodium majus, Daucaceae, Daucus carota, Ammi* type, *Daucus carota* type, *Daucus* type, *Echinophora, Eryngium, Eryngium ilicifolium, Eryngium* type, *Falcaria* type, *Ferula, Ferula* type, *Heracleum, Angelica, Heracleum laciniatum* type, *Heracleum sphondylium, Heracleum* type, *Laserpitium latifolium* type, *Laserpitium prutenicum, Ligusticum mutellina, Malabaila, Meum, Meum athamanticum, Neogaya simplex* type, *Angelica archangelica, Oenanthe, Oenanthe* type, *Orlaya, Orlaya grandiflora, Pastinaca* type, *Peucedanum, Peucedanum ostruthium, Peucedanum* type, *Pimpinella, Pimpinella major* type, *Angelica* type, *Pimpinella* type, *Pleurospermum austriacum, Sanicula, Sanicula europaea, Sanicula type, Scandix, Seseli* type, *Torilis, Torilis arvensis, Turgenia* type, *Anisosciadium* type, *Anthriscus, Anthriscus sylvestris*
Genus	*Aquilegia*	*Aquilegia* type
Family	Araceae	Araceae
Genus	*Arbutus*	*Arbutus, Arbutus* type, *Arbutus unedo*
Genus	*Arctostaphylos*	*Arctostaphylos, Arctostaphylos uva-ursi*
Genus	*Argania*	*Argania spinosa*
Family	Aristolochiaceae	*Aristolochia*
Genus	*Artemisia*	*Artemisia, Artemisia genipii/Artemisia mutellina, Artemisia herba-alba* type, *Artemisia* type, *Artemisia vulgaris* type
Family	Asclepiadaceae	Asclepiadaceae

Family	Asparagaceae	Asparagaceae, *Asparagus*, *Asparagus* type, *Convallaria*, *Convallaria* type, *Maianthemum bifolium*, *Maianthemum* type, *Ornithogalum type*, *Scilla* type
Family	Asphodelaceae	*Eremurus*
Family	Asphodeliaceae	*Asphodeline*, *Asphodelus*, *Asphodelus albus*, *Asphodelus albus* type, *Asphodelus fistulosus* type, *Asphodelus* type
Family	Asteraceae	Asteraceae
Family sub-group	Asteraceae (Liguliflorae)	Asteraceae (Liguliflorae)
Family sub-group	Asteroideae	*Achillea*, *Antennaria*, *Antennaria* type, *Anthemis*, *Anthemis* type, *Arnica montana*, *Aster*, *Aster bellidiastrum*, *Aster* type, *Aster/Achillea*, *Aster/Achillea* type, *Achillea* type, Asteraceae (Tubuliflorae), Asteroideae, *Bellis*, *Bellis* type, *Bidens*, *Bidens* type, *Calendula*, *Calendula* type, *Chrysanthemum alpinum*, *Doronicum*, *Achillea/Anthemis* type, *Erigeron*, *Eupatorium*, *Eupatorium* type, *Filago* type, *Filifolium sibiricum*, *Gnaphalium*, *Gnaphalium* type, *Helianthus*, *Helianthus* type, *Homogyne*, *Achillea/Aster*, *Homogyne alpina*, *Inula*, *Inula* type, *Logfia* type, *Matricaria* type, *Petasites*, *Petasites* type, *Senecio*, *Senecio* type, *Solidago*, *Adenostyles* type, *Solidago* type, *Solidago virgaurea* type, *Tussilago farfara*, *Tussilago* type, *Xanthium*, *Xanthium spinosum*, *Xanthium strumarium*, *Xanthium* type, *Ambrosia*, *Ambrosia artemisiifolia* type, *Ambrosia* type, *Ambrosia/Xanthium*
Genus	*Astragalus*	*Astragalus*, *Astragalus alpinus* type, *Astragalus* type
Family	Berberidaceae	Berberidaceae
Genus	*Berberis*	*Berberis*, *Berberis vulgaris*, *Mahonia*
Genus	*Betula*	*Betula*, *Betula* type, *Betula alba*, *Betula alba* type, *Betula pendula*, *Betula pendula/Betula pubescens*, *Betula pubescens*, *Betula pubescens* type, *Betula sect. Albae*, *Betula tortuosa*
Genus	*Betula (Chamaebetula)*	*Betula fruticosa*, *Betula humilis/Betula nana*, *Betula nana*, *Betula nana* type

Family	Boraginaceae	*Alkanna, Cynoglossum creticum, Echium, Echium* type, *Echium vulgare, Heliotropium* type, *Lithospermum, Myosotis, Myosotis arvensis* type, *Myosotis* type, *Onosma, Anchusa, Pulmonaria, Pulmonaria* type, *Symphytum, Symphytum* type, *Anchusa arvensis, Anchusa type,* Boraginaceae, *Borago officinalis, Cerinthe, Cerinthe minor, Cerinthe type*
Family	Brassicaceae	*Arabidopsis, Cardamine pratensis* type, *Cardamine* type, *Crambe, Descurainia, Draba, Draba type, Hornungia* type, *Lepidium* type, *Matthiola, Sinapis, Barbarea* type, *Sinapis* type, *Brassica, Brassica* type, Brassicaceae, Brassicaceae type, *Capsella bursa-pastoris* type, *Capsella* type, *Cardamine*
Genus	*Bruckenthalia*	*Bruckenthalia*
Genus	*Buxus*	*Buxus, Buxus sempervirens*
Genus	*Calluna*	*Calluna, Calluna* type, *Calluna vulgaris, Calluna vulgaris* type
Family	Campanulaceae	*Campanula, Phyteuma, Phyteuma* type, *Campanula* type, Campanulaceae, *Jasione, Jasione montana, Jasione* type, *Legousia, Lobelia dortmanna, Lobelia* type
Family	Capparaceae	Capparidaceae, *Capparis, Capparis spinosa, Capparis* type
Family	Caprifoliaceae	Caprifoliaceae, *Scabiosa columbaria* type, *Scabiosa rotata* type, *Scabiosa* type, *Scabiosa/Succisa* type, *Succisa, Succisa pratensis, Succisa pratensis* type, *Succisa* type, *Dipsacaceae, Dipsacus, Dipsacus fullonum* type, *Dipsacus* type, *Knautia, Knautia arvensis, Knautia* type, *Scabiosa*
Genus	*Carduoideae*	*Arctium, Centaurea, Centaurea collina, Centaurea collina* type, *Centaurea cyanus, Centaurea cyanus* type, *Centaurea depressa* type, *Centaurea jacea, Centaurea jacea* type, *Centaurea montana, Centaurea montana* type, *Arctium* type, *Centaurea nigra, Centaurea nigra* type, *Centaurea rhenana* type, *Centaurea scabiosa, Centaurea scabiosa* type, *Centaurea solstitialis, Centaurea solstitialis* type, *Centaurea* type, *Cirsium, Cirsium* type, *Arctium/Jurinea, Cirsium/Carduus, Cirsium/Gundelia, Cousinia, Echinops, Gundelia* type, *Jurinea* type, *Onopordum, Onopordum* type, *Saussurea, Saussurea alpina, Carduoideae, Saussurea* type,

		Serratula, *Serratula* type, *Carduus*, *Carduus* type, *Carlina*, *Carlina* type, *Carthamus*
Genus	*Carpinus betulus*	*Carpinus*, *Carpinus betulus*, *Carpinus betulus* type, *Carpinus* type
Genus	*Carpinus orientalis/Ostrya*	*Carpinus orientalis*, *Carpinus orientalis* type, *Carpinus orientalis/Ostrya*, *Carpinus orientalis/Ostrya carpinifolia*, *Carpinus orientalis/Ostrya carpinifolia* type, *Carpinus/Ostrya*, *Carpinus/Ostrya* type, *Ostrya*, *Ostrya* type
Family	Caryophyllaceae	*Agrostemma githago*, *Cerastium cerastioides* type, *Cerastium fontanum* type, *Cerastium* type, *Cerastium/Stellaria* type, *Corrigiola*, *Dianthus*, *Dianthus superbus* type, *Dianthus* type, *Frankenia*, *Frankenia* type, *Agrostemma* type, *Gypsophila*, *Gypsophila fastigiata*, *Gypsophila repens* type, *Gypsophila* type, *Herniaria*, *Herniaria glabra*, *Herniaria* type, *Herniaria/Paronychia*, *Illecebrum*, *Loeflingia*, *Arenaria*, *Lychnis*, *Lychnis flos-cuculi*, *Lychnis flos-cuculi* type, *Lychnis* type, *Lychnis viscaria* type, *Minuartia*, *Minuartia rubra* type, *Minuartia* type, *Minuartia verna* type, *Moehringia* type, *Arenaria* type, *Paronychia*, *Paronychia type*, *Polycarpon*, *Sagina*, *Sagina procumbens*, *Sagina* type, *Saponaria*, *Scleranthus*, *Scleranthus annuus*, *Scleranthus perennis*, *Caryophyllaceae*, *Scleranthus* type, Silenaceae, *Silene*, *Silene acaulis*, *Silene acaulis* type, *Silene alba* type, *Silene dioica* type, *Silene latifolia*, *Silene rupestris*, *Silene* type, Caryophyllaceae subfam. Silenoideae, *Silene vulgaris type*, *Spergula*, *Spergula arvensis*, *Spergula* type, *Spergularia*, *Spergularia* type, *Stellaria*, *Stellaria holostea*, *Stellaria holostea* type, *Stellaria nemorum*, *Cerastium*, *Stellaria nemorum* type, *Stellaria palustris*, *Stellaria* type, *Vaccaria* type, *Cerastium alpinum* type, *Cerastium arvense* type
Genus	*Cassiope*	*Cassiope*, *Cassiope* type
Genus	*Castanea*	*Castanea*, *Castanea sativa*
Genus	*Cedrus*	*Cedrus*, *Cedrus atlantica*, *Cedrus atlantica* type, *Cedrus libani*
Family	Celastraceae	Celastraceae, *Parnassia*, *Parnassia palustris*
Genus	*Celtis*	*Celtis*, *Celtis australis*
Genus	*Ceratonia*	*Ceratonia*, *Ceratonia siliqua*, *Ceratonia* type

Genus	*Cercis*	*Cercis siliquastrum*
Genus	*Chamaedaphne*	*Chamaedaphne, Chamaedaphne calyculata*
Genus	*Chamaerops*	*Chamaerops*
Genus	*Chimaphila*	*Chimaphila umbellata*
Genus	*Cichorioideae*	*Cichorioideae, Lactuca sativa* type, *Lactuca* type, *Leontodon helveticus, Leontodon* type, *Scorzonera humilis* type, *Scorzonera* type, *Sonchus* type, *Taraxacum, Taraxacum* type, *Cichorium, Cichorium intybus* type, *Cichorium* type, *Crepis, Crepis aurea, Crepis* type, *Hieracium* type, *Lactuca*
Family	Cistaceae	Cistaceae, *Halimium/Tuberaria, Tuberaria*
Genus	*Cistus*	*Cistus, Cistus salviifolius* type, *Cistus* type, *Cistus villosus* type, *Cistus albidus* type, *Cistus incanus, Cistus ladanifer, Cistus ladanifer* type, *Cistus monspeliensis* type, *Cistus populifolius* type, *Cistus salvifolius, Cistus salviifolius*
Genus	*Clematis*	*Clematis, Clematis* type, *Clematis vitalba* type
Genus	*Clethra*	*Clethra*
Family	Clusiaceae	*Guttiferae*
Family	Colchicaceae	*Colchicum, Colchicum autumnale* type, *Colchicum* type, *Colchicum/Merendera, Merendera*
Genus	*Colutea*	*Colutea*
Family	Convolvulaceae	*Calystegia, Calystegia sepium,* Convolvulaceae, *Convolvulus, Convolvulus arvensis, Convolvulus arvensis* type, *Corema album* type, *Cuscuta, Cuscuta europaea* type
Genus	*Coriaria*	*Coriaria, Coriaria myrtifolia*
Genus	*Cornus*	Cornaceae, *Cornus, Cornus mas, Cornus mas/Cornus suecica, Cornus sanguinea, Cornus suecica*

Genus	*Corylus*	*Corylus, Corylus avellana, Corylus avellana* type*, Corylus maxima, Corylus* type
Genus	*Cotinus*	*Cotinus, Cotinus coggygria*
Genus	*Cotoneaster*	*Cotoneaster*
Family	Crassulaceae	*Crassula,* Crassulaceae*, Sedum, Sedum rosea, Sedum* type*, Sempervivum, Umbilicus, Umbilicus rupestris* type
Genus	*Crataegus*	*Crataegus, Crataegus* type
Family	Cucurbitaceae	Cucurbitaceae
Family	Cupressaceae	Cupressaceae*, Taxodiaceae, Taxodium, Cupressus, Cupressus type, Juniperus, Juniperus communis, Juniperus communis* type*, Juniperus excelsa/Juniperus oxycedrus, Juniperus sabina, Juniperus* type
Genus	*Cynomorium*	*Cynomorium*
Family	Cyperaceae	*Carex, Fimbristylis, Rhynchospora, Rhynchospora alba, Rhynchospora* type*, Schoenoplectus, Schoenoplectus lacustris ssp lacustris, Schoenoplectus* type*, Schoenus* type*, Scirpus, Scirpus lacustris* type*, Carex hirta type, Scirpus* type*, Trichophorum caespitosum, Carex* type*,* Cyperaceae*, Cyperus, Cyperus* type*, Eleocharis palustris, Eriophorum angustifolium/Eriophorum vaginatum, Eriophorum* type
Family	Cytinaceae	*Cytinus hypocistis* type
Genus	*Daphne*	*Daphne, Daphne gnidium, Daphne gnidium* type*, Daphne* type
Genus	*Datisca*	*Datisca*
Genus	*Delphinium*	*Delphinium* type
Family	Dennstaedtiaceae	*Pteridium, Pteridium aquilinum, Pteridium aquilinum type, Pteridium* type
Genus	*Diapensia*	*Diapensia, Diapensia lapponica*

Genus	*Dryas*	*Dryas, Dryas octopetala*
Genus	*Elaeagnus*	*Elaeagnus*
Genus	*Empetrum*	*Empetrum, Empetrum nigrum, Empetrum* type
Genus	*Ephedra*	*Ephedra, Ephedra major* type, *Ephedra* type, *Ephedra alata* type, *Ephedra distachya, Ephedra distachya* type, *Ephedra fragilis, Ephedra fragilis ssp campylopoda, Ephedra fragilis* type, *Ephedra fragilis var campylopoda, Ephedra major*
Genus	*Equisetum*	*Equisetum*
Genus	*Erica*	*Erica, Erica lusitanica* type, *Erica scoparia* type, *Erica tetralix, Erica tetralix* type, *Erica* type, *Erica umbellata* type, *Erica arborea, Erica arborea* type, *Erica australis, Erica australis* type, *Erica cinerea, Erica cinerea* type, *Erica erigena* type, *Erica lusitanica*
Family	Ericaceae	Ericaceae, *Ericales, Lecythis, Moneses, Orthilia, Phyllodoce, Pyrola*
Genus	*Euonymus*	*Euonymus, Euonymus europaeus*
Family	Euphorbiaceae	*Acalypha, Euphorbia, Euphorbia* type, Euphorbiaceae
Family	Fabaceae	Fabaceae, *Glycine*
Family	Fabaceae (herbs)	*Anthyllis, Lathyrus/Vicia, Lotus, Lotus corniculatus, Lotus corniculatus type, Lotus type, Lotus uliginosus, Medicago, Medicago littoralis* type, *Medicago sativa, Medicago* type, *Coronilla, Melilotus, Melilotus* type, *Onobrychis, Onobrychis* type, *Oxytropis, Phaseolus type, Trifolium, Trifolium alpinum* type, *Trifolium badium* type, *Trifolium montanum, Ebenus/Hedysarum, Trifolium pratense, Trifolium pratense* type, *Trifolium repens, Trifolium repens* type, *Trifolium spadiceum* type, *Trifolium* type, *Vicia, Vicia cracca, Vicia cracca* type, *Vicia faba* type, *Hedysarum hedysaroides, Vicia sylvatica* type, *Vicia* type, Viciaceae, *Hippocrepis comosa, Hippocrepis* type, *Lathyrus, Lathyrus* type, *Lathyrus/Vicia*
Genus	*Fagus*	*Fagus, Fagus orientalis, Fagus sylvatica*

Genus	*Ficus*	*Ficus, Ficus carica*
Genus	*Flueggea*	*Securinega tinctoria* type
Genus	*Frangula*	*Frangula, Frangula alnus*
Genus	*Fraxinus*	*Fraxinus, Fraxinus angustifolia, Fraxinus angustifolia subsp. oxycarpa, Fraxinus angustifolia* type, *Fraxinus excelsior, Fraxinus excelsior* type, *Fraxinus ornus, Fraxinus ornus* type, *Fraxinus oxycarpa* type
Genus	*Genisteae*	*Cytisus* type, *Ulex, Ulex* type, *Cytisus/Genista, Cytisus/Genista* type, *Cytisus/Ulex, Genista, Genista* type, *Genista/Ulex, Sarothamnus scoparius, Spartium*
Family	Gentianaceae	*Centaurium, Gentiana purpurea* type, Gentianaceae, *Gentianella, Gentianella campestris type, Swertia perennis, Centaurium maritimum, Centaurium* type, *Gentiana, Gentiana lutea/Gentiana pneumonanthe, Gentiana nivalis* type, *Gentiana pneumonanthe, Gentiana pneumonanthe* type, *Gentiana purpurea*
Family	Geraniaceae	*Erodium*, Geraniaceae, *Geranium, Geranium sylvaticum* type, *Geranium* type
Genus	*Halimium*	*Halimium, Halimium* type
Genus	*Hedera*	*Hedera, Hedera helix, Hedera* type
Genus	*Helianthemum*	*Helianthemum, Helianthemum croceum type, Helianthemum nummularium* type, *Helianthemum salicifolium* type, *Helianthemum* type
Genus	*Helleborus*	*Helleborus, Helleborus foetidus, Helleborus viridis* type
Genus	*Hippophae*	*Hippophae, Hippophae rhamnoides*
Genus	*Huperzia*	*Huperzia selago, Lycopodium selago*
Family	Hymenophyllaceae	*Hymenophyllum tunbrigense, Hymenophyllum wilsonii, Trichomanes speciosum*

Family	Hypericaceae	*Hypericum, Hypericum hyssopifolium, Hypericum perforatum* type, *Hypericum pulchrum* type, *Hypericum* type
Genus	*Ilex*	*Ilex, Ilex aquifolium*
Genus	*Impatiens*	*Impatiens*
Family	Iridaceae	*Crocus,* Iridaceae, *Iris, Iris pseudacorus, Iris pseudacorus* type, *Iris* type
Genus	*Jasminum*	*Jasminum, Jasminum fruticans, Jasminum* type
Family	Juglandaceae	Juglandaceae
Genus	*Juglans*	*Juglans, Juglans regia*
Family	Juncaceae	Juncaceae, *Juncus, Luzula*
Genus	*Kalmia*	*Loiseleuria procumbens*
Genus	*Koenigia*	*Koenigia islandica*
Genus	*Laburnum*	*Laburnum anagyroides*
Family	Lamiaceae	*Ajuga, Lycopus* type, *Lycopus/Mentha, Marrubium, Mentha, Mentha* type, *Mentha/Thymus, Origanum vulgare, Phlomis, Prunella, Prunella* type, *Ballota, Prunella vulgaris* type, *Scutellaria, Scutellaria* type, *Sideritis, Stachys, Stachys sylvatica* type, *Stachys sylvestris, Stachys* type, *Thymus, Thymus serpyllum, Galeopsis, Thymus* type, *Galeopsis* type, *Glechoma* type, Lamiaceae, *Lamium, Lamium* type, *Lycopus*
Genus	*Larix*	*Larix, Larix decidua, Larix decidua* type, *Larix/Pseudotsuga*
Genus	*Lavandula*	*Lavandula stoechas* type
Genus	*Ledum*	*Ledum, Ledum palustre, Ledum* type
Genus	*Ligustrum*	*Ligustrum, Ligustrum vulgare, Ligustrum vulgare* type

Family	Liliaceae	*Allium, Lilium martagon* type, *Lloydia serotina, Allium* type, *Anthericum, Anthericum* type, *Fritillaria lusitanica, Fritillaria* type, *Gagea,* Liliaceae, *Lilium*
Family	Linaceae	Linaceae, *Radiola linoides*
Genus	*Linnaea*	*Linnaea, Linnaea borealis*
Genus	*Linum*	*Linum, Linum bienne* type, *Linum catharticum, Linum catharticum* type, *Linum* type
Genus	*Lonicera*	*Lonicera, Lonicera caerulea, Lonicera hispida, Lonicera implexa, Lonicera periclymenum, Lonicera periclymenum* type, *Lonicera* type, *Lonicera xylosteum* type
Family	Loranthaceae	Loranthaceae
Genus	*Lycopodiella*	*Lepidotis inundata, Lycopodium inundatum*
Genus	*Lycopodium*	*Diphasiastrum, Lycopodium alpinum, Lycopodium annotinum, Lycopodium annotinum* type, *Lycopodium clavatum, Lycopodium clavatum* type, *Lycopodium complanatum, Lycopodium dubium, Lycopodium* type, *Diphasiastrum alpinum, Diphasium, Diphasium alpinum, Diphasium alpinum* type, *Diphasium complanatum, Diphasium tristachyum, Diphasium* type, *Lycopodium*
Genus	*Lysimachia*	*Lysimachia, Lysimachia maritima, Lysimachia nemorum, Lysimachia thyrsiflora, Lysimachia* type, *Lysimachia vulgaris, Lysimachia vulgaris* type
Family	Lythraceae	Lythraceae, *Lythrum, Lythrum salicaria, Lythrum salicaria* type, *Lythrum salicaria/Lythrum hyssopifolia, Peplis*
Family	Magnoliaceae	Magnoliaceae
Genus	*Malus*	*Malus, Malus* type
Family	Malvaceae	*Hibiscus, Lavatera* type, *Malva, Malva sylvestris* type, Malvaceae, *Sterculia*
Family	Melanthiaceae	*Veratrum, Veratrum* type

Genus	*Mercurialis*	*Mercurialis, Mercurialis annua, Mercurialis annua* type, *Mercurialis perennis, Mercurialis perennis* type
Genus	*Moltkia*	*Moltkia*
Family	Montiaceae	*Montia*
Family	Moraceae	Moraceae, *Morus, Morus alba, Morus alba* type, *Morus nigra*
Genus	*Myrica*	*Corylus/Myrica, Myrica, Myrica gale, Myrica gale* type, *Myrica* type
Genus	*Myricaria*	*Myricaria*
Family	Myrtaceae	Myrtaceae, *Myrtus, Myrtus communis*
Family	Nartheciaceae	*Narthecium, Narthecium ossifragum, Narthecium* type
Genus	*Nerium*	*Nerium, Nerium oleander*
Genus	*Nigella*	*Nigella*
Family	Nitrariaceae	*Nitraria, Peganum harmala*
Genus	*Olea*	*Olea, Olea europaea, Olea* type
Family	Oleaceae	*Fontanesia/Phillyrea, Olea/Ligustrum,* Oleaceae
Family	Onagraceae	*Chamaenerion, Chamaenerion angustifolium, Circaea, Epilobium, Epilobium* type, Onagraceae
Genus	*Ononis*	*Ononis, Ononis* type
Family	Ophioglossaceae	*Botrychium, Botrychium lunaria, Botrychium lunaria* type, *Botrychium* type, Ophioglossaceae, *Ophioglossum, Ophioglossum vulgatum*
Family	Orchidaceae	*Neottia* type, Orchidaceae

Family	Orobanchaceae	*Euphrasia, Euphrasia* type, *Melampyrum, Pedicularis, Pedicularis oederi* type, *Pedicularis palustris* type, *Pedicularis* type, *Rhinanthus, Rhinanthus* type
Family	Osmundaceae	*Osmunda, Osmunda regalis*
Family	Oxalidaceae	Oxalidaceae, *Oxalis, Oxalis acetosella, Oxalis stricta*
Genus	*Oxyria/Rumex*	*Oxyria, Rumex acetosa/Rumex acetosella, Rumex acetosa/Rumex acetosella* type, *Rumex acetosa/Rumex scutatus* type, *Rumex acetosella, Rumex acetosella* type, *Rumex alpestris, Rumex alpinus, Rumex alpinus* type, *Rumex aquaticus, Rumex aquaticus* type, *Oxyria digyna, Rumex conglomeratus* type, *Rumex crispus, Rumex crispus* type, *Rumex hydrolapathum, Rumex hydrolapathum* type, *Rumex longifolius, Rumex longifolius* type, *Rumex obtusifolius* type, *Rumex patentia* type, *Rumex sanguineus* type, *Oxyria* type, *Rumex* type, *Oxyria/Rumex, Oxyria/Rumex* type, *Rumex, Rumex acetosa, Rumex acetosa* type, *Rumex acetosa/Oxyria* type
Genus	*Paeonia*	*Paeonia*
Genus	*Paliurus*	*Paliurus, Paliurus spina-christi*
Family	Papaveraceae	*Chelidonium majus, Papaver, Papaver argemone, Papaver rhoeas* type, *Papaver* type, Papaveraceae, *Roemeria, Corydalis, Corydalis solida* type, *Corydalis* type, *Fumana, Fumaria, Fumaria officinalis* type, *Glaucium, Hypecoum*
Genus	*Parrotia*	*Parrotia persica*
Genus	*Periploca*	*Periploca*
Genus	*Phillyrea*	*Olea/Phillyrea, Phillyrea, Phillyrea angustifolia, Phillyrea angustifolia* type, *Phillyrea media, Phillyrea* type
Family	Phyllanthaceae	*Andrachne, Andrachne telephioides*
Genus	*Picea*	*Picea, Picea abies, Picea abies subsp abies*
Genus	*Picea orientalis*	*Picea orientalis*

Genus	*Pinus*	*Pinus*
Genus sub-group	*Pinus (diploxylon)*	*Pinus (Diploxylon), Pinus subg. Pinus, Pinus sylvestris, Pinus sylvestris* type, *Pinus sylvestris/Pinus nigra* type, *Pinus* type, *Pinus halepensis, Pinus nigra* type, *Pinus non-cembra, Pinus pinaster, Pinus pinaster* type, *Pinus pinaster/Pinus halepensis, Pinus pinea* type, *Pinus pinea/Pinus halepensis* type
Genus sub-group	*Pinus (haploxylon)*	*Pinus (Haploxylon), Pinus cembra, Pinus cembra* type, *Pinus peuce, Pinus sibirica*
Genus	*Pistacia*	*Pistacia, Pistacia lentiscus, Pistacia lentiscus* type, *Pistacia terebinthus, Pistacia terebinthus* type, *Pistacia* type
Family	Plantaginaceae	*Globularia, Plantago coronopus* type, *Plantago cylindrica* type, *Plantago lanceolata, Plantago lanceolata* type, *Plantago lusitanica, Plantago major, Plantago major* type, *Plantago major/Plantago media, Plantago maririma, Plantago maritima, Gratiola officinalis, Plantago maritima* type, *Plantago media, Plantago media* type, *Plantago media/Plantago major, Plantago media/Plantago major* type, *Plantago montana* type, *Plantago ovata* type, *Plantago psyllium* type, *Plantago tenuiflora* type, *Plantago* type, Plantaginaceae, *Plantago, Plantago afra* type, *Plantago albicans, Plantago alpina, Plantago alpina* type, *Plantago coronopus*
Genus	*Platanus*	*Platanus, Platanus orientalis, Platanus* type
Family	Plumbaginaceae	*Acantholimon, Limonium vulgare,* Plumbaginaceae, *Plumbago, Armeria, Armeria maritima, Armeria maritima subsp elongata, Armeria* type, *Armeria/Limonium, Armeria/Limonium type, Limonium, Limonium* type
Family	Poaceae	*Anthoxanthum, Stipa, Deschampsia, Elymus, Lygeum, Lygeum spartum, Nardus, Poa/Festuca* type, Poaceae, *Setaria*
Family	Polemoniaceae	Polemoniaceae, *Polemonium*
Family	Polygalaceae	*Polygala, Polygala* type, *Polygala vulgaris, Polygala vulgaris* type, Polygalaceae, *Polygaloides chamaebuxus*

Family	Polygonaceae	*Atraphaxis*, *Persicaria amphibia*, Polygonaceae, *Pteropyrum*, *Rheum*, *Rheum ribes*, *Rheum* type, *Bilderdykia convolvulus*, *Bilderdykia convolvulus* type, *Bistorta officinalis* type, *Bistorta vivipara*, *Calligonum*, *Fallopia convolvulus*, *Fallopia convolvulus* type, *Persicaria*
Genus	*Polygonum*	*Polygonum*, *Polygonum convolvulus*, *Polygonum convolvulus* type, *Polygonum oxyspermum* type, *Polygonum persicaria*, *Polygonum persicaria* type, *Polygonum sect. Persicaria*, *Polygonum* type, *Polygonum viviparum*, *Polygonum alpinum*, *Polygonum amphibium*, *Polygonum amphibium* type, *Polygonum aviculare*, *Polygonum aviculare* type, *Polygonum bistorta*, *Polygonum bistorta* type, *Polygonum bistorta/Polygonum viviparum*
Genus	*Polypodiales*	*Aspidium*, *Blechnum*, *Blechnum spicant*, *Cystopteris*, *Cystopteris fragilis*, *Cystopteris* type, *Dryopteridaceae/Polypodiaceae*, *Dryopteris*, *Dryopteris carthusiana*, *Dryopteris carthusiana* type, *Dryopteris cristata*, *Asplenium*, *Dryopteris cristata* type, *Dryopteris dilatata*, *Dryopteris dilatata* type, *Dryopteris filix-mas*, *Dryopteris filix-mas* type, *Dryopteris* type, *Dryopteris/Thelypteris*, *Grammitis*, *Gymnocarpium*, *Gymnocarpium dryopteris*, *Asplenium nidus*, *Pilularia*, Polypodiaceae, Polypodiales, *Polypodium*, *Polypodium vulgare*, *Polypodium vulgare* type, *Polystichum*, *Polystichum* type, *Thelypteris*, *Thelypteris palustris*, *Asplenium* type, *Thelypteris palustris* type, *Thelypteris phegopteris*, *Thelypteris* type, *Asplenium viride*, *Athyrium*, *Athyrium alpestre* type, *Athyrium distentifolium* type, *Athyrium filix-femina*
Genus	*Populus*	*Populus*, *Populus tremula*, *Populus tremula* type
Family	Portulacaceae	Portulacaceae
Genus	*Potentilla*	*Potentilla*, *Potentilla aurea*, *Potentilla micrantha* type, *Potentilla recta*, *Potentilla* type
Family	Primulaceae	*Anagallis*, *Primula*, *Primula clusiana* type, *Primula farinosa*, *Primula farinosa* type, *Primula hirsuta* type, *Primula* type, *Primula veris* type, *Primula vulgaris* type, Primulaceae, *Soldanella*, *Anagallis arvensis*, *Trientalis*, *Trientalis europaea*, *Anagallis arvensis* type, *Anagallis tenella*, *Anagallis* type, *Androsace*, *Androsaceae*, *Cyclamen*, *Cyclamen hederifolium*
Genus	*Prosopis*	*Lagonychium* type, *Prosopis*

Genus	*Prunus*	*Prunus, Prunus avium, Prunus padus, Prunus spinosa* type, *Prunus* type
Family	Pteridaceae	*Adiantum, Cheilanthes, Cryptogramma, Cryptogramma crispa, Cryptogramma crispa* type, *Pteris*
Genus	*Pterocarya*	*Pterocarya, Pterocarya fraxinifolia*
Genus	*Punica*	*Punica*
Genus	*Pyrus*	*Pyrus, Pyrus* type
Genus	*Quercus* (deciduous)	*Quercus, Quercus robur* type, *Quercus robur/Quercus petraea, Quercus (deciduous), Quercus cerris, Quercus cerris* type, *Quercus deciduous, Quercus ithaburensis, Quercus ithaburensis* type, *Quercus petraea, Quercus robur*
Genus	*Quercus* (evergreen)	*Quercus (evergreen), Quercus rotundifolia* type, *Quercus suber, Quercus suber* type, *Quercus calliprinos, Quercus calliprinos* type, *Quercus coccifera, Quercus coccifera* type, *Quercus coccifera/Quercus ilex, Quercus evergreen, Quercus ilex, Quercus ilex* type
Genus	*Quercus* (intermediate)	*Quercus canariensis type, Quercus cerris/Quercus suber, Quercus cerris/Quercus suber* type, *Quercus faginea, Quercus faginea/Quercus pubescens, Quercus faginea/Quercus pyrenaica, Quercus pubescens* type, *Quercus pyrenaica* type, *Quercus robur/Quercus pubescens* type
Family	Ranunculaceae	*Anemone, Anemone nemorosa, Anemone nemorosa type, Anemone nemorosa* type/*Hepatica nobilis, Anemone nemorosa/Anemone ranunculoides, Anemone* type, *Hepatica, Pulsatilla*, Ranunculaceae
Genus	*Ranunculus*	*Ranunculus, Ranunculus ficaria* type, *Ranunculus flammula* type, *Ranunculus glacialis* type, *Ranunculus montanus* type, *Ranunculus muricatus* type, *Ranunculus nivalis* type, *Ranunculus parviflorus, Ranunculus repens* type, *Ranunculus sceleratus* type, *Ranunculus* type, *Ranunculus acer* type, *Ranunculus aconitifolius, Ranunculus aconitifolius* type, *Ranunculus acris, Ranunculus acris* type, *Ranunculus arvensis, Ranunculus arvensis* type, *Ranunculus asiaticus* type
Family	Resedaceae	*Reseda, Reseda lutea* type, Resedaceae

Family	Rhamnaceae	Rhamnaceae
Genus	*Rhamnus*	*Rhamnus, Rhamnus catharticus, Rhamnus* type
Genus	*Rhododendron*	*Rhododendron, Rhododendron ferrugineum, Rhododendron* type
Genus	*Rhus*	*Rhus, Rhus coriaria*
Genus	*Ribes*	*Ribes, Ribes* type
Family	Rosaceae	*Agrimonia, Fragaria* type, *Geum, Geum rivale* type, *Geum* type, *Pirus* type, *Prunus/Rubus* type, *Pyrus/Malus, Rosa, Rosa canina* type, *Rosa* type, *Agrimonia eupatoria, Rosa/Prunus,* Rosaceae, *Spiraea, Alchemilla, Alchemilla* type, *Filipendula, Filipendula* type, *Filipendula ulmaria, Filipendula vulgaris, Fragaria*
Genus	*Rosmarinus*	*Rosmarinus, Rosmarinus* type
Family	Rubiaceae	*Asperula, Galium, Galium* type, Rubiaceae, *Theligonum*
Genus	*Rubus*	*Rubus, Rubus arcticus, Rubus arcticus* type, *Rubus chamaemorus, Rubus fruticosus* type, *Rubus idaeus* type, *Rubus saxatilis, Rubus* type
Genus	*Ruscus*	*Ruscus*
Family	Rutaceae	*Haplophyllum, Ruta,* Rutaceae
Genus	*Salix*	*Salix, Salix glauca* type, *Salix helvetica* type, *Salix herbacea, Salix herbacea* type, *Salix herbacea/Salix reticulata, Salix pentandra* type
Genus	*Salvia*	*Salvia, Salvia verticillata* type
Genus	*Sambucus*	*Sambucus, Sambucus ebulus, Sambucus nigra, Sambucus nigra* type, *Sambucus nigra/Sambucus racemosa, Sambucus racemosa, Sambucus* type
Genus	*Sanguisorba group*	*Poterium, Sanguisorba, Sanguisorba minor, Sanguisorba minor ssp minor, Sanguisorba minor* type, *Sanguisorba officinalis, Sanguisorba* type, *Sarcopoterium*

Family	Santalaceae	*Arceuthobium oxycedri, Comandra elegans, Osyris alba* type, *Thesium*
Family	Saxifragaceae	*Chrysosplenium, Saxifraga oppositifolia, Saxifraga oppositifolia* type, *Saxifraga paniculata* type, *Saxifraga stellaris, Saxifraga stellaris* type, *Saxifraga tricuspidata,* Saxifragaceae, *Chrysosplenium* type, *Micranthes nivalis* type, *Saxifraga, Saxifraga cernua* type, *Saxifraga cespitosa* type, *Saxifraga foliolosa* type, *Saxifraga granulata, Saxifraga granulata* type
Family	Scrophulariaceae	*Antirrhinum* type, *Scrophularia/Verbascum,* Scrophulariaceae, *Verbascum, Verbascum* type, *Veronica, Veronica* type, *Antirrhinum/Linaria, Digitalis, Digitalis purpurea* type, *Digitalis* type, *Linaria, Linaria* type, *Scrophularia, Scrophularia* type
Genus	*Smilax*	*Smilax*
Family	Solanaceae	*Capsicum* type, *Lycium,* Solanaceae, *Solanum, Solanum dulcamara, Solanum nigrum, Solanum nigrum* type
Genus	*Sorbus*	*Sorbus, Sorbus aria, Sorbus aucuparia, Sorbus aucuparia* type, *Sorbus* type
Genus	*Styrax*	*Styrax officinalis*
Genus	*Suaeda*	*Suaeda, Suaeda* type
Genus	*Syringa*	*Syringa*
Genus	*Tamarix*	*Tamarix*
Genus	*Taxus*	*Taxus, Taxus baccata*
Genus	*Teucrium*	*Teucrium, Teucrium* type
Genus	*Thalictrum*	*Thalictrum, Thalictrum alpinum, Thalictrum aquilegiifolium, Thalictrum flavum* type, *Thalictrum lucidum, Thalictrum* type
Family	Thymelaeaceae	*Thymelaea,* Thymelaeaceae

Genus	*Tilia*	*Tilia, Tilia cordata, Tilia cordata* type, *Tilia platyphyllos, Tilia platyphyllos* type
Genus	*Tofieldia*	*Tofieldia*
Genus	*Trollius*	*Trollius, Trollius europaeus, Trollius* type
Genus	*Ulmus*	*Ulmus, Ulmus glabra, Ulmus glabra* type, *Ulmus minor*
Genus	*Ulmus/Zelkova*	*Ulmus/Zelkova, Zelkova, Zelkova* type
Family	Urticaceae	*Parietaria, Parietaria/Urtica, Urtica, Urtica dioica, Urtica dioica* type, *Urtica pilulifera* type, *Urtica* type, *Urtica urens,* Urticaceae
Genus	*Vaccinium*	*Vaccinium, Vaccinium myrtillus, Vaccinium myrtillus type, Vaccinium oxycoccos, Vaccinium* type, *Vaccinium uliginosum* type, *Vaccinium/Oxycoccus*
Family	Valerianaceae	*Centranthus, Valerianella, Valeriana, Valeriana dioica* type, *Valeriana officinalis, Valeriana officinalis* type, *Valeriana sambucifolia* type, *Valeriana tripteris* type, *Valeriana* type, Valerianaceae
Family	Verbenaceae	*Verbena, Verbena officinalis*
Genus	*Viburnum*	*Viburnum, Viburnum opulus, Viburnum opulus* type, *Viburnum* type
Family	Violaceae	*Viola, Viola arvensis* type, *Viola canina* type, *Viola palustris, Viola palustris* type, *Viola tricolor, Viola tricolor/Viola arvensis,* Violaceae
Genus	*Viscum*	*Viscum, Viscum album, Viscum album* type, *Viscum* type
Genus	*Vitex*	*Vitex*
Genus	*Ziziphus*	*Ziziphus* type, *Zizyphus, Zizyphus lotus*
Family	Zygophyllaceae	*Tribulus, Tribulus terrestris,* Zygophyllaceae, *Zygophyllum*

Supplementary Table 2.2: Comparison of the quality of reconstructions based on training datasets constructed in different ways or the modern data set for the whole of the SPECIAL Modern Pollen Data Set (SMPDS) and for the data set encompassing only the Eastern Mediterranean-Black Sea Caspian Corridor (EMBSeCBIO) region. Assessments are made on the accuracy with respect to only the dominant biome and to the dominant and sub-dominant biomes identified in a 20 x 20 km2 search window around each sampling point according to the Potential Natural Vegetation (PNV) Map of Hengl et al. (2018). We give both the accuracy and the balanced accuracy metrics for each split of the training and testing datasets.

		SMPDS region				EMBSeCBIO region			
		Dominant biome		Dominant and sub-dominant		Dominant biome		Dominant and sub-dominant	
Training dataset	Testing dataset	Accuracy	Balanced accuracy	Accuracy	Balanced accuracy	Accuracy	Balanced accuracy	Accuracy	Balanced accuracy
Random selection of 70% of the data	Random selection of 30% of the data	67.30	62.07	78.89	77.78	65.36	58.76	79.45	75.64
Random selection with 0% from SMPDS, 50% from EMBSeCBIO.	Random selection of combined data set to produce test data sets the same size as the training set	63.93	57.00	75.63	71.49	71.18	67.03	82.10	78.46
Random selection with 50% of the samples for each biome from SMPDS and 50% from EMBSeCBIO; each class limited to number of samples of the median size class.	Random selection of samples of the same size as the training set	64.66	63.55	75.73	78.00	68.74	64.40	79.45	77.10
Optimum sampling of bioclimatic space of each class to have a maximum of 1000 samples the training dataset	All the samples not used for the training dataset	63.86	62.80	75.18	78.34	64.70	56.92	77.70	72.01
Random down-sampling of classes towards the median size class (GRAM). 70% of down-sampled data used for training	30% of down-sampled data for testing	65.75	65.88	75.68	75.58	62.30	64.22	74.21	77.34
Samples from large lakes removed; random down-sampling of classes towards the median size class (GRAM); 70% of down-sampled data used for training.	30% of down-sampled data used for testing	66.32	66.49	77.49	76.52	63.82	64.54	75.42	78.32

Supplementary Table 2.3: Comparison of the quality of reconstructions based on using different areas around each sample to determine the observed vegetation type and on using different training and testing data partitioning ratios. The size of the search window is given in km. For the ratio of the size of the training and testing data sets, a value of 70:30 means that 70% of the data are used as the training set and 30% of the data are used as the test set. Assessments are made on the accuracy with respect to only the dominant biome and to the dominant and sub-dominant biomes identified in each search window around each sampling point according to the Potential Natural Vegetation (PNV) Map of Hengl et al. (2018) for the modern data set for the whole of the SPECIAL Modern Pollen Data Set (SMPDS) and for the data set encompassing only the Eastern Mediterranean-Black Sea Caspian Corridor (EMBSeCBIO) region. We give both the accuracy and the balanced accuracy metrics for each assessment.

		SMPDS REGION				EMBSECBIO REGION			
		Dominant		Dominant and subdominant		Dominant		Dominant and subdominant	
Size of the search window (km)	Training - testing data partitioning ratio	Accuracy	Balanced accuracy	Accuracy	Balanced accuracy	Accuracy	Balanced accuracy	Accuracy	Balanced accuracy
12x12	50:50	58.76	58.80	73.71	73.23	62.25	57.23	77.79	75.84
12x12	60:40	62.00	63.18	73.50	74.22	62.32	57.81	76.45	74.05
12x12	70:30	63.09	63.41	75.17	75.53	64.18	66.15	77.88	80.03
12x12	75:25	62.35	62.55	72.06	72.31	62.91	62.66	76.04	74.96
12x12	80:20	59.18	59.59	73.98	74.45	62.47	60.19	76.04	74.07
20x20	50:50	61.76	62.19	74.03	74.55	62.73	60.07	76.28	78.22
20x20	60:40	61.24	61.52	73.90	73.93	61.20	57.90	74.75	73.94
20x20	70:30	65.75	65.88	75.68	75.58	62.30	64.22	74.21	77.34
20x20	75:25	64.58	64.75	76.25	76.49	64.48	59.51	76.50	75.70
20x20	80:20	68.37	69.23	75.00	75.36	63.72	59.42	76.72	75.95
25x25	50:50	60.34	60.85	73.21	73.43	63.48	54.85	74.81	71.72
25x25	60:40	60.85	61.42	73.54	73.76	66.04	63.39	76.92	75.90
25x25	70:30	60.42	61.07	74.20	74.33	63.96	58.03	76.04	75.44
25x25	75:25	61.92	62.58	71.13	71.45	65.82	58.88	78.24	75.08
25x25	80:20	66.32	66.38	74.21	74.91	66.37	59.28	78.57	76.10
40x40	50:50	63.29	63.76	77.03	76.74	59.45	54.70	73.19	76.14
40x40	60:40	65.27	65.26	76.75	76.26	61.98	55.93	76.48	77.19
40x40	70:30	67.41	67.69	76.30	76.31	62.57	54.29	75.19	74.56
40x40	75:25	68.58	68.93	76.55	77.15	64.65	56.08	79.14	77.45
40x40	80:20	67.96	68.07	80.11	80.30	64.76	57.59	77.50	76.29
50x50	50:50	65.27	65.92	76.36	76.28	61.43	61.16	75.52	76.00
50x50	60:40	68.07	65.31	82.06	82.26	65.38	63.54	80.36	78.44
50x50	70:30	67.13	65.61	77.97	77.99	66.93	64.12	80.50	79.10
50x50	75:25	64.98	65.67	78.06	79.04	66.25	65.29	79.13	78.97
50x50	80:20	65.63	66.12	79.17	78.73	67.54	64.47	80.70	79.69

Supplementary Table 2.4: Comparison of the quality of reconstructions for the modern data set for the whole of the SPECIAL Modern Pollen Data Set (SMPDS) and for the data set encompassing only the Eastern Mediterranean-Black Sea Caspian Corridor (EMBSeCBIO) region based on using different values for ε in equation 1 (range from 0.01 to 1). Assessments are made on the accuracy with respect to only the dominant biome and to the dominant and sub-dominant biomes identified in a 20 x 20 km2 search window around each sampling point according to the Potential Natural Vegetation (PNV) Map of Hengl et al. (2018). We give both the accuracy and the balanced accuracy metrics for assessment.

	SMPDS region				EMBSeCBIO region			
	Dominant biome		Dominant and Subdominant		Dominant biome		Dominant and Subdominant	
Value for ε	Accuracy	Balanced accuracy	Accuracy	Balanced accuracy	Accuracy	Balanced accuracy	Accuracy	Balanced accuracy
0.01	66.10	65.93	73.63	72.59	66.92	60.06	78.86	77.16
0.05	63.70	63.64	71.92	71.15	66.01	62.23	77.38	77.80
0.1	64.04	64.17	73.29	73.07	65.03	63.03	77.16	79.58
0.5	65.75	65.88	75.68	75.58	62.30	64.22	74.21	77.34
0.8	66.78	66.86	75.68	75.60	62.19	63.68	74.43	78.25
1	66.78	66.86	75.68	75.67	61.60	62.99	74.18	77.69

Supplementary Table 2.5: Plant functional types (PFTs) included in each biome in the biomisation procedure. The allocations of PFTs to biomes follows Marinova et al. (2018), but has been modified to take account of the amalgamation of some biomes in our analyses.

Biomes	Biomes in Marinova et al. (2017)	Constituent plant functional types
TUND	Tundra (TUND)	Arctic forb, sedge graminoid, arctic dwarf shrub, arctic low-to-high shrub
DESE	Desert (DESE)	Halophyte, rosette or cushion forb, succulent, switch plant, tuft tree
GRAM	Graminoids with forbs (GRAM)	Grass graminoid, geophyte, other forb
XSHB	Xeric shrubland (XSHB)	Drought-tolerant forb, switch plant, xerophytic shrub
WTSFS	Warm-temperate evergreen sclerophyll broadleaf shrubland (WTSHB), Warm-temperate deciduous malacophyll broadleaf forest (WTDF), Warm-temperate evergreen needleleaf and sclerophyll broadleaf forest (WTEF)	Warm-temperate low-to-high shrub, temperate low-to-high shrub, warm-temperate sclerophyll tree, temperate (spring frost tolerant) cold-deciduous malacophyll broadleaved tree temperate (spring frost intolerant) cold-deciduous malacophyll broadleaved tree, climber/liana/vine, warm-temperate needle-leaved evergreen tree, warm-temperate evergreen malacophyll broadleaved tree, eurythermic evergreen needle-leaved tree
CENF	Cold evergreen needleleaf forest (CENF), Cool evergreen needleleaf forest (COOL)	Boreal low-to-high shrub, boreal cold-deciduous malacophyll broadleaved tree, boreal evergreen needle-leaved tree, boreal needle-leaved deciduous tree, eurythermic evergreen needle-leaved tree, Boreal cold-deciduous malacophyll broadleaved tree, cool-temperate evergreen needle-leaved tree, temperate (spring frost tolerant) cold-deciduous malacophyll broadleaved tree, temperate evergreen needle-leaved tree
TEDE	Temperate deciduous malacophyll broadleaf forest (TEDE)	Temperate (frost-induced late budburst) cold-deciduous malacophyll broadleaved tree, temperate (spring frost intolerant) cold-deciduous malacophyll broadleaved tree, temperate (spring frost tolerant) cold-deciduous malacophyll broadleaved tree, eurythermic evergreen needle-leaved tree, climber/liana/vine
CMIX	Cool mixed evergreen needleleaf and deciduous broadleaf forest (CMIX)	Cool-temperate evergreen needle-leaved tree, eurythermic evergreen needle-leaved tree, temperate (frost-induced late budburst) cold-deciduous malacophyll broadleaved tree, temperate (spring frost tolerant) cold-deciduous malacophyll broadleaved tree, temperate evergreen needle-leaved tree
ENWD	Evergreen needleleaf woodland (ENWD), Deciduous broadleaf woodland (DBWD)	Warm-temperate low-to-high shrub, other forb, eurythermic evergreen needle-leaved tree, warm-temperate needle-leaved evergreen tree, warm-temperate evergreen malacophyll broadleaved tree, temperate (spring frost intolerant) cold-deciduous malacophyll broadleaved tree, temperate low-to-high shrub

Supplementary Table 2.6: Taxon allocation to plant functional types (PFTs) used in the biomisation reconstructions. The allocations of taxa to PFTs es follows Marinova et al. (2018) but has been modified to take account of the amalgamation of some biomes in our analyses.

Plant functional type	**Constituent taxa**
Arctic forb	*Aconitum*, *Aconitum* type, Androsace, *Anemone*, *Anemone nemorosa* type, *Anemone* type, *Aquilegia* type,Campanulaceae, *Cardamine*, *Drosera*, *Gentiana*, *Gentiana nivalis* type, *Gentiana pneumonanthe* type, Gentianaceae, *Gentianella campestris* type, Herbs, *Jasione*, *Parnassia*, *Parnassia palustris*, *Phyteuma*, *Phyteuma* type, *Pinguicula*, Polygonaceae, *Polygonum*, *Polygonum* type, *Pulsatilla*, Ranunculaceae, *Rosa*, *Rosa* type, *Sagina*, *Saussurea*, *Saxifraga*, *Saxifraga hirsuta* type, *Saxifraga nivalis* type, *Saxifraga oppositifolia*, *Saxifraga oppositifolia* type, *Saxifraga rosacea*, *Saxifraga stellaris* type, Saxifragaceae, Scrophulariaceae, *Thalictrum*, *Thalictrum aquilegifolium*, *Trollius*, *Valeriana*, Valerianaceae, *Veratrum* type
Rosette or cushion forb	*Artemisia*, *Artemisia herba-alba* type, *Artemisia* type, Asteraceae, Asteraceae (Liguliflorae), Asteraceae (Tubuliflorae), *Astragalus*, *Astragalus* type, Crassulaceae, *Euphorbia*, *Gundelia* type, Herbs, *Marrubium*, *Phlomis*, *Scabiosa*, *Scabiosa columbaria* type, *Scleranthus*, *Scleranthus* type, *Tribulus*, *Zygophyllum*
Drought-tolerant forb	*Achillea*, *Achillea* type, *Adonis* , *Adonis aestivalis* type, *Adonis* type, Amaranthaceae/Chenopodiaceae, *Ambrosia*, *Ambrosia* type, *Armeria*, *Armeria/Limonium*, *Artemisia*, *Artemisia* type, *Artemisia vulgaris* type, *Aster*, *Aster* type, *Aster/Achillea*, *Aster/Achillea* type, Asteraceae, Asteraceae (Liguliflorae), Asteraceae (Tubuliflorae), *Astragalus*, *Astragalus* type, *Astrantia* type, *Atriplex*, Cannabaceae, *Cannabis*, *Cannabis sativa*, *Carduus*, *Carduus* type, *Carthamus*, Caryophyllaceae, *Centaurea*, *Centaurea cyanus*, *Centaurea cyanus* type, *Centaurea depressa*, *Centaurea depressa* type, *Centaurea jacea*, *Centaurea jacea* type, *Centaurea nigra* type, *Centaurea scabiosa*, *Centaurea scabiosa* type, *Centaurea solstitialis* type, Chenopodiaceae, Dipsacaceae, *Dipsacus*, *Dipsacus* type, *Echinops*, *Eryngium* type, *Euphorbia*, *Fagopyrum*, *Fagopyrum esculentum*, *Fagopyrum tataricum*, *Glaucium*, *Gundelia* type, *Gypsophila*, *Gypsophila* type, *Helichrysum*, *Heliotropium* type, Herbs, *Herniaria* type, *Hornungia* type, *Jurinea*, *Jurinea* type, *Knautia*, *Knautia arvensis*, *Limonium*, *Noaea* type, *Salvia*, *Scabiosa*, *Scabiosa columbaria* type, *Scabiosa rotata* type, Scrophulariaceae, *Serratula*, *Seseli libanotis* type, *Sideritis*, *Succisa*, *Thymus*, *Verbascum*, *Verbascum* type

Other forb	*Acanthus*, *Achillea*, *Achillea* type, *Aconitum*, *Aconitum* type, *Adoxa* type, *Agrimonia*, *Agrimonia eupatoria*, *Agrostemma* type, *Alchemilla*, Amaranthaceae/Chenopodiaceae, *Ambrosia*, *Ambrosia* type, *Ammi* type, *Anagallis*, *Anemone*, *Anemone* type, *Anthemis* type, *Anthriscus* type, Apiaceae, *Apium* type, *Arctium*, *Arctium/Jurinea*, *Asperula* type, *Aster*, *Aster* type, *Aster/Achillea*, *Aster/Achillea* type, Asteraceae, Asteraceae (Liguliflorae), Asteraceae(Tubuliflorae), *Bellis* type, *Beta*, *Bidens* type, Boraginaceae, *Brassica* type, Brassicaceae, Brassicaceae type, *Bunium* type, *Bupleurum*, *Bupleurum* type, *Caltha*, *Caltha* type, *Campanula*, *Campanula* type, Campanulaceae, Cannabaceae, *Capsella* type, *Carduus*, *Carduus* type, Caryophyllaceae, *Centaurea*, *Centranthus*, *Cerastium* type, *Chaerophyllum* type, *Cheilanthes*, *Chelidonium*, Chenopodiaceae, *Chrysosplenium*, *Chrysosplenium* type, Cichoriaceae, *Circaea*, *Cirsium*, *Cirsium* type, *Cirsium/Carduus*, *Cirsium/Gundelia*, *Conium maculatum*, *Consolida*, Convolvulaceae, *Convolvulus*, *Daucus* type, *Delphinium*, *Delphinium* type, *Dianthus*, *Dianthus* type, *Digitalis*, *Digitalis purpurea* type, *Diphasium alpinum* type, Dipsacaceae, *Dipsacus*, *Dipsacus* type, *Echium*, *Echium* type, *Echium violaceum*, *Epilobium*, *Epilobium* type, *Erodium*, *Euphrasia*, *Falcaria* type, *Ferula*, *Ferula* type, *Filago* type, *Filifolium sibiricum*, *Filipendula*, *Flammula* type, *Fragaria* type, *Fumaria*, *Galium*, *Galium* type, Geraniaceae, *Geranium*, *Geum*, *Geum* type, *Gnaphalium*, *Hedysarum* type, *Helleborus*, *Heracleum*, *Heracleum* type, *Hippocrepis* type, *Hyoscyamus*, *Hypericum*, *Hypericum assyriacum* type, *Hypericum hyssopifolium*, *Hypericum perforatum* type, *Hypericum* type, *Impatiens*, *Lactuca*, *Lathyrus*, *Lathyrus* type, *Legousia*, Leguminosae, *Lepidium*, *Lepidium* type, *Linaceae*, *Linaria*, *Linum*, *Linum* type, *Lithospermum*, *Lotus* type, *Lychnis* type, *Lysimachia*, *Malabaila*, *Malabaila* type, *Malva*, Malvaceae, *Matricaria* type, *Matthiola*, *Medicago*, *Melampyrum*, *Mercurialis*, *Mercurialis annua*, *Mercurialis perennis*, *Myosotis*, *Myosotis* type, *Nigella*, Onagraceae, *Onobrychis*, *Onobrychis* type, *Onosma*, *Origanum vulgare*, *Oxalis*, *Oxyria*, *Oxyria/Rumex*, *Papaver*, *Papaver rhoeas* type, Papaveraceae, *Parietaria*, *Paronychia*, *Paronychia/Polycnemum*, *Peucedanum* type, *Pimpinella*, *Pimpinella anisum* type, *Pimpinella major* type, *Pimpinella* type, Plantaginaceae, *Plantago*, *Plantago coronopus*, *Plantago coronopus* type, *Plantago lanceolata*, *Plantago lanceolata* type, *Plantago major*, *Plantago major* type, *Plantago major/Plantago media*, *Plantago maritima*, *Plantago maritima* type, *Plantago media*, *Plantago media* type, *Plantago ovate*, *Plantago ovata* type, Plumbaginaceae, Polemoniaceae, *Polemonium*, *Polygala*, Polygonaceae, *Polygonum*, *Polygonum* type, Portulacaceae, *Potentilla*, *Potentilla* type, *Primula*, Primulaceae, *Prunella* type, *Pulmonaria* type, Ranunculaceae, *Reseda*, Resedaceae, *Rhinanthus*, *Rhinanthus* type, *Rumex*, *Rumex acetosa*, *Rumex acetosa* type, *Rumex acetosa/Rumex acetosella*, *Rumex acetosella*, *Rumex acetosella* type, *Rumex cyprius*, *Rumex hydrolapathum*, *Rumex hydrolapathum* type, *Rumex patentia*, *Rumex patentia* type, *Rumex scutatus* type, *Rumex* type, *Sagina*, *Salvia*, *Sanguisorba*, *Sanguisorba minor*, *Sanguisorba minor* type, *Sanguisorba officinalis*, *Sanguisorba* type, *Sanicula* type, Scrophulariaceae, *Scutellaria*, *Senecio*, *Senecio* type, *Silene*, *Silene dioica* type, *Silene* type, *Silene vulgaris* type, *Sinapis* type, Solanaceae, *Solanum*, *Solanum nigrum*, *Spergula*, *Spergula arvensis* , *Spergula* type, *Spergula/Spergularia*, *Spergularia* type, *Stachys*, *Stachys* type, *Stellaria*, *Symphytum*, *Symphytum* type, *Taraxacum*, *Taraxacum* type, *Teucrium*, *Thesium*, *Torilis arvensis* type, *Torilis japonica* type, *Trifolium*, *Trifolium alpestre* type, *Trifolium pratense*, *Trifolium pratense* type, *Trifolium* type, *Turgenia* type, *Urtica*, *Urtica dioica*, *Urtica dioica* type, *Urtica pilulifera* type, *Urtica* type, Urticaceae, *Vaccaria* type, *Valeriana*, Valerianaceae,

	Verbascum, *Verbascum* type, *Verbena*, *Veronica* type, *Vicia*, *Vicia* type, *Viola*, Violaceae, *Xanthium*
Halophyte	Amaranthaceae/Chenopodiaceae, *Atriplex*, *Calligonum*, *Ceratoides*, Chenopodiaceae, *Crambe*, *Frankenia*, *Frankenia* hirsute, *Halogeton*, *Halothamnus* type, *Hammada* type, *Lycium*, *Nitraria*, *Peganum*, *Peganum harmala*, *Salsola*, *Salsola* type, *Suaeda*, *Suaeda* type, *Tamarix*
Geophyte	*Allium*, *Allium* type, *Anthericum* type, Araceae, *Asparagus* type, *Asphodeline*, *Asphodelus*, *Calamus*, *Colchicum*, *Cyclamen*, *Eremurus*, *Fritillaria* type, *Iridaceae*, *Iris*, Liliaceae, *Lilium*, *Maianthemum* type, *Muscari*, *Narthecium* type, *Ornithogalum* type, *Scilla* type, *Scorzonera*, *Scorzonera humilis* type, *Scorzonera* type, *Tulipa sylvestris* type, *Tulipa systola* type
Succulent	*Aellenia* type, Amaranthaceae/Chenopodiaceae, Chenopodiaceae, Crassulaceae, *Euphorbia*, *Sedum*, *Sedum* type, Zygophyllum
Grass graminoid	*Glyceria* type, *Lygeum*, Poaceae, *Secale*, *Secale* type, *Stipa*
Sedge graminoid	*Carex*, *Carex* type, *Cladium*, *Cladium mariscus*, Cyperaceae, *Cyperus*, *Fimbristylis*, Juncaceae, *Juncus*/*Luzula*, *Rhynchospora* type, *Scheuchzeria palustris*, *Schoenoplectus*
Arctic dwarf shrub	*Betula*, *Bruckenthalia*, *Dryas* type, Ericaceae, Ericaceae type, *Potentilla*, *Potentilla* type, *Primula*, Primulaceae, *Rheum*, *Rheum* type, *Rubus arcticus*, *Rubus chamaemorus*, *Salix*, *Vaccinium*, *Vaccinium* type, *Vaccinium uliginosum* type, *Veratrum* type
Switch plants	*Ephedra*, *Ephedra alata* type, *Ephedra distachya*, *Ephedra distachya* type, *Ephedra fragilis*, *Ephedra fragilis* type, *Ephedra fragilis* var *campylopoda*, *Ephedra major type*
Climber/liana/vine	*Calystegia*, *Calystegia sepium*, *Clematis*, *Clematis* type, Convolvulaceae, *Convolvulus*, *Convovulus arvensis*, *Cuscuta*, *Glycine*, *Hedera*, *Hedera helix*, *Humulus*, *Humulus lupulus*, *Lonicera*, *Periploca*, Ranunculaceae, *Smilax*, Solanaceae, *Solanum*, *Solanum dulcamara*, *Tamus communis*, *Vitis*, *Vitis vinifera*
Boreal low-to-high shrub	Cotoneaster, *Erica*, *Erica* type, Ericaceae, Ericaceae type, *Myrica*, Pinaceae, *Pinus*, *Pinus* (Diploxylon), *Pinus* subg. *Pinus*, *Ribes*, *Ribes* cf. *montigenum*, *Vaccinium*, *Vaccinium* type
Temperate low-to-high shrub	Amaranthaceae/Chenopodiaceae, *Atropa*, Berberidaceae, *Berberis*, *Calluna*, *Calluna vulgaris* type, Chenopodiaceae, Cistaceae, *Cistus*, Convolvulaceae, *Cornus*, *Cornus mas*, *Cornus mas*/*Cornus suecica*, *Cornus sanguinea*, *Cotoneaster*, *Crataegus*, *Crataegus* type, *Daphne*, *Erica*, *Erica* type, Ericaceae, Ericaceae type, *Hippophae*, *Hippophae rhamnoides*, *Lycium*, *Prunus*, *Prunus spinosa* type, *Prunus* type, Rhamnaceae, *Rhamnus*, *Rhododendron*, *Rhododendron ponticum*, *Ribes*, *Rosa*, *Rosa* type, *Rubus fruticosus*, Rutaceae, *Sambucus*, *Sambucus ebulus*, *Sambucus nigra* type, *Sambucus* type, Scrophulariaceae, Thymelaeaceae, *Thymus*, *Viburnum*, *Viburnum* type

Warm-temperate low-to-high shrub/small tree	*Abutilon*, Amaranthaceae/Chenopodiaceae, *Arceuthobium*, Berberidaceae, *Caragana*, *Carpinus*, *Carpinus orientalis*, *Carpinus orientalis* type, *Carpinus orientalis*/*Ostrya*, *Celastrus*, *Cercis siliquastrum*, Chenopodiaceae, Cistaceae, *Cistus*, *Cistus incanus*, *Cistus salviifolius*, *Colutea*, Convolvulaceae, *Convolvulus*, *Cornus*, *Cornus mas*, *Cornus mas*/*Cornus suecica*, *Cotinus*, *Daphne*, *Elaeagnus*, *Erica*, *Erica* type, Ericaceae, Ericaceae type, *Euonymus*, *Fontanesia phillireoides*, *Frangula*, *Frangula alnus*, *Fraxinus ornus*, *Genista* type, *Jasminum*, *Jasminum fruticans*, *Juniperus*, *Juniperus communis*, *Juniperus* type, *Lagonychium* type, *Lavatera* type, Leguminosae, *Ligustrum*, *Morus*, Myrtaceae, *Myrtus*, Oleaceae, *Paeonia*, *Paliurus*, *Paliurus spina-christi*/*Rhamnus*, *Paliurus*/*Rhamnus*, *Phillyrea*, *Phillyrea angustifolia*, *Pistacia*, *Prosopis*, Rhamnaceae, *Rhamnus*, *Rhamnus* subg. *Frangula*, *Rhododendron*, *Rhus*, *Rhus coriaria*, *Ruta*, Rutaceae, *Sambucus*, *Sambucus* type, Solanaceae, *Solanum*, *Syringa*, Thymelaeaceae, *Thymus*, *Ulex* type, *Vitex agnus-castus*
Xerophytic shrub	*Alhagi*, Amaranthaceae/Chenopodiaceae, *Artemisia*, *Artemisia* type, *Atraphaxis*, Capparidaceae, *Capparis*, Chenopodiaceae, *Chrozophora*, *Cistaceae*, *Cistus*, *Cistus ladanifer*, *Cistus salviifolius*, *Cotinus*, *Erica*, *Erica* type, Ericaceae, Ericaceae type, *Euphorbia*, *Juniperus*, *Juniperus* type, *Lycium*, *Myricaria*, *Nitraria*, *Ononis* type, *Paliurus*, *Paliurus spina-christi*/*Rhamnus*, *Paliurus*/*Rhamnus*, Rhamnaceae, *Rhamnus*, *Ruta*, Rutaceae, *Sarcopoterium*, Thymelaeaceae, *Thymus*, *Trachomitum*, *Zygophyllum*
Boreal cold-deciduous malacophyll broadleaved tree	*Alnus incana*, *Alnus viridis*, *Betula*, *Populus*, *Salix*
Boreal evergreen needle-leaved tree	*Abies*, *Picea*, *Picea abies*, Pinaceae, *Pinus*, *Pinus* (Haploxylon), *Pinus cembra*, *Pinus peuce*
Boreal needle-leaved deciduous tree	*Larix*, Pinaceae
Cool-temperate evergreen needle-leaved tree	*Picea*, *Picea orientalis*, Pinaceae
Eurythermic evergreen needle-leaved tree	Cupressaceae, *Cupressus*, *Juniperus*, *Juniperus communis*, *Juniperus* type, *Pinaceae*, *Pinus*, *Pinus* (Diploxylon), *Pinus* subg. *Pinus*
Temperate (frost-induced late budburst) cold-deciduous malacophyll broadleaved tree	*Acer*, *Acer platanoides*, Aceraceae, *Cornus*, *Cornus mas*, *Cornus mas*/*Cornus suecica*, *Corylus*, *Corylus avellana*, *Fraxinus*, *Fraxinus angustifolia*, *Fraxinus excelsior*, *Fraxinus excelsior* type, *Malus*, *Malus sylvestris* type, *Malus* type, *Populus*, *Prunus*, *Prunus spinosa* type, *Prunus* type, *Pyrus*, *Quercus*, *Quercus* (deciduous), *Quercus robur* type, *Salix*, *Sorbus*, *Sorbus* type, *Tilia*

Temperate (spring frost tolerant) cold-deciduous malacophyll broadleaved tree	*Acer campestre* type, *Aesculus*, *Carpinus*, *Carpinus betulus*, *Cercis siliquastrum*, *Fagus*, *Fagus sylvatica*, *Frangula*, *Frangula alnus*, *Fraxinus ornus*, Leguminosae, *Morus*, *Pistacia*, *Prunus* type, *Quercus*, *Quercus cerris*, *Quercus cerris* type, *Quercus frainetto*, *Quercus ithaburensis*, *Rhamnus* subg. *Frangula*, *Syringa*, *Ulmus*, *Ulmus glabra*, *Ulmus laevis*, *Ulmus*/*Zelkova*
Temperate (spring frost intolerant) cold-deciduous malacophyll broadleaved tree	*Carpinus*, *Carpinus orientalis* type, *Carpinus orientalis*/*Ostrya*, *Carya*, *Castanea*, *Castanea sativa*, *Celtis*, *Celtis reticulate*, *Ceratonia*, *Fagus*, *Fagus orientalis*, Juglandaceae, *Juglans*, *Juglans regia*, Leguminosae, *Liquidambar*, *Ostrya*, *Ostrya* type, *Parrotia persica*, *Platanus*, *Pterocarya*, *Pterocarya fraxinifolia*, *Punica*, Rhamnaceae, *Rhamnus*, *Styrax*, *Ulmus*/*Zelkova*, *Zelkova*
Temperate evergreen needle-leaved tree	*Abies*, *Abies nordmanniana*, *Cedrus*, Pinaceae, *Pinus*, *Pinus* (Diploxylon), *Pinus* (Haploxylon), *Pinus* subg. *Pinus*, *Pinus sylvestris*, *Taxus*
Warm-temperate evergreen malacophyll broadleaved tree	*Acacia*, *Acacia greggii*, *Acalypha*, *Citrus*, *Diospyros*, *Ficus carica*, *Ilex*, Leguminosae
Warm-temperate sclerophyll tree	*Acalypha*, *Arbutus*, *Buxus*, Leguminosae, *Nerium*, *Olea*, Oleaceae, *Quercus*, *Quercus* (evergreen), *Quercus calliprinos*, *Quercus coccifera*, *Quercus coccifera* type, *Quercus ilex*, *Quercus ilex* type, Rutaceae
Warm-temperate needle-leaved evergreen tree	Cupressaceae, *Cupressus*, *Juniperus*, *Juniperus sabina*, *Juniperus scopulorum*, *Juniperus* type, Pinaceae, *Pinus*, *Pinus* (Diploxylon), *Pinus* (Haploxylon), *Pinus pinaster*
Tuft tree	*Phoenix*

Supplementary Table 2.7: Comparison of percent changes in biomes between adjacent samples for selected high-resolution Holocene pollen records using the new method and the standard biomisation approach. The biome with the lowest percentage of changes is highlighted in bold.

				Biome change percentage	
Entity name	**Lat - Lon**	**No. of samples**	**Age interval (cal. Years BP)**	**New approach**	**Standard biomisation**
Didachara core	41.68 - 42.5	52	0 - 4071	**8**	45
Lake Blatisto	41.62 - 24.68	142	0 - 1626	**15**	43
Kumisi core 1	41.58 - 44.83	30	0 - 1128	**0**	69
Ispani II core 1	41.87 - 41.8	21	0 - 1862	**0**	10
Imera core 1	41.65 - 44.22	34	0 - 2208	**39**	55
Dead Sea DS7-1SC core	31.49 - 35.44	55	0 - 2360	**7**	24
Kumata Core	42.59 - 23.25	19	0 - 1285	50	**28**
Asi Gonia 2	35.25 - 24.28	41	0 - 1102	**10**	20
Demiryurt Gölü Bottema Core	39.73 - 37.38	21	0 - 1551	65	65
Litochoro_core	40.14 - 22.55	35	0 - 2234	**24**	29
Aligol core 1	41.63 - 44.02	28	0 - 1360	26	26
Iaz Core	47.11 - 22.66	105	15 - 5315	**13**	30
Capatana core	46.47 - 23.14	60	16 - 2335	8	**2**
Lake Almalou	37.67 - 46.63	53	157 - 3402	27	**15**
Melen Gölü	40.77 - 31.05	76	165 - 4051	**3**	15
Tsavkisi core 1	41.68 - 44.72	73	174 - 4575	**31**	33
Amtkel 1	43.28 - 41.29	24	560 - 2002	**17**	26
Sapanca long core SA03R6	40.72 - 30.26	31	776 - 1865	**27**	50
Dry Lake 2	42.04 - 23.53	81	1295 - 6475	**6**	34
Voulkaria	38.87 - 20.83	51	1809 - 2947	**0**	18
Maharlou Lake	29.48 - 52.76	38	3625 - 5902	27	**0**

Arkutino AR2	42.37 - 27.73	59	3702 - 7314	**0**	7
Arkutino AR1	42.37 - 27.73	31	4705 - 6876	**13**	23
Lake Varna (Beloslav-Poveljanovo)	43.2 - 27.83	27	4986 - 6861	8	**0**
Mohos1	46.08 - 25.92	92	5428 - 10991	23	**9**
Giannitsa B	40.67 - 22	28	7237 - 8674	**41**	59
Steregoiu	47.81 - 23.54	142	7273 - 12159	11	**1**
GeoTü SL152	40.1 - 24.36	76	7531 - 10073	**16**	31
Van - Wick Core	38.53 - 42.47	137	8597 - 11705	**1**	13
Taul Zanogutii core	45.33 - 22.8	28	10556 - 11857	**22**	37

Supplementary Table 2.8: Optimal threshold for each biome used for detection of potential non-analogue assemblages.

Biome	Threshold
CENF	0.8245
CMIX	0.8812
DESE	0.8751
ENWD	0.8665
GRAM	0.8817
TEDE	0.8694
TUND	0.8835
WTFS	0.8450
XSHB	0.7987

References

Harrison, S. P. (2019). Modern pollen data for climate reconstructions, version 1 (SMPDS) [Data set]. University of Reading. https://doi.org/10.17864/1947.194

Hengl, T., Walsh, M. G., Sanderman, J., Wheeler, I., Harrison, S. P., & Prentice, I. C. (2018). Global mapping of potential natural vegetation: An assessment of machine learning algorithms for estimating land potential. PeerJ, 6, e5457. https://doi.org/10.7717/peerj.5457

Marinova, E., Harrison, S. P., Bragg, F., Connor, S., Laet, V. de, Leroy, S. A. G., Mudie, P., Atanassova, J., Bozilova, E., Caner, H., Cordova, C., Djamali, M., Filipova-Marinova, M., Gerasimenko, N., Jahns, S., Kouli, K., Kotthoff, U., Kvavadze, E., Lazarova, M., … Tonkov, S. (2018). Pollen-derived biomes in the Eastern Mediterranean–Black Sea–Caspian-Corridor. Journal of Biogeography, 45(2), 484–499. https://doi.org/10.1111/jbi.13128

Wei, D., Prentice, I. C., & Harrison, S. P. (2020). The climatic space of European pollen taxa. Ecology, 101(8), e03055. https://doi.org/10.1002/ecy.3055

Chapter 3. Holocene vegetation dynamics of the Eastern Mediterranean region: old controversies addressed by a new analysis

This chapter has been published as: **Cruz-Silva, E.**, Harrison, S. P., Prentice, I. C. & Marinova, E.,. (2023). Holocene vegetation dynamics of the Eastern Mediterranean region: Old controversies addressed by a new analysis. Journal of Biogeography, 00, 1–17. https://doi.org/10.1111/jbi.14749 . It has been written according to the guidelines of the journal.

3.1 Abstract

Aim: We reconstruct vegetation changes since 12 ky in the Eastern Mediterranean to examine four features of the regional vegetation history that are controversial: the extent of non-analogue vegetation assemblages in the transition from the Late Glacial to the early Holocene, the synchroneity of postglacial forest expansion, the geographical extent of temperate deciduous forest during the mid-Holocene and the timing and trigger for the re-establishment of drought-tolerant vegetation during the late Holocene.Location: The Eastern Mediterranean–Black Sea Caspian Corridor.Ta xo n: Vascular plants.

Methods: We reconstruct vegetation changes for 122 fossil pollen records using a method that accounts for within-biome variability in pollen taxon abundance to deter-mine the biome with which a sample has greatest affinity. Per-biome affinity thresh-old values were used to identify samples that do not belong to any modern biome. We apply time series analysis and mapping to examine space and time changes.

Results: Sites with non-analogue vegetation were most common between 11.5 and 9.5 ky and mostly in the Carpathians. The transition from open vegetation to forest occurred at 10.64 ± 0.65 ky across the whole region. Temperate deciduous forest was not more extensive at 6 ky; maximum expansion occurred between 5.5 and 5 ky. Expansion of forest occurred between c. 4 and 2.8 k, followed by an abrupt decrease and a subsequent recovery. This pattern is not consistent with a systematic decline of forest towards more drought-tolerant vegetation in the late Holocene but is consistent with centennial-scale speleothem patterns linked to variations in moisture availability.

Main Conclusions: We show the occurrence of non-analogue vegetation types peaked during early Holocene, forest expansion was synchronous across the region and there was an expansion of moisture-demanding temperate trees around 5.5 to 5 ky. There is no signal of a continuous late Holocene aridification, but changes in forest cover appear to reflect climatic rather than anthropogenic influences

3.2. Introduction

The Eastern Mediterranean–Black Sea Caspian Corridor (EMBSeCBIO) region (33°–49° N, 20°–60° E) provides opportunities to examine Holocene vegetation changes and how these have been shaped by climate and human activities, because it is characterised by large climate and elevation gradients and has a long history of human occupation stretching back to the introduction of Neolithic farming in the early Holocene. Several works have summarised vegetation changes for parts of the region or specific time periods (e.g. Bottema et al., 1994; Bozilova & Tonkov, 1995; Connor & Sagona,2007; Elenga et al., 2000; Magyari et al., 2019; Prentice et al., 1996 ; Tarasov et al., 1998; Zeist & Bottema, 1991). However, the limited spatio-temporal coverage of these analyses means that there is no comprehensive overview of the vegetation history of the EMBSeCBIO region and several features of the Holocene record are still a matter of debate, including the extent of non-analogue vegetation in the transition from the Late Glacial to the early Holocene, the timing of postglacial afforestation across the region, the geographical extent of temperate deciduous forest during the mid-Holocene and the exact timing of the expansion of drought-tolerant vegetation during the late Holocene. The large number of pollen records from individual sites across the region compiled by the EMBSeCBIO project (Cordova et al., 2009; Marinova et al., 2018) allows a more comprehensive analysis of Holocene vegetation changes to be made.

Pollen records from the northern extratropics indicate that some vegetation assemblages during the Late Glacial and early Holocene combined species that are not present together today, so-called non-analogue vegetation types (Magyari et al., 2014, 2018, 2019; Williams & Jackson, 2007; Zanon et al., 2018). The existence of non-analogue vegetation types in the EMBSeCBIO region has not been explored in a systematic way. However, it has been argued that some areas of the Carpathians (Feurdean et al., 2007), western Georgia (Connor & Kvavadze, 2009) and the southwestern Black Sea (Bottema et al., 1994) were refugia for tree taxa, including species of Fagus, Ulmus and Acer, during the glacial period. The pollen percentages of these tree taxa are much higher in some early Holocene samples than in samples from vegetation where they occur today, but are consistently associated with a high abundance of grasses (Bottema et al., 1994; Feurdean et al., 2007; Robles et al., 2022). There has been no systematic evaluation of whether these anomalous values exceed observed variability across the full environmental range of the biomes in which these tree species occur today, and therefore whether these samples genuinely represent non-analogue vegetation.

The postglacial timing of forest spread in the EMBSeCBIO region is also controversial. It has been suggested that forest development in the western part of the region began in the early Holocene, while further east the increase in forests occurred 2–5 millennia after the beginning of the Holocene (Djamali et al., 2010; Messager et al., 2017). This delay has been attributed to dry conditions during the early Holocene in the east (Djamali et al., 2010; Joannin et al., 2014; Messager et al., 2013; Wright et al., 2003). However, δ18O isotopes from lake carbonates and speleothems and leaf wax δ13C isotopes from the region have been interpreted as showing humid

conditions since the beginning of the Holocene (Bar-Matthews et al., 2003; Bliedtner et al., 2020; Cheng et al., 2015; Eastwood et al., 2007; Fleitmann et al., 2009; Göktürk et al., 2011; Roberts et al., 2008; Stevens et al., 2001). Several hypotheses have been proposed to explain the apparent delay in forest development, including the time lag for tree mi-gration from glacial refugia (Connor & Kvavadze, 2009; Messager et al., 2017), the impact of fire (Roberts, 2002; Turner et al., 2010), the fact that increases in precipitation were concentrated out-side the growing season (Brayshaw et al., 2011; Dean et al., 2015; Göktürk et al., 2011), a negative feedback from the freshwater lake which occupied the Black Sea basin before it was joined to the Mediterranean (Göktürk et al., 2011; Messager et al., 2017) and potential anthropogenic modification of the landscape (Asouti & Kabukcu, 2014). However, the extent of dry conditions and the inhibition of forest growth in the eastern part of the EMBSeCBIO region are still unclear, making it difficult to evaluate these hypotheses.

Early analyses of vegetation patterns in the mid-Holocene suggested that temperate deciduous forest was more extensive in southern Europe at 6 ky (cal. yr BP) than today, replacing cool mixed and conifer forest in the mountains of southern Europe and Mediterranean vegetation in the lowlands (Huntley & Prentice, 1993; Peyron et al., 1998; Prentice et al., 1996). The replacement of xerophytic vegetation by temperate deciduous forest implies an increase in plant available moisture during the growing season, while winters remained cooler than today. Collins et al. (2012) also showed an expansion of temperate deciduous forest at 6 ky compared to present but argued that the extent of this expansion was overestimated in earlier reconstructions which considered all sites with a mid-Holocene record and did not measure the expansion relative to reconstructions of modern day vegetation at the same site. According to the Collins et al. (2012) reconstruction, drought-tolerant, open vegetation was still present in southern Europe, including in the Eastern Mediterranean region which is the focus of this study, implying the continuation of a pronounced seasonality in the precipitation regime. However, none of these vegetation reconstructions consider possible with-in-biome variability of temperate deciduous forest and all of them either focus only on the 6 ky window or have limited coverage of the EMBSeCBIO region. Thus, the question of the extent of temperate deciduous forests during the middle Holocene is still unanswered.

It has been suggested that there has been a general increase in drought-tolerant vegetation, reflecting a trend towards more arid conditions, since the mid-Holocene in the Mediterranean region (Jalut et al., 1997, 2009; Magny et al., 2002; Roberts, Brayshaw, et al., 2011; Roberts, Eastwood, et al., 2011; Roberts et al., 2001, 2004, 2008). However, there is debate about whether this occurred simultaneously across the region or indeed was ubiquitous (Herzschuh et al., 2022). Isolating a long-term trend is further complicated by the fact that multi-centennial oscillations in precipitation have been inferred from pollen and speleothem records in the Eastern Mediterranean, but these oscillations are neither simultaneously nor seen everywhere (Bar-Matthews & Ayalon,2011; Bini et al., 2019; Burstyn et al., 2019; Göktürk et al., 2011; Kaniewski et al., 2018). Furthermore, there is some debate about whether the increase in drought-tolerant vegetation was a consequence of changes in climate or the effect of changes in

land use on runoff (Jacobson et al., 2021; Schilman et al., 2001). In this article, we use a recently developed method to reconstruct vegetation from pollen samples which takes account of within-biome variability in taxon abundance and also identifies assemblages that are not typical of any modern biome (Cruz-Silva et al., 2022). This allows us to address whether existing controversies are in part a reflection of the use of subjective approaches to vegetation reconstruction. We address four questions: (1) the extent of non-analogue vegetation during the postglacial period; (2) the synchroneity of forest expansion during the early Holocene; (3) the extent of temperate deciduous forest in the mid-Holocene and (4) the expansion of drought-tolerant vegetation during the late Holocene.

3.3. Materials and Methods

Vegetation reconstructions for fossil pollen sites in the EMBSeCBIO region were made using the technique described by Cruz-Silva et al. (2022) (Supplementary Appendix 3.1), using 5765 modern pollen samples from Europe, the Middle East and northern Eurasia de-rived from the EMSeCBIO and SPECIAL databases (Harrison, 2019; Harrison et al., 2021), which were assigned to biomes based on potential natural vegetation reconstructions (Hengl et al., 2018) (Figure 3.1) using a previously tested search window of 20 × 20 km [close to the theoretical pollen source area for small (<1 km2) basins accordingly to Prentice (1988) and Sugita (1993)] to characterise the within-biome means and standard deviations of the abundances of individual taxa (see details of the methods in Cruz-Silva et al., 2022). This technique is an improved method of vegetation reconstruction compared to the biomisation approach that was previously applied to the EMBSeCBIO region (Marinova et al., 2018) because it allows the identification of non-analogue vegetation types, i.e. assemblages that consist of associations of taxa with abundances very different from those seen in any modern biome.

The new method produces a substantial increase in the prediction accuracy for individual biomes compared to biomisation and a reduction in the number of misassigned samples (Cruz-Silva et al., 2022). We have made a further evaluation of the method to determine how accurate it is in predicting the vegetation represented by core top samples (age <150 cal. yrs. BP) from fossil pollen cores from the EMBSeCBIO region. We discuss the application of this method to fossil records from the EMBSeCBIO region and then describe the analyses of the fossil reconstructions to address the four questions posed earlier.

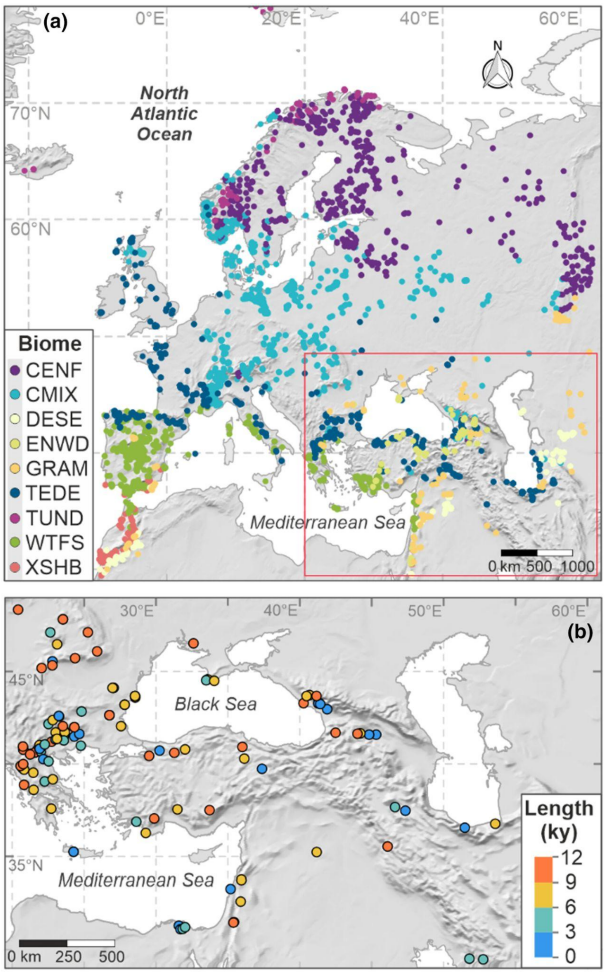

Figure 3.1. Distribution of modern and fossil pollen sites (WGS84 Mercator projection). (a) Distribution of modern pollen entities from the SPECIAL modern pollen dataset (SMPDS) and the Eastern Mediterranean–Black Sea Caspian corridor (EMBSeCBIO) database. The colours represent the biome at each site derived from the Hengl et al. (2018) reconstruction of potential natural vegetation. The biome codes are: CENF, cold evergreen needleleaf forest; CMIX, cool mixed evergreen needleleaf and deciduous broadleaf forest; DESE, desert; ENWD, evergreen needleleaf woodland; GRAM, graminoids with forbs; TEDE, temperate deciduous malacophyll broadleaf forest; TUND, tundra; WTFS, warm-temperate evergreen needleleaf and sclerophyll broadleaf forest; XSHB, xeric shrubland. (b) Distribution of the fossil pollen records from the EMBSeCBIO region that completely or partially span the last 12 ky. The colour represents the time length of the record.

3.3.1. Application to fossil records

Fossil pollen data were obtained from the EMBSeCBIO database (Harrison et al., 2021), which contains records derived from public-access databases and the original authors. The database contains 187 Holocene records. Vegetation reconstructions were made after filtering to remove records (a) with no radiocarbon dating, (b) where the age of the uppermost pollen sample was unknown (e.g. because they come from extinct lakes or stratigraphic sequences), (c) where there is a major hiatus after the youngest radiocarbon date, (d) where more than half of the radiocarbon dates were rejected by the original authors, (e) where more than half of the ages are based on pollen correlation with other radiocarbon-dated records and (f) marine records or cores from very large lakes (>500 km2). We kept records where the original publication indicates a

major hiatus but where there are radiocarbon dates above this hiatus allowing an age model to be constructed for the post-hiatus part of the record. As a result of this filtering, vegetation reconstructions were made for 122 continental records from basins ranging in size from <0.01 to 500 km2. New age-depth models were produced for these 122 records using the IntCal20 calibration curve (Reimer et al., 2020) and the 'rbacon' R package (Blaauw et al., 2021) in the 'AgeR' R package (Villegas-Diaz et al., 2021). This package provides an optimum model for each record, based on the lowest quantified area between prior and posterior accumulation rate distribution curves (see Harrison et al., 2022). The selected model was checked manually and through visual inspection to ensure that the final age models represented the date information accurately and did not manifest abrupt shifts in accumulation rates or changes at the dated depth. The records have a mean length of 6700 years (Figure 3.1) and a mean resolution of 265 years (Supplementary Figure 3.1). We calculated dissimilarity and similarity scores (Supplementary Appendix 3.1) for each fossil sample with respect to each biome in turn.

3.3.2. Non-analogue vegetation types

We applied the per-biome threshold values determined by Cruz-Silva et al. (2022) to detect whether a given sample exceeded the threshold for assignment to a given biome. Samples that exceeded this threshold for all biomes were considered to represent non-analogue vegetation. Since there is some uncertainty in the matches between fossil and modern samples, we used a 5% threshold to distinguish false positives, and only consider samples that exceed this threshold as actual non-analogues. We quantified the proportion of sites with at least one non-analogue sample in 300-year windows with 50% overlap to produce a time series of the occurrence of non-analogues through time. The size of the window was chosen to approximate the mean resolution of the records (265 years). Since the time series are expressed as a percentage of total records in each window, we examined the number of pollen records available in each window to verify that changes were not an artefact of data availability. We also checked that individual samples were not depauperate and the counts sufficiently large to ensure an adequate representation of the vegetation in the pollen assemblage. Previous research has shown that high-elevation records may be contaminated by upward transport of pollen from lower elevation sites (Takahara et al., 2000), and this might provide an explanation for apparently non-analogue samples. To test this, we created separate time series for high (>1500 m a.s.l.), medium (between 500 and 1500 m a.s.l.) and low (<500 m a.s.l.) elevation sites.

3.3.3. Timing of the early Holocene forest expansion

We used terrestrial sites spanning at least 3000 years during the period between 7 and 11.6 ky, with at least 13 pollen samples during this interval, and where the oldest pollen sample had an age of at least 11.2 ky to analyse the timing of forest expansion. Temperate deciduous malacophyll broadleaf forest (TEDE) and cool mixed evergreen needle leaf and deciduous broadleaf forest (CMIX) were considered as forest; samples classified as belonging to other bi-omes were considered together since they represent less moisture-demanding vegetation types. The non-normalised similarity scores for each pollen sample were summed separately for both forest and other vegetation and then expressed as a percentage. The resulting curve was smoothed

using the mean value in windows of 300 years with 50% overlap. This compositing approach has been used with other types of data, for example charcoal and speleothem data (Parker et al., 2021; Power et al., 2010), to minimise the effect of age uncertainty and differences in sampling resolution between records and to emphasise the common signal across sites. Breakpoint analysis (Zeileis et al., 2003) was applied on the time series for each individual site to obtain the optimal number (smallest magnitude of residuals) of break points in the trends in the sequence (score ~ age) using the R package 'strucchange'. Linear regressions were performed between the identified break points in each sequence. The earliest point indicating a change from zero or negative slope (no change or decrease in forest) to a positive slope (increase in forest) was taken as the start of forest expansion. The mean and standard deviation between all estimated inception points was calculated to obtain the approximate age of the start of forest expansion at each site. We explored whether there were differences in the timing of initial forest expansion as a function of latitude, longitude and elevation.

3.3.4. Timing of mid-Holocene expansion of temperate deciduous forest

We examined all continental records that wholly or partially covered the mid-Holocene, defined here as the interval from 7 to 4 ky. We determined the predicted biome in successive non-over-lapping 300-year windows centred on 7.0, 6.5, 6.0, 5.5, 5.0, 4.5 and 4.0 ky for each record, where the width of the window allows for potential chronological uncertainties. In cases where more than one biome was predicted during a time window at a given site, we used the most common biome across all samples (following Bigelow et al., 2003) or, in the case of a tie, the biome with the highest sum of similarity scores. In order to express the changes of TEDE through time, we filtered the sites predicted as TEDE and expressed as the percentage of TEDE per time window relative to the total number of sites. To express the changes of TEDE through space as maps, in each time window, we categorised the sites predicted as TEDE into one of the following categories: 'Remains as TEDE' for records where TEDE had been present in the previous interval and persisted, 'change to TEDE' for records which were not TEDE in the previous interval and became TEDE and 'TEDE' for sites which were TEDE in the selected time window but had no record in the previous time window.

3.3.5. Evaluation of the expansion of drought-tolerant vegetation in the late Holocene

We examined the vegetation trends from 6 ky onwards and through the late Holocene by creating a composite time series of the number of sites classified as forest, where forest includes samples allocated to TEDE and CMIX, in 300-year windows with 50% overlap. As the intention was to compare the vegetation time series with evidence for changes in both human population density and speleothem oxygen isotope records of hydroclimate, we focused these analyses on the region where there are speleothem isotope records covering at least 3000 years from 6 ky to the present. Additionally, we assessed the robustness of the relationships between changes in forest cover, human population and climate by examining these trends at a sub-regional scale. We

focus on the three regions where there is sufficient archaeological data to construct reliable summed probability distribution (SPD) curves: Greece, Anatolia and the Levant.

The SPD of archaeological radiocarbon dates has been widely used as a measure of changes in human population density (see Rick, 1987; Robinson et al., 2019), including in the Eastern Mediterranean (Palmisano, Lawrence, et al., 2021; Weiberg, Bevan, et al., 2019). We extracted data from the Mediterranean basin region from the p3k14c global database of archaeological radiocarbon dates (Bird et al., 2022). An SPD curve covering the interval from 6 to 2.5 ky was produced using 5979 calibrated radiocarbon dates (using the Intcal20 calibration curve) from 620 sites, without normalising and using the 'rcarbon' R package (Bevan et al., 2022). This approach cannot be used for intervals younger than 2.5 ky because dating of archaeological records in the more recent period tends to rely on typo-chronological schemes defined by short-lived pottery types and coins rather than radiocarbon (Palmisano, Bevan, et al., 2021; Roberts et al., 2019; Weiberg, Hughes, et al., 2019). Settlement data from archaeological surveys have been used to reconstruct populations changes in the interval younger than 2.5 ky (e.g. Palmisano et al., 2017; Roberts et al., 2019), but are only available for a few limited sub-regions, for example for the Peloponnese and Macedonia (Weiberg et al., 2016) in Greece, the Sagalassos basin and the Burdur province in south western Anatolia (De Cupere et al., 2017; Dusar et al., 2012) and thus cannot be used to construct a regional com-posite. Intervals of higher and lower than average human population density according to the regional SPD curve between 6 and 2.5 ka were identified using an exponential null model of population growth, where the periods of growth (and decline) were those intervals in the SPD that were significantly different from the fitted model (Timpson et al., 2014). An exponential null model was used because theoretically, this accounts for constant homogeneous taphonomic loss of archaeological sites without having to resort to any other cor-rection bias (Timpson et al., 2014). We also compared the regional SPD with SPD curves constructed for sub-regions, Greece, Anatolia and Levant, using the same dataset.

Oxygen isotope records from speleothems are generally interpreted as indicating changes in moisture in the region above the cave site (Bar-Matthews et al., 2003; Burstyn et al., 2019; Cheng et al., 2015; Fleitmann et al., 2009). We extracted five oxygen isotope records in the EMBSeCBIO region from the SISAL v2.2 database (Comas-Bru et al., 2020, b). The SISAL database contains multiple age models for each record; we preferentially used models built with Bchron (which is the most common model type in the database), followed by Bacon or the originally provided ages.

3.4. Results

3.4.1. Prediction accuracy of the modern core-top reconstructions

The quantitative evaluation of the ability of the training set to predict modern core-top pollen samples from the EMBSeCBIO region showed a balanced accuracy of 54% when only the dominant biome within a 21 km search window was considered (Supplementary Appendix 3.1; Supplementary Table 3.1). As in the evaluation using the modern samples from the region (Cruz-Silva et al., 2022), the accuracy increased substantially when both the dominant biome and the sub-dominant biome were considered, reaching 69% (Supplementary Table 3.1). This level of

accuracy is not as good as the values obtained using modern pollen samples (with ages <50 years) from the region (64% and 76% respectively), most likely reflecting the wider time interval (c. 150 years) covered by the core-top samples. Nevertheless, the technique correctly predicted modern vegetation patterns in the region including grasslands in the southeastern Caucasus, Mesopotamia and the Levant, temperate forest in the Balkans and warm temperate shrublands and forest in the Mediterranean lowlands. As in the case of the modern evaluation, misallocations occurred between closely related biomes (e.g. TEDE and CMIX) and were frequently in the Carpathian region (Supplementary Figure 3.2) where such misallocations likely reflect pollen transport up elevational gradients.

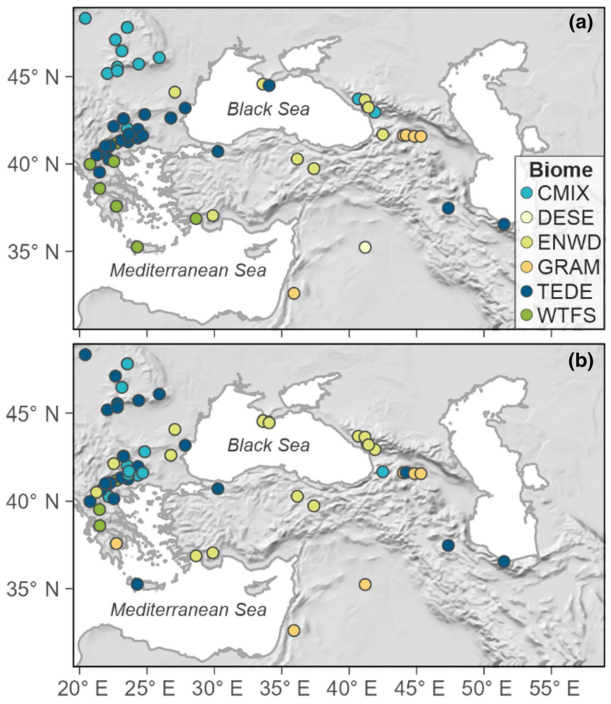

Figure 3.2. Comparison of (a) observed and (b) reconstructed biomes from modern samples in the Eastern Mediterranean–Black Sea Caspian corridor (EMBSeCBIO) region (WGS84 Mercator projection). The observed biomes are derived from the Hengl et al. (2018) reconstruction of potential natural vegetation. The biome codes are: CMIX, cool mixed evergreen needleleaf and deciduous broadleaf forest; DESE, desert; ENWD, evergreen needleleaf woodland; GRAM, graminoids with forbs; TEDE, temperate deciduous malacophyll broadleaf forest; WTFS, warm-temperate evergreen needleleaf and sclerophyll broadleaf forest

3.4.2. Non-analogue vegetation types

The percentage of records with non-analogue samples in the earliest part of the record, between c. 12.3 and 11.8 ky, does not exceed the 5% threshold for false positives (Figure 3.3a). There is a rapid increase in the number of records with non-analogue samples after c. 11.8 ky, and the highest values of the entire record occur between c. 11.5 and 9.5 ky (Supplementary Figure 3.2). There is a gradual decrease in the percentage of records with non-analogue samples until c. 6.0 ky, after which the values do not exceed the 5% threshold for false positives. There is no obvious relationship between changes in the number of sites with non-analogue samples and the total number of sites per time window, and there are no windows with less than 20 records (Figure 3.3a), so it is unlikely that the changes in the representation of non-analogues are an artefact.

Most (~40%) of the records with non-analogue samples during the interval characterised by the maximum occurrence of non-analogues are from sites above 1500 m a.s.l. (Supplementary Figure 3.3). The records are concentrated in the Carpathian region (Figure 3.3b), where there are seven sites with non-analogue samples. There is a single record west of Georgia, and one from the mountains south of the Black Sea. Non-analogue samples are generally characterised by atypical abundances of specific pollen types rather than simply the presence or absence of specific pollen types. The taxonomic composition of samples with no modern analogue, aggregated for the Carpathian region (Supplementary Figure 3.4), showed that the most abundant taxon is Ulmus (>20%), but other tree species including Pinus, Alnus, Picea, Betula, Fraxinus and Coryluswere present and herbaceous taxa including Cyperaceae, Artemisia, Oxyria/Rumex and Ericaceae were also abundant. The taxonomic composition of samples from the Gagra site, eastern Georgia, showed that the most abundant taxa are Abies (>20%), followed by Alnus, Carpinus, Pinus, Fagus, Ulmus, and non-arboreal taxa including Amaranthaceae, Artemisia and Asteraceae. In general, non-analogue samples from the Carpathians and eastern Georgia are characterised by assemblages dominated by moisture-demanding trees, but taxa indicative of open landscapes were present in high abundance. On the other hand, non-analogue samples from the Yenicaga site, south-west of the Black Sea, have a different taxonomic composition, being dominated by Equisetum (>20%), followed by Poaceae, Cyperaceae, Pinus, Abies and deciduous Quercus. Although the high abundances of tree taxa suggest that the assemblages represent in situ vegetation, nevertheless the co-occurrence of moisture-demanding trees with high abundance of non-arboreal taxa raises questions about whether these samples could represent contributions from nearby wetland or alluvial settings.

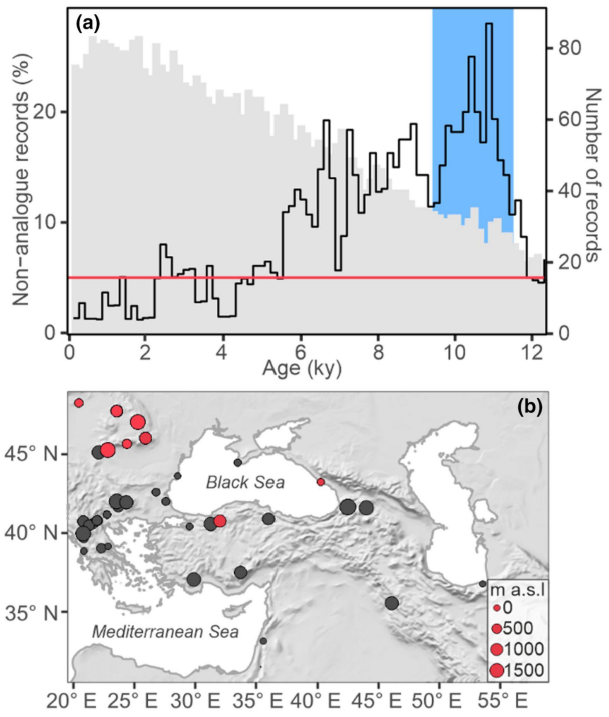

Figure 3.3. (a) Proportion of records from the Eastern Mediterranean–Black Sea Caspian corridor (EMBSeCBIO) region having at least one sample identified as non-analogue in a 300-year time-window over the past 12,000 years, where the time windows were constructed with 50% overlap. The red line indicates the 5% threshold to separate false

positives (values below the threshold). The blue highlighted area corresponds to the period of maximum occurrence of non-analogues. The grey histogram shows the number of records through time in 300-year time window with 50% overlap. (b) The location of sites with more than 5% non-analogues samples during the interval between 11,500 to 9500 yr BP (red circles); sites with less than 5% non-analogues samples are shown as grey circles (WGS84 Mercator projection). The size of the circles represents the elevation of the site.

3.4.3. Post-glacial forest expansion

Comparison of the similarity scores for forest versus other vegetation shows a transition from a predominantly open or drought-tolerant Late Glacial vegetation to dominance of moisture-demanding forests during the early Holocene (Supplementary Figure 3.2 and Supplementary Figure 3.5). However, the nature of this transition varies geographically. At some sites in the Carpathians (e.g. Kismohos, Avrig 1, Mohos1, Sterogoiu), the Rila and Rhodope mountains (e.g. Dry Lake 2, Kupena) and eastern Caucasus (e.g. Didachara), the increase in the forest was large and it became the dominant vegetation type in a matter of centuries. Other sites in the Aegean region (e.g. Gramousti, Orestias G25, Lake Maliq, Supplementary Figure 3.1) show a more gradual and fluctuating increase in forest, while sites in Zagros (e.g. Lake Zeribar) show only a limited and slower increase. Considering all sites, the mean date of the start of forest increase is 10.64 ± 0.65 ky (Figure 4). The individualistic response of each site is consistent with the fact that there is no discernible difference in the timing of the transition from open vegetation to forest either with latitude, longitude or elevation across the sites (Figure 3.4).

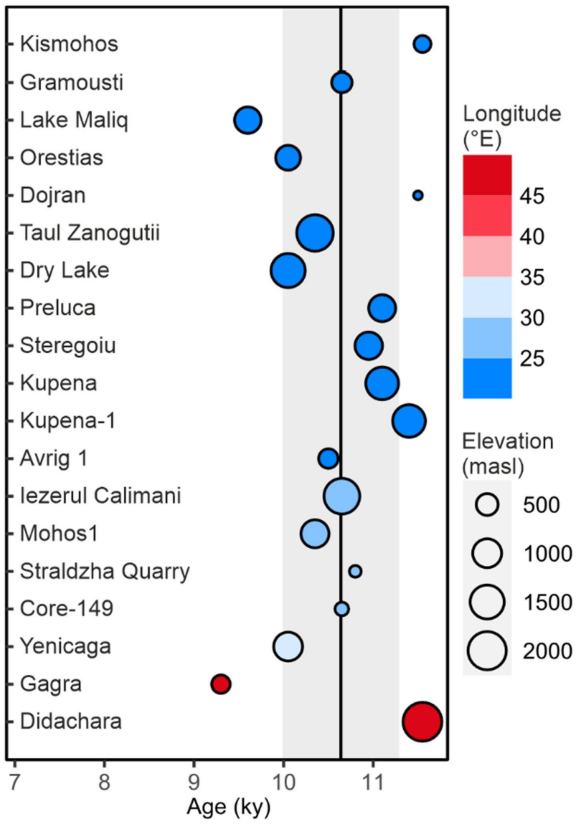

Figure 3.4. The timing of initial forest expansion during the early Holocene in the Eastern Mediterranean–Black Sea Caspian corridor (EMBSeCBIO) region. The sites are organised by latitude (from north to south) and colour coded to

show longitude. The size of the circles shows the elevation of the sites. The black line at 10.64 ky indicates the mean value of forest inception, while the grey bar shows the standard deviation of ±0.65 ky.

3.4.4. Temperate deciduous forest

There is no obvious expansion of TEDE at 6.0 ± 0.15 ky compared to the previous intervals (Figure 3.5), but rather changes in the geographic distribution of these forests (Figure 3.6). The distribution of TEDE at 7.0 ± 0.15 ky was restricted to montane areas in the Carpathians, Zagros, Balkans and Caucasus, and the Euxine region around the Black Sea (Supplementary Figure 3.2; Figure 3.6). TEDE had disappeared from the Carpathian region in the next time window but was present at 6.0 ± 0.2 ky, and also appeared at sites in the Euxine region and in the Aegean region. The maximum expansion of TEDE occurs after 6.0 ky (Figure 3.5; Supplementary Figure 3.6), with additional sites appearing in the Balkans and in Greece in the 5.5 ky time window and several additional sites showing a shift to TEDE in the 5.0 ky time window. Subsequently, TEDE disappeared from lowland sites around the Aegean and on the Greek peninsula, though TEDE persisted or expanded in the Balkans and the northwestern Caucasus.

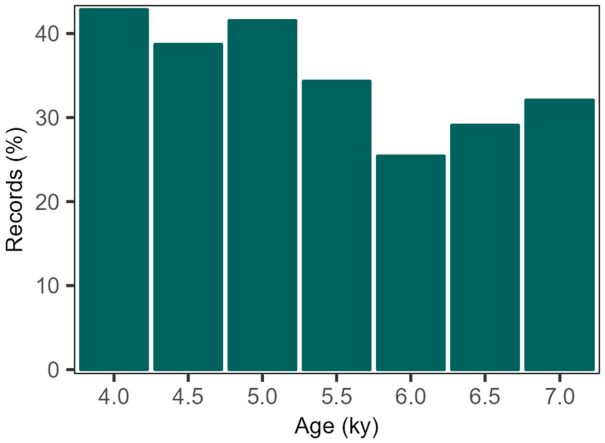

Figure 3.5. Proportion of records reconstructed as temperate deciduous malacophyll broadleaf forest (TEDE) in a 300-year window centred on a specific time slice in the mid-Holocene, here defined as 7 to 4 ky.

3.4.5. Late Holocene forest dynamics

The maximum in forest cover occurred between c. 4.5 and 3.6 ky (Figure 3.7c; Supplementary Figure 3.2), when more than 50% of the sites are reconstructed as forest. There is an abrupt decline in forest cover from 50% to 30%, starting at c. 3.3 and reaching a minimum at 2.6 ky. Forest cover gradually increased after c. 2.3 ky to reach levels of around 45% between c. 2.3 and 1 ky. Although there are fluctuations in the number of forest sites after 1 ky, the number remains relatively high until the present. Thus, there is no explicit evidence of a systematic decrease in forest over the late Holocene; the pattern rather points to centennial-scale variations in forest abundance and corresponding increases in more open vegetation, as represented by samples

reconstructed as tundra (TUND), desert (DESE), graminoids with forbs (GRAM), xeric shrubland (XSHB) and evergreen needle-leaved woodland (ENWD) (Supplementary Figure 3.7). Warm-temperate evergreen needleleaf and sclerophyll broadleaf forest (WTSFS), though also exhibiting considerable centennial-scale variability, showed a general decline during the late Holocene (Supplementary Figure 3.7).

There is no obvious coherence between the changes in forest cover and population changes as evidenced by the SPD curve. The interval of highest forest cover overlaps with a period of high human population density; the decrease in human population density around 3.5 ky occurs before the abrupt decrease in forest sites at 3.3 ky. Although the brief increase in forest cover around 2.8 ky corresponds to an interval of declining population, the subsequent interval of low forest cover is not associated with an increase in population, though this may reflect uncertainties in the SPD. However, the lack of coherency at a regional scale does not preclude the possibility that there were anthropogenic impacts on vegetation at more local scales.

The changes in the number of forest sites does show a close resemblance to intervals of wetter/drier conditions as inferred from the oxygen isotope records (Figure 3.7). The records from Jeita, Mavri Trypa, Skala Marion and Sofular show wetter conditions when the percentage of forest sites is high, particularly between 4.5 and 3.3. They also show a sharp increase in aridity near 3 ky (though this occurs somewhat later at c. 2.8 ky in Skala Marion) that persists until at least c. 2.3 ky. All of the speleothem records show somewhat wetter conditions corresponding to the forest expansion between c. 2.3 and 1.3 ky, though this is most marked at Mavri Trypa and Skala Marion. The Sofular record shows increasing aridity during the last millennium, and this would be consistent with the cessation of speleothem formation at Jeita, Mavri Trypa and Skala Marion, but is inconsistent with the relatively high number of forest sites. However, the Kocain record does not show a strong increase in aridity in the recent 1000 years, suggesting that there may be considerable spatial heterogeneity in the nature of late Holocene moisture changes.

Further analyses of radiocarbon data for specific sub-regions (Figure 3.8) reveal distinct human population density trajectories. Population levels were low in Greece during the mid-Holocene and maximum population levels were reached around 3 ky. In contrast, the Levant and Anatolia exhibited high population levels during the mid-Holocene, followed by a general population decline. There are limited numbers of pollen records (Supplementary Figure 3.8) for some of these sub-regions, with an average of only 7.5 records per time window for Anatolia sites, and an average of only three sites for the Levant, which may affect the reliability of the composite forest cover curves. Nevertheless, the forest curves for Greece and Anatolia show a closer resemblance to changes in moisture, as shown by speleothem isotope records, than to human population changes. In both regions, increases in forest cover correspond to both increases and decreases in population; there is a similar lack of synchroneity with population changes in times of decreasing forest cover. The forest cover for the Levant does not align well with either humidity or population changes, but this likely reflects the very limited number of records from the region.

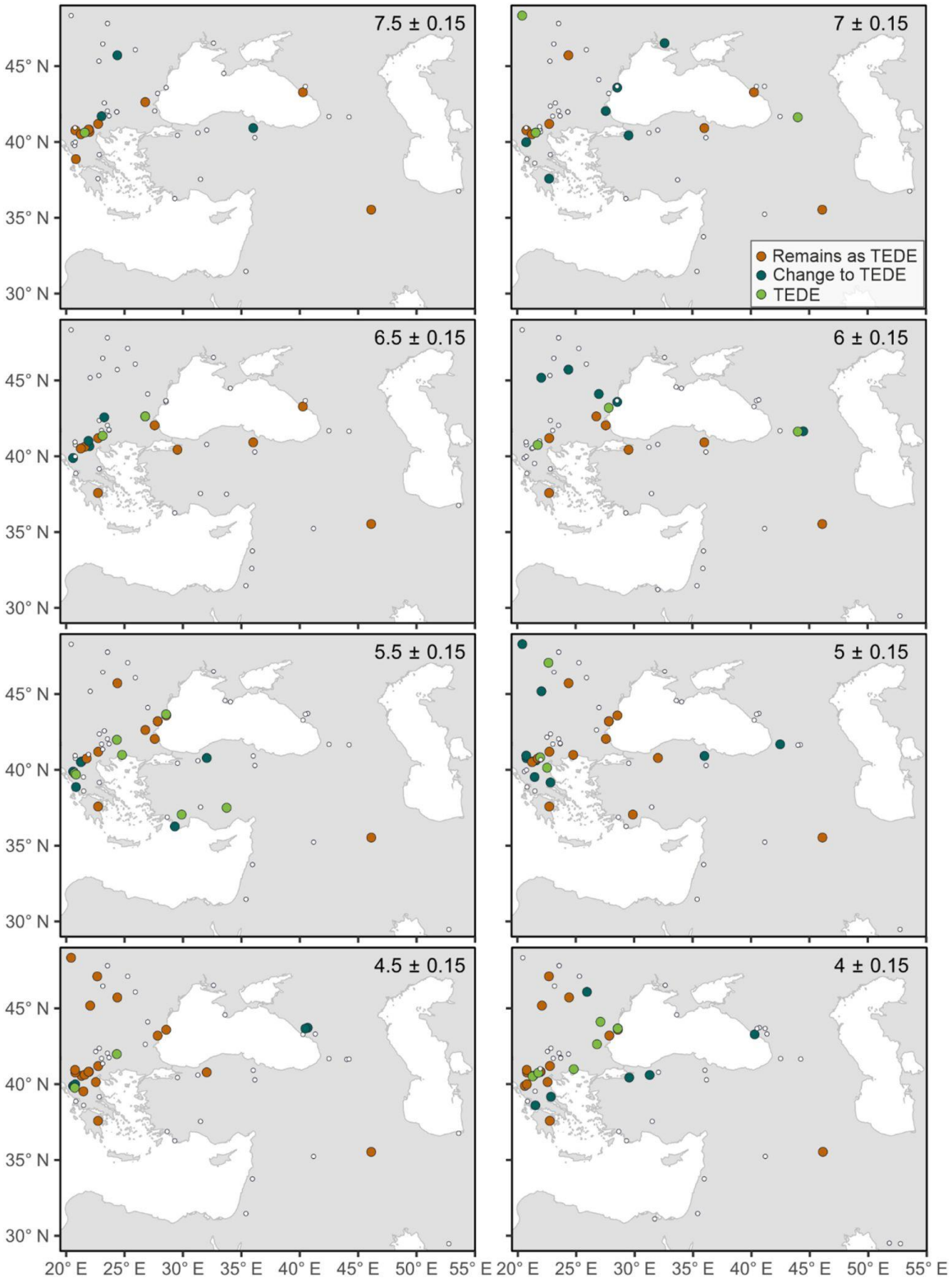

Figure 3.6. Dynamics of temperate deciduous forest during the mid-Holocene in the Eastern Mediterranean–Black Sea Caspian corridor (EMBSeCBIO) region. The plots show sites where temperate deciduous malacophyll broadleaf forest (TEDE) was inferred as the dominant biome within specific 300-year windows, where the colours show whether these were records where TEDE had been present in the previous interval and persisted (remains as TEDE), records which were not TEDE in the previous interval and became TEDE (change to TEDE) or records which were TEDE in the selected time window but had no record in the previous time window (TEDE). Sites where the predicted biome is not TEDE are shown as open circles. The biome reconstructions for these sites are shown in Supplementary Figure 3.2.

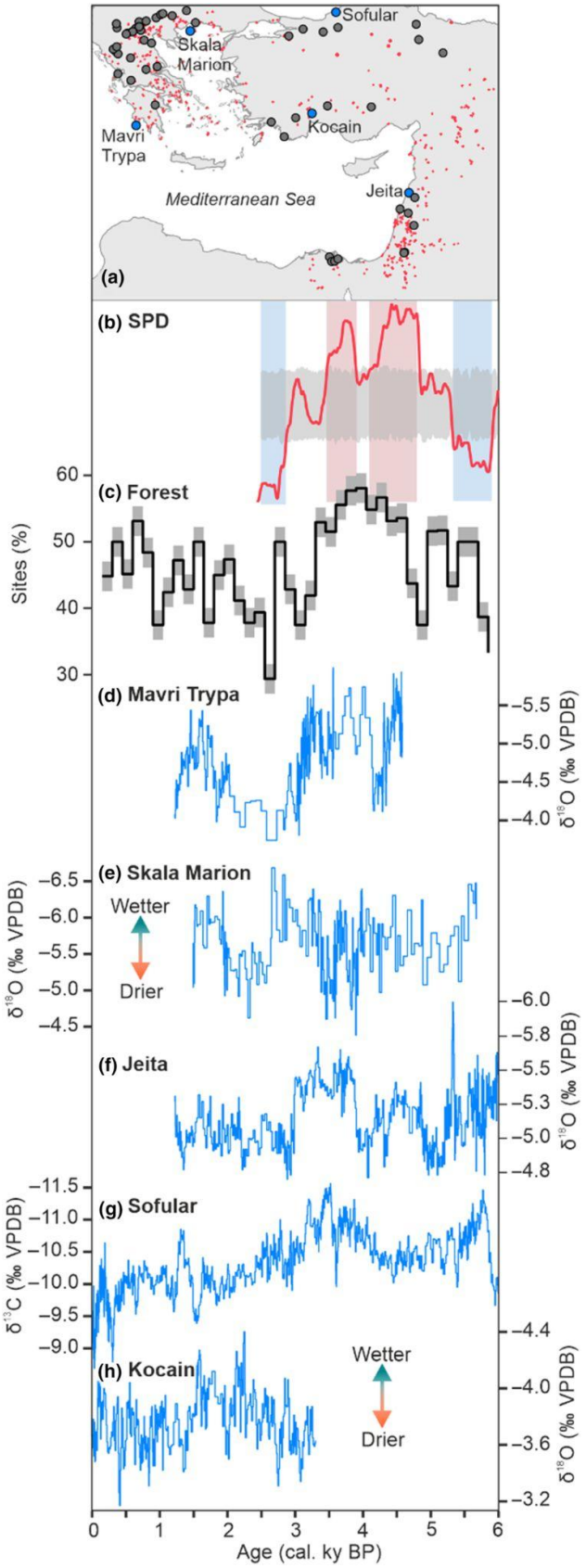

Figure 3.7. Comparison of reconstructed changes in vegetation in over the past 6000 years with evidence for changes in human population and palaeoclimate in the Eastern Mediterranean–Black Sea Caspian corridor (EMBSeCBIO) region. The map (a) shows sites used in the reconstruction of biome changes. Changes in human population density

(b) are shown by the summed probability distribution (SPD) of radiocarbon dates on archaeological material. The biome plot (c) shows the proportion of records in the region characterised by forest in a 300-year time-window through the past 6000 years, where the time windows were constructed with 50% overlap. Changes in palaeoclimate are inferred from the oxygen isotope records (δ18O) from individual speleothem records (d–h), where more negative values are taken to indicate wetter conditions.

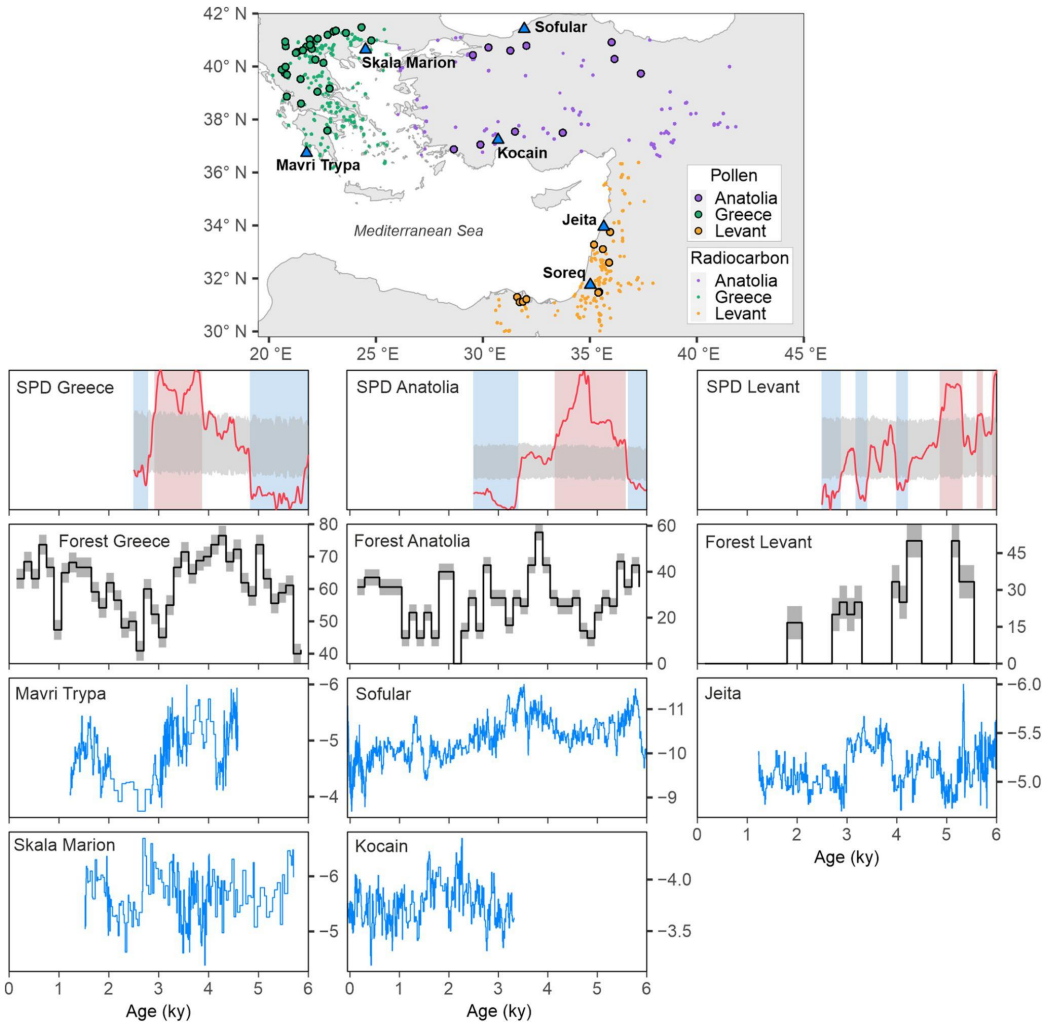

Figure 3.8. Comparison of reconstructed changes in vegetation in over the past 6000 years with evidence for changes in human population and palaeoclimate at sub-regional scale (Anatolia, Greece and Levant). The small coloured dots on the map indicate sites of archaeological radiocarbon dates (Bird et al., 2022), the coloured dots with black border on the map indicates sites of pollen records and the triangles on the map show location of oxygen isotope records (δ18O) from speleothems.

3.5. Discussion

The Late Glacial in the EMBSeCBIO region was characterised by open vegetation analogous to modern cold and dry affinity assemblages. However, a large number of early Holocene records represent vegetation types that are not present in the region today. The maximum number of records with non-analogue samples occurred from c. 11.5 to 9.5 ky. Samples from records from c. 6.0 ky onwards were all attributed to existing biome types (Figure 3.3a). This pattern is consistent

with the analysis of vegetation changes across Europe using a modern analogue approach (Zanon et al., 2018), which also found an increase in the number of non-analogue records from the start of the Holocene, reaching a peak between 9.0 and 6.0 ky. This pattern contrasts with records from e.g. North America, where non-analogue vegetation is more typical of the Late Glacial than the early Holocene (Williams & Jackson, 2007).

Almost all of the sites with non-analogue samples come from the Carpathians (Figure 3.3b). This region has been identified as a glacial refugium for a number of coniferous and deciduous trees. High-resolution pollen records and macrofossils have shown the occurrence of Pinus, Juniperus, Betula, Salix and Picea in lowland areas and the Romanian Carpathians prior to 14.7 ky (Feurdean et al., 2007, 2010; Pató et al., 2020; Tanţău et al., 2014). Plant genetic data also point to this region as a glacial refugium (Magri et al., 2006; Petit et al., 2003), while genetic evidence of canopy forest snails also supports the existence of temperate trees in the Carpathians during the Late Glacial (Juřičková et al., 2019). Evidence for a very rapid expansion of Larix, Pinus and Ulmus in the early Holocene strongly supports the idea of a glacial refugium for these species in Romania (Feurdean et al., 2007). The extremely high values (>20%) of Ulmus in the non-analogue samples in the early Holocene (Supplementary Figure 3.4), when this taxon does not exceed a mean of 0.4% in spectra from forest biomes where it is found today (Cruz-Silva et al., 2022), support the idea of rapid expansion from refugial conditions. Similarly, the lowlands of eastern Georgia on the edge of the Black Sea, where the Gagra site is located, has also been previously identified as a Late Glacial refugium where Abies was the dominant taxon (Connor & Kvavadze, 2009). This is consistent with the fact that Abies was the dominant taxon at this site (Supplementary Figure 3.4), though Ulmus is also present in relatively high abundance (3.5%). Quantitative reconstructions of Last Glacial Maximum climates (Davis et al., 2022) indicate somewhat moderate cooling in regions to the west and south of the Black Sea accompanied by increased growing season precipitation, which could favour the persistence of moisture-demanding broad-leaved trees along with conifers.

The timing of forest expansion after the Younger Dryas in response to increasing temperature and humidity occurred between 10.64 ± 0.65 ky (Supplementary Figure 3.4). There is no evidence of systematic differences in timing between the western and eastern parts of the EMBSeCBIO region, or between high and low elevation sites. For instance, at 10.5 ± 0.15 ky (Supplementary Figure 3.2), sites located at both easternmost and westernmost longitudes, spanning from the Caucasus to the Balkans, underwent a transition from predominantly open biomes, primarily GRAM, to forested biomes including CMIX and TEDE. This spatial distribution aligns with the broader shift from open or drought-tolerant Late Glacial vegetation to moisture-de-manding forests during the early Holocene. Differences in the speed of forest expansion, and hence the timing of peak forest cover, indicate a somewhat individualistic response at different sites. This is consistent with previous studies which have shown that vegetation changes were of variable amplitude and timing and have explained this in terms of interactions of external and internal drivers including glacial refugia, dispersal abilities, migration patterns, climate, soil development, competition and disturbance regimes (Feurdean et al., 2007, 2010; Finsinger et al., 2017; Huntley & Prentice, 1993; Jamrichová et al., 2017; Prentice, 1985; Tantau et al., 2003; Tanţău et al., 2011, 2014). There is,

however, a tendency for sites in the western part of the region and high-elevation sites to show more abrupt increases in forest cover than those in the eastern part of the region. This, coupled with the fact that forest density in the eastern sites never reached the levels observed in the western sites, may underpin the perception that forest expansion was delayed in the eastern part of the EMBSecBIO region.

Temperate deciduous forests were present in Anatolia and southern Greece by 6 ky (Figure 3.6) and temperate deciduous trees were an important component of the vegetation across much of the region at that time. This is consistent with earlier findings (e.g. Huntley & Prentice, 1993 ; Peyron et al., 2017; Prentice et al., 1996, 2000; Roberts et al., 2004) and with quantitative climate reconstructions showing that most of the Mediterranean region was characterised by lower temperatures and greater plant-available moisture during the mid-Holocene (e.g. Bartlein et al., 2011; Cheddadi et al., 1997; Davis et al., 2003). It is also consistent with speleothem oxygen isotope records from the Middle East, which show higher precipitation than present during the mid-Holocene (Burstyn et al., 2019). However, our analyses suggest that the expansion of TEDE occurred later than this, since both the 5.5 and 5.0 ky time windows registered a higher abundance of TEDE than at 6 ky (Figure 3.6). The focus on 6 ky in earlier studies was motivated by the fact that this was an inter-val chosen for palaeoclimate modelling (Prentice et al., 2000), being a compromise between the maximum changes in northern hemisphere insolation and the relict presence of northern hemisphere ice sheets (Joussaume et al., 1999), rather than the idea that this might represent the maximum expression of climate-driven vegetation changes. The increase in TEDE after 6 ky is consistent with warm and wet conditions inferred from marine and terrestrial biological and biogeochemical proxies in sediment cores from North and SE Aegean and Levant Seas (Triantaphyllou et al., 2014).

Late Holocene forest cover exhibited centennial-scale variations rather than a systematic decline. The abundance of forest sites shows millennial-scale variability with peaks between 4.5 and 2.3 ky, at 2.7 ky, and 2.3 and 1 ky. The early interval of high forest cover is coincident with a wetter interval starting at 4.8 ky in the Jeita record and 4.5 ky in the Skala Marion record and lasting until 2.9 ky (Cheng et al., 2015). The δ13C record from Sofular also shows increased humidity between c. 4.5 and 3 ky (Fleitmann et al., 2009 ; Göktürk et al., 2011). The gradual increase in forest cover after 2.3 ky is also consistent with the speleothem evidence of increased humidity. The cessation of speleothem formation at Mavri Trypa, Skala Marion and Jeita at varying times after 2 ky could reflect aridification, but this is not supported by the Sofular and Kocain records which show a continuation of relatively moist but fluctuating conditions, consistent with the moderate fluctuations in forest cover.

Intervals of high forest cover occur during intervals of both high and low population density. At a regional scale, population dynamics and forest cover showed limited coherence, emphasising the importance of considering climate influences on forest changes. Even at sub-regional scale, there is no relationship between population density and forest cover in Greece and Anatolia. In regions where there are sufficient pollen data to construct a reliable composite curve, the fluctuations in late Holocene forest cover seem to follow centennial-scale patterns that are more tied to

variations in climate. An improvement in the coverage of vegetation records for other parts of the EMBSeCBIO region is required to test the relationship between human activities and vegetation more thoroughly. It is not possible to use the SPD 'dates as data' approach to reconstruct changes in population density after 2.5 ky in the EMBSeCBIO region and thus we are unable to evaluate the role of humans in the fluctuations of forest cover during the most recent interval. However, the abrupt drop in population at c. 3 ky is robust and has been documented previously (Palmisano, Lawrence, et al., 2021; Weiberg, Bevan, et al., 2019; Weiberg, Hughes, et al., 2019) and is thought to correspond to a period of political collapse and social transformation (Knapp & Manning, 2016). While the short-lived increase in forest cover at 2.9 ky might be associated with this abrupt decline, the subsequent interval of reduced forest cover cannot be explained as a consequence of human activities since population levels remained low during this time. Thus, while there is scope for more thorough investigations of the role of human activities on the landscape at a local scale, the evidence currently available suggests that late Holocene vegetation changes were more likely to have been driven by changes in climate than human activities.

We have used a new approach taking account of within-biome variability in pollen assemblages to make vegetation reconstructions (Cruz-Silva et al., 2022), and shown that this provides more reliable reconstructions than the classic biomisation method. Nevertheless, it is not perfect since there are still some mismatches between the predicted and observed vegetation. These mismatches may, in part, reflect the diversity of site types or differences in the size of the basin since both of these factors can influence the pollen source area and the quality of pollen preservation (Davis, 2000; Prentice, 1985). However, the rigorous filtering applied to the records, for example by removing large basins and records that showed obvious indications of poor preservation, should have minimised the impact of site differences on the vegetation reconstructions. Even in the early Holocene there are at least 20 records from the region after this filtering. Our focus on the regional picture of vegetation changes to address specific controversies should also minimise the impact of potential uncertainties in the reconstructions.

We have largely focused on vegetation changes that reflect changing plant-available moisture and the seasonality of precipitation, and have used speleothem data as an independent source of information on moisture changes through the Holocene. Although quantitative reconstructions of climate variables have been made at some sites from the EMBSeCBIO region (e.g. Davis et al., 2003; Herzschuh et al., 2022; Robles et al., 2022), they either use a PFT-based modern-analogue approach or local calibrations, which may provide reasonable reconstruction statistics but tends to underestimate climate variability. Furthermore, these reconstructions focus on mean annual precipitation rather than plant-available moisture. It would be useful to develop robust reconstructions of bioclimatic variables for the EMBSeCBIO region in order to be able to determine how far the observed vegetation changes reflect changes in climate factors influencing plant growth.

3.6. Conclusions

Vegetation with no modern analogue occurred from c. 11.8 to c. 6 ky, mostly in the Carpathians, with a maximum number of records between 11.5 and 9.5 ky. The composition of non-analogue

samples and the location of the records suggest that these vegetation types arose because of rapid expansion of individual species from Late Glacial refugia. There is no discernible difference in the timing of forest expansion in the early Holocene either with latitude, longitude or elevation across the sites. Differences in the exact timing and speed of forest increase between sites suggests multiple factors, including relative location of refugia, plant dispersal abilities, competition and disturbance regimes, could have influenced the response to early Holocene climate change. Temperate deciduous forest was not more extensive than today at 6 ky; the maximum mid-Holocene expansion occurred at c. 5.5 and 5.0 ky. Late Holocene forest cover exhibited centennial-scale variations rather than a systematic decline, at both regional and sub-regional scale. Fluctuations in forest cover during this interval are broadly consistent with speleothem records of changing moisture availability than aggregate regional changes in human population. However, more well-dated pollen cores and archaeological evidence on human population density are necessary to establish definitive conclusions about the interaction of climate, vegetation and people at sub-regional scales.

3.7. References

Asouti, E., & Kabukcu, C. (2014). Holocene semi-arid oak woodlands in the Irano-Anatolian region of Southwest Asia: Natural or anthropogenic? Quaternary Science Reviews, 90, 158–182. https://doi.org/10.1016/j.quascirev.2014.03.001

Bar-Matthews, M., & Ayalon, A. (2011). Mid-Holocene climate variations revealed by high-resolution speleothem records from Soreq Cave, Israel and their correlation with cultural changes. The Holocene, 21(1), 163–171. https://doi.org/10.1177/0959683610384165

Bar-Matthews, M., Ayalon, A., Gilmour, M., Matthews, A., & Hawkesworth, C. J. (2003). Sea–land oxygen isotopic relationships from planktonic foraminifera and speleothems in the Eastern Mediterranean region and their implication for paleorainfall during interglacial intervals. Geochimica et Cosmochimica Acta, 67(17), 3181–3199. https://doi.org/10.1016/S0016-7037(02)01031-1

Bartlein, P. J., Harrison, S. P., Brewer, S., Connor, S., Davis, B. A. S., Gajewski, K., Guiot, J., Harrison-Prentice, T. I., Henderson, A., Peyron, O., Prentice, I. C., Scholze, M., Seppä, H., Shuman, B., Sugita, S., Thompson, R. S., Viau, A., Williams, J., & Wu, H. (2011). Pollen-based continental climate reconstructions at 6 and 21 ka: A global synthesis. Climate Dynamics, 37, 775–802. https://doi.org/10.1007/s00382-010-0904-1

Bevan, A., Crema, E., Bocinsky, R. K., Hinz, M., Riris, P., & Silva, F. (2022). rcarbon: Calibration and analysis of radiocarbon dates (1.4.4). https://CRAN.R-project.org/package=rcarbon

Bigelow, N. H., Brubaker, L. B., Edwards, M. E., Harrison, S. P., Prentice, I. C., Anderson, P. M., Andreev, A. A., Bartlein, P. J., Christensen, T. R., Cramer, W., Kaplan, J. O., Lozhkin, A. V., Matveyeva, N. V., Murray, D. F., McGuire, A. D., Razzhivin, V. Y., Ritchie, J. C., Smith, B., Walker, D. A., … Volkova, V. S. (2003). Climate change and Arctic ecosystems: 1. Vegetation changes north of 55° N between

the last glacial maximum, mid-Holocene, and present. Journal of Geophysical Research: Atmospheres, 108(D19), https://doi.org/10.1029/2002JD002558

Bini, M., Zanchetta, G., Perşoiu, A., Cartier, R., Català, A., Cacho, I., Dean, J. R., Di Rita, F., Drysdale, R. N., Finnè, M., Isola, I., Jalali, B., Lirer, F., Magri, D., Masi, A., Marks, L., Mercuri, A. M., Peyron, O., Sadori, L., … Brisset, E. (2019). The 4.2 ka BP event in the Mediterranean region: An overview. Climate of the Past, 15(2), https://doi.org/10.5194/cp-15-555-2019

Bird, D., Miranda, L., Vander Linden, M., Robinson, E., Bocinsky, R. K., Nicholson, C., Capriles, J. M., Finley, J. B., Gayo, E. M., Gil, A., d'Al-poim Guedes, J., Hoggarth, J. A., Kay, A., Loftus, E., Lombardo, U., Mackie, M., Palmisano, A., Solheim, S., Kelly, R. L., & Freeman, J. (2022). P3k14c, a synthetic global database of archaeological radiocarbon dates. Scientific Data, 9(1), https://doi.org/10.1038/s41597-022-01118-7

Blaauw, M., Christen, J. A., Lopez, M. A. A., Vazquez, J. E., Gonzalez V., O. M., Belding, T., Theiler, J., Gough, B., & Karney, C. (2021). rbacon: Age-depth modelling using Bayesian statistics (2.5.6) [R]. https://CRAN.R-project.org/package=rbacon

Bliedtner, M., Zech, R., Zech, J., Schäfer, I., & von Suchodoletz, H. (2020). A first Holocene leaf wax isotope-based paleoclimate record from the semi-humid to semi-arid southeastern Caucasian lowlands. Journal of Quaternary Science, 35(5), https://doi.org/10.1002/jqs.

Bottema, S., Woldring, H., & Aytuğ, B. (1994). Late Quaternary vegetation history of northern Turkey. Palaeohistoria, 36, 13–72. https://doi.org/10.1177/095968369603600317

Bozilova, E., & Tonkov, S. (Eds.). (1995). Advances in Holocene palaeoecology in Bulgaria. Pensoft Publishers. https://doi.org/10.1177/095968369603600317

Brayshaw, D. J., Rambeau, C. M. C., & Smith, S. J. (2011). Changes in Mediterranean climate during the Holocene: Insights from global and regional climate modelling. The Holocene, 21(1), 15–31. https://doi.org/10.1177/095968361037528

Burstyn, Y., Martrat, B., Lopez, J. F., Iriarte, E., Jacobson, M. J., Lone, M. A., & Deininger, M. (2019). Speleothems from the Middle East: An example of water-limited environments in the SISAL database. Quaternary, 2(2), 16. https://doi.org/10.3390/quat2020016

Cheddadi, R., Yu, G., Guiot, J., Harrison, S. P., & Prentice, I. C. (1997). The climate of Europe 6000 years ago. Climate Dynamics, 13, 1–9.

Cheng, H., Sinha, A., Verheyden, S., Nader, F. H., Li, X. L., Zhang, P. Z., Yin, J. J., Yi, L., Peng, Y. B., Rao, Z. G., Ning, Y. F., & Edwards, R. L. (2015). The climate variability in northern Levant over the past 20,000 years. Geophysical Research Letters, 42(20), 8641–8650. https://doi.org/10.1002/2015GL065397

Collins, P. M., Davis, B. A. S., & Kaplan, J. O. (2012). The mid-Holocene vegetation of the Mediterranean region and southern Europe, and comparison with the present day. Journal of Biogeography, 39(10), 1848–1861. https://doi.org/10.1111/j.1365-2699.2012.02738.x

Comas-Bru, L., Atsawawaranunt, K., Harrison, S., & Members of the SISAL Working Group. (2020). SISAL (Speleothem Isotopes Synthesis and Analysis Working Group) database version 2.0 [Data set]. University of Reading. https://doi.org/10.17864/1947.256

Comas-Bru, L., Rehfeld, K., Roesch, C., Amirnezhad-Mozhdehi, S., Harrison, S. P., Atsawawaranunt, K., Ahmad, S. M., Brahim, Y. A., Baker, A., Bosomworth, M., Breitenbach, S. F. M., Burstyn, Y., Columbu, A., Deininger, M., Demény, A., Dixon, B., Fohlmeister, J., Hatvani, I. G., Hu, J., … SISAL Working Group Members. (2020). SISALv2: A comprehensive speleothem isotope database with multiple age-depth models. Earth System Science Data, 12(4), 2579–2606. https://doi.org/10.5194/essd-12-2579-2020

Connor, S., & Kvavadze, E. V. (2009). Modelling late Quaternary changes in plant distribution, vegetation and climate using pollen data from Georgia, Caucasus. Journal of Biogeography, 36(3), 529–545. https://doi.org/10.1111/j.1365-2699.2008.02019.x

Connor, S., & Sagona, A. (2007). Environment and society in the late prehistory of southern Georgia, Caucasus. In B. Lyonnet (Ed.), The cultures of the Caucasus (6th to 3rd centuries B.C.E): Their relations with the Near East (Vol. 3, pp. 21–36). CNRS Editions.

Cordova, C. E., Harrison, S. P., Mudie, P. J., Riehl, S., Leroy, S. A. G., & Ortiz, N. (2009). Pollen, plant macrofossil and charcoal records for palaeovegetation reconstruction in the Mediterranean-Black Sea corridor since the last glacial maximum. Quaternary International, 197(1–2), 12–26. https://doi.org/10.1016/j.quaint.2007.06.015

Cruz-Silva, E., & Harrison, S. P. (2023). esmeraldacs/EMBSECBIO_Holoc_vegetation: Initial release (0.1.0) [software]. Zenodo, https://doi.org/10.5281/zenodo.10026596

Cruz-Silva, E., Harrison, S. P., Marinova, E., & Prentice, I. C. (2022). A new method based on surface-sample pollen data for reconstructing palaeovegetation patterns. Journal of Biogeography, 49(7), 1381–1396. https://doi.org/10.1111/jbi.14448

Davis, B. A. S., Brewer, S., Stevenson, A. C., & Guiot, J. (2003). The temperature of Europe during the Holocene reconstructed from pollen data. Quaternary Science Reviews, 22, 1701–1716. https://doi.org/10.1016/S0277-3791(03)00173-2

Davis, B. A. S., Fasel, M., Kaplan, J. O., Russo, E., & Burke, A. (2022). The climate and vegetation of Europe, North Africa and the Middle East during the last glacial maximum (21,000 years BP) based on pollen data. Climate of the Past Discussions [preprint]. https://doi.org/10.5194/cp-2022-59 . In review.

Davis, M. B. (2000). Palynology after Y2K—Understanding the source area of pollen in sediments. Annual Review of Earth and Planetary Sciences, 28(1), 1–18. https://doi.org/10.1146/annurev.earth.28.1.1

De Cupere, B., Frémondeau, D., Kaptijn, E., Marinova, E., Poblome, J., Vandam, R., & Van Neer, W. (2017). Subsistence economy and land use strategies in the Burdur province (SW Anatolia) from

prehis-tory to the Byzantine period. Quaternary International, 436, 4–17. https://doi.org/10.1016/j.quaint.2015.11.097

Dean, J. R., Jones, M. D., Leng, M. J., Noble, S. R., Metcalfe, S. E., Sloane, H. J., Sahy, D., Eastwood, W. J., & Roberts, C. N. (2015). Eastern Mediterranean hydroclimate over the Late Glacial and Holocene, reconstructed from the sediments of Nar lake, Central Turkey, using stable isotopes and carbonate mineralogy. Quaternary Science Reviews, 124, 162–174. https://doi.org/10.1016/j.quascirev.2015.07.023

Djamali, M., Akhani, H., Andrieu-Ponel, V., Braconnot, P., Brewer, S., de Beaulieu, J.-L., Fleitmann, D., Fleury, J., Gasse, F., Guibal, F., Jackson, S. T., Lézine, A.-M., Médail, F., Ponel, P., Roberts, N., & Stevens, L. (2010). Indian summer monsoon variations could have affected the early-Holocene woodland expansion in the near east. The Holocene, 20(5), 813–820. https://doi.org/10.1177/0959683610362813

Dusar, B., Verstraeten, G., D'haen, K., Bakker, J., Kaptijn, E., & Waelkens, M. (2012). Sensitivity of the Eastern Mediterranean geomorphic system towards environmental change during the late Holocene: A chronological perspective. Journal of Quaternary Science, 27(4), 371–382. https://doi.org/10.1002/jqs.1555

Eastwood, W. J., Leng, M. J., Roberts, N., & Davis, B. (2007). Holocene climate change in the Eastern Mediterranean region: A comparison of stable isotope and pollen data from Lake Gölhisar, Southwest Turkey. Journal of Quaternary Science, 22(4), 327–341. https://doi.org/10.1002/jqs.1062

Elenga, H., Peyron, O., Bonnefille, R., Jolly, D., Cheddadi, R., Guiot, J., Andrieu, V., Bottema, S., Buchet, G., Beaulieu, J.-L. D., Hamilton, A. C., Maley, J., Marchant, R., Perez-Obiol, R., Reille, M., Riollet, G., Scott, L., Straka, H., Taylor, D., … Jonson, H. (2000). Pollen-based biome reconstruction for southern Europe and Africa 18,000 yr BP. Journal of Biogeography, 27(3), 621–634. https://doi.org/10.1046/j.1365-2699.2000.00430.x

Feurdean, A., Willis, K. J., Parr, C. L., Tanţău, I., & Fărcaş, S. (2010). Post-glacial patterns in vegetation dynamics in Romania: Homogenization or differentiation? Journal of Biogeography, 37(11), 2197–2208. https://doi.org/10.1111/j.1365-2699.2010.02370.x

Feurdean, A., Wohlfarth, B., Björkman, L., Tantau, I., Bennike, O., Willis, K. J., Farcas, S., & Robertsson, A. M. (2007). The influence of refugial population on Late Glacial and early Holocene vegetational changes in Romania. Review of Palaeobotany and Palynology, 145(3), 305–320. https://doi.org/10.1016/j.revpalbo.2006.12.004

Finsinger, W., Giesecke, T., Brewer, S., & Leydet, M. (2017). Emergence patterns of novelty in European vegetation assemblages over the past 15,000 years. Ecology Letters, 20(3), 336–346. https://doi.org/10.1111/ele.12731

Fleitmann, D., Cheng, H., Badertscher, S., Edwards, R. L., Mudelsee, M., Göktürk, O. M., Fankhauser, A., Pickering, R., Raible, C. C., Matter, A., Kramers, J., & Tüysüz, O. (2009). Timing and climatic

impact of Greenland interstadials recorded in stalagmites from northern Turkey. Geophysical Research Letters, 36(19), L19707. https://doi.org/10.1029/2009GL040050

Göktürk, O. M., Fleitmann, D., Badertscher, S., Cheng, H., Edwards, R. L., Leuenberger, M., Fankhauser, A., Tüysüz, O., & Kramers, J. (2011). Climate on the southern Black Sea coast during the Holocene: Implications from the Sofular cave record. Quaternary Science Reviews, 30(19), 2433–2445. https://doi.org/10.1016/j.quascirev.2011.05.007

Harrison, S. P. (2019). Modern pollen data for climate reconstructions, version 1 (SMPDS) [Data set]. University of Reading. https://doi.org/10.17864/1947.194

Harrison, S. P., Marinova, E., & Cruz-Silva, E. (2021). EMBSeCBIO pollen database [Data set]. University of Reading. https://doi.org/10.17864/1947.309

Harrison, S. P., Villegas-Diaz, R., Cruz-Silva, E., Gallagher, D., Kesner, D., Lincoln, P., Shen, Y., Sweeney, L., Colombaroli, D., Ali, A., Barhoumi, C., Bergeron, Y., Blyakharchuk, T., Bobek, P., Bradshaw, R., Clear, J. L., Czerwiński, S., Daniau, A.-L., Dodson, J., … Paillard, J. (2022). The Reading Palaeofire database: An expanded global resource to document changes in fire regimes from sedimentary charcoal records. Earth System Science Data, 14, 1109–1124. https://doi.org/10.5194/essd-14-1109-2022

Hengl, T., Walsh, M. G., Sanderman, J., Wheeler, I., Harrison, S. P., & Prentice, I. C. (2018). Global mapping of potential natural vegetation: An assessment of machine learning algorithms for estimating land potential. PeerJ, 6, e5457. https://doi.org/10.7717/peerj.5457

Herzschuh, U., Böhmer, T., Li, C., Cao, X., Hébert, R., Dallmeyer, A., Telford, R. J., & Kruse, S. (2022). Reversals in temperature-precipitation correlations in the northern hemisphere extratropics during the Holocene. Geophysical Research Letters, 49, e2022GL099730. https://doi.org/10.1029/2022GL099730

Huntley, B., & Prentice, I. C. (1993). Holocene vegetation and climates in Europe. In H. E. Wright, J. E. Kutzbach, T. Webb, W. F. Ruddiman, F. A. Street-Perrott, & P. J. Bartlein (Eds.), Global climates since the last glacial maximum (pp. 136–168). University of Minnesota.

Jacobson, M. J., Flohr, P., Gascoigne, A., Leng, M. J., Sadekov, A., Cheng, H., Edwards, R. L., Tüysüz, O., & Fleitmann, D. (2021). Heterogeneous late Holocene climate in the Eastern Mediterranean—The Kocain cave record from SW Turkey. Geophysical Research Letters, 48(20), e2021GL094733. https://doi.org/10.1029/2021GL094733

Jalut, G., Dedoubat, J. J., Fontugne, M., & Otto, T. (2009). Holocene circum-Mediterranean vegetation changes: Climate forcing and human impact. Quaternary International, 200(1), 4–18. https://doi.org/10.1016/j.quaint.2008.03.012

Jalut, G., Esteban Amat, A., Mora, S. R. i., Fontugne, M., Mook, R., Bonnet, L., & Gauquelin, T. (1997). Holocene climatic changes in the western Mediterranean: Installation of the Mediterranean climate. Comptes Rendus de l'Académie des Sciences - Series IIA - Earth and Planetary Science, 325(5), 327–334. https://doi.org/10.1016/S1251-8050(97)81380-8

Jamrichová, E., Petr, L., Jiménez-Alfaro, B., Jankovská, V., Dudová, L., Pokorný, P., Kołaczek, P., Zernitskaya, V., Čierniková, M., Břízová, E., Syrovátka, V., Hájková, P., & Hájek, M. (2017). Pollen-inferred millennial changes in landscape patterns at a major biogeographical interface within Europe. Journal of Biogeography, 44(10), 2386–2397. https://doi.org/10.1111/jbi.13038

Joannin, S., Ali, A. A., Ollivier, V., Roiron, P., Peyron, O., Chevaux, S., Nahapetyan, S., Tozalakyan, P., Karakhanyan, A., & Chataigner, C. (2014). Vegetation, fire and climate history of the Lesser Caucasus: A new Holocene record from Zarishat fen (Armenia). Journal of Quaternary Science, 29(1), 70–82. https://doi.org/10.1002/jqs.2679

Joussaume, S., Taylor, K. E., Braconnot, P., Mitchell, J. F. B., Kutzbach, J. E., Harrison, S. P., Prentice, I. C., Broccoli, A. J., Abe-Ouchi, A., Bartlein, P. J., Bonfils, C., Dong, B., Guiot, J., Herterich, K., Hewitt, C. D., Jolly, D., Kim, J. W., Kislov, A., Kitoh, A., … Wyputta, U. (1999). Monsoon changes for 6000 years ago: Results of 18 simulations from the Paleoclimate Modeling Intercomparison Project (PMIP). Geophysical Research Letters, 26, 859–862. https://doi.org/10.1029/1999GL900126

Juřičková, L., Horáčková, J., Jansová, A., Kovanda, J., Harčár, J., & Ložek, V. (2019). A glacial refugium and zoogeographic boundary in the Slovak eastern Carpathians. Quaternary Research, 91(1), 383–398. https://doi.org/10.1017/qua.2018.68

Kaniewski, D., Marriner, N., Cheddadi, R., Guiot, J., & Van Campo, E. (2018). The 4.2 ka BP event in the Levant. Climate of the Past, 14(10), 1529–1542. https://doi.org/10.5194/cp-14-1529-2018

Knapp, A. B., & Manning, S. W. (2016). Crisis in context: The end of the late bronze age in the Eastern Mediterranean. American Journal of Archaeology, 120, 99–149.

Magny, M., Miramont, C., & Sivan, O. (2002). Assessment of the impact of climate and anthropogenic factors on Holocene Mediterranean vegetation in Europe on the basis of palaeohydrological records. Palaeogeography, Palaeoclimatology, Palaeoecology, 186(1), 47–59. https://doi.org/10.1016/S0031-0182(02)00442-X

Magri, D., Vendramin, G. G., Comps, B., Dupanloup, I., Geburek, T., Gömöry, D., Latałowa, M., Litt, T., Paule, L., Roure, J. M., Tantau, I., Van Der Knaap, W. O., Petit, R. J., & De Beaulieu, J.-L. (2006). A new scenario for the quaternary history of European beech populations: Palaeobotanical evidence and genetic consequences. New Phytologist, 171(1), 199–221. https://doi.org/10.1111/j.1469-8137.2006.01740.x

Magyari, E., Vincze, I., Orbán, I., Bíró, T., & Pál, I. (2018). Timing of major forest compositional changes and tree expansions in the Retezat Mts during the last 16,000 years. Quaternary International, 477, 40–58. https://doi.org/10.1016/j.quaint.2017.12.054

Magyari, E. K., Kuneš, P., Jakab, G., Sümegi, P., Pelánková, B., Schäbitz, F., Braun, M., & Chytrý, M. (2014). Late Pleniglacial vegetation in eastern-central Europe: Are there modern analogues in Siberia? Quaternary Science Reviews, 95, 60–79. https://doi.org/10.1016/j.quascirev.2014.04.020

Magyari, E. K., Pál, I., Vincze, I., Veres, D., Jakab, G., Braun, M., Szalai, Z., Szabó, Z., & Korponai, J. (2019). Warm Younger Dryas summers and early Late Glacial spread of temperate deciduous trees

in the Pannonian Basin during the last glacial termination (20-9 kyr cal BP). Quaternary Science Reviews, 225, 105980. https://doi.org/10.1016/j.quascirev.2019.105980

Marinova, E., Harrison, S. P., Bragg, F., Connor, S., de Laet, V., Leroy, S. A. G., Mudie, P., Atanassova, J., Bozilova, E., Caner, H., Cordova, C., Djamali, M., Filipova-Marinova, M., Gerasimenko, N., Jahns, S., Kouli, K., Kotthoff, U., Kvavadze, E., Lazarova, M., … Tonkov, S. (2018). Pollen-derived biomes in the Eastern Mediterranean–Black Sea–Caspian-Corridor. Journal of Biogeography, 45(2), 484–499. https://doi.org/10.1111/jbi.13128

Messager, E., Belmecheri, S., Von Grafenstein, U., Vincent, O., Voinchet, P., Puaud, S., Courtin-nomade, A., Guillou, H., Mgeladze, A., Dumoulin, J.-P., Mazuy, A., & Lordkipanidze, D. (2013). Late quaternary record of the vegetation and catchment-related changes from Lake Paravani (Javakheti, South Caucasus). Quaternary Science Reviews, 77, 125–140. https://doi.org/10.1016/j.quascirev.2013.07.011

Messager, E., Nomade, S., Wilhelm, B., Joannin, S., Scao, V., von Grafenstein, U., Martkoplishvili, I., Ollivier, V., Mgeladze, A., Dumoulin, J., Mazuy, A., Belmecheri, S., & Lordkipanidze, D. (2017). New pollen evidence from Nariani (Georgia) for delayed postglacial forest expansion in the South Caucasus. Quaternary Research, 87(1), 121–132. https://doi.org/10.1017/qua.2016.3

Palmisano, A., Bevan, A., Kabelindde, A., Roberts, N., & Shennan, S. (2021). Long-term demographic trends in prehistoric Italy: Climate impacts and regionalised socio-ecological trajectories. Journal of World Prehistory, 34(3), 381–432. https://doi.org/10.1007/s10963-021-09159-3

Palmisano, A., Bevan, A., & Shennan, S. (2017). Comparing archaeological proxies for long-term population patterns: An example from central Italy. Journal of Archaeological Science, 87, 59–72. https://doi.org/10.1016/j.jas.2017.10.001

Palmisano, A., Lawrence, D., de Gruchy, M. W., Bevan, A., & Shennan, S. (2021). Holocene regional population dynamics and climatic trends in the Near East: A first comparison using archaeo-demographic proxies. Quaternary Science Reviews, 252, 106739. https://doi.org/10.1016/j.quascirev.2020.106739

Parker, S. E., Harrison, S. P., Comas-Bru, L., Kaushal, N., LeGrande, A. N., & Werner, M. (2021). A data–model approach to interpreting speleothem oxygen isotope records from monsoon regions. Climate of the Past, 17(3), 1119–1138. https://doi.org/10.5194/cp-17-1119-2021

Pató, Z. A., Standovár, T., Gałka, M., Jakab, G., Molnár, M., Szmorad, F., & Magyari, E. (2020). Exposure matters: Forest dynamics reveal an early Holocene conifer refugium on a north-facing slope in Central Europe. The Holocene, 30(12), 1833–1848. https://doi.org/10.1177/0959683620950452

Petit, R. J., Aguinagalde, I., de Beaulieu, J.-L., Bittkau, C., Brewer, S., Cheddadi, R., Ennos, R., Fineschi, S., Grivet, D., Lascoux, M., Mohanty, A., Müller-Starck, G., Demesure-Musch, B., Palmé, A.,

Martín, J. P., Rendell, S., & Vendramin, G. G. (2003). Glacial refugia: Hotspots but not melting pots of genetic diversity. Science, 300(5625), 1563–1565. https://doi.org/10.1126/science.1083264

Peyron, O., Combourieu-Nebout, N., Brayshaw, D., Goring, S., Andrieu-Ponel, V., Desprat, S., Fletcher, W., Gambin, B., Ioakim, C., Joannin, S., Kotthoff, U., Kouli, K., Montade, V., Pross, J., Sadori, L., & Magny, M. (2017). Precipitation changes in the Mediterranean basin during the Holocene from terrestrial and marine pollen records: A model–data comparison. Climate of the Past, 13(249–265), 2017–2265. https://doi.org/10.5194/cp-13-249-2017

Peyron, O., Guiot, J., Cheddadi, R., Tarasov, P., Reille, M., de Beaulieu, J.-L., Bottema, S., & Andrieu, V. (1998). Climatic reconstruction in Europe for 18,000 YR B.P. from pollen data. Quaternary Research, 49(2), 183–196. https://doi.org/10.1006/qres.1997.1961

Power, M. J., Marlon, J. R., Bartlein, P. J., & Harrison, S. P. (2010). Fire history and the global charcoal database: A new tool for hypothesis testing and data exploration. Palaeogeography, Palaeoclimatology, Palaeoecology, 291(1), 52–59. https://doi.org/10.1016/j.palaeo.2009.09.014

Prentice, I. C. (1985). Pollen representation, source area, and basin size: Toward a unified theory of pollen analysis. Quaternary Research, 23(1), 76–86. https://doi.org/10.1016/0033-5894(85)90073-0

Prentice, I. C. (1988). Records of vegetation in time and space: the principles of pollen analysis. In B. Huntley & T. Webb, III (Eds.), Vegetation History (pp. 17–42). Kluwer.

Prentice, I. C., Guiot, J., Huntley, B., Jolly, D., & Cheddadi, R. (1996). Reconstructing biomes from palaeoecological data: A general method and its application to European pollen data at 0 and 6 ka. Climate Dynamics, 12, 185–194. https://doi.org/10.1007/BF00211617

Prentice, I. C., Jolly, D., & BIOME 6000 Participants. (2000). Mid-Holocene and glacial-maximum vegetation geography of the northern continents and Africa. Journal of Biogeography, 27, 507–519.

Reimer, P., Austin, W. E. N., Bard, E., Bayliss, A., Blackwell, P. G., Ramsey, C. B., Butzin, M., Cheng, H., Edwards, R. L., Friedrich, M., Grootes, P. M., Guilderson, T. P., Hajdas, I., Heaton, T. J., Hogg, A. G., Hughen, K. A., Kromer, B., Manning, S. W., Muscheler, R., … Talamo, S. (2020). The IntCal20 northern hemisphere radiocarbon age calibration curve (0-55 cal kBP). Radiocarbon, 62(4), 725–757. https://doi.org/10.1017/RDC.2020.41

Rick, J. W. (1987). Dates as data: An examination of the Peruvian preceramic radiocarbon record. American Antiquity, 52(1), 55–73. https://doi.org/10.2307/281258

Roberts, C. N., Woodbridge, J., Palmisano, A., Bevan, A., Fyfe, R., & Shennan, S. (2019). Mediterranean landscape change during the Holocene: Synthesis, comparison and regional trends in population, land cover and climate. The Holocene, 29(5), 923–937. https://doi.org/10.1177/0959683619826697

Roberts, N. (2002). Did prehistoric landscape management retard the post-glacial spread of woodland in Southwest Asia? Antiquity, 76(294), 1002–1010. https://doi.org/10.1017/S0003598X0009181X

Roberts, N., Brayshaw, D., Kuzucuoğlu, C., Perez, R., & Sadori, L. (2011). The mid-Holocene climatic transition in the Mediterranean: Causes and consequences. The Holocene, 21(1), 3–13. https://doi.org/10.1177/0959683610388058

Roberts, N., Eastwood, W. J., Kuzucuoğlu, C., Fiorentino, G., & Caracuta, V. (2011). Climatic, vegetation and cultural change in the Eastern Mediterranean during the mid-Holocene environmental transition. The Holocene, 21(1), 147–162. https://doi.org/10.1177/0959683610386819

Roberts, N., Jones, M. D., Benkaddour, A., Eastwood, W. J., Filippi, M. L., Frogley, M. R., Lamb, H. F., Leng, M. J., Reed, J. M., Stein, M., Stevens, L., Valero-Garcés, B., & Zanchetta, G. (2008). Stable isotope records of late quaternary climate and hydrology from Mediterranean lakes: The ISOMED synthesis. Quaternary Science Reviews, 27(25), 2426–2441. https://doi.org/10.1016/j.quascirev.2008.09.005

Roberts, N., Reed, J. M., Leng, M. J., Kuzucuoğlu, C., Fontugne, M., Bertaux, J., Woldring, H., Bottema, S., Black, S., Hunt, E., & Karabiyikoglu, M. (2001). The tempo of Holocene climatic change in the Eastern Mediterranean region: New high-resolution crater-lake sediment data from Central Turkey. The Holocene, 11(6), 721–736. https://doi.org/10.1191/095968301957214

Roberts, N., Stevenson, T., Davis, B., Cheddadi, R., Brewster, S., & Rosen, A. (2004). Holocene climate, environment and cultural change in the circum-Mediterranean region. In R. W. Battarbee, F. Gasse, & C. E. Stickley (Eds.), Past climate variability through Europe and Africa (Vol. 6, pp. 343–362). Springer Netherlands. https://doi.org/10.1007/978-1-4020-2121-3_17

Robinson, E., Zahid, H. J., Codding, B. F., Haas, R., & Kelly, R. L. (2019). Spatiotemporal dynamics of prehistoric human population growth: Radiocarbon 'dates as data' and population ecology models. Journal of Archaeological Science, 101, 63–71. https://doi.org/10.1016/j.jas.2018.11.006

Robles, M., Peyron, O., Brugiapaglia, E., Ménot, G., Dugerdil, L., Ollivier, V., Ansanay-Alex, S., Develle, A.-L., Tozalakyan, P., Meliksetian, K., Sahakyan, K., Sahakyan, L., Perello, B., Badalyan, R., Colombié, C., & Sébastien Joannin, S. (2022). Impact of climate changes on vegetation and human societies during the Holocene in the South Caucasus (Vanevan, Armenia): A multi-proxy approach including pollen, NPPs and brGDGTs. Quaternary Science Reviews, 277, 107297. https://doi.org/10.1016/j.quascirev.2021.107297

Schilman, B., Bar-Matthews, M., Almogi-Labin, A., & Luz, B. (2001). Global climate instability reflected by Eastern Mediterranean marine records during the late Holocene. Palaeogeography, Palaeoclimatology, Palaeoecology, 176(1), 157–176. https://doi.org/10.1016/S0031-0182(01)00336-4

Stevens, L. R., Wright, H. E., & Ito, E. (2001). Proposed changes in seasonality of climate during the Lateglacial and Holocene at Lake Zeribar, Iran. The Holocene, 11(6), 747–755. https://doi.org/10.1191/095968301957762

Sugita, S. (1993). A model of pollen source area for an entire lake surface. Quaternary Research, 39, 239–244. https://doi.org/10.1006/qres.1993.1027

Takahara, H., Sugita, S., Harrison, S. P., Miyoshi, N., Morita, Y., & Uchiyama, T. (2000). Pollen-based reconstructions of Japanese biomes at 0, 6000 and 18,000 14C yr BP. Journal of Biogeography, 27(3), 665–683. https://doi.org/10.1046/j.1365-2699.2000.00432.x

Tanţău, I., Feurdean, A., de Beaulieu, J.-L., Reille, M., & Fărcaş, S. (2011). Holocene vegetation history in the upper forest belt of the eastern Romanian Carpathians. Palaeogeography, Palaeoclimatology, Palaeoecology, 309(3), 281–290. https://doi.org/10.1016/j.palaeo.2011.06.011

Tanţău, I., Feurdean, A., De Beaulieu, J.-L., Reille, M., & Fărcaş, S. (2014). Vegetation sensitivity to climate changes and human impact in the Harghita Mountains (eastern Romanian Carpathians) over the past 15,000 years. Journal of Quaternary Science, 29(2), 141–152. https://doi.org/10.1002/jqs.2688

Tantau, I., Reille, M., de Beaulieu, J.-L., Farcas, S., Goslar, T., & Paterne, M. (2003). Vegetation history in the eastern Romanian Carpathians: Pollen analysis of two sequences from the Mohoş crater. Vegetation History and Archaeobotany, 12(2), 113–125. https://doi.org/10.1007/s00334-003-0015-6

Tarasov, P. E., Webb, T., III, Andreev, A. A., Afanas'eva, N. B., Berezina, N. A., Bezusko, L. G., Blyakharchuk, T. A., Bolikhovskaya, N. S., Cheddadi, R., Chernavskaya, M. M., Chernova, G. M., Dorofeyuk, N. I., Dirksen, V. G., Elina, G. A., Filimonova, L. V., Glebov, F. Z., Guiot, J., Gunova, V. S., Harrison, S. P., … Zernitskaya, V. P. (1998). Present-day and mid-Holocene biomes reconstructed from pollen and plant macrofossil data from the former Soviet Union and Mongolia. Journal of Biogeography, 25(6), 1029–1053. https://doi.org/10.1046/j.1365-2699.1998.00236.x

Timpson, A., Colledge, S., Crema, E. R., Edinborough, K., Kerig, T., Manning, K., Thomas, M. G., & Shennan, S. (2014). Reconstructing regional population fluctuations in the European Neolithic using radiocarbon dates: A new case-study using an improved method. Journal of Archaeological Science, 52, 549–557. https://doi.org/10.1016/j.jas.2014.08.011

Triantaphyllou, M. V., Gogou, A., Bouloubassi, I., Dimiza, M., Kouli, K., Rousakis, G., Kotthoff, U., Emeis, K.-C., Papanikolaou, M., Athanasiou, M., Parinos, C., Ioakim, C., & Lykousis, V. (2014). Evidence for a warm and humid mid-Holocene episode in the Aegean and northern Levantine seas (Greece, NE Mediterranean). Regional Environmental Change, 14(5), 1697–1712. https://doi.org/10.1007/s10113-013-0495-6

Turner, R., Roberts, N., Eastwood, W. J., Jenkins, E., & Rosen, A. (2010). Fire, climate and the origins of agriculture: Micro-charcoal records of biomass burning during the last glacial–interglacial transition in Southwest Asia. Journal of Quaternary Science, 25(3), 371–386. https://doi.org/10.1002/jqs.1332

Villegas-Diaz, R., Cruz-Silva, E., & Harrison, S. P. (2021). ageR: Supervised age models [R]. Zenodo, https://doi.org/10.5281/zenodo.463716

Weiberg, E., Bevan, A., Kouli, K., Katsianis, M., Woodbridge, J., Bonnier, A., Engel, M., Finné, M., Fyfe, R., Maniatis, Y., Palmisano, A., Panajiotidis, S., Roberts, C. N., & Shennan, S. (2019). Long-term trends of land use and demography in Greece: A comparative study. The Holocene, 29(5), 742–760. https://doi.org/10.1177/0959683619826641

Weiberg, E., Hughes, R. E., Finné, M., Bonnier, A., & Kaplan, J. O. (2019). Mediterranean land use systems from prehistory to antiquity: A case study from Peloponnese (Greece). Journal of Land Use Science, 14(1), 1–20. https://doi.org/10.1080/1747423X.2019.1639836

Weiberg, E., Unkel, I., Kouli, K., Holmgren, K., Avramidis, P., Bonnier, A., Dibble, F., Finné, M., Izdebski, A., Katrantsiotis, C., Stocker, S. R., Andwinge, M., Baika, K., Boyd, M., & Heymann, C. (2016). The socio-environmental history of the Peloponnese during the Holocene: Towards an integrated understanding of the past. Quaternary Science Reviews, 136, 40–65. https://doi.org/10.1016/j.quascirev.2015.10.042

Williams, J. W., & Jackson, S. T. (2007). Novel climates, no-analog communities, and ecological surprises. Frontiers in Ecology and the Environment, 5(9), 475–482. https://doi.org/10.1890/070037

Wright, H. E., Ammann, B., Stefanova, I., Atanassova, J., Margalitadze, N., Wick, L., & Blyakharchuk, T. (2003). Late-glacial and early-Holocene dry climates from the Balkan Peninsula to southern Siberia. In S. Tonkov (Ed.), Aspects of Palynology and Palaeoecology (pp. 127–136). Pensoft Publishing.

Zanon, M., Davis, B. A. S., Marquer, L., Brewer, S., & Kaplan, J. O. (2018). European forest cover during the past 12,000 years: A palynological reconstruction based on modern analogs and remote sensing. Frontiers in Plant Science, 9, 253. https://doi.org/10.3389/fpls.2018.00253

Zeileis, A., Kleiber, C., Krämer, W., & Hornik, K. (2003). Testing and dating of structural changes in practice. Computational Statistics & Data Analysis, 44, 109–123. https://doi.org/10.1016/S0167-9473(03)00030-6

van Zeist, W., & Bottema, S. (1991). Late quaternary vegetation of the near east. Dr Ludwig Reichert Verlag.

3.8. Supplement

Supplementary appendix 3.1: The vegetation reconstruction method

Cruz-Silva et al. (2022) used 5765 modern pollen samples from Europe, the Middle East and northern Eurasia derived from the EMSeCBIO and SPECIAL databases (Harrison, 2019; Harrison et al., 2021), which were taxonomically harmonised (Cruz-Silva et al., 2022) and assigned to biomes based on potential natural vegetation reconstructions (Hengl et al., 2018) to characterise the within-biome means and standard deviations of the abundances of individual taxa. These values were then used to calculate first a dissimilarity index and subsequently a similarity index between any pollen sample and every biome and thus assign each pollen sample to the biome which it is most likely to represent:

$$D_{ik} = \sqrt{\Sigma_{jk} \frac{(p_{jk} - \mu_{ji})^2}{(s_{ji} + \varepsilon)^2}}, \quad (1)$$

where *Dik* is the dissimilarity of pollen sample k from biome i; pjk is the pollen percentage of taxon j in sample k; μji is the mean of taxon j in biome i, sji is the sample standard deviation of taxon j in biome i and ε is a parameter assigned a value of 0.5%. Summation is over all taxa in sample k.

The dissimilarity values were converted to similarities by:

$$S_{ik} = e^{-D_{ik}/100}, \quad (2)$$

where Sik is an approximation of the likelihood of biome i given pollen sample k. A sample was then assigned to the biome with which it had the greatest similarity.

Biome reconstructions were evaluated using confusion matrices based on dominant and subdominant biomes in the sample search window. The balanced accuracy metric was used to assess performance, especially for imbalanced classes. The balanced accuracy metric is given by:

$$\mathrm{BA} = \frac{1}{l} \sum_{i=1}^{l} \frac{k_i}{n_i}, \quad (3)$$

Where where ki is the number of sites correctly predicted for biome i, l is the number of biomes and ni is the number of sites in biome i.

Cruz-Silva et al (2022) showed that reconstructions of the modern vegetation using a modern pollen dataset covering Europe, the Middle East and northern Eurasia used to derive the training data reached a balanced accuracy (i.e. the average accuracy of assignments to all classes: Carrillo et al., 2014) of 66%, which improved to 76% when both dominant and subdominant biomes within a search window of 21 km around the sample were considered. They also showed that the method captured the modern vegetation in the EMBSeCBIO region only with a balanced accuracy

of 64%, which improved to 77% when both the dominant and subdominant biomes were considered. The present study includes a further evaluation of the method to determine how accurate it is in predicting the vegetation represented by core top samples (age < 150 cal. yrs. BP) from fossil pollen cores from the EMBSeCBIO region.

Supplementary Table 3.1. Quantitative comparison of predicted and observed dominant and (sub-dominant) biomes in modern (<150 years) samples from long pollen records of the eastern Mediterranean-Black Sea Caspian corridor region. The observed dominant and sub-dominant biomes are taken from the Hengl et al. (2018) potential natural vegetation map. The biome codes are: CENF, cold evergreen needleleaf forest; CMIX, cool mixed evergreen needleleaf and deciduous broadleaf forest; DESE, desert; ENWD, evergreen needleleaf woodland; GRAM, graminoids with forbs; TEDE, temperate deciduous malacophyll broadleaf forest; TUND, tundra; WTFS, warm-temperate evergreen needleleaf and sclerophyll broadleaf forest; XSHB, xeric shrubland. The total number of predicted and observed records for each biome are also shown (Σ). The grey diagonal shows the number of correctly predicted samples, while off-diagonal elements are those incorrectly predicted.

		Predicted									
		DESE	XSHB	WTSFS	GRAM	ENWD	TEDE	CMIX	CENF	TUND	Σ
Observed	DESE	0	0	0	0	0	0	0	0	0	0
	XSHB	0	0	0	0	0	0	0	0	0	0
	WTSFS	0	0	2[1]	1	1	4	0	0	0	9
	GRAM	0	0	0	4[1]	0	1	0	0	0	6
	ENWD	0	0	0	0	7[2]	0	0	0	0	9
	TEDE	0	0	1	0	6	13[3]	1	0	0	24
	CMIX	0	0	0	0	1	4	4[6]	0	0	15
	CENF	0	0	0	0	0	0	0	0	0	0
	TUND	0	0	0	0	0	0	0	0	0	0
	Σ	0	0	4	6	17	25	11	0	0	63

Supplementary Figure 3.1. Plot showing the resolution and length of the records from the Eastern Mediterranean-Black Sea Caspian corridor (EMBSeCBIO) region.

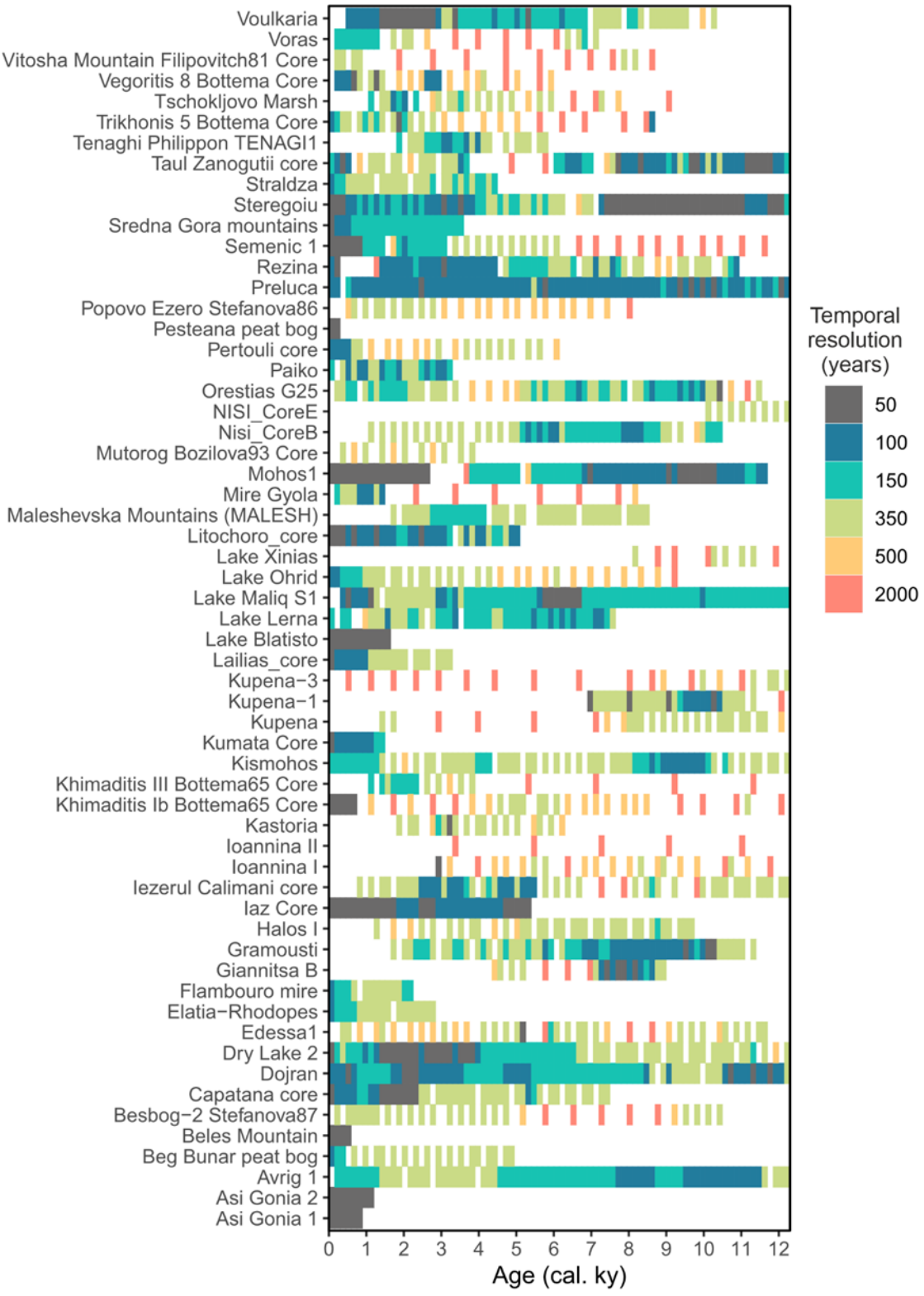

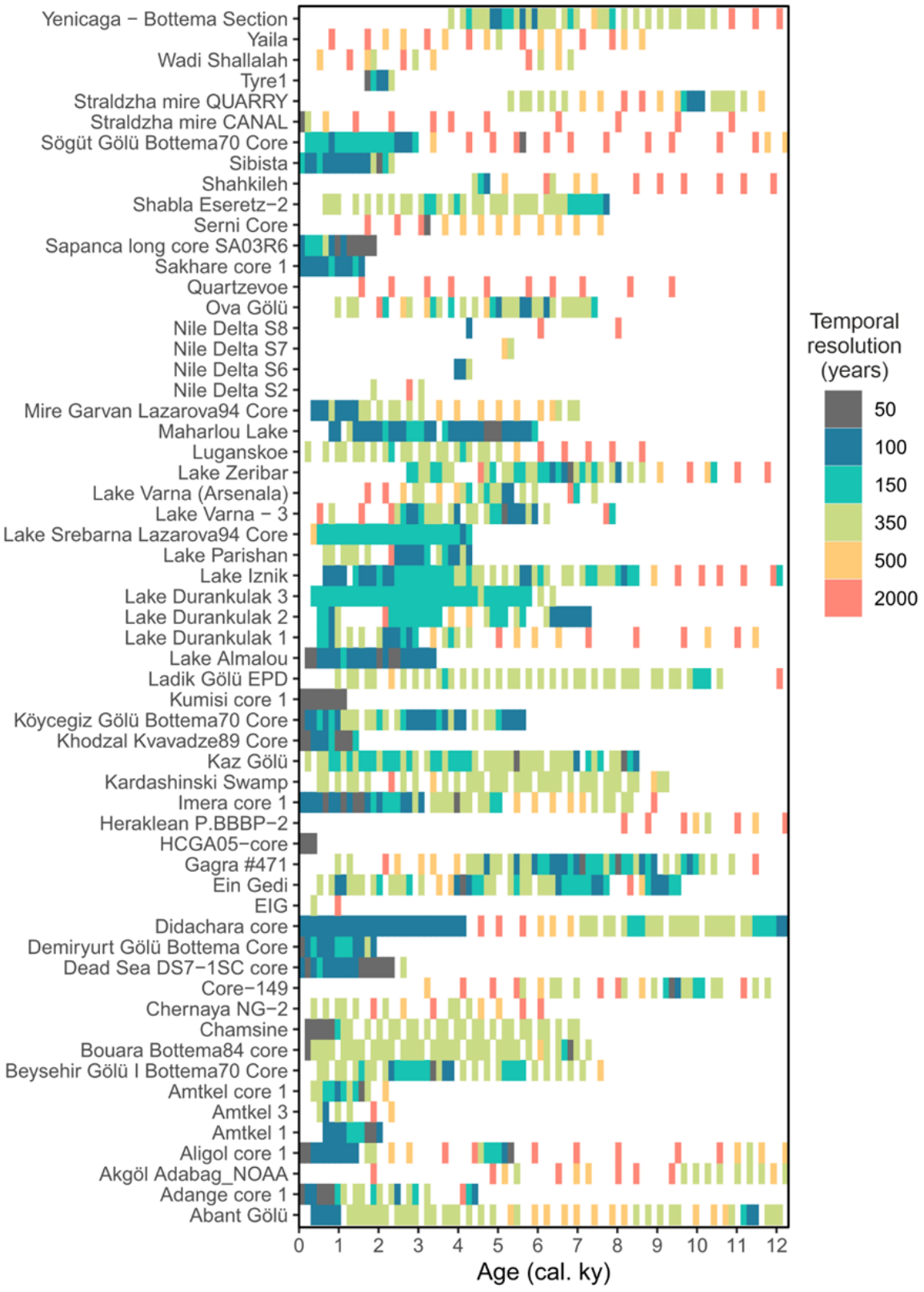
Yenicaga − Bottema Section
Yaila
Wadi Shallalah
Tyre1
Straldzha mire QUARRY
Straldzha mire CANAL
Sögüt Gölü Bottema70 Core
Sibista
Shahkileh
Shabla Eseretz−2
Serni Core
Sapanca long core SA03R6
Sakhare core 1
Quartzevoe
Ova Gölü
Nile Delta S8
Nile Delta S7
Nile Delta S6
Nile Delta S2
Mire Garvan Lazarova94 Core
Maharlou Lake
Luganskoe
Lake Zeribar
Lake Varna (Arsenala)
Lake Varna − 3
Lake Srebarna Lazarova94 Core
Lake Parishan
Lake Iznik
Lake Durankulak 3
Lake Durankulak 2
Lake Durankulak 1
Lake Almalou
Ladik Gölü EPD
Kumisi core 1
Köycegiz Gölü Bottema70 Core
Khodzal Kvavadze89 Core
Kaz Gölü
Kardashinski Swamp
Imera core 1
Heraklean P.BBBP−2
HCGA05−core
Gagra #471
Ein Gedi
EIG
Didachara core
Demiryurt Gölü Bottema Core
Dead Sea DS7−1SC core
Core−149
Chernaya NG−2
Chamsine
Bouara Bottema84 core
Beysehir Gölü I Bottema70 Core
Amtkel core 1
Amtkel 3
Amtkel 1
Aligol core 1
Akgöl Adabag_NOAA
Adange core 1
Abant Gölü
0
1
2
3
4
5
6
7
8
9
10
11
12
Age (cal. ky)
Temporal resolution (years)
50
100
150
350
500
2000

Supplementary Figure 3.2. Plots showing reconstructed biomes at 0.5 ky intervals from 12 ky to the present. each plot shows the dominant biome within the 300-year window around each time point. The biome codes are: CMIX, cool mixed evergreen needleleaf and deciduous broadleaf forest; DESE, desert; ENWD, evergreen needleleaf woodland; GRAM, graminoids with forbs; TEDE, temperate deciduous malacophyll broadleaf forest; WTFS, warm-temperate evergreen needleleaf and sclerophyll broadleaf forest; XSHB, xeric shrubland. Note that cold evergreen needleleaf forest (CENF) and tundra (TUND) do not occur in these time intervals, although they were reconstructed for other samples. Sites which had samples that were considered to have no modern analogue are indicated as NONA.

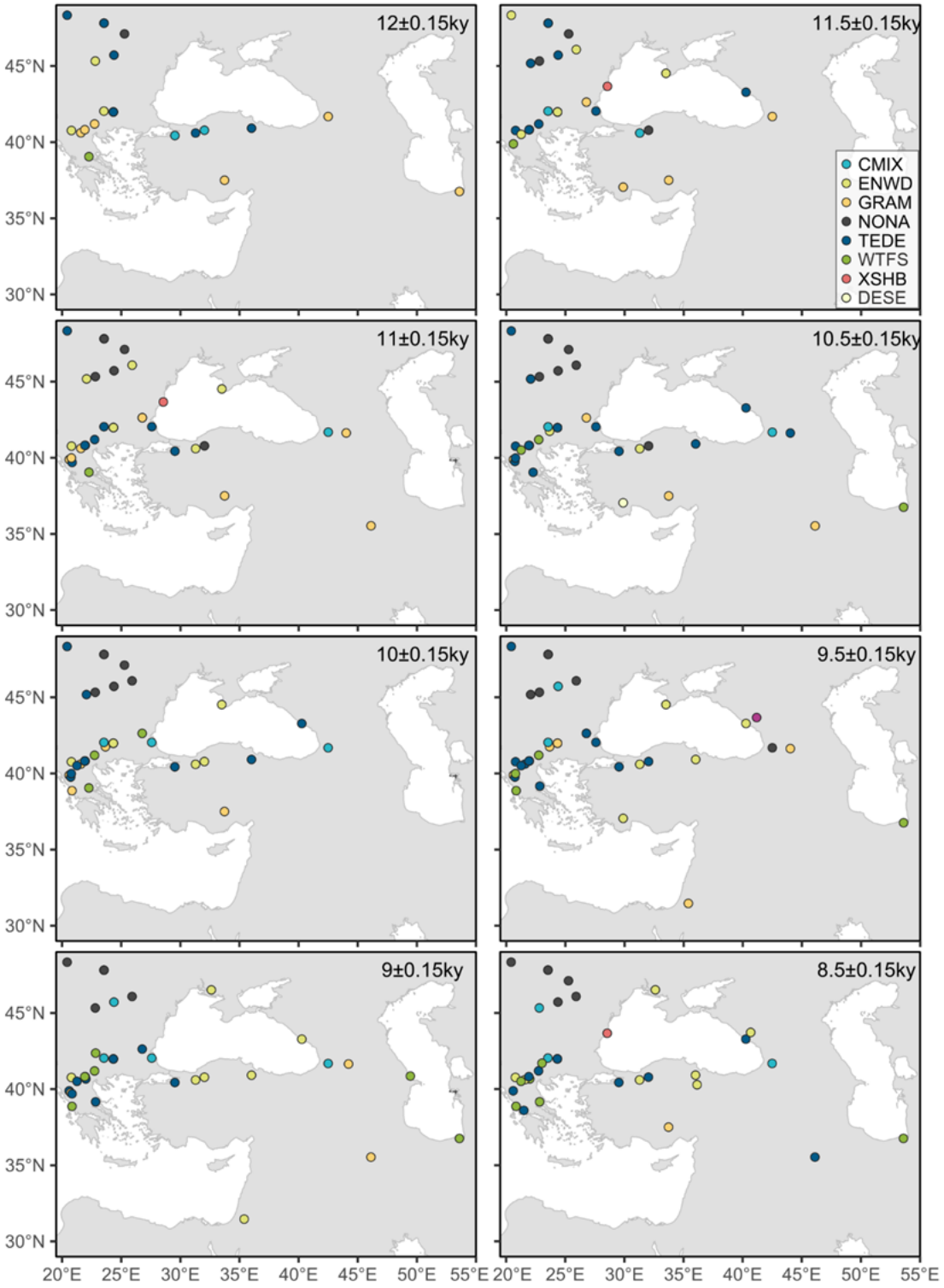

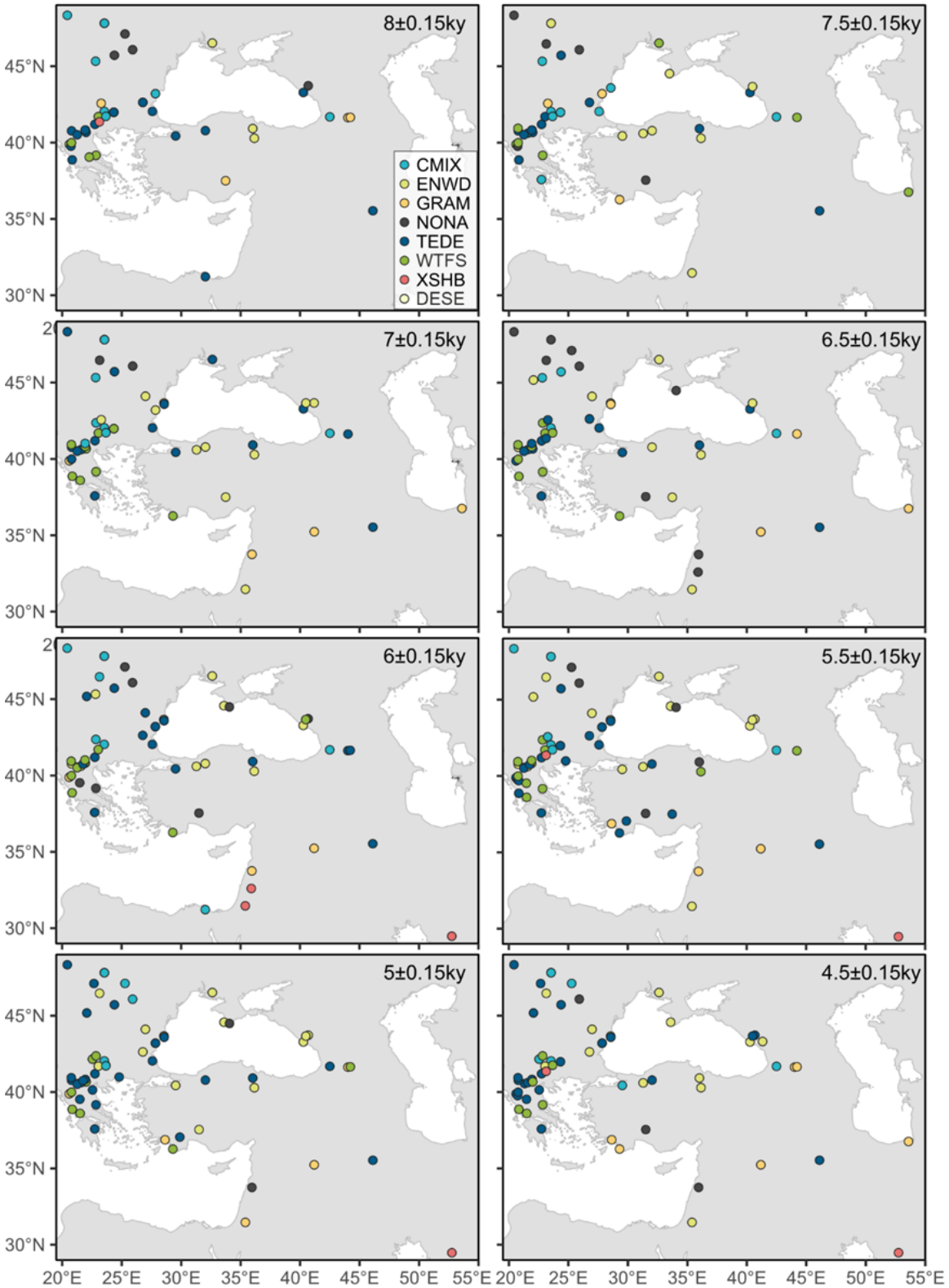
8±0.15ky
7.5±0.15ky
7±0.15ky
6.5±0.15ky
6±0.15ky
5.5±0.15ky
5±0.15ky
4.5±0.15ky
CMIX
ENWD
GRAM
NONA
TEDE
WTFS
XSHB
DESE
45°N
40°N
35°N
30°N
20°E
25°E
30°E
35°E
40°E
45°E
50°E
55°E

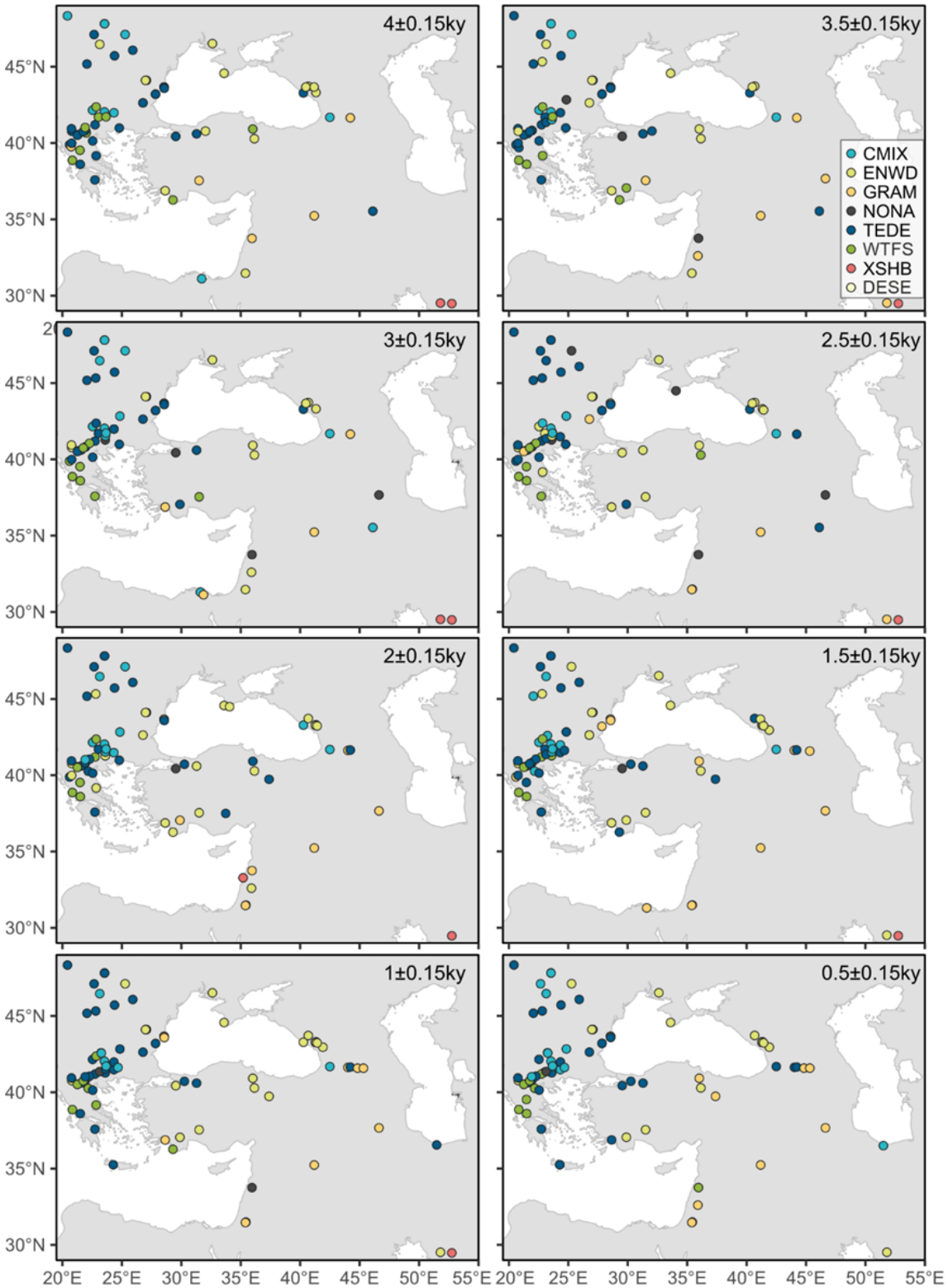
4±0.15ky
3.5±0.15ky
3±0.15ky
2.5±0.15ky
2±0.15ky
1.5±0.15ky
1±0.15ky
0.5±0.15ky
CMIX
ENWD
GRAM
NONA
TEDE
WTFS
XSHB
DESE
45°N
40°N
35°N
30°N
20°E
25°E
30°E
35°E
40°E
45°E
50°E
55°E

Supplementary Figure 3.3. Proportion of records in different elevation bands (> 1500m, between 500 and 1500m, < 500m) in the Eastern Mediterranean-Black Sea Caspian corridor (EMBSeCBIO) region having at least one sample identified as non-analogue in a 300-year time-window over the past 12 ky, where the time windows were constructed with 50% overlap. The red line indicates the 5% threshold to separate false positives (values below the threshold).

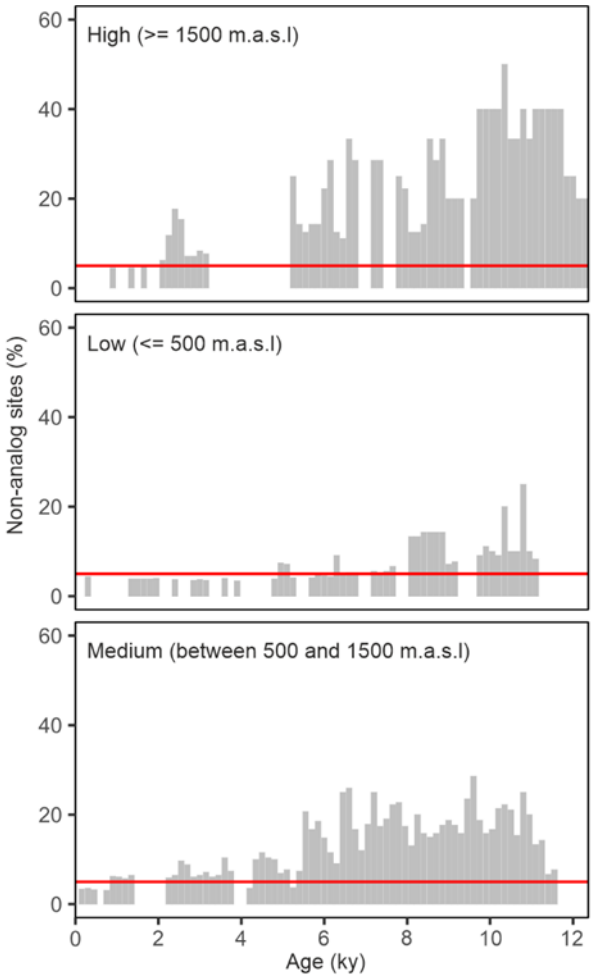

Supplementary Figure 3.4. Taxon abundance in non-analogue samples from the interval between 11 and 8 ky from (a) the Carpathians, (b) Gagra, and (c) Yenicaga. The box plots represent the mean and interquartile range across all the non-analogue samples.

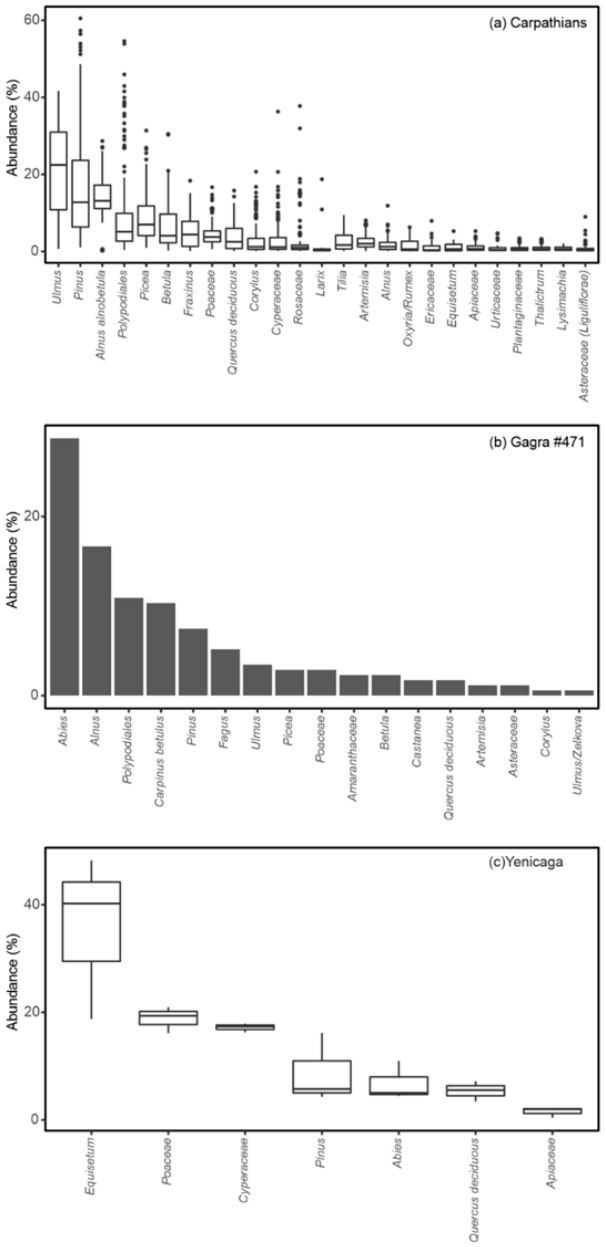

Supplementary Figure 3.5. Identification of the starting point of Holocene forest growth in sequences spanning at least the last 12.3 ky with at least 13 samples in the interval. The curves were produced considering the similarity score ratio of biomes defined as moisture-demanding forest types to other vegetation types for each pollen sample. The forest types are temperate deciduous malacophyll broadleaf forest (TEDE), cool mixed evergreen needleleaf and deciduous broadleaf forest (CMIX) and cold evergreen needleleaf forest (CENF). The curves were smoothed using a 300-year window with 50% overlap. A break point analysis was applied to the forest curve to obtain the optimal number (least amount of residuals) of break points that allowed identifying trend changes in the sequence (score ~ age). Linear regressions were performed between the identified break points in each sequence (formula: y ~ x + {x - breaking} * ifelse(x > breaking,1,0)). The earliest point indicating a change from a zero or negative slope (no change or decrease of forest) to a positive slope (an increase of forest) was cidnetified as the starting point of forest growth. The period evaluated was from 7 to 11.6 ky before present. In the plot, the colours represent the proportion of forest vegetation (blue shading) versus other vegetation (orange shading). The red lines indicate the breakpoint identified as the start of forest growth. The white lines represent the linear regressions between adjacent breakpoints.

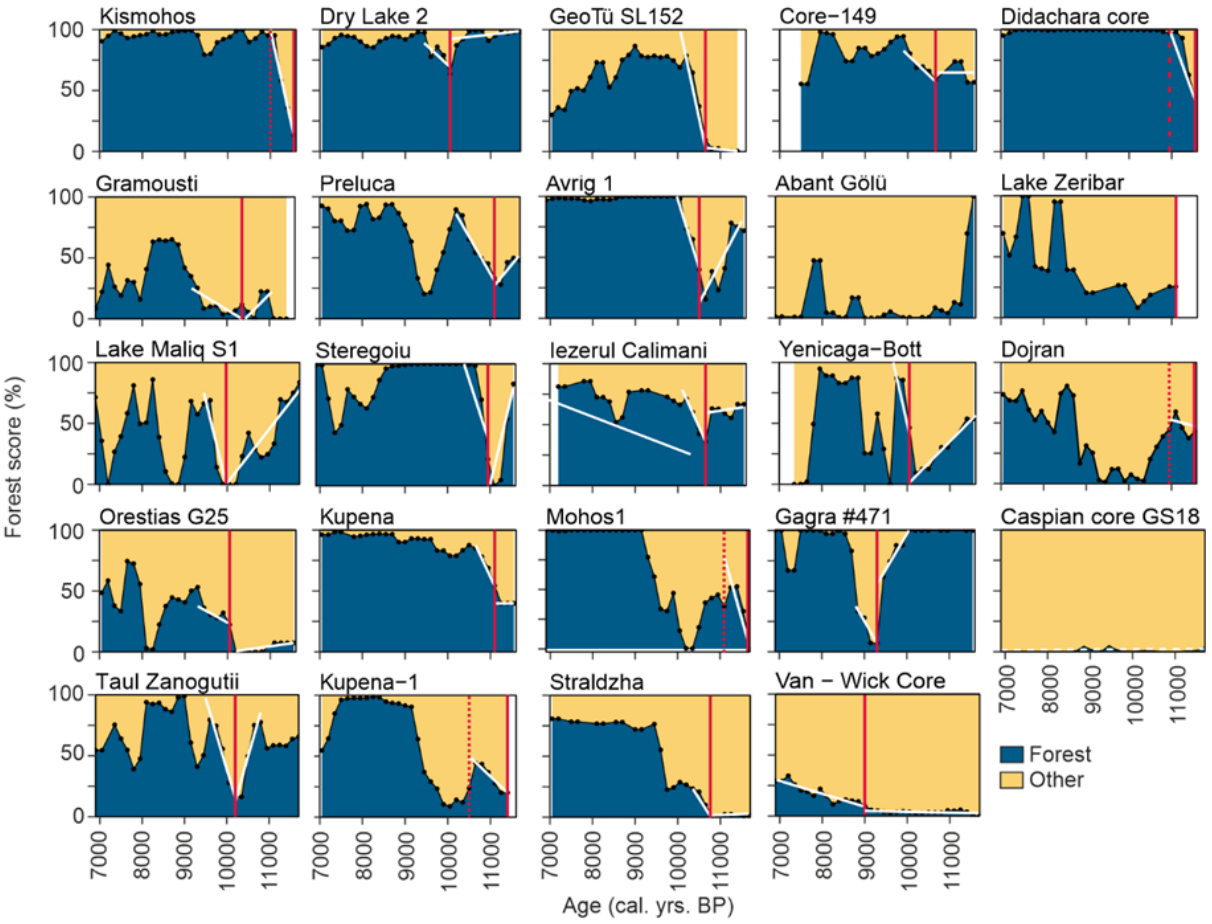

Supplementary Figure 3.6. Proportion of records the eastern Mediterranean-Black Sea Caspian corridor (EMBSeCBIO) region identified as temperate deciduous malacophyll broadleaf forest (TEDE) in successive 300-year windows during the Holocene.

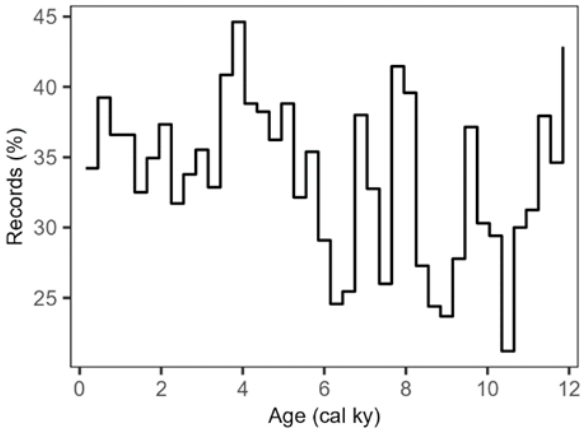

Supplementary Figure 3.7. Holocene dynamics of forest vegetation during the Holocene. The uppermost panel shows the proportion of records in the region characterised by moisture-demanding forest, as represented temperate deciduous malacophyll broadleaf forest (TEDE), cool mixed evergreen needleleaf and deciduous broadleaf forest (CMIX) and cold evergreen needleleaf forest (CENF), in 300-year windows with 50% overlap. The lowermost panel shows warm-temperate evergreen needleleaf and sclerophyll broadleaf forest (WTSFS), represented in the same way. The central panel represents more open vegetation types, including samples reconstructed as tundra (TUND), desert (DESE), graminoids with forbs (GRAM), xeric shrubland (XSHB), evergreen needleleaved woodland (ENWD).

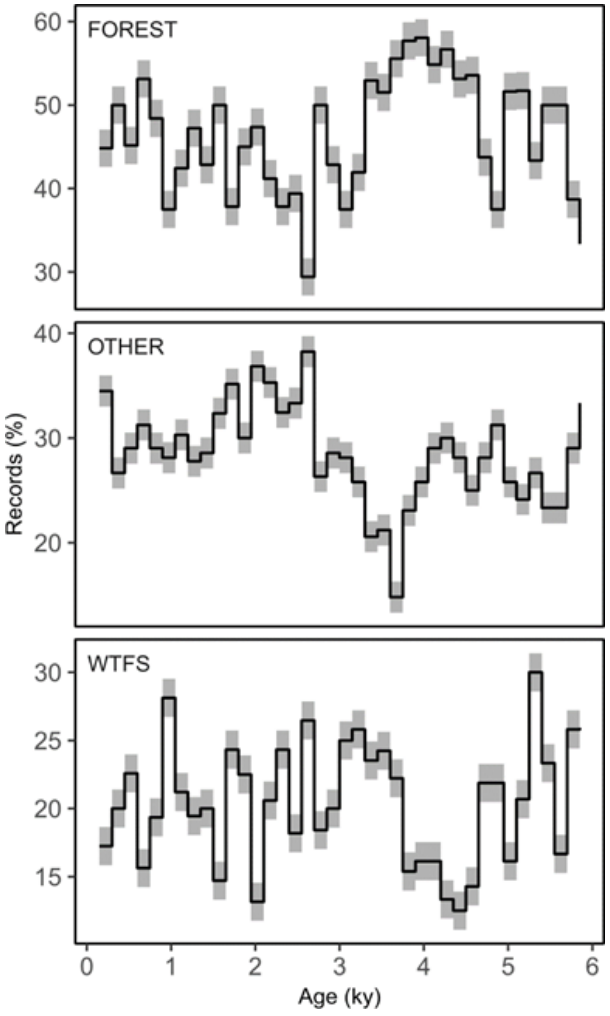

Suppelentary Figure 3.8. Forest curve at subregional scale (green line) alongside the count of utilized sites within each time-window (represented by the grey bars in the background).

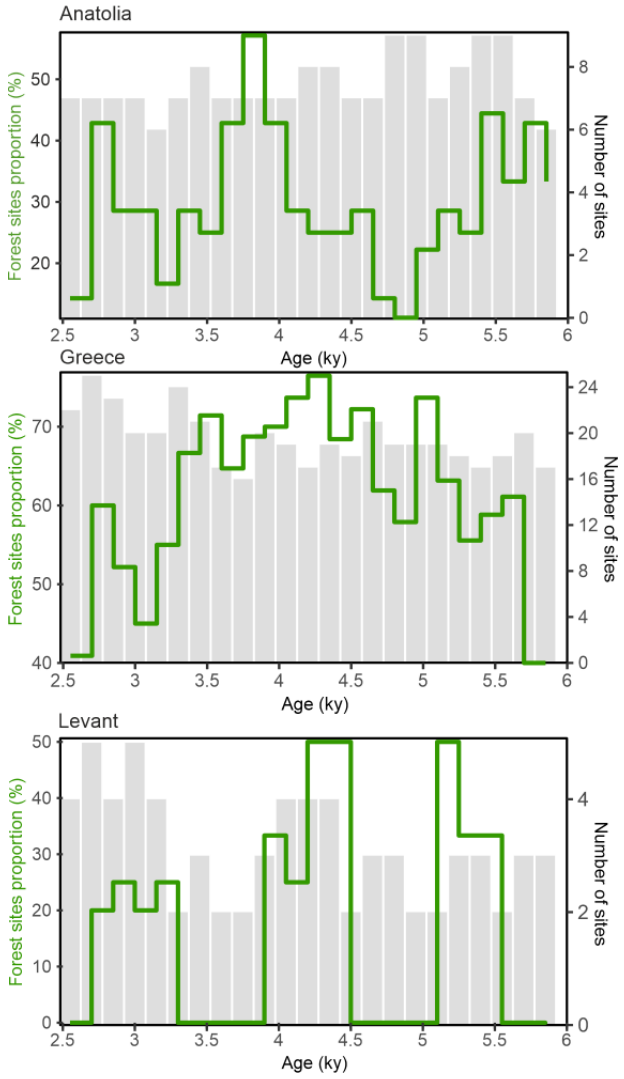

Chapter 4. Pollen-based reconstructions of Holocene climate trends in the eastern Mediterranean region

This chapter has been published as: **Cruz-Silva, E.**, Harrison, S. P., Prentice, I. C., Marinova, E., Bartlein, P. J., Renssen, H., and Zhang, Y. (2023). Pollen-based reconstructions of Holocene climate trends in the eastern Mediterranean region. Clim. Past, 19, 2093–2108, https://doi.org/10.5194/cp-19-2093-2023, 2023. It has been written according to the guidelines of the journal

4.1 Abstract

There has been considerable debate about the degree to which climate has driven societal changes in the eastern Mediterranean region, partly through reliance on a limited number of qualitative records of climate changes and partly reflecting the need to disentangle the joint impact of changes in different aspects of climate. Here, we use tolerance-weighted, weighted-averaging partial least squares to derive reconstructions of the mean temperature of the coldest month (MTCO), mean temperature of the warmest month (MTWA), growing degree days above a threshold of 0 ◦C (GDD0), and plant-available moisture, which is represented by the ratio of modelled actual to equilibrium evapotranspiration (α) and corrected for past CO2 changes. This is done for 71 individual pollen records from the eastern Mediterranean region covering part or all of the interval from 12.3 ka to the present. We use these reconstructions to create regional composites that illustrate the long-term trends in each variable. We compare these composites with transient climate model simulations to explore potential causes of the observed trends. We show that the glacial–Holocene transition and the early part of the Holocene was characterised by conditions colder than the present. Rapid increases in temperature occurred between ca. 10.3 and 9.3 ka, considerably after the end of the Younger Dryas. Although the time series are characterised by centennial to millennial oscillations, the MTCO showed a gradual increase from 9 ka to the present, consistent with the expectation that winter temperatures were forced by orbitally induced increases in insolation during the Holocene. The MTWA also showed an increasing trend from 9 ka and reached a maximum of ca. 1.5 ◦C greater than the present at ca. 4.5 and 5 ka, followed by a gradual decline towards present-day conditions. A delayed response to summer insolation changes is likely a reflection of the persistence of the Laurentide and Fennoscandian ice sheets; subsequent summer cooling is consistent with the expected response to insolation changes. Plant-available moisture increased rapidly after 11 ka, and conditions were wetter than today between 10 and 6 ka, but thereafter, α declined gradually. These trends likely reflect changes in atmospheric circulation and moisture advection into the region and were probably too small to influence summer temperature through land–surface feedbacks. Differences in the simulated trajectory of α in different models highlight the difficulties in reproducing circulation-driven moisture advection into the eastern Mediterranean.

4.2. Introduction

The eastern Mediterranean region is a critical region for examining the long-term interactions between climate and past societies because of the early adoption of agriculture in the region, which has been widely associated with the rapid warming at the end of the Younger Dryas (Belfer-Cohen and Goring-Morris, 2011). Societal collapse and large-scale migrations have been associated with climates less favourable to agriculture during the 8.2 ka event (Weninger et al., 2006) or to major changes in agricultural practices (Roffet-Salque et al., 2018). Subsequent periods of less favourable climate, particularly prolonged droughts, have been associated with the fall of the Akkadian Empire, ca. 4.2 ka (Cookson et al., 2019), and the end of the Late Bronze Age and the beginning of the Greek Dark Ages, ca. 3.2 ka (Kaniewski et al., 2013; Drake, 2012). However, the attribution of changes in human society to climate changes is not universally accepted. Flohr et al. (2016), for example, analysed radiocarbon-dated archaeological sites for evidence of societal changes in response to climate changes in the early Holocene, particularly the 8.2 ka event, and found no evidence of large-scale site abandonment or migration, although there were indications of local adaptations. However, since Flohr et al. (2016) did not compare the archaeological records to region-specific climate reconstructions, it is difficult to assess how far local responses might reflect differences in climate between the sites. Even the societal response to the early Holocene warming appears to have differed across the region (Roberts et al., 2018).

The need to understand the interactions between climate and past societies in the eastern Mediterranean is given further impetus because human modification of the landscape has the potential to affect climate directly through changes in land surface properties. The degree to which human modifications of the landscape had a significant impact on global climate before the pre-industrial period is debated (Ruddiman, 2003; Joos et al., 2004; Kaplan et al., 2011; Singarayer et al., 2011; Mitchell et al., 2013; Stocker et al., 2017), but these impacts were likely to be more important in regions with a long history of settlement and agricultural activities (Harrison et al., 2020).

Much of our current understanding of climate changes in the eastern Mediterranean region is based on the qualitative interpretation of individual records (e.g. Roberts et al., 2019). Oxygen isotope records from speleothems or lake sediments have been used to infer changes in moisture availability through the Holocene (e.g. Bar-Matthews et al., 1997; Cheng et al., 2015; Dean et al., 2015; Burstyn et al., 2019), as have pollen-based reconstructions of changes in vegetation (e.g. Bottema, 1995; Denèfle et al., 2000; Sadori et al., 2011). Pollen records can also be used to make quantitative reconstructions of seasonal temperatures and precipitation or plant-available water (Bartlein et al., 2011; Chevalier et al., 2020). Quantitative reconstructions of past climates have been made for individual records from the eastern Mediterranean region (e.g. Cheddadi and Khater, 2016; Magyari et al., 2019), and syntheses of pollen-based quantitative climate reconstructions have included sites from this region (Davis et al., 2003; Mauri et al., 2015;

Herzschuh et al., 2022). Davis et al. (2003) provided a composite curve of seasonal temperature changes but not moisture changes; both summer and winter temperatures showed very little variation (<1 ◦C) through most of the Holocene. Mauri et al. (2015) is an updated version of the Davis et al. (2003) reconstructions, with more sites included but showing similarly muted temperate changes in the eastern Mediterranean region. Herzschuh et al. (2022) showed more homogenous changes in both temperature and precipitation across the eastern Mediterranean region, but it is difficult to compare the two reconstructions directly because they used different reconstruction techniques. None of the existing reconstructions takes account of the impact of changing CO2 levels on vegetation, which could potentially affect the reconstructions of moisture variables (Prentice et al., 2022a). Thus, there is a need for well-founded reconstructions of climate, particularly climate variables that are relevant for human occupation and agriculture, to be able to address questions about the interactions between climate and society in the eastern Mediterranean region.

Here, we provide new quantitative reconstructions of seasonal temperature and plant-available moisture for 71 sites from the eastern Mediterranean region (defined by the eastern Mediterranean–Black Sea–Caspian corridor, EMBSeCBIO, project as the region between 29–49◦ N, 20 and 62◦ E), including a correction for the impact of changing CO2 levels on plant-available moisture reconstructions. We use these reconstructions to document the regional trends in climate from 12.3 ka to the present. We then explore how far these trends can be explained by changes in external forcing by comparing the reconstructions with transient climate model simulations.

4.3. Methods

4.3.1. Modern pollen and climate data

The modern pollen data set was obtained from version 1 of the SPECIAL Modern Pollen Data Set for Climate Reconstructions (SMPDSv1; Harrison, 2019), which provides relative abundance data from 6459 terrestrial sites from Europe, the Middle East, and northern Eurasia and has been assembled from multiple public sources or provided by the original authors. The SMPDS pollen records have been taxonomically standardised, filtered to remove obligate aquatics, insectivorous species, introduced species, or taxa that only occur in cultivation. The removal of cultivars is designed to minimise the influence of anthropogenic signals on the reconstructions. We then grouped taxa with only sporadic occurrences into higher taxonomic levels (genus, sub-family, or family). Consequently, the data set provides relative abundance data for 247 pollen taxa (Supplementary Table 4.1). We used the 5840 SMPDS sites from the area between 29 and 75◦ N and 20◦ W, 62◦ E to construct the training data set (Supplementary Figure 4.1); the sampling outside this box is limited and likely not representative of the diversity of the climate gradients. At sites with multiple modern samples, we averaged the taxon abundances across all samples to minimise the over-representation of some localities and hence specific climates, in the training

data set. We used the 195 pollen taxa that occurred at more than 10 sites (Supplementary Table 4.1) to derive climate–abundance relationships.

We focus on reconstructing bioclimatic variables that fundamentally control plant distribution, specifically related to winter temperature limits, accumulated summer warmth, and plant-available moisture (Harrison et al., 2010). The bioclimatic data for each modern site was obtained from Harrison et al. (2019) through a data set that provides estimates of mean temperature of the coldest month (MTCO), growing degree days above a base level of 0 ◦C (GDD0), and a moisture index (MI) defined as the ratio of annual precipitation to annual potential evapotranspiration at each modern pollen site, which is derived using a geographically weighted regression of version 2.0 of the Climate Research Unit (CRU) long-term gridded climatology at 10 arcmin resolution (CRU CL v2.0; New et al., 2002). MTCO and GDD0 were taken directly from the data set. Since Harrison (2019) do not provide mean temperature of the warmest month (MTWA), we calculated this based on the relationship between MTCO and GDD0 given in Wei et al. (2021). We derived an alternative moisture index, α, which is the ratio between modelled actual and equilibrium evapotranspiration from MI, following Liu et al. (2020). MI and α both provide good indices of plant-available moisture, but since α has a natural limit in wetter conditions, it is more suitable for discriminating differences in drier climates.

4.3.2. Fossil pollen data

The fossil pollen data set for the eastern Mediterranean region was obtained from the eastern Mediterranean–Black Sea–Caspian corridor (EMBSeCBIO) database (Harrison et al., 2021), which contains information from 187 records from the region between 29 and 49◦ N and between 20 and 62◦ E. (Note that this is a more limited region than the one used for the modern training data set.) We discarded records (a) from marine environments or very large lakes (>500 km2), (b) with no radiocarbon dating, (c) where the age of the youngest pollen sample was unknown, (d) where there is a hiatus after the youngest radiocarbon date, (e) where more than half of the radiocarbon dates were rejected by the original authors, and (f) where more than half of the ages were based on pollen correlation with other radiocarbon-dated records. However, we kept records where there is a hiatus but where there are sufficient radiocarbon dates above the hiatus to create an age model for the post-hiatus part of the record. We constructed new age models for all the remaining sites (121) using the IntCal20 calibration curve (Reimer et al., 2020) and the rbacon R package (Blaauw et al., 2021) in the framework of the AgeR R package (Villegas-Diaz et al., 2021). Some of these records have no modern samples, where modern was defined as 0–300 years before present, and thus could not be used to calculate climate anomalies. As a result, 71 pollen records (Figure 4.1; Supplementary Table 4.2) were used for the climate reconstructions. These records have a mean length of 6594 years and a mean resolution of 228 years. The records were taxonomically standardised for consistency with the training data set.

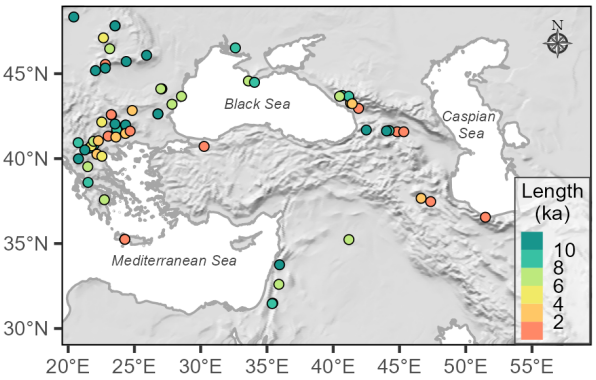

Figure 4.1. Distribution of pollen records used in the climate reconstructions. The colour coding shows the length of the record.

4.3.3. Climate reconstructions

We used tolerance-weighted, weighted-averaging partial least squares (fxTWA-PLS; Liu et al., 2020) regression to model the relationships between taxon abundances and individual climate variables in the modern training data set and then applied these relationships to reconstruct past climate using the fossil assemblages. fxTWA-PLS reduces the known tendency of regression methods to compress climate reconstructions towards the middle of the sampled range by applying a sampling frequency correction to reduce the influence of uneven sampling of climate space and by weighting the contribution of individual taxa according to their climate tolerance (Liu et al., 2020). Version 2 of fxTWA-PLS (fxTWA-PLS2; Liu et al., 2023), applied here, uses P-spline smoothing to derive the frequency correction and also applies the correction both in estimating climate optima and in the regression itself, producing a further improvement in model performance relative to version 1, as published by Liu et al. (2020).

We evaluated the fxTWA-PLS models by comparing the reconstructions against observations using pseudo-removed leave-out cross-validation, where one site was randomly selected as a test site and geographically and climatically similar sites (pseudo sites) were removed from the training set to avoid redundancy in the climate information inflating the cross-validation. We selected the last significant component (p value ≤ 0.01) and assessed model performance using the root mean square error of the prediction (RMSEP). The degree of compression was assessed using linear regression, and local compression was assessed by loess regression (locfit). Climate reconstructions were made for every sample in each fossil record using the best models, and sample-specific errors were estimated via bootstrapping. We applied a correction factor (Prentice et al., 2022a) to the reconstructions of α to account for the impact of changes in atmospheric CO_2 levels on water use efficiency, specifically the increased water use efficiency under high CO_2 levels characteristic of the recent past and the low CO_2 levels that would have reduced water use efficiency during the Late Glacial period and thus could have influenced the reconstructions during the earliest part of the records. The correction was implemented through the package codos: 0.0.2 (Prentice et al., 2022b), with past CO_2 concentration values derived from the EPICA Dome C record (Bereiter et al., 2015).

4.3.4. Construction of climate time series

To obtain climate time series representative of the regional trends in climate, we first screened the reconstructions to remove individual samples with (a) low effective diversity (< 2), as measured using Hill's N2 diversity measure (Hill, 1973), which could indicate low pollen counts or local contamination; and (b) sample-specific errors above the 0.95 quantile to remove obvious outliers. This screening resulted in the exclusion of only a small number of individual samples (see Supplementary Figure 4.2). We then averaged the reconstructed values in 300-year bins (slightly larger than the average resolution of the records at 228 years) with 50% overlap. The first bin centred on 150 years before present, and subsequent bins were centred at 150-year increments throughout the record. We excluded any bins with only one sample. The binned values of individual sites were averaged to produce a regional composite of the anomalies for each climate variable, where the modern baseline was taken as the first 300-year bin centred on 150 years before present. These time series were smoothed using locally weighted regression (Cleveland and Devlin, 1988), with a window width of 1000 years (half-window width 500 years) and fixed target points in time to highlight the long-term trends. Confidence intervals (5th and 95th percentiles) for each composite were generated by bootstrap resampling by site over 1000 iterations. We examined the impact of the CO_2 correction on reconstructed α (Supplementary Figure 4.3); this had no major effect on the reconstructed trends, except during the earliest part of the record.

4.3.5. Climate model simulations

We compared the reconstructed climate changes with transient climate model simulations of the response to external forcing to determine the extent that the reconstructed climate changes reflect changes in known forcing. We used transient simulations of the response to orbital and greenhouse gas forcing in the later Holocene from the following four models participating in the PAleao-Constraints on Monsoon Evolution and Dynamics (PACMEDY) project (Carré et al., 2021): the MPI (Max Planck Institute) Earth System Model version 1.2 (Dallmeyer et al., 2020), the AWI (Alfred Wegener Institute) Earth System Model version 2 (Sidorenko et al., 2019), and two versions of the IPSL (Institut Pierre-Simon Laplace) Earth System Model. The IPSL and AWI simulations were run from 6 ka to 1950 CE and the MPI simulation from 7.95 ka to 1850 CE. We used a longer transient simulation covering the period from 11.5 ka that was made with the LOVECLIM model (Goosse et al., 2010), which, in addition to orbital and greenhouse gas forcing, accounts for the waning of the Laurentide and Fennoscandian ice sheets (Zhang et al., 2016). Finally, we used two transient simulations from 22 ka to the present that were made using the Community Climate System Model (CCSM3; Collins et al., 2006). Both were forced by changes in orbital configuration, atmospheric greenhouse gas concentrations, continental ice sheets, and meltwater fluxes but differ in the configuration of the meltwater forcing applied after the Bølling warming (14.7 ka).

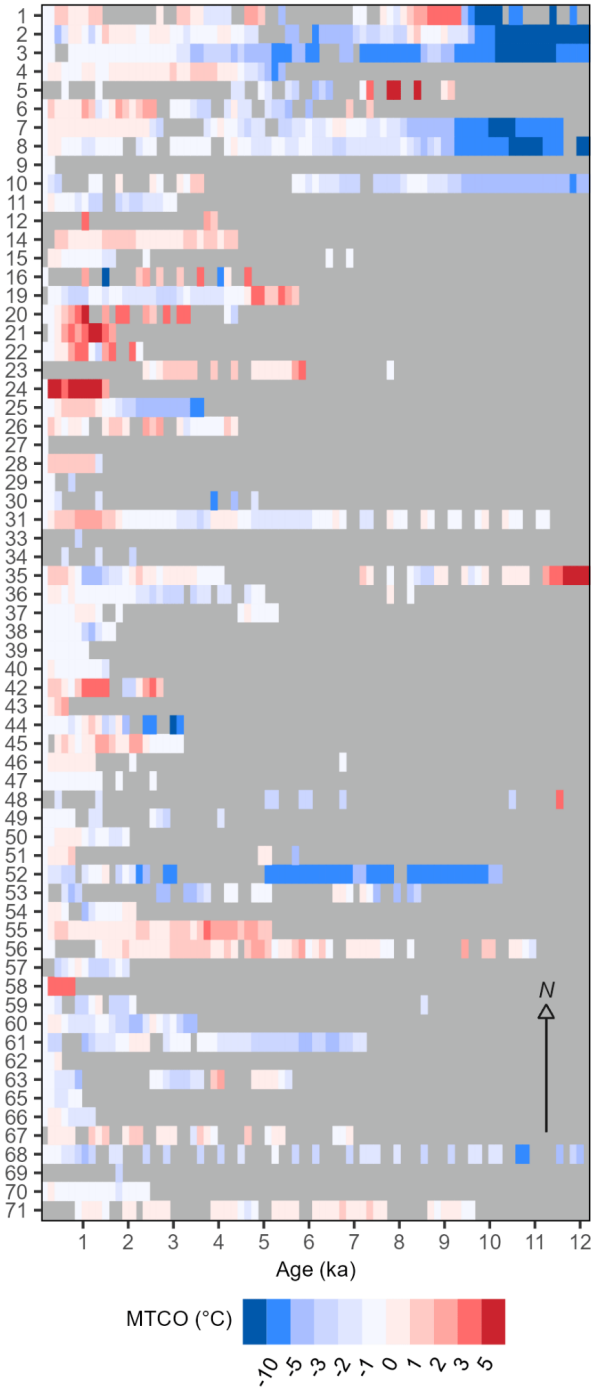

Figure 4.2. Time series of reconstructed anomalies of mean temperature of the coldest month (MTCO) for individual records. Entities are arranged by latitude (N-S). Information about the numbered individual sites can be found in Supplementary table 4.1.

In the first simulation (TRACE-21k-I; Liu et al., 2009), there was a sustained meltwater flux of ~ 0.1 Sv from the Northern Hemisphere ice sheets to the Arctic and North Atlantic until ca. 6 ka and a continuous inflow of water from the North Pacific into the Arctic after the opening of the Bering Strait. The second simulation (TRACE-21k-II; He and Clark, 2022) had no meltwater flux during the Bølling warming or the Holocene but applied a flux of ~ 0.17 Sv to the North Atlantic during the

Younger Dryas (12.9–11.7 ka). The difference in meltwater forcing results in a much stronger Atlantic Meridional Overturning Circulation during the Holocene in the TRACE-21k-II simulation compared to the TRACE-21k-I simulation. Details of the model simulations are given in Supplementary Table 4.3. The use of multiple simulations allows the identification of robust signals that are not model-dependent (see, e.g., Carré et al., 2021) and also the separation of the effects of different forcings. The TRACE-21k-I data were adjusted to reflect the changing length of months during the Holocene (related to the eccentricity of Earth's orbit and the precession-determined time of year of perihelion), whereas the other simulations were not. However, this makes little practical difference for the selection of variables used here.

Outputs from each simulation were extracted for land grid cells in the EMBSeCBIO domain (29–49◦ N, 20–55◦ E; this region extends slightly less far eastwards than the EMBSeCBIO region as originally defined, but there are no pollen sites beyond 55◦ E). The MTCO and MTWA were extracted directly; GDD0 was obtained by deriving daily temperature values from monthly data using a mean-preserving autoregressive interpolation function (Rymes and Myers, 2001). Daily values of cloud cover fraction and precipitation were obtained from monthly data in the same way and used to estimate MI, i.e. the ratio of annual precipitation to annual potential evapotranspiration, through the R package smpds (Villegas-Diaz and Harrison, 2022) before converting this to α, following Liu et al. (2020). For consistency with the reconstructed time series, climate anomalies for 30-year bins for each land grid cell within the EMBSeCBIO domain were calculated using the interval after 300 years before present as the modern baseline. Since the spatial resolution of the models varies (Supplementary Table 4.3), and in any case is coarser than the sampling resolution of the individual pollen records precluding direct comparisons except at a regional scale, we used all of the land grid cells within the EMBSeCBIO domain and did not attempt to select grid cells coincident with the location of pollen data. A composite was produced by averaging the grid cell time series, which was then smoothed, using locally weighted regression (Cleveland and Devlin, 1988) with a window width of 1000 years (i.e. a half-window width of 500 years) and fixed target points in time. Confidence intervals (5th and 95th percentiles) for each composite were generated by bootstrap resampling by grid cell over 1000 iterations.

4.4. Results

4.4.1. Performance of the fxTWA-PLS statistical model

The assessment of the model through cross-validation showed that it reproduces the modern climate variables reasonably well (Table 4.1; Supplementary Table 4.4). The best performance is achieved by α (R^2=0.73; RMSEP=0.15) and MTCO (R^2=0.73; RMSEP 3.67). The models for GDD0 (R^2=0.69; RMSEP=880) and MTWA (R^2=0.63, RMSEP=3.22) were also acceptable. The slopes of the regressions ranged from 0.78 (MTWA) to 0.86 (MTCO), indicating that the degree of

compression in the reconstructions in small (Table 4.1). Thus, the downcore fxTWA-PLS reconstructions of all the climate variables can be considered to be robust and reliable.

Variable	Selected component	R^2	Average bias	RMSEP	P	b1	b1.se
MTCO	4	0.73	−0.22	3.67	0.001	0.86	0.01
MTWA	2	0.63	−0.10	3.22	0.001	0.78	0.01
GDD0	2	0.69	56.46	880.33	0.001	0.79	0.01
α	2	0.73	−0.01	0.15	0.001	0.80	0.01

Table 4.1. Leave-out cross-validation fitness of fxTWA-PLSv2 for the mean temperature of the coldest month (MTCO), mean temperature of the warmest month (MTWA), growing degree days above base level 0 ◦C (GDD0), and plant-available moisture (α), with a P-spline-smoothed fx estimation, using bins of 0.02, 0.02, and 0.002, showing results for the selected component for each variable. RMSEP is the root mean square error of the prediction. P assesses whether using the current number of components is significantly different from using one component less. The degree of overall compression is assessed by linear regression of the cross-validated reconstructions onto the climate variable, where b1 and b1.se are the slope and the standard error of the slope, respectively. The overall compression is reduced as the slope approaches 1. Full details for all the components are given in Supplementary Table 4.4.

4.4.2. Holocene climate evolution in the region

Down-core reconstructions showed broadly coherent signals, although there was variation in both the timing and magnitude of climate changes across the sites that reflected differences in latitude and elevation (Figures 4.2, 4.3, 4.4). Nevertheless, the records indicated coherent regional trends over the past 12 kyr.

Winter temperature showed a cooling trend between 12 and 11 ka, with the reconstructed MTCO ca. 8 ◦C lower than the present at 11 ka (Figure 4.5). There was a moderate increase in the MTCO after 11 ka, followed by a more pronounced increase of ca. 5 ◦C between 10.3 and 9.3 ka. Winter temperatures were only ca. 2 ◦C lower than the present at the end of this rapid warming phase. There are relatively large uncertainties in the MTCO reconstructions prior to 10.3 ka, so the trends in the early part of the record are not well constrained. However, the phase of rapid warming between 10.3 and 9.3 ka (and the subsequent part of the record) is well constrained. MTCO continued to increase gradually through the Holocene, although multi-centennial to millennial oscillations were superimposed on the general trend.

The initial trends in the summer temperature were broadly similar to those in MTCO, with a cooling between 12.3 and 11 ka and the reconstructed MTWA ca. 2 ◦C lower than the present at 11 ka (Figure 4.5). Summer temperature increased thereafter, although with pronounced millennial oscillations, up to ca. 4.5 ka when the MTWA was ca. 1.5 ◦C higher than the present. There was a gradual decrease in summer temperature after ca. 4.5 ka. The GDD0 reconstructions

showed similar trends to the MTWA, reaching maximum values around 4.5 ka when the growing season was ca. 150 degree days greater than today. The subsequent decline in GDD0 was somewhat flatter, which presumably reflects the influence of still-increasing winter temperatures on the length of the growing season.

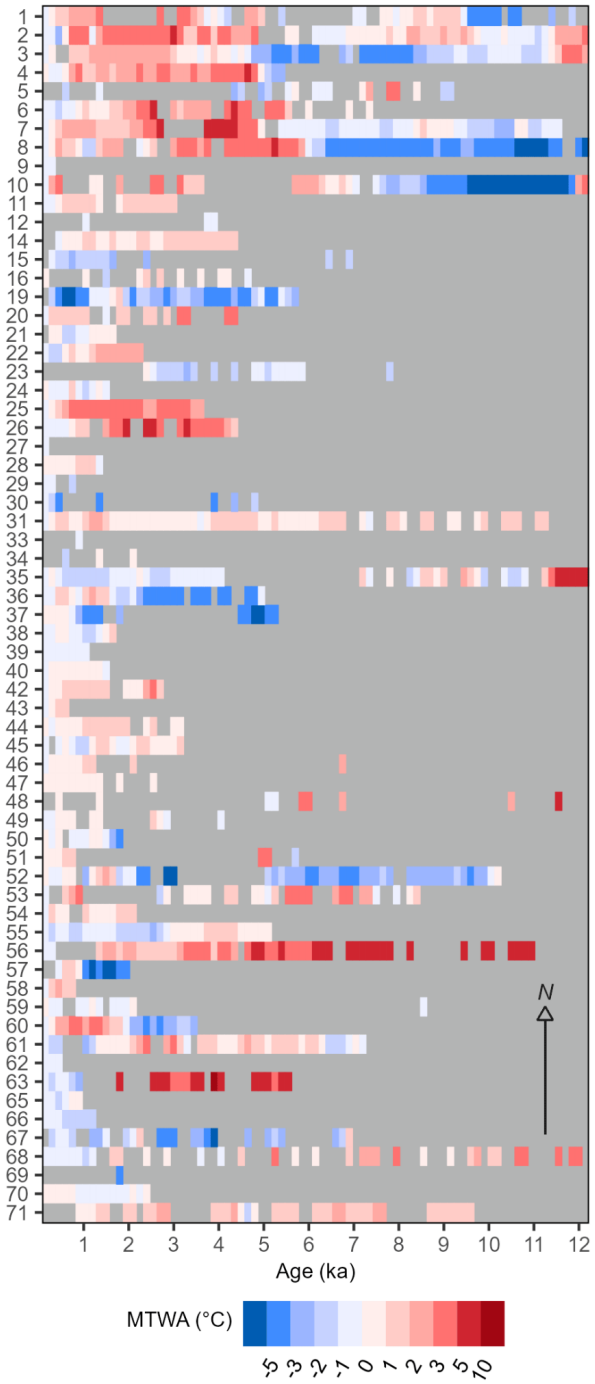

Figure 4.3. Time series of reconstructed anomalies of mean temperature of the warmest month (MTWA) for individual records. Entities are arranged by latitude (N–S). Information about the numbered individual sites can be found in Supplementary Table 4.2.

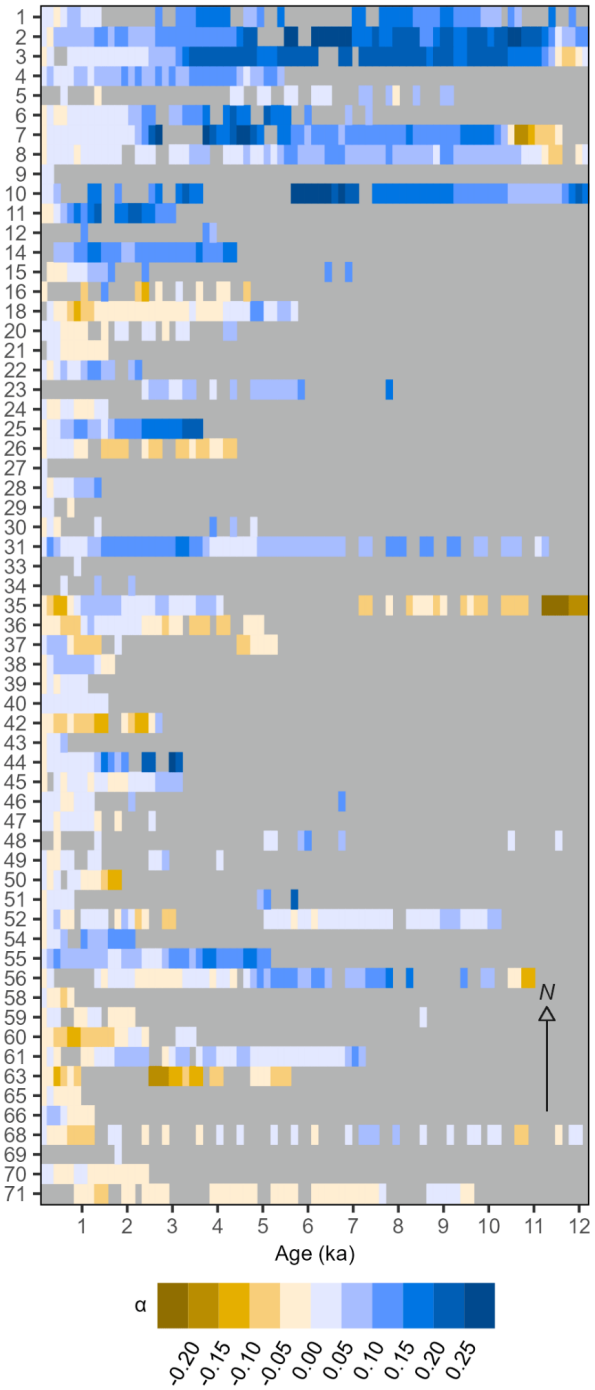

Figure 4.4. Time series of reconstructed anomalies of plant-available moisture, expressed as the ratio between potential and actual evapotranspiration (α), at individual sites. A correction to account for the direct physiological impacts of CO2 on plant growth has been applied to the reconstructed α. Entities are arranged by latitude (N–S). Information about the numbered individual sites can be found in Supplementary Table 4.2.

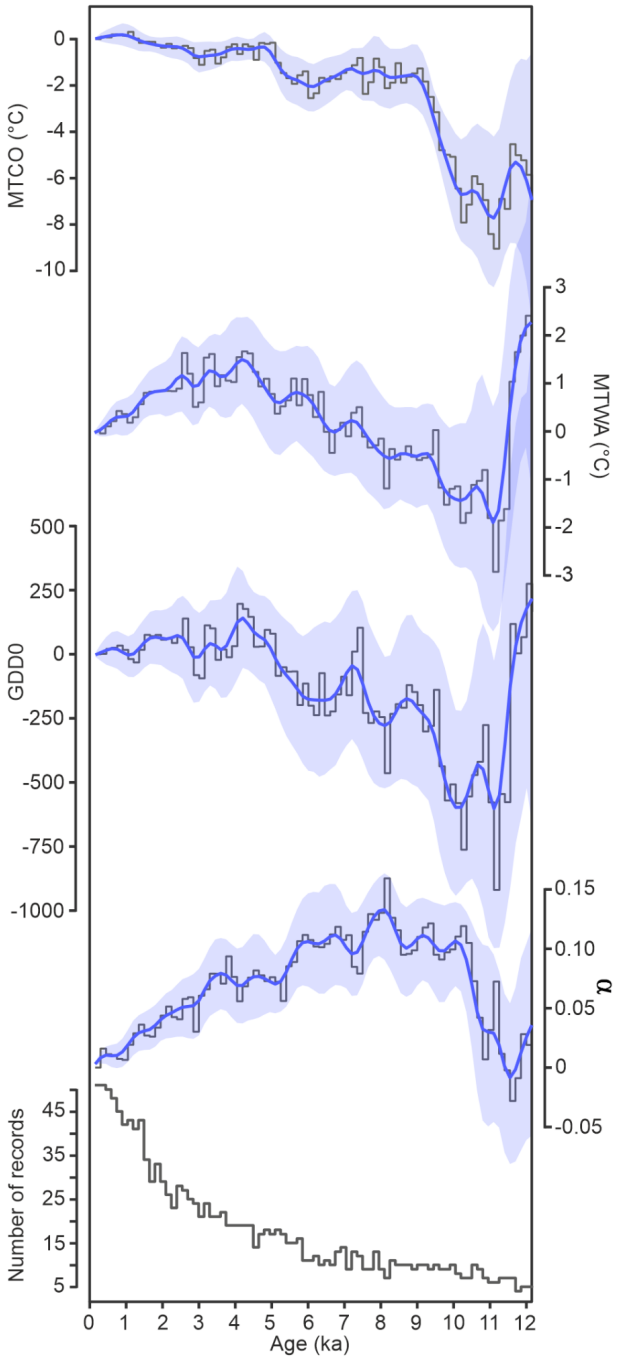

Figure 4.5. Composite changes in reconstructed mean temperature of the coldest month (MTCO), mean temperature of the warmest month (MTWA), growing degree days above a base level of 0 ◦C (GDD0), and plant-available moisture expressed as the ratio between potential and actual evapotranspiration (α). A correction to account for the direct physiological impacts of CO2 on plant growth has been applied to the reconstructions of α. The dark blue line is a loess smoothed curve through the reconstruction, with a window half-width of 500 years; the green shading shows the uncertainties based on 1000 bootstrap resampling of the records. The bottom plot shows the number of records used to create the composite through time.

The trends in α differ from the trends in temperature. Conditions were similar to the present at around 11.5 ka (Figure 4.5). Between 11 and 10 ka, there was a rapid increase in α. Values of α were higher than the present (>0.1) between 10 to 6 ka. Subsequently, there was a gradual and continuous decrease in α until the present time. The correction for the physiological impact of CO2 levels was, as expected, largest during intervals when CO2 was lowest (i.e. prior to 11 ka; Figure 4.4). The reconstructions with and without the correction are not statistically different between 10 and 5 ka, when taking account the uncertainties in the reconstructions, but the correction produced marginally wetter reconstructions after 5 ka, with a maximum difference of 0.08. However, the gradually declining trend in moisture availability towards the present is not affected by the CO2 correction.

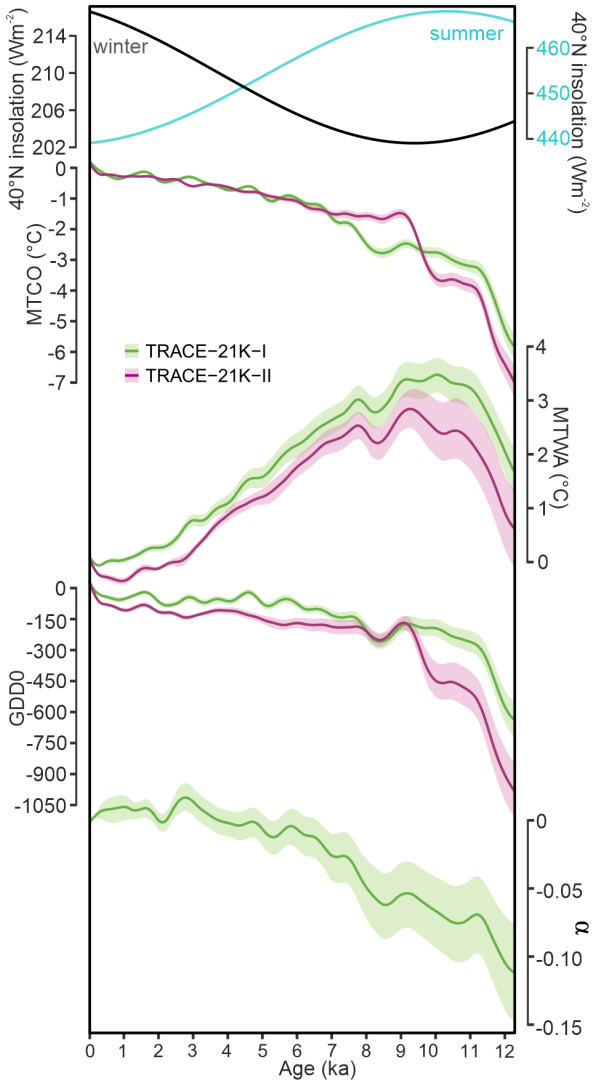

Figure 4.6. Simulated regional changes in mean temperature of the coldest month (MTCO), mean temperature of the warmest month (MTWA), growing degree days above a base level of 0 ◦C (GDD0), and plant-available moisture expressed as the ratio between potential and actual evapotranspiration (α) in the EMBSeCBIO domain from the TRACE-21K-I (green) and TRACE-21K-II (red) transient simulations. It is not possible to calculate changes in α for the TRACE-21K-II simulation from the available data. Loess smoothed curves were drawn using a window half-width of

500 years, and the envelope was obtained through 1000 bootstrap resampling of the sequences. The top plot shows the changes in summer and winter insolation (Wm–2) at 40◦ N.

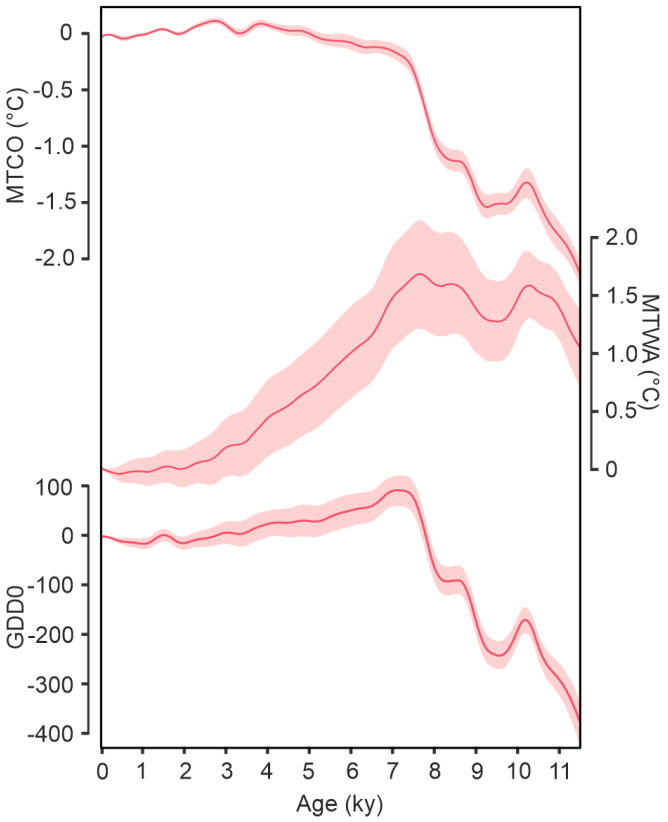

Figure 4.7. Simulated regional changes in mean temperature of the coldest month (MTCO), mean temperature of the warmest month (MTWA), and growing degree days above a base level of 0 ◦C (GDD0) in the EMBSeCBIO domain from the LOVECLIM transient simulation. It is not possible to calculate the changes in α for the LOVECLIM simulation from the available data. Loess smoothed curves were drawn using a window half-width of 500 years, and the envelope was obtained through 1000 bootstrap resampling of the sequences.

4.4.3. Comparison with climate simulations

The TRACE-21k-I simulation (Figure 4.6) shows an initial winter warming between 12 and 11 ka, but the MTCO is still ca. 3 ◦C lower than the present at 11 ka. There is a gradual increase in MTCO from 11 ka onwards, although with centennial-scale variability and a more pronounced oscillation corresponding to the 8.2 ka event. The TRACE-21k-II simulation is initially slightly colder and displays a two-step warming, with a peak at 8.5 ka, when MTCO is ca. 1.5 ◦C lower than the present. The later Holocene trend is similar to that shown in TRACE-21k-I. The LOVECLIM simulation produced generally warmer conditions than either of the TRACE simulations, where MTCO is ca. 2.5 ◦C lower than the present at 11 ka, but the two-step warming is more pronounced, and peak warming occurs somewhat later, at ca. 7.5 ka, when the MTCO was only ca. 0.25 ◦C lower than the present (Figure 4.7). While all three models show a rapid warming comparable to the

reconstructed warming between 10.3 and 9.3 ka, it is clear that the differences in the ice sheet and meltwater forcings affect both the magnitude and the timing of this trend. The overall magnitude of the warming after 9 ka in the TRACE-21k-I simulation is consistent with the reconstructions of the MTCO (anomalies of 2.4 and 2.6 ◦C for model and data, respectively). The mid to late Holocene trend is similar in the PACMEDY simulations (Figure 4.8) to both TRACE-21k simulations, both in sign and in magnitude (ca. 1 ◦C between 6 ka and the present), and both are consistent with the reconstructions (-0.9±0.7 ◦C). The continuous increase in MTCO is consistent with the change in winter insolation. Given the similarities between the PACMEDY simulations (which only include orbital and greenhouse gas forcing) and the LOVECLIM and TRACE simulations, which also include the forcing associated with the relict Laurentide and Fennoscandian ice sheets, it seems likely that orbital forcing was the main driver of winter temperatures in the EMBSeCBIO region during the later Holocene.

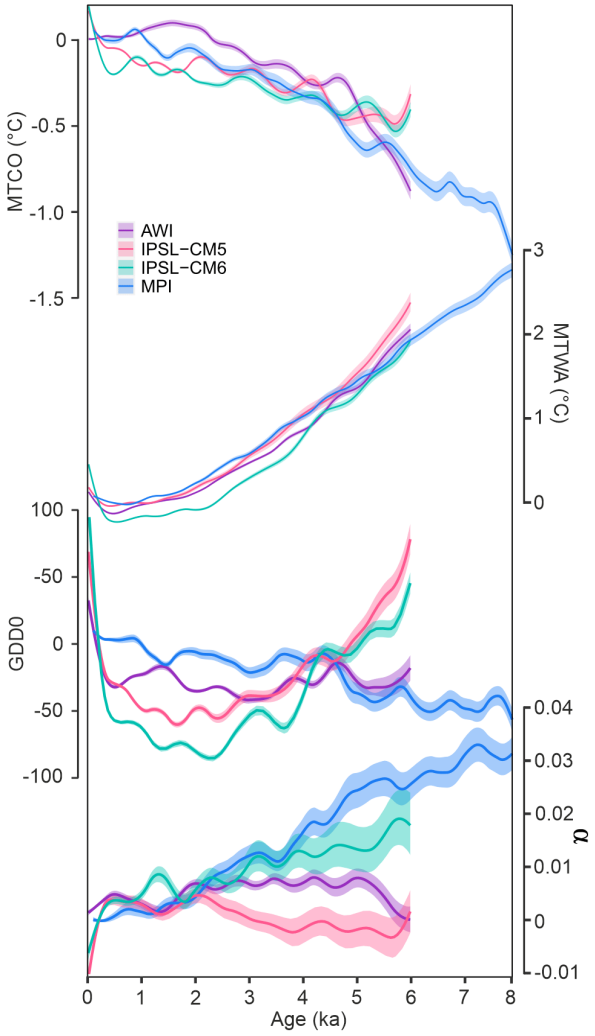

Figure 4.8. Simulated regional changes in the mean temperature of the coldest month (MTCO), mean temperature of the warmest month (MTWA), and growing degree days above a base level of 0 ◦C (GDD0) in the EMBSeCBIO domain from the four PACMEDY simulations. The models are the Max Plank Institute Earth System Model (MPI), Alfred Wegener Institute Earth System Model simulations (AWI), Institut Pierre-Simon Laplace Climate Model TR5AS simulation (IPSL-CM5), and Institut Pierre-Simon Laplace Climate Model TR6A V simulation (IPSL-CM6). Loess smoothed curves were drawn using a window half-width of 500 years and the envelope was obtained through 1000 bootstrap resampling of the sequences.

The TRACE-21k-I simulation shows peak summer temperatures between 11 and 9 ka, when the MTWA was ca. 3 °C greater than the present (Figure 4.6). The TRACE-21K-II simulations are initially colder than the TRACE-21k-I simulation, and the peak in summer temperatures occurs at 9 ka, when the MTWA was ca. 2.5 °C greater than the present (Figure 4.6). The LOVECLIM simulation is warmer than the present from 11.5 ka, but peak warming is only reached at 7.5 ka when the MTWA is ca. 2 °C (Figure 4.7). All three simulations show a gradual decrease in the summer temperature through the Holocene after this initial peak. This decreasing trend is also seen in the PACMEDY simulations from 6 ka (or 8 ka in the case of the MPI simulation) onwards (Figure 4.8), and the magnitude of the change over this interval (ca. 2 °C from 6 ka onwards) is similar to that shown by the TRACE and the LOVECLIM simulations. This similarity suggests that the simulated response is a direct reflection of the change in orbital forcing. However, the reconstructed changes in summer temperature do not show this gradual decline. Reconstructed MTWA is ca. 4 °C colder than the model predictions at 9 ka. The reconstructions show a gradual increase in the MTWA from 9 to 4.5 ka. Changes in reconstructed temperatures at 4.5 ka are of a similar magnitude to the simulated temperatures at this time (ca. 1 °C greater than the present), although the late Holocene is marked by a cooling trend, as seen in the simulations. Thus, while the simulated late Holocene trend is consistent with orbital forcing being the main driver of summer temperatures in the EMBSeCBIO region, the early to mid Holocene trend is not. Previous modelling studies have suggested that the timing of peak warmth differs in different regions of Europe and is associated with the impact of the Fennoscandian ice sheet on regional climates (Renssen et al., 2009; Blascheck and Renssen, 2013; Zhang et al., 2016). The differences in the timing of peak warmth in the EMBSeCBIO region in the TRACE-21k-II and LOVECLIM simulations would be consistent with this argument but suggest that the timing and magnitude are model-dependent. It is therefore plausible that the reconstructed trend in the MTWA at least during the early Holocene reflects the influence of the relict Laurentide and Fennoscandian ice sheets in modulating the impact of increased summer insolation until the mid Holocene. Given that GDD0 is a reflection of both changes in season length, as influenced by winter temperatures and summer warming, the difference between the simulated and reconstructed MTWA are also seen in GDD0 trends during the early part of the Holocene (Figure 4.6).

The simulations do not show consistent patterns for the trend in α. The TRACE-21k-I simulation (Figure 4.6) shows a gradual increase, with minor multi-centennial oscillations from 12 ka to present. (Available model output variables are not sufficient to calculate α for the TRACE-21k-II or LOVECLIM simulations.) One of the PACMEDY simulations (IPSL-CM5) shows an increase from the mid Holocene (Figure 4.8), although the simulated change is an order of magnitude smaller than over the comparable period in the TRACE-21k-I simulation. The AWI model shows no trend in α over this period; the remaining two models show increasing aridity from the mid Holocene to the present (Figure 4.8). These three models are all broadly consistent with the reconstructions, since the reconstructed decrease in α is small. However, the differences in the sign of the trend between the different models indicates that changes in moisture are not a straightforward consequence of the forcing but must reflect model-dependent changes in moisture supply via changes in

atmospheric circulation. Reconstructions of Holocene climates in Iberia have suggested that land–surface feedbacks associated with changes in moisture availability have a strong influence on summer temperature (Liu et al., 2023). There does not seem to be strong evidence for this in the EMBSeCBIO region, given the difference in the trends of α and the MTWA and the muted nature of the trend in α.

4.5. Discussion

The three temperature-related variables, MTCO, MTWA, and GDD0, all show relatively warm conditions around the late glacial–Holocene transition (ca. 12 ka), followed by a cooling that was greatest between ca. 11 and 10 ka. This pattern is also shown in regional composites (Figure 4.9) derived from the reconstructions by Mauri et al. (2015) and Herzschuh et al. (2022). However, the magnitude of the cooling shown in the Mauri et al. (2015) and Herzschuh et al. (2022) reconstructions is small compared to our reconstructions. The cool interval starts somewhat later and persists until 9 ka in the Mauri et al. (2015) reconstructions, but this is partly a reflection of the fact that these reconstructions were only made at 1 ka intervals, and thus, the transitions are less well constrained than in either our reconstructions or those of Herzschuh et al. (2022). This cool interval and the marked warming seen after 10.3 ka in our reconstructions does not correspond to the Younger Dryas and the subsequent warming. Although the Younger Dryas is considered to be a globally synchronous event (Cheng et al., 2020) and is generally considered coeval with Greenland stadial 1 (Larsson et al., 2022), it does not appear to be strongly registered in the EMBSeCBIO region in any of the quantitative climate reconstructions. This is consistent with earlier suggestions, based on vegetation changes, that the Younger Dryas was not a clearly marked feature over much of this region (Bottema, 1995).

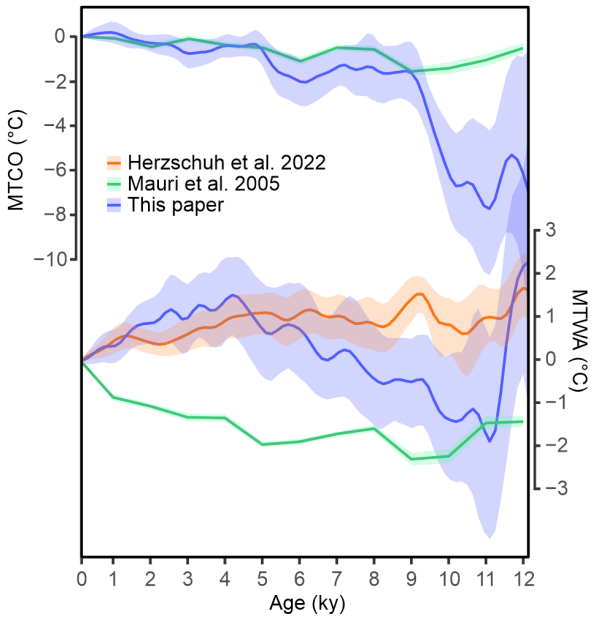

Figure 4.9. Comparison of regional composites of reconstructed seasonal temperatures from this study with those derived from Mauri et al. (2015) and Herzschuh et al. (2022). Mauri et al. (2015 provide the mean temperature of the coldest month (MTCO) and mean temperature of the warmest month (MTWA) reconstructions, which can be directly

compared with our reconstructions. Herzschuh et al. (2022) only provide reconstructions of July temperature. Our reconstructions are shown in blue, reconstructions based on the Mauri et al. (2015) data set are shown in green, and reconstructions based on the Herzschuh et al. (2022) reconstruction are shown in orange. The solid line is a loess smoothed curve through the reconstruction with a window half-width of 500 years; the shading shows the uncertainties based on 1000 bootstrap resampling of the records.

We have shown that winter temperatures increased sharply between 10.3 and 9.3 ka but then continued to increase at a more gradual rate through the Holocene. The increase of ca. 7.5 °C is of the same order of magnitude to the increase shown in the TRACE-21K-II simulation (ca. 5 °C) and in the LOVECLIM simulation (ca. 3 °C). This increasing trend is also seen in the Mauri et al. (2015) reconstructions of MTCO (Figure 4.9), although the change from the early Holocene to the present is much smaller (ca. 0.5–1 °C) in these reconstructions than in our reconstructions, and Mauri et al. (2015) do not show marked cooling around 11 ka. Nevertheless, the consistency between the two reconstructions and between our reconstruction and the simulated changes in MTCO supports the idea that these trends are a response to orbital forcing during the Holocene. Our reconstructions show a gradual increase in summer temperature, as measured by both MTWA and GDD0, from ca. 10 to 5 ka, when the MTWA was ca. 1 °C warmer than the present, followed by a gradual decrease towards the present. This is not consistent with previous reconstructions. Mauri et al. (2015) show an overall increasing trend from 9 ka to present. The Herzschuh et al. (2022) study shows a completely different pattern, with the maximum in July temperature at ca. 9 ka and an oscillating but declining trend thereafter (Figure 4.9).

These differences between the three sets of reconstructions are too large to be caused by differences in the age models applied. They are also unlikely to reflect differences in sampling, since the number of sites used is roughly similar across all three reconstructions (71 sites versus 67 sites from Herzschuh et al., 2022, and 409 grid points, based on 57 sites, from Mauri et al., 2015); most sites are common to all three analyses. The differences must therefore be related to the reconstruction method. Herzshuch et al. (2022) used the regression-based approach, weighted-average partial least squares (WA-PLS) that is the basis for our reconstruction technique, fxTWA-PLSv2. Mauri et al. (2015) used the modern analogue technique. However, after taking the differences caused by the temporal resolution into account, there is greater similarity between our reconstructions and those of Mauri et al. (2015) than between either of these reconstructions and the Herzschuh et al. (2022) reconstructions.

Several methodological issues could be responsible for the differences between the three sets of reconstructions and, in particular, the anomalous moisture trends shown by Herzschuh et al. (2022). Specifically, Herzschuh et al. (2022) used (1) a unique calibration data set for each fossil site, based on modern samples within a 2000 km radius of that site, rather than relying on a single training data set; (2) a limited set of 70 dominant taxa rather than the whole pollen assemblage; and (3) marine records, including those from, e.g., the Black Sea, which were excluded in the other reconstructions because they sample an extremely large area and thus are unrepresentative of the local climate. However, inclusion of records from the Black Sea in our reconstructions does not have a substantial impact on either the magnitude or the trends in climate. Thus, it seems likely

that the differences between these two reconstructions reflects the use of a unique calibration data set for each fossil site and the limited set of taxa included.

The reconstructed MTWA shows a gradual increase through the early Holocene with maximum values of around 1.5 °C greater than the present reached at ca. 4.5 ka. Previous modelling studies have shown that the timing of maximum warmth during the Holocene in Europe was delayed compared to the maximum of insolation forcing and varied regionally as a consequence of the impact of the Fennoscandian ice sheet on surface albedo, atmospheric circulation, and heat transport (Renssen et al., 2009; Blascheck and Renssen, 2013; Zhang et al., 2016; Zhang et al., 2018). Two of the simulations examined here show a delay in the timing of peak warmth, which occurred ca. 9 ka in the TRACE-21k-II simulation and ca. 7.5 ka in the LOVECLIM simulation. Although both sets of simulations include the relict Laurentide and Fennoscandian ice sheets, neither has realistic ice sheet and meltwater forcing. In the LOVECLIM simulation, for example, the Fennoscandian ice sheet was gone by 10 ka, whereas in reality it persisted until at least 8.7 ka (Patton et al., 2017). Thus, the impact of the Fennoscandian ice sheet in delaying orbitally induced warming would likely have been greater than shown in this simulation. In addition to differences in the way in which ice sheets and meltwater forcing are implemented in different models, models are also differentially sensitive to the presence of the same prescribed ice sheet (Kapsch et al., 2022). Thus, it would be useful to examine the influence of more realistic prescriptions of the relict ice sheets on the climate of the EMBSeCBIO region using multiple models and, preferably, transient simulations at a higher resolution or with regional climate models. It has been suggested that meltwater was routed to the Black and Caspian seas via the Dnieper and Volga rivers during the early phase of deglaciation (e.g. Yanchilina et al., 2019; Aksu et al., 2022; Vadsaria et al., 2022), and it would also be useful to investigate the impact of this on the regional climate.

We have shown that α was similar to today around 11 ka, but there was a rapid increase in moisture availability after ca. 10.5 ka, such that α values were noticeably higher than the present between 10 to 6 ka, followed by a gradual and continuous decrease until the present time. Changes in the late Holocene are small even at centennial scale (Figure 4.5). The reconstructed trends in α are not captured in the simulations, which show different trends during the late Holocene. Thus, it is unlikely that the gradual increase in aridity during the late Holocene is a straightforward response to orbital forcing. Changes in α in the EMBSeCBIO region are likely to be primarily driven by precipitation changes, which in turn are driven by changes in atmospheric circulation. Differences in the trend of moisture availability between the models imply that the nature of the changes in circulation varies between models and thus the simulations do not provide a strong basis for explaining the observed patterns of change in moisture availability. Earlier studies, focusing on the western Mediterranean (Liu et al., 2023), Europe (Mauri et al., 2014), and central Eurasia (Bartlein et al., 2017), have shown that models have difficulty in simulating the enhanced moisture transport into the Eurasian continent shown by palaeoenvironmental data during the mid Holocene and during the late Holocene. Changes in precipitation can also affect land–surface feedbacks. Liu et al. (2023), for example, have argued that enhanced moisture transport into the Iberian peninsula during the mid Holocene led to more vegetation cover and increased

evapotranspiration and had a significant impact on the reduction of growing season temperatures. Differences in the reconstructed trends of summer temperature and plant-available moisture through the Holocene suggests that this land–surface feedback was not an important factor influencing summer temperatures in the EMBSeCBIO region. Nevertheless, differences in the strength of land–surface feedbacks between models could also contribute to the divergences seen in the simulations. It would be useful to investigate the role of changes in atmospheric circulation for precipitation patterns during the Holocene in the EMBSeCBIO region using transient simulations at a higher resolution or with regional climate models.

The timing of the transition to an agriculture economy in the eastern Mediterranean is still debated (Asouti and Fuller, 2012). It has been argued that climatic deterioration and population growth during the Younger Dryas triggered a shift to farming (Weiss and Bradley, 2001; Bar-Yosef, 2017). The presence of morphologically altered cereals by the end of the Pleistocene has been put forward as evidence for an early transition to agriculture (Bar-Yosef et al., 2017), but it has also been pointed out that the evidence for cereal domestication before ca. 10.5 ka is poorly dated and insufficiently documented (Nesbitt, 2002) and that crops did not replace foraging economies until well into the Holocene (Smith, 2001; Willcox, 2012; Zeder, 2011). The availability of water is a crucial factor in the viability of early agriculture (Richerson et al., 2001; Zeder, 2011). We have shown that moisture availability was higher than today during the first part of the Holocene (10–6 ka) but similar to today until ca. 10.5 ka. Wetter conditions during the early Holocene could have been a crucial factor in the transition to agriculture, and our findings support the idea that this transition did not happen until much later than the Younger Dryas or late glacial–Holocene transition. Further exploration of the role of climate in the transition to agriculture would require a more comprehensive assessment of the archaeobotanical evidence. The issue could also be addressed by using modelling to explore how the reconstructed changes in regional moisture availability and seasonal temperatures would impact crop viability (see, e.g., Contreras et al., 2019).

We have focused on the composite picture of regional changes across the EMBSeCBIO region, in order to investigate whether these changes could be explained as a consequence of known changes in forcing. The data set also provides information on the trends in climate at individual sites. These data could be used to address the question of whether population density or cultural changes reflect shifts in climate (e.g. Weninger et al., 2006; Drake, 2012; Kaniewski et al., 2013; Cookson et al., 2019; Weiberg et al., 2019; Palmisano et al., 2021). In addition, it would also be possible to use these data to explore the impact of climate changes on the environment, including the natural resources available for people (Harrison et al., 2023).

4.6. Conclusions

We have reconstructed changes in seasonal temperature and in plant-available moisture from 12.3 ka to the present from 71 sites from the EMBSeCBIO domain to examine changes in the

regional climate of the eastern Mediterranean region. We show that there are regionally coherent trends in these variables. The large increase in both summer and winter temperatures during the early Holocene considerably post-dates the warming observed elsewhere at the end of the Younger Dryas, supporting the idea that the impact of the Younger Dryas in the EMBSeCBIO region was muted. Subsequent changes in winter temperature are consistent with the expected response to insolation changes. The timing of peak summer warming occurred later than expected as a consequence of insolation changes and likely, at least in part, reflects the influence of the relict Laurentide and Fennoscandian ice sheets on the regional climate. There is a rapid increase in plant-available moisture between 11 and 10 ka, which could have promoted the adoption of agriculture in the region.

4.7. References

Aksu, A. E. and Hiscott, R. N.: Persistent Holocene outflow from the Black Sea to the eastern Mediterranean Sea still contradicts the Noah's Flood Hypothesis: A review of 1997–2021 evidence and a regional paleoceanographic synthesis for the latest Pleistocene–Holocene, Earth Sci. Rev., 227, 103960, https://doi.org/10.1016/j.earscirev.2022.103960, 2022.

Asouti, E. and Fuller, D. Q.: From foraging to farming in the southern Levant: The development of Epipalaeolithic and Pre-pottery Neolithic plant management strategies, Veg. Hist. Archaeobot., 21, 149–162, https://doi.org/10.1007/s00334-011-0332-0, 2012.

Bar-Matthews, M., Ayalon, A., and Kaufman, A.: Late Quaternary paleoclimate in the eastern Mediterranean region from stable isotope analysis of speleothems at Soreq Cave, Israel, Quaternary Res., 47, 155–168, https://doi.org/10.1006/qres.1997.1883, 1997.

Bartlein, P. J., Harrison, S. P., Brewer, S., Connor, S., Davis, B. A. S., Gajewski, K., Guiot, J., Harrison-Prentice, T. I., Henderson, A., Peyron, O., Prentice, I. C., Scholze, M., Seppä, H., Shuman, B., Sugita, S., Thompson, R. S., Viau, A., Williams, J., and Wu, H.: Pollen-based continental climate reconstructions at 6 and 21 ka: a global synthesis, Clim. Dynam., 37, 775–802, 2011.

Bartlein, P. J., Harrison, S. P., and Izumi, K.: Underlying causes of Eurasian mid-continental aridity in simulations of mid-Holocene climate, Geophys, Res. Lett., 44, 9020–9028, https://doi.org/10.1002/2017GL074476, 2017.

Bar-Yosef, O.: Multiple Origins of Agriculture in Eurasia and Africa, in: On Human Nature, edited by: Tibayrenc, M. Ayala, F. J., Academic Press, 297–331, https://doi.org/10.1016/B978-0-12-420190-3.00019-3, 2017.

Belfer-Cohen, A. and Goring-Morris, A. N. Becoming Farmers: The Inside Story, Curr. Anthropol., 52, S209–S220, https://doi.org/10.1086/658861, 2011.

Bereiter, B., Eggleston, S., Schmitt, J., Nehrbass-Ahles, C., Stocker, T. F., Fischer, H., Kipfstuhl, S., and Chappellaz, J.: Revision of the EPICA Dome C CO2 record from 800 to 600 kyr before present, Geophys. Res. Lett., 42, 542–549, https://doi.org/10.1002/2014GL061957, 2015.

Blaauw, M., Christen, J. A., Aquino Lopez, M. A., Vazquez, J. E., Gonzalez V. O. M., Belding, T., Theiler, J., Gough, B., and Karney, C.: rbacon: Age-Depth Modelling using Bayesian Statistics (2.5.6) [R], https://CRAN.R-project.org/package=rbacon (last access: 17 April 2023), 2021.

Blaschek, M. and Renssen, H.: The Holocene thermal maximum in the Nordic Seas: the impact of Greenland Ice Sheet melt and other forcings in a coupled atmosphere–sea-ice–ocean model, Clim. Past, 9, 1629–1643, https://doi.org/10.5194/cp-9-1629-2013, 2013.

Bottema, S.: The Younger Dryas in the eastern Mediterranean, Quaternary Sci. Rev., 14, 883–891, https://doi.org/10.1016/0277-3791(95)00069-0, 1995.

Burstyn, Y., Martrat, B., Lopez, J. F., Iriarte, E., Jacobson, M. J., Lone, M. A., and Deininger, M.: Speleothems from the Middle East: An example of water limited environments in the SISAL database, Quaternary, 2, 16, https://doi.org/10.3390/quat2020016, 2019.

Carré, M., Braconnot, P., Elliot, M., d'Agostino, R., Schurer, A., Shi, X., Marti, O., Lohmann, G., Jungclaus, J., Cheddadi, R., Abdelkader di Carlo, I., Cardich, J., Ochoa, D., Salas Gismondi, R., Pérez, A., Romero, P. E., Turcq, B., Corrège, T., and Harrison, S. P.: High-resolution marine data and transient simulations support orbital forcing of ENSO amplitude since the mid-Holocene, Quaternary Sci. Rev., 268, 107125, https://doi.org/10.1016/j.quascirev.2021.107125, 2021.

Cheddadi, R. and Khater, C.: Climate change since the last glacial period in Lebanon and the persistence of Mediterranean species, Quaternary Sci. Rev., 150, 146–157, https://doi.org/10.1016/j.quascirev.2016.08.010, 2016.

Cheng, H., Sinha, A., Verheyden, S., Nader, F. H., Li, X. L., Zhang, P. Z., Yin, J. J., Yi, L., Peng, Y. B., Rao, Z. G., Ning, Y. F., and Edwards, R. L.: The climate variability in northern Levant over the past 20,000 years, Geophys. Res. Lett., 42, 8641–8650, https://doi.org/10.1002/2015GL065397, 2015.

Cheng, H., Zhang, H., Spötl, C., Baker, J., Sinha, A., Li, H., Bartolomé, M., Moreno, A., Kathayat, G., Zhao, J., Dong, X., Li, Y., Ning, Y., Jia, X., Zong, B., Ait Brahim, Y., Pérez-Mejías, C., Cai, Y., Novello, V. F., Cruz, F. W., Severinghaus, J. P., An, Z., and Edwards, R. L.: Timing and structure of the Younger Dryas event and its underlying climate dynamics, P. Natl. Acad. Sci. USA, 117, 23408–23417, https://doi.org/10.1073/pnas.2007869117, 2020.

Chevalier, M., Davis, B. A. S., Heiri, O., Seppä, H., Chase, B. M., Gajewski, K., Lacourse, T., Telford, R. J., Finsinger, W., Guiot, J., Kühl, N., Maezumi, S. Y., Tipton, J. R., Carter, V. A., Brussel, T., Phelps, L. N., Dawson, A., Zanon, M., Vallé, F., Nolan, C., Mauri, A., de Vernal, A., Izumi, K., Holmström, L., Marsicek, J., Goring, S., Sommer, P. S., Chaput, M., and Kupriyanov, D.: Pollen-based climate reconstruction techniques for late Quaternary studies, Earth Sci. Rev., 210, 103384, https://doi.org/10.1016/j.earscirev.2020.103384, 2020.

Cleveland, W. S. and Devlin, S. J.: Locally weighted regression: An approach to regression analysis by local fitting, J. Am. Stat. Assoc., 83, 596–610, https://doi.org/10.1080/01621459.1988.10478639, 1988.

Cookson, E., Hill, D. J., and Lawrence, D.: Impacts of long term climate change during the collapse of the Akkadian Empire, J. Archael. Sci., 106, 1–9, https://doi.org/10.1016/j.jas.2019.03.009, 2019.

Collins, W. D., Bitz, C. M., Blackmon, M. L., Bonan, G. B., Bretherton, C. S., Carton, J. A., Chang, P., Doney, S. C., Hack, J. J., Henderson, T. B., Kiehl, J. T., Large, W. G., McKenna, D. S., Santer, B. D., and Smith, R. D.: The Community Climate System Model version 3 (CCSM3), J. Climate, 19, 2122–2143, https://doi.org/10.1175/JCLI3761.1, 2006.

Contreras, D. A., Bondeau, A., Guiot, J., Kirman, A., Hiriart, E., Bernard, L., Suarez, R., and Fader, M.: From paleoclimate variables to prehistoric agriculture: Using a process-based agro-ecosystem model to simulate the impacts of Holocene climate change on potential agricultural productivity in Provence, France, Quatern. Int., 501, 303–316 2019.

Cruz-Silva, E.: EMBSeCBIO_Holocene_climate: First release (0.1.0), Zenodo [code], https://doi.org/10.5281/zenodo.10040708, 2023.

Dallmeyer, A., Claussen, M., Lorenz, S. J., and Shanahan, T.: The end of the African humid period as seen by a transient comprehensive Earth system model simulation of the last 8000 years, Clim. Past, 16, 117–140, https://doi.org/10.5194/cp-16-117-2020, 2020.

Davis, B. A. S., Brewer, S., Stevenson, A. C., and Guiot, J.: The temperature of Europe during the Holocene reconstructed from pollen data, Quaternary Sci. Rev., 22, 1701–1716, https://doi.org/10.1016/S0277-3791(03)00173-2, 2003.

Dean, J. R., Jones, M. D., Leng, M. J., Noble, S. R., Metcalfe, S. E., Sloane, H. J., Sahy, D., Eastwood, W. J., and Roberts, C. N.: Eastern Mediterranean hydroclimate over the late glacial and Holocene, reconstructed from the sediments of Nar lake, central Turkey, using stable isotopes and carbonate mineralogy, Quaternary Sci. Rev., 124, 162–174, https://doi.org/10.1016/j.quascirev.2015.07.023, 2015.

Denèfle, M., Lézine, A., Fouache, E., and Dufaure, J.: A 12,000-Year pollen record from Lake Maliq, Albania, Quaternary Res., 54, 423–432, https://doi.org/10.1006/qres.2000.2179, 2000.

Drake, B. L.: The influence of climatic change on the Late Bronze Age Collapse and the Greek Dark Ages, J. Archaeol. Sci., 39, 1862–1870, https://doi.org/10.1016/j.jas.2012.01.029, 2012.

Flohr, P., Fleitmann, D., Matthews, R., Matthews, W., and Black, S.: Evidence of resilience to past climate change in Southwest Asia: Early farming communities and the 9.2 and 8.2 ka events, Quaternary Sci. Rev., 136, 23–39, https://doi.org/10.1016/j.quascirev.2015.06.022, 2016.

Goosse, H., Brovkin, V., Fichefet, T., Haarsma, R., Huybrechts, P., Jongma, J., Mouchet, A., Selten, F., Barriat, P.-Y., Campin, J.-M., Deleersnijder, E., Driesschaert, E., Goelzer, H., Janssens, I., Loutre, M.-F., Morales Maqueda, M. A., Opsteegh, T., Mathieu, P.-P., Munhoven, G., Pettersson, E. J., Renssen, H., Roche, D. M., Schaeffer, M., Tartinville, B., Timmermann, A., and Weber, S. L.: Description of the Earth system model of intermediate complexity LOVECLIM version 1.2, Geosci. Model Dev., 3, 603–633, https://doi.org/10.5194/gmd-3-603-2010, 2010.

Harrison, S. P.: SPECIAL Modern Pollen Data Set for Climate Reconstructions, version 1 (SMPDS), University of Reading [data set], https://doi.org/10.17864/1947.194, 2019

Harrison, S. P., Prentice, I. C., Sutra, J.-P., Barboni, D., Kohfeld, K. E., and Ni, J.: Ecophysiological and bioclimatic foundations for a global plant functional classification, J. Veg. Sci., 21, 300–317, 2010.

Harrison, S. P., Gaillard, M.-J., Stocker, B. D., Vander Linden, M., Klein Goldewijk, K., Boles, O., Braconnot, P., Dawson, A., Fluet-Chouinard, E., Kaplan, J. O., Kastner, T., Pausata, F. S. R., Robinson, E., Whitehouse, N. J., Madella, M., and Morrison, K. D.: Development and testing scenarios for implementing land use and land cover changes during the Holocene in Earth system model experiments, Geosci. Model Dev., 13, 805–824, https://doi.org/10.5194/gmd-13-805-2020, 2020.

Harrison, S. P., Marinova, E., and Cruz-Silva, E.: EMBSeCBIO pollen database, University of Reading [data set], https://doi.org/10.17864/1947.309, 2021.

Harrison, S. P., Cruz-Silva, E., Haas, O., Liu, M., Parker, S. E., Qiao, S., Shen, Y., and Sweeney, L.: Tools and approaches to addressing the climate-humans nexus during the Holocene, in: Proceedings of the 12th International Congress on the Archaeology of the Ancient Near East, edited by: Marchetti, N., Campeggi, M., Cavaliere, F., D'Orazio, C., Giacosa, G., and Mariani, E., Harrassowitz Verlag, https://doi.org/10.13173/9783447118736, 2023.

He, F. and Clark, P. U.: Freshwater forcing of the Atlantic Meridional Overturning Circulation revisited, Nat. Clim. Change, 12, 449–454, https://doi.org/10.1038/s41558-022-01328-2, 2022.

Herzschuh, U., Böhmer, T., Li, C., Cao, X., Hébert, R., Dallmeyer, A., Telford, R. J., and Kruse, S.: Reversals in temperature-precipitation correlations in the Northern Hemisphere extratropics during the Holocene, Geophys. Res. Lett., 49, e2022GL099730, https://doi.org/10.1029/2022GL099730, 2022.

Hill, M. O.: Diversity and evenness: A unifying notation and its consequences, Ecol., 54, 427–432, https://doi.org/10.2307/1934352, 1973.

Joos, F., Gerber, S., Prentice, I. C., Otto-Bliesner, B. L., and Valdes, P. J.: Transient simulations of Holocene atmospheric carbon dioxide and terrestrial carbon since the last glacial maximum, Globzl Biogeochem. Cy., 18, GB2002, https://doi.org/10.1029/2003GB002156, 2004.

Kaniewski, D., Van Campo, E., Guiot, J., Le Burel, S., Otto, T., and Baeteman, C.: Environmental roots of the Late Bronze Age Crisis, PLoS ONE, 8, e71004, https://doi.org/10.1371/journal.pone.0071004, 2013.

Kaplan, J. O., Krumhardt, K. M., Ellis, E. C., Ruddiman, W. F., Lemmen, C., and Klein Goldewijk, K.: Holocene carbon emissions as a result of anthropogenic land cover change, Holocene, 21, 775–791, 2011.

Kapsch, M.-L., Mikolajewicz, U., Ziemen, F., and Schannwell, C.: Ocean response in transient simulations of the last deglaciation dominated by underlying ice-sheet reconstruction and method of meltwater distribution, Geophys. Res. Lett., 49, e2021GL096767, https://doi.org/10.1029/2021GL096767, 2022.

Larsson, S. A., Kylander, M. E., Sannel, A. B. K., and Hammarlund, D.: Synchronous or not? The timing of the Younger Dryas and Greenland Stadial-1 reviewed using tephrochronology, Quaternary, 5, 19, https://doi.org/10.3390/quat5020019, 2022.

Liu, M., Prentice, I. C., ter Braak, C. J. F., and Harrison, S. P.: An improved statistical approach for reconstructing past climates from biotic assemblages, P. R. Soc. A, 476, 20200346, https://doi.org/10.1098/rspa.2020.0346, 2020.

Liu, M., Shen, Y., González-Sampériz, P., Gil-Romera, G., ter Braak, C. J. F., Prentice, I. C., and Harrison, S. P.: Holocene climates of the Iberian Peninsula: pollen-based reconstructions of changes in the west–east gradient of temperature and moisture, Clim. Past, 19, 803–834, https://doi.org/10.5194/cp-19-803-2023, 2023.

Liu, Z., Otto-Bliesner, B. L., He, F., Brady, E. C., Tomas, R., Clark, P. U., Carlson, A. E., Lynch-Stieglitz, J., Curry, W., Brook, E., Erickson, D., Jacob, R., Kutzbach, J., and Cheng, J.: Transient Simulation of Last Deglaciation with a New Mechanism for Bolling-Allerod Warming, Science, 325, 310–314, https://doi.org/10.1126/science.1171041, 2009.

Magyari, E. K., Pál, I., Vincze, I., Veres, D., Jakab, G., Braun, M., Szalai, Z., Szabó, Z., and Korponai, J.: Warm Younger Dryas summers and early late glacial spread of temperate deciduous trees in the Pannonian Basin during the last glacial termination (20–9 kyr cal BP), Quaternary Sci. Rev., 225, 105980, https://doi.org/10.1016/j.quascirev.2019.105980, 2019.

Mauri, A., Davis, B. A. S., Collins, P. M., and Kaplan, J. O.: The influence of atmospheric circulation on the mid-Holocene climate of Europe: a data–model comparison, Clim. Past, 10, 1925–1938, https://doi.org/10.5194/cp-10-1925-2014, 2014.

Mauri, A., Davis, B. A. S., Collins, P. M., and Kaplan, J. O.: The climate of Europe during the Holocene: a gridded pollen-based reconstruction and its multi-proxy evaluation, Quaternary Sci. Rev., 112, 109–127, https://doi.org/10.1016/j.quascirev.2015.01.013, 2015.

Mitchell, L., Brook, E., Lee, J., Buizert, C., and Sowers, T.: Constraints on the late Holocene anthropogenic contribution to the atmospheric methane budget, Science, 342, 964–966, https://doi.org/10.1126/science.1238920, 2013.

Nesbitt, M.: When and where did domesticated cereals first occur in southwest Asia?, in: The dawn of farming in the Near East, edited by: Cappers, R. T. J. and Bottema, S., Ex Oriente, 113–132, https://www.researchgate.net/publication/234002845_When_and_where_did_domesticated_cereals_first_occur_in_southwest_Asia (last access: 27 October 2023), 2002.

New, M., Lister, D., Hulme, M., and Makin, I.: A high-resolution data set of surface climate over global land areas, Clim. Res., 21, 1–25, https://doi.org/10.3354/cr021001, 2002.

Palmisano, A., Bevan, A., Kabelindde, A., Roberts, N., and Shennan, S.: Long-term demographic trends in prehistoric Italy: Climate impacts and regionalised socio-ecological trajectories, J. World Prehist., 34, 381–432, https://doi.org/10.1007/s10963-021-09159-3, 2021.

Patton, H., Hubbard, A., Andreassen, K., Auriac, A., Whitehouse, P. L., Stroeven, A. P., Shackleton, C., Winsborrow, M., Heyman, J., and Hall, A. M.: Deglaciation of the Eurasian ice sheet complex, Quaternary Sci. Rev., 169, 148–172, https://doi.org/10.1016/j.quascirev.2017.05.019, 2017.

Prentice, I. C., Villegas-Diaz, R., and Harrison, S. P.: Accounting for atmospheric carbon dioxide variations in pollen-based reconstruction of past hydroclimates, Global Planet. Change, 211, 103790, https://doi.org/10.1016/j.gloplacha.2022.103790, 2022a.

Prentice, I. C., Villegas-Diaz, R., and Harrison, S. P.: codos: 0.0.2 (0.0.2), Zenodo [code], https://doi.org/10.5281/zenodo.5083309, 2022b.

Reimer, P., Austin, W. E. N., Bard, E., Bayliss, A., Blackwell, P. G., Ramsey, C. B., Butzin, M., Cheng, H., Edwards, R. L., Friedrich, M., Grootes, P. M., Guilderson, T. P., Hajdas, I., Heaton, T. J., Hogg, A. G., Hughen, K. A., Kromer, B., Manning, S. W., Muscheler, R., Palmer, J. G., Pearson, C., Plicht, J. van der, Reimer, R., Richards, D. A., Scott, E. M., Southon, J. R., Turney, C. S. M., Wacker, L., Adolphi, F., Büntgen, U., Capano, M., Fahrni, S., Fogtmann-Schulz, A., Friedrich, R., Miyake, F., Olsen, J., Reinig, F., Sakamoto, M., Sookdeo, A., and Talamo, S.: The IntCal20 Northern Hemisphere radiocarbon age calibration curve (0–55 cal kBP), Radiocarbon, 62, 725–757, https://doi.org/10.1017/RDC.2020.41, 2020.

Renssen, H., Seppä, H., Heiri, O., Roche, D. M., Goosse, H., and Fichefet, T.: The spatial and temporal complexity of the Holocene thermal maximum, Nat. Geosci., 2, 411–414, https://doi.org/10.1038/ngeo513, 2009.

Richerson, P. J., Boyd, R., and Bettinger, R. L.: Was agriculture impossible during the Pleistocene but mandatory during the Holocene? A climate change hypothesis, Am. Antiqquity, 66, 387–411, https://doi.org/10.2307/2694241, 2001.

Rick, J. W. (1987). Dates as data: An examination of the Peruvian preceramic radiocarbon record. American Antiquity, 52(1), 55–73. https://doi.org/10.2307/281060

Roberts, N., Cassis, M., Doonan, O., Eastwood, W., Elton, H., Haldon, J., Izdebski, A., and Newhard, J.: Not the End of the World? Post-classical decline and recovery in rural Anatolia, Hum. Ecol., 46, 305–322, https://doi.org/10.1007/s10745-018-9973-2, 2018.

Roberts, C. N., Woodbridge, J., Palmisano, A., Bevan, A., Fyfe, R., and Shennan, S.: Mediterranean landscape change during the Holocene: Synthesis, comparison and regional trends in population, land cover and climate, Holocene, 29, 923–937, https://doi.org/10.1177/0959683619826697, 2019.

Robinson, E., Zahid, H. J., Codding, B. F., Haas, R., & Kelly, R. L. (2019). Spatiotemporal dynamics of prehistoric human population growth: Radiocarbon 'dates as data' and population ecology models. Journal of Archaeological Science, 101, 63–71. https://doi.org/10.1016/j.jas.2018.11.006

Roffet-Salque, M., Marciniak, A., Valdes, P. J., Pawłowska, K., Pyzel, J., Czerniak, L., Krüger, M., Roberts, C. N., Pitter, S., and Evershed, R. P.: Evidence for the impact of the 8.2-ky BP climate event on Near Eastern early farmers, P. Natl. Acad. Sci. USA, 115, 8705–8709, https://doi.org/10.1073/pnas.1803607115, 2018.

Ruddiman, W. F.: The anthropogenic greenhouse era began thousands of years ago, Clim. Change, 61, 261–293, https://doi.org/10.1023/B:CLIM.0000004577.17928.fa, 2003.

Rymes, M. D. and Myers, D. R.: Mean preserving algorithm for smoothly interpolating averaged data, Sol. Energy, 71, 225–231, https://doi.org/10.1016/S0038-092X(01)00052-4, 2001.

Sadori, L., Jahns, S., and Peyron, O.: Mid-Holocene vegetation history of the central Mediterranean, Holocene, 21, 117–129, https://doi.org/10.1177/0959683610377530, 2011.

Sidorenko, D., Goessling, H. f., Koldunov, N. v., Scholz, P., Danilov, S., Barbi, D., Cabos, W., Gurses, O., Harig, S., Hinrichs, C., Juricke, S., Lohmann, G., Losch, M., Mu, L., Rackow, T., Rakowsky, N., Sein, D., Semmler, T., Shi, X., Stepanek, C., Streffing, J., Wang, Q., Wekerle, C., Yang, H., and Jung, T.: Evaluation of FESOM2.0 coupled to ECHAM6.3: Preindustrial and HighResMIP simulations, J. Adv. Model. Earth Sy., 11, 3794–3815, https://doi.org/10.1029/2019MS001696, 2019.

Singarayer, J. S., Valdes, P. J., Friedlingstein, P., Nelson, S., and Beerling, D. J.: Late Holocene methane rise caused by orbitally controlled increase in tropical sources, Nature, 470, 82–85, https://doi.org/10.1038/nature09739, 2011.

Smith, B. D.: Low-Level Food Production, J. Archaeol. Res., 9, 1–43, https://doi.org/10.1023/A:1009436110049, 2001.

Stocker, B. D., Yu, Z., Massa, C., and Joos, F.: Holocene peatland and ice-core data constraints on the timing and magnitude of CO2 emissions from past land use, P. Natl. Acad. Sci. USA, 114, 1492–1497, https://doi.org/10.1073/pnas.1613889114, 2017.

Vadsaria, T., Zaragosi, S., Ramstein, G., Dutay, J.-C., Li, L., Siani, G., Revel, M., Obase, T., and Abe-Ouchi, A.: Freshwater influx to the Eastern Mediterranean Sea from the melting of the Fennoscandian ice sheet during the last deglaciation, Sci. Rep., 12, 8466, https://doi.org/10.1038/s41598-022-12055-1, 2022.

Villegas-Diaz, R. and Harrison, S. P.: The SPECIAL Modern Pollen Data Set for Climate Reconstructions, version 2 (SMPDSv2), University of Reading [data set], https://doi.org/10.17864/1947.000389, 2022.

Villegas-Diaz, R., Cruz-Silva, E., and Harrison, S. P.: 90 ageR: Supervised Age Models, Zenodo [code], https://doi.org/10.5281/zenodo.4636716, 2021.

Wei, D., González-Sampériz, P., Gil-Romera, G., Harrison, S. P., and Prentice, I. C.: Seasonal temperature and moisture changes in interior semi-arid Spain from the last interglacial to the Late Holocene, Quaternary Res., 101, 143–155, https://doi.org/10.1017/qua.2020.108, 2021.

Weiberg, E., Bevan, A., Kouli, K., Katsianis, M., Woodbridge, J., Bonnier, A., Engel, M., Finné, M., Fyfe, R., Maniatis, Y., Palmisano, A., Panajiotidis, S., Roberts, C. N., and Shennan, S.: Long-term trends of land use and demography in Greece: A comparative study, Holocene, 29, 742–760, https://doi.org/10.1177/0959683619826641, 2019.

Weiss, H. and Bradley, R. S.: What Drives Societal Collapse? Science, 291, 609–610, https://doi.org/10.1126/science.1058775, 2001.

Weninger, B., Alram-Stern, E., Bauer, E., Clare, L., Danzeglocke, U., Jöris, O., Kubatzki, C., Rollefson, G., Todorova, H., and van Andel, T.: Climate forcing due to the 8200 cal yr BP event observed at Early Neolithic sites in the eastern Mediterranean, Quaternary Res., 66, 401-420, https://doi.org/10.1016/j.yqres.2006.06.009, 2006.

Willcox, G.: Searching for the origins of arable weeds in the Near East, Vegetation History and Archaeobotany, 21, 163–167, https://doi.org/10.1007/s00334-011-0307-1, 2012.

Yanchilina, A. G., Ryan, W. B. F., Kenna, T. C., and McManus, J. F.: Meltwater floods into the Black and Caspian Seas during Heinrich Stadial 1, Earth Sci. Rev., 198, 102931, https://doi.org/10.1016/j.earscirev.2019.102931, 2019.

Zeder, M. A.: The origins of agriculture in the Near East, Curr. Anthropol., 52, S221–S235, https://doi.org/10.1086/659307, 2011.

Zhang, Y., Renssen, H., and Seppä, H.: Effects of melting ice sheets and orbital forcing on the early Holocene warming in the extratropical Northern Hemisphere, Clim. Past, 12, 1119–1135, https://doi.org/10.5194/cp-12-1119-2016, 2016.

Zhang, Y., Renssen, H., Seppä, H., and Valdes, P. J.: Holocene temperature trends in the extratropical Northern Hemisphere based on inter-model comparisons, J. Quaternary Sci., 33, 464–476. https://doi.org/10.1002/jqs.3027, 2018.

4.8. Supplementary

Supplementary Table 4.1. Allocation of pollen taxa found in samples of the Eastern Mediterranean-Black Sea Caspian Corridor (EMBSeCBIO) pollen database into the 247 types represented in the SPECIAL Modern Pollen Data Set (SMPDS) (Harrison, 2019). The table indicates the taxonomic level of aggregation, the name used for the amalgamated taxon, and the component species or genera included in this taxon.

Taxonomic level	**Amalgamated taxon name**	**Individual taxa included**
Genus	*Abies*	*Abies, Abies alba, Abies cilicica, Abies nordmanniana, Abies pinsapo subsp marocana*
Family	Acanthaceae	*Acanthus mollis*
Genus	*Acer*	*Acer, Acer campestre, Acer campestre* type, *Acer pseudoplatanus, Acer* type
Genus	*Aconitum*	*Aconitum, Aconitum group, Aconitum napellus* type, *Aconitum septentrionale, Aconitum* type
Family	Actinidiaceae	*Actinidia*
Genus	*Adonis*	*Adonis, Adonis aestivalis* type, *Adonis* type
Family	Adoxaceae	*Adoxa, Adoxa moschatellina, Adoxa* type
Genus	*Aesculus*	*Aesculus, Aesculus hippocastanum*
Genus	*Ailanthus*	*Ailanthus*
Family	Aizoaceae	*Carpobrotus*
Genus sub-group	*Alnus*	*Alnus, Alnus glutinosa, Alnus glutinosa* type, *Alnus glutinosa/Alnus incana, Alnus incana, Alnus incana* type, *Alnus incana/Alnus cordata* type, *Alnus non-viridis, Alnus* type
Genus sub-group	*Alnus alnobetula*	*Alnus viridis*
Family	Amaranthaceae	*Aellenia* type, Amaranthaceae, *Amaranthus, Atriplex nudicaulis, Chenopodium, Chenopodium album, Halothamnus* type, *Noaea* type
Family	Amaryllidaceae	Amaryllidaceae, *Narcissus*
Family	Anacardiaceae	Anacardiaceae
Genus	*Andromeda*	*Andromeda*

Family	Apiaceae	*Aegopodium, Anthriscus sylvestris* type, *Anthriscus* type, Apiaceae, *Apium, Apium* type, *Astrantia, Astrantia* type, *Athamanta cretensis, Berula erecta* type, *Bunium* type, *Aegopodium podagraria, Bupleurum, Bupleurum* type, *Carum carvi, Chaerophyllum, Chaerophyllum hirsutum* type, *Chaerophyllum* type, *Conopodium, Conopodium majus, Daucaceae, Daucus carota, Ammi* type, *Daucus carota* type, *Daucus* type, *Echinophora, Eryngium, Eryngium ilicifolium, Eryngium* type, *Falcaria* type, *Ferula, Ferula* type, *Heracleum, Angelica, Heracleum laciniatum* type, *Heracleum sphondylium, Heracleum* type, *Laserpitium latifolium* type, *Laserpitium prutenicum, Ligusticum mutellina, Malabaila, Meum, Meum athamanticum, Neogaya simplex* type, *Angelica archangelica, Oenanthe, Oenanthe* type, *Orlaya, Orlaya grandiflora, Pastinaca* type, *Peucedanum, Peucedanum ostruthium, Peucedanum* type, *Pimpinella, Pimpinella major* type, *Angelica* type, *Pimpinella* type, *Pleurospermum austriacum, Sanicula, Sanicula europaea, Sanicula type, Scandix, Seseli* type, *Torilis, Torilis arvensis, Turgenia* type, *Anisosciadium* type, *Anthriscus, Anthriscus sylvestris*
Genus	*Aquilegia*	*Aquilegia* type
Family	Araceae	Araceae
Genus	*Arbutus*	*Arbutus, Arbutus* type, *Arbutus unedo*
Genus	*Arctostaphylos*	*Arctostaphylos, Arctostaphylos uva-ursi*
Genus	*Argania*	*Argania spinosa*
Family	Aristolochiaceae	*Aristolochia*
Genus	*Artemisia*	*Artemisia, Artemisia genipii/Artemisia mutellina, Artemisia herba-alba* type, *Artemisia* type, *Artemisia vulgaris* type
Family	Asclepiadaceae	Asclepiadaceae
Family	Asparagaceae	Asparagaceae, *Asparagus, Asparagus* type, *Convallaria, Convallaria* type, *Maianthemum bifolium, Maianthemum* type, *Ornithogalum type, Scilla* type
Family	Asphodelaceae	*Eremurus*
Family	Asphodeliaceae	*Asphodeline, Asphodelus, Asphodelus albus, Asphodelus albus* type, *Asphodelus fistulosus* type, *Asphodelus* type
Family	Asteraceae	Asteraceae
Family sub-group	Asteraceae (Liguliflorae)	Asteraceae (Liguliflorae)

Family sub-group	Asteroideae	*Achillea*, *Antennaria*, *Antennaria* type, *Anthemis*, *Anthemis* type, *Arnica montana*, *Aster*, *Aster bellidiastrum*, *Aster* type, *Aster/Achillea*, *Aster/Achillea* type, *Achillea* type, Asteraceae (Tubuliflorae), Asteroideae, *Bellis*, *Bellis* type, *Bidens*, *Bidens* type, *Calendula*, *Calendula* type, *Chrysanthemum alpinum*, *Doronicum*, *Achillea/Anthemis* type, *Erigeron*, *Eupatorium*, *Eupatorium* type, *Filago* type, *Filifolium sibiricum*, *Gnaphalium*, *Gnaphalium* type, *Helianthus*, *Helianthus* type, *Homogyne*, *Achillea/Aster*, *Homogyne alpina*, *Inula*, *Inula* type, *Logfia* type, *Matricaria* type, *Petasites*, *Petasites* type, *Senecio*, *Senecio* type, *Solidago*, *Adenostyles* type, *Solidago* type, *Solidago virgaurea* type, *Tussilago farfara*, *Tussilago* type, *Xanthium*, *Xanthium spinosum*, *Xanthium strumarium*, *Xanthium* type, *Ambrosia*, *Ambrosia artemisiifolia* type, *Ambrosia* type, *Ambrosia/Xanthium*
Genus	*Astragalus*	*Astragalus*, *Astragalus alpinus* type, *Astragalus* type
Family	Berberidaceae	Berberidaceae
Genus	*Berberis*	*Berberis*, *Berberis vulgaris*, *Mahonia*
Genus	*Betula*	*Betula*, *Betula* type, *Betula alba*, *Betula alba* type, *Betula pendula*, *Betula pendula/Betula pubescens*, *Betula pubescens*, *Betula pubescens* type, *Betula sect. Albae*, *Betula tortuosa*
Genus	*Betula (Chamaebetula)*	*Betula fruticosa*, *Betula humilis/Betula nana*, *Betula nana*, *Betula nana* type
Family	Boraginaceae	*Alkanna*, *Cynoglossum creticum*, *Echium*, *Echium* type, *Echium vulgare*, *Heliotropium* type, *Lithospermum*, *Myosotis*, *Myosotis arvensis* type, *Myosotis* type, *Onosma*, *Anchusa*, *Pulmonaria*, *Pulmonaria* type, *Symphytum*, *Symphytum* type, *Anchusa arvensis*, *Anchusa type*, Boraginaceae, *Borago officinalis*, *Cerinthe*, *Cerinthe minor*, *Cerinthe type*
Family	Brassicaceae	*Arabidopsis*, *Cardamine pratensis* type, *Cardamine* type, *Crambe*, *Descurainia*, *Draba*, *Draba type*, *Hornungia* type, *Lepidium* type, *Matthiola*, *Sinapis*, *Barbarea* type, *Sinapis* type, *Brassica*, *Brassica* type, Brassicaceae, Brassicaceae type, *Capsella bursa-pastoris* type, *Capsella* type, *Cardamine*
Genus	*Bruckenthalia*	*Bruckenthalia*
Genus	*Buxus*	*Buxus*, *Buxus sempervirens*
Genus	*Calluna*	*Calluna*, *Calluna* type, *Calluna vulgaris*, *Calluna vulgaris* type
Family	Campanulaceae	*Campanula*, *Phyteuma*, *Phyteuma* type, *Campanula* type, Campanulaceae, *Jasione*, *Jasione montana*, *Jasione* type, *Legousia*, *Lobelia dortmanna*, *Lobelia* type
Family	Capparaceae	Capparidaceae, *Capparis*, *Capparis spinosa*, *Capparis* type

Family	Caprifoliaceae	Caprifoliaceae, *Scabiosa columbaria* type, *Scabiosa rotata* type, *Scabiosa* type, *Scabiosa/Succisa* type, *Succisa*, *Succisa pratensis*, *Succisa pratensis* type, *Succisa* type, *Dipsacaceae*, *Dipsacus*, *Dipsacus fullonum* type, *Dipsacus* type, *Knautia*, *Knautia arvensis*, *Knautia* type, *Scabiosa*
Genus	*Carduoideae*	*Arctium*, *Centaurea*, *Centaurea collina*, *Centaurea collina* type, *Centaurea cyanus*, *Centaurea cyanus* type, *Centaurea depressa* type, *Centaurea jacea*, *Centaurea jacea* type, *Centaurea montana*, *Centaurea montana* type, *Arctium* type, *Centaurea nigra*, *Centaurea nigra* type, *Centaurea rhenana* type, *Centaurea scabiosa*, *Centaurea scabiosa* type, *Centaurea solstitialis*, *Centaurea solstitialis* type, *Centaurea* type, *Cirsium*, *Cirsium* type, *Arctium/Jurinea*, *Cirsium/Carduus*, *Cirsium/Gundelia*, *Cousinia*, *Echinops*, *Gundelia* type, *Jurinea* type, *Onopordum*, *Onopordum* type, *Saussurea*, *Saussurea alpina*, *Carduoideae*, *Saussurea* type, *Serratula*, *Serratula* type, *Carduus*, *Carduus* type, *Carlina*, *Carlina* type, *Carthamus*
Genus	*Carpinus betulus*	*Carpinus*, *Carpinus betulus*, *Carpinus betulus* type, *Carpinus* type
Genus	*Carpinus orientalis/Ostrya*	*Carpinus orientalis*, *Carpinus orientalis* type, *Carpinus orientalis/Ostrya*, *Carpinus orientalis/Ostrya carpinifolia*, *Carpinus orientalis/Ostrya carpinifolia* type, *Carpinus/Ostrya*, *Carpinus/Ostrya* type, *Ostrya*, *Ostrya* type
Family	Caryophyllaceae	*Agrostemma githago*, *Cerastium cerastioides* type, *Cerastium fontanum* type, *Cerastium* type, *Cerastium/Stellaria* type, *Corrigiola*, *Dianthus*, *Dianthus superbus* type, *Dianthus* type, *Frankenia*, *Frankenia* type, *Agrostemma* type, *Gypsophila*, *Gypsophila fastigiata*, *Gypsophila repens* type, *Gypsophila* type, *Herniaria*, *Herniaria glabra*, *Herniaria* type, *Herniaria/Paronychia*, *Illecebrum*, *Loeflingia*, *Arenaria*, *Lychnis*, *Lychnis flos-cuculi*, *Lychnis flos-cuculi* type, *Lychnis* type, *Lychnis viscaria* type, *Minuartia*, *Minuartia rubra* type, *Minuartia* type, *Minuartia verna* type, *Moehringia* type, *Arenaria* type, *Paronychia*, *Paronychia type*, *Polycarpon*, *Sagina*, *Sagina procumbens*, *Sagina* type, *Saponaria*, *Scleranthus*, *Scleranthus annuus*, *Scleranthus perennis*, *Caryophyllaceae*, *Scleranthus* type, Silenaceae, *Silene*, *Silene acaulis*, *Silene acaulis* type, *Silene alba* type, *Silene dioica* type, *Silene latifolia*, *Silene rupestris*, *Silene* type, Caryophyllaceae subfam. Silenoideae, *Silene vulgaris type*, *Spergula*, *Spergula arvensis*, *Spergula* type, *Spergularia*, *Spergularia* type, *Stellaria*, *Stellaria holostea*, *Stellaria holostea* type, *Stellaria nemorum*, *Cerastium*, *Stellaria nemorum* type, *Stellaria palustris*, *Stellaria* type, *Vaccaria* type, *Cerastium alpinum* type, *Cerastium arvense* type
Genus	*Cassiope*	*Cassiope*, *Cassiope* type
Genus	*Castanea*	*Castanea*, *Castanea sativa*
Genus	*Cedrus*	*Cedrus*, *Cedrus atlantica*, *Cedrus atlantica* type, *Cedrus libani*
Family	Celastraceae	Celastraceae, *Parnassia*, *Parnassia palustris*
Genus	*Celtis*	*Celtis*, *Celtis australis*

Genus	*Ceratonia*	*Ceratonia, Ceratonia siliqua, Ceratonia* type
Genus	*Cercis*	*Cercis siliquastrum*
Genus	*Chamaedaphne*	*Chamaedaphne, Chamaedaphne calyculata*
Genus	*Chamaerops*	*Chamaerops*
Genus	*Chimaphila*	*Chimaphila umbellata*
Genus	*Cichorioideae*	*Cichorioideae, Lactuca sativa* type, *Lactuca* type, *Leontodon helveticus, Leontodon* type, *Scorzonera humilis* type, *Scorzonera* type, *Sonchus* type, *Taraxacum, Taraxacum* type, *Cichorium, Cichorium intybus* type, *Cichorium* type, *Crepis, Crepis aurea, Crepis* type, *Hieracium* type, *Lactuca*
Family	Cistaceae	Cistaceae, *Halimium/Tuberaria, Tuberaria*
Genus	*Cistus*	*Cistus, Cistus salviifolius* type, *Cistus* type, *Cistus villosus* type, *Cistus albidus* type, *Cistus incanus, Cistus ladanifer, Cistus ladanifer* type, *Cistus monspeliensis* type, *Cistus populifolius* type, *Cistus salvifolius, Cistus salviifolius*
Genus	*Clematis*	*Clematis, Clematis* type, *Clematis vitalba* type
Genus	*Clethra*	*Clethra*
Family	Clusiaceae	*Guttiferae*
Family	Colchicaceae	*Colchicum, Colchicum autumnale* type, *Colchicum* type, *Colchicum/Merendera, Merendera*
Genus	*Colutea*	*Colutea*
Family	Convolvulaceae	*Calystegia, Calystegia sepium,* Convolvulaceae, *Convolvulus, Convolvulus arvensis, Convolvulus arvensis* type, *Corema album* type, *Cuscuta, Cuscuta europaea* type
Genus	*Coriaria*	*Coriaria, Coriaria myrtifolia*
Genus	*Cornus*	Cornaceae, *Cornus, Cornus mas, Cornus mas/Cornus suecica, Cornus sanguinea, Cornus suecica*
Genus	*Corylus*	*Corylus, Corylus avellana, Corylus avellana* type, *Corylus maxima, Corylus* type
Genus	*Cotinus*	*Cotinus, Cotinus coggygria*
Genus	*Cotoneaster*	*Cotoneaster*
Family	Crassulaceae	*Crassula,* Crassulaceae, *Sedum, Sedum rosea, Sedum* type, *Sempervivum, Umbilicus, Umbilicus rupestris* type
Genus	*Crataegus*	*Crataegus, Crataegus* type

Family	Cucurbitaceae	Cucurbitaceae
Family	Cupressaceae	Cupressaceae, *Taxodiaceae, Taxodium, Cupressus, Cupressus type, Juniperus, Juniperus communis, Juniperus communis* type, *Juniperus excelsa/Juniperus oxycedrus, Juniperus sabina, Juniperus* type
Genus	*Cynomorium*	*Cynomorium*
Family	Cyperaceae	*Carex, Fimbristylis, Rhynchospora, Rhynchospora alba, Rhynchospora* type, *Schoenoplectus, Schoenoplectus lacustris ssp lacustris, Schoenoplectus* type, *Schoenus* type, *Scirpus, Scirpus lacustris* type, *Carex hirta type, Scirpus* type, *Trichophorum caespitosum, Carex* type, Cyperaceae, *Cyperus, Cyperus* type, *Eleocharis palustris, Eriophorum angustifolium/Eriophorum vaginatum, Eriophorum* type
Family	Cytinaceae	*Cytinus hypocistis* type
Genus	*Daphne*	*Daphne, Daphne gnidium, Daphne gnidium* type, *Daphne* type
Genus	*Datisca*	*Datisca*
Genus	*Delphinium*	*Delphinium* type
Family	Dennstaedtiaceae	*Pteridium, Pteridium aquilinum, Pteridium aquilinum type, Pteridium* type
Genus	*Diapensia*	*Diapensia, Diapensia lapponica*
Genus	*Dryas*	*Dryas, Dryas octopetala*
Genus	*Elaeagnus*	*Elaeagnus*
Genus	*Empetrum*	*Empetrum, Empetrum nigrum, Empetrum* type
Genus	*Ephedra*	*Ephedra, Ephedra major* type, *Ephedra* type, *Ephedra alata* type, *Ephedra distachya, Ephedra distachya* type, *Ephedra fragilis, Ephedra fragilis ssp campylopoda, Ephedra fragilis* type, *Ephedra fragilis var campylopoda, Ephedra major*
Genus	*Equisetum*	*Equisetum*
Genus	*Erica*	*Erica, Erica lusitanica* type, *Erica scoparia* type, *Erica tetralix, Erica tetralix* type, *Erica* type, *Erica umbellata* type, *Erica arborea, Erica arborea* type, *Erica australis, Erica australis* type, *Erica cinerea, Erica cinerea* type, *Erica erigena* type, *Erica lusitanica*
Family	Ericaceae	Ericaceae, *Ericales, Lecythis, Moneses, Orthilia, Phyllodoce, Pyrola*
Genus	*Euonymus*	*Euonymus, Euonymus europaeus*
Family	Euphorbiaceae	*Acalypha, Euphorbia, Euphorbia* type, Euphorbiaceae
Family	Fabaceae	Fabaceae, *Glycine*

Family	Fabaceae (herbs)	*Anthyllis*, *Lathyrus/Vicia*, *Lotus*, *Lotus corniculatus*, *Lotus corniculatus type*, *Lotus type*, *Lotus uliginosus*, *Medicago*, *Medicago littoralis* type, *Medicago sativa*, *Medicago* type, *Coronilla*, *Melilotus*, *Melilotus* type, *Onobrychis*, *Onobrychis* type, *Oxytropis*, *Phaseolus type*, *Trifolium*, *Trifolium alpinum* type, *Trifolium badium* type, *Trifolium montanum*, *Ebenus/Hedysarum*, *Trifolium pratense*, *Trifolium pratense* type, *Trifolium repens*, *Trifolium repens* type, *Trifolium spadiceum* type, *Trifolium* type, *Vicia*, *Vicia cracca*, *Vicia cracca* type, *Vicia faba* type, *Hedysarum hedysaroides*, *Vicia sylvatica* type, *Vicia* type, Viciaceae, *Hippocrepis comosa*, *Hippocrepis* type, *Lathyrus*, *Lathyrus* type, *Lathyrus/Vicia*
Genus	*Fagus*	*Fagus*, *Fagus orientalis*, *Fagus sylvatica*
Genus	*Ficus*	*Ficus*, *Ficus carica*
Genus	*Flueggea*	*Securinega tinctoria* type
Genus	*Frangula*	*Frangula*, *Frangula alnus*
Genus	*Fraxinus*	*Fraxinus*, *Fraxinus angustifolia*, *Fraxinus angustifolia subsp. oxycarpa*, *Fraxinus angustifolia* type, *Fraxinus excelsior*, *Fraxinus excelsior* type, *Fraxinus ornus*, *Fraxinus ornus* type, *Fraxinus oxycarpa* type
Genus	*Genisteae*	*Cytisus* type, *Ulex*, *Ulex* type, *Cytisus/Genista*, *Cytisus/Genista* type, *Cytisus/Ulex*, *Genista*, *Genista* type, *Genista/Ulex*, *Sarothamnus scoparius*, *Spartium*
Family	Gentianaceae	*Centaurium*, *Gentiana purpurea* type, Gentianaceae, *Gentianella*, *Gentianella campestris type*, *Swertia perennis*, *Centaurium maritimum*, *Centaurium* type, *Gentiana*, *Gentiana lutea/Gentiana pneumonanthe*, *Gentiana nivalis* type, *Gentiana pneumonanthe*, *Gentiana pneumonanthe* type, *Gentiana purpurea*
Family	Geraniaceae	*Erodium*, Geraniaceae, *Geranium*, *Geranium sylvaticum* type, *Geranium* type
Genus	*Halimium*	*Halimium*, *Halimium* type
Genus	*Hedera*	*Hedera*, *Hedera helix*, *Hedera* type
Genus	*Helianthemum*	*Helianthemum*, *Helianthemum croceum type*, *Helianthemum nummularium* type, *Helianthemum salicifolium* type, *Helianthemum* type
Genus	*Helleborus*	*Helleborus*, *Helleborus foetidus*, *Helleborus viridis* type
Genus	*Hippophae*	*Hippophae*, *Hippophae rhamnoides*
Genus	*Huperzia*	*Huperzia selago*, *Lycopodium selago*
Family	Hymenophyllaceae	*Hymenophyllum tunbrigense*, *Hymenophyllum wilsonii*, *Trichomanes speciosum*

Family	Hypericaceae	*Hypericum*, *Hypericum hyssopifolium*, *Hypericum perforatum* type, *Hypericum pulchrum* type, *Hypericum* type
Genus	*Ilex*	*Ilex*, *Ilex aquifolium*
Genus	*Impatiens*	*Impatiens*
Family	Iridaceae	*Crocus*, Iridaceae, *Iris*, *Iris pseudacorus*, *Iris pseudacorus* type, *Iris* type
Genus	*Jasminum*	*Jasminum*, *Jasminum fruticans*, *Jasminum* type
Family	Juglandaceae	Juglandaceae
Genus	*Juglans*	*Juglans*, *Juglans regia*
Family	Juncaceae	Juncaceae, *Juncus*, *Luzula*
Genus	*Kalmia*	*Loiseleuria procumbens*
Genus	*Koenigia*	*Koenigia islandica*
Genus	*Laburnum*	*Laburnum anagyroides*
Family	Lamiaceae	*Ajuga*, *Lycopus* type, *Lycopus/Mentha*, *Marrubium*, *Mentha*, *Mentha* type, *Mentha/Thymus*, *Origanum vulgare*, *Phlomis*, *Prunella*, *Prunella* type, *Ballota*, *Prunella vulgaris* type, *Scutellaria*, *Scutellaria* type, *Sideritis*, *Stachys*, *Stachys sylvatica* type, *Stachys sylvestris*, *Stachys* type, *Thymus*, *Thymus serpyllum*, *Galeopsis*, *Thymus* type, *Galeopsis* type, *Glechoma* type, Lamiaceae, *Lamium*, *Lamium* type, *Lycopus*
Genus	*Larix*	*Larix*, *Larix decidua*, *Larix decidua* type, *Larix/Pseudotsuga*
Genus	*Lavandula*	*Lavandula stoechas* type
Genus	*Ledum*	*Ledum*, *Ledum palustre*, *Ledum* type
Genus	*Ligustrum*	*Ligustrum*, *Ligustrum vulgare*, *Ligustrum vulgare* type
Family	Liliaceae	*Allium*, *Lilium martagon* type, *Lloydia serotina*, *Allium* type, *Anthericum*, *Anthericum* type, *Fritillaria lusitanica*, *Fritillaria* type, *Gagea*, Liliaceae, *Lilium*
Family	Linaceae	Linaceae, *Radiola linoides*
Genus	*Linnaea*	*Linnaea*, *Linnaea borealis*
Genus	*Linum*	*Linum*, *Linum bienne* type, *Linum catharticum*, *Linum catharticum* type, *Linum* type
Genus	*Lonicera*	*Lonicera*, *Lonicera caerulea*, *Lonicera hispida*, *Lonicera implexa*, *Lonicera periclymenum*, *Lonicera periclymenum* type, *Lonicera* type, *Lonicera xylosteum* type

Family	Loranthaceae	Loranthaceae
Genus	*Lycopodiella*	*Lepidotis inundata*, *Lycopodium inundatum*
Genus	*Lycopodium*	*Diphasiastrum*, *Lycopodium alpinum*, *Lycopodium annotinum*, *Lycopodium annotinum* type, *Lycopodium clavatum*, *Lycopodium clavatum* type, *Lycopodium complanatum*, *Lycopodium dubium*, *Lycopodium* type, *Diphasiastrum alpinum*, *Diphasium*, *Diphasium alpinum*, *Diphasium alpinum* type, *Diphasium complanatum*, *Diphasium tristachyum*, *Diphasium* type, *Lycopodium*
Genus	*Lysimachia*	*Lysimachia*, *Lysimachia maritima*, *Lysimachia nemorum*, *Lysimachia thyrsiflora*, *Lysimachia* type, *Lysimachia vulgaris*, *Lysimachia vulgaris* type
Family	Lythraceae	Lythraceae, *Lythrum*, *Lythrum salicaria*, *Lythrum salicaria* type, *Lythrum salicaria/Lythrum hyssopifolia*, *Peplis*
Family	Magnoliaceae	Magnoliaceae
Genus	*Malus*	*Malus*, *Malus* type
Family	Malvaceae	*Hibiscus*, *Lavatera* type, *Malva*, *Malva sylvestris* type, Malvaceae, *Sterculia*
Family	Melanthiaceae	*Veratrum*, *Veratrum* type
Genus	*Mercurialis*	*Mercurialis*, *Mercurialis annua*, *Mercurialis annua* type, *Mercurialis perennis*, *Mercurialis perennis* type
Genus	*Moltkia*	*Moltkia*
Family	Montiaceae	*Montia*
Family	Moraceae	Moraceae, *Morus*, *Morus alba*, *Morus alba* type, *Morus nigra*
Genus	*Myrica*	*Corylus/Myrica*, *Myrica*, *Myrica gale*, *Myrica gale* type, *Myrica* type
Genus	*Myricaria*	*Myricaria*
Family	Myrtaceae	Myrtaceae, *Myrtus*, *Myrtus communis*
Family	Nartheciaceae	*Narthecium*, *Narthecium ossifragum*, *Narthecium* type
Genus	*Nerium*	*Nerium*, *Nerium oleander*
Genus	*Nigella*	*Nigella*
Family	Nitrariaceae	*Nitraria*, *Peganum harmala*
Genus	*Olea*	*Olea*, *Olea europaea*, *Olea* type
Family	Oleaceae	*Fontanesia/Phillyrea*, *Olea/Ligustrum*, Oleaceae

Family	Onagraceae	*Chamaenerion, Chamaenerion angustifolium, Circaea, Epilobium, Epilobium* type, Onagraceae
Genus	*Ononis*	*Ononis, Ononis* type
Family	Ophioglossaceae	*Botrychium, Botrychium lunaria, Botrychium lunaria* type, *Botrychium* type, Ophioglossaceae, *Ophioglossum, Ophioglossum vulgatum*
Family	Orchidaceae	*Neottia* type, Orchidaceae
Family	Orobanchaceae	*Euphrasia, Euphrasia* type, *Melampyrum, Pedicularis, Pedicularis oederi* type, *Pedicularis palustris* type, *Pedicularis* type, *Rhinanthus, Rhinanthus* type
Family	Osmundaceae	*Osmunda, Osmunda regalis*
Family	Oxalidaceae	Oxalidaceae, *Oxalis, Oxalis acetosella, Oxalis stricta*
Genus	*Oxyria/Rumex*	*Oxyria, Rumex acetosa/Rumex acetosella, Rumex acetosa/Rumex acetosella* type, *Rumex acetosa/Rumex scutatus* type, *Rumex acetosella, Rumex acetosella* type, *Rumex alpestris, Rumex alpinus, Rumex alpinus* type, *Rumex aquaticus, Rumex aquaticus* type, *Oxyria digyna, Rumex conglomeratus* type, *Rumex crispus, Rumex crispus* type, *Rumex hydrolapathum, Rumex hydrolapathum* type, *Rumex longifolius, Rumex longifolius* type, *Rumex obtusifolius* type, *Rumex patentia* type, *Rumex sanguineus* type, *Oxyria* type, *Rumex* type, *Oxyria/Rumex, Oxyria/Rumex* type, *Rumex, Rumex acetosa, Rumex acetosa* type, *Rumex acetosa/Oxyria* type
Genus	*Paeonia*	*Paeonia*
Genus	*Paliurus*	*Paliurus, Paliurus spina-christi*
Family	Papaveraceae	*Chelidonium majus, Papaver, Papaver argemone, Papaver rhoeas* type, *Papaver* type, Papaveraceae, *Roemeria, Corydalis, Corydalis solida* type, *Corydalis* type, *Fumana, Fumaria, Fumaria officinalis* type, *Glaucium, Hypecoum*
Genus	*Parrotia*	*Parrotia persica*
Genus	*Periploca*	*Periploca*
Genus	*Phillyrea*	*Olea/Phillyrea, Phillyrea, Phillyrea angustifolia, Phillyrea angustifolia* type, *Phillyrea media, Phillyrea* type
Family	Phyllanthaceae	*Andrachne, Andrachne telephioides*
Genus	*Picea*	*Picea, Picea abies, Picea abies subsp abies*
Genus	*Picea orientalis*	*Picea orientalis*
Genus	*Pinus*	*Pinus*

Genus sub-group	*Pinus (diploxylon)*	*Pinus (Diploxylon), Pinus subg. Pinus, Pinus sylvestris, Pinus sylvestris* type, *Pinus sylvestris/Pinus nigra* type, *Pinus* type, *Pinus halepensis, Pinus nigra* type, *Pinus non-cembra, Pinus pinaster, Pinus pinaster* type, *Pinus pinaster/Pinus halepensis, Pinus pinea* type, *Pinus pinea/Pinus halepensis* type
Genus sub-group	*Pinus (haploxylon)*	*Pinus (Haploxylon), Pinus cembra, Pinus cembra* type, *Pinus peuce, Pinus sibirica*
Genus	*Pistacia*	*Pistacia, Pistacia lentiscus, Pistacia lentiscus* type, *Pistacia terebinthus, Pistacia terebinthus* type, *Pistacia* type
Family	Plantaginaceae	*Globularia, Plantago coronopus* type, *Plantago cylindrica* type, *Plantago lanceolata, Plantago lanceolata* type, *Plantago lusitanica, Plantago major, Plantago major* type, *Plantago major/Plantago media, Plantago maririma, Plantago maritima, Gratiola officinalis, Plantago maritima* type, *Plantago media, Plantago media* type, *Plantago media/Plantago major, Plantago media/Plantago major* type, *Plantago montana* type, *Plantago ovata* type, *Plantago psyllium* type, *Plantago tenuiflora* type, *Plantago* type, Plantaginaceae, *Plantago, Plantago afra* type, *Plantago albicans, Plantago alpina, Plantago alpina* type, *Plantago coronopus*
Genus	*Platanus*	*Platanus, Platanus orientalis, Platanus* type
Family	Plumbaginaceae	*Acantholimon, Limonium vulgare,* Plumbaginaceae, *Plumbago, Armeria, Armeria maritima, Armeria maritima subsp elongata, Armeria* type, *Armeria/Limonium, Armeria/Limonium type, Limonium, Limonium* type
Family	Poaceae	*Anthoxanthum, Stipa, Deschampsia, Elymus, Lygeum, Lygeum spartum, Nardus, Poa/Festuca* type, Poaceae, *Setaria*
Family	Polemoniaceae	Polemoniaceae, *Polemonium*
Family	Polygalaceae	*Polygala, Polygala* type, *Polygala vulgaris, Polygala vulgaris* type, Polygalaceae, *Polygaloides chamaebuxus*
Family	Polygonaceae	*Atraphaxis, Persicaria amphibia,* Polygonaceae, *Pteropyrum, Rheum, Rheum ribes, Rheum* type, *Bilderdykia convolvulus, Bilderdykia convolvulus* type, *Bistorta officinalis* type, *Bistorta vivipara, Calligonum, Fallopia convolvulus, Fallopia convolvulus* type, *Persicaria*
Genus	*Polygonum*	*Polygonum, Polygonum convolvulus, Polygonum convolvulus* type, *Polygonum oxyspermum* type, *Polygonum persicaria, Polygonum persicaria* type, *Polygonum sect. Persicaria, Polygonum* type, *Polygonum viviparum, Polygonum alpinum, Polygonum amphibium, Polygonum amphibium* type, *Polygonum aviculare, Polygonum aviculare* type, *Polygonum bistorta, Polygonum bistorta* type, *Polygonum bistorta/Polygonum viviparum*

Genus	*Polypodiales*	*Aspidium*, *Blechnum*, *Blechnum spicant*, *Cystopteris*, *Cystopteris fragilis*, *Cystopteris* type, *Dryopteridaceae/Polypodiaceae*, *Dryopteris*, *Dryopteris carthusiana*, *Dryopteris carthusiana* type, *Dryopteris cristata*, *Asplenium*, *Dryopteris cristata* type, *Dryopteris dilatata*, *Dryopteris dilatata* type, *Dryopteris filix-mas*, *Dryopteris filix-mas* type, *Dryopteris* type, *Dryopteris/Thelypteris*, *Grammitis*, *Gymnocarpium*, *Gymnocarpium dryopteris*, *Asplenium nidus*, *Pilularia*, Polypodiaceae, Polypodiales, *Polypodium*, *Polypodium vulgare*, *Polypodium vulgare* type, *Polystichum*, *Polystichum* type, *Thelypteris*, *Thelypteris palustris*, *Asplenium* type, *Thelypteris palustris* type, *Thelypteris phegopteris*, *Thelypteris* type, *Asplenium viride*, *Athyrium*, *Athyrium alpestre* type, *Athyrium distentifolium* type, *Athyrium filix-femina*
Genus	*Populus*	*Populus*, *Populus tremula*, *Populus tremula* type
Family	Portulacaceae	Portulacaceae
Genus	*Potentilla*	*Potentilla*, *Potentilla aurea*, *Potentilla micrantha* type, *Potentilla recta*, *Potentilla* type
Family	Primulaceae	*Anagallis*, *Primula*, *Primula clusiana* type, *Primula farinosa*, *Primula farinosa* type, *Primula hirsuta* type, *Primula* type, *Primula veris* type, *Primula vulgaris* type, Primulaceae, *Soldanella*, *Anagallis arvensis*, *Trientalis*, *Trientalis europaea*, *Anagallis arvensis* type, *Anagallis tenella*, *Anagallis* type, *Androsace*, *Androsaceae*, *Cyclamen*, *Cyclamen hederifolium*
Genus	*Prosopis*	*Lagonychium* type, *Prosopis*
Genus	*Prunus*	*Prunus*, *Prunus avium*, *Prunus padus*, *Prunus spinosa* type, *Prunus* type
Family	Pteridaceae	*Adiantum*, *Cheilanthes*, *Cryptogramma*, *Cryptogramma crispa*, *Cryptogramma crispa* type, *Pteris*
Genus	*Pterocarya*	*Pterocarya*, *Pterocarya fraxinifolia*
Genus	*Punica*	*Punica*
Genus	*Pyrus*	*Pyrus*, *Pyrus* type
Genus	*Quercus* (deciduous)	*Quercus*, *Quercus robur* type, *Quercus robur/Quercus petraea*, *Quercus (deciduous)*, *Quercus cerris*, *Quercus cerris* type, *Quercus deciduous*, *Quercus ithaburensis*, *Quercus ithaburensis* type, *Quercus petraea*, *Quercus robur*
Genus	*Quercus* (evergreen)	*Quercus (evergreen)*, *Quercus rotundifolia* type, *Quercus suber*, *Quercus suber* type, *Quercus calliprinos*, *Quercus calliprinos* type, *Quercus coccifera*, *Quercus coccifera* type, *Quercus coccifera/Quercus ilex*, *Quercus evergreen*, *Quercus ilex*, *Quercus ilex* type
Genus	*Quercus* (intermediate)	*Quercus canariensis type*, *Quercus cerris/Quercus suber*, *Quercus cerris/Quercus suber* type, *Quercus faginea*, *Quercus faginea/Quercus pubescens*, *Quercus faginea/Quercus pyrenaica*, *Quercus pubescens*

		type, *Quercus pyrenaica* type, *Quercus robur/Quercus pubescens* type
Family	Ranunculaceae	*Anemone*, *Anemone nemorosa*, *Anemone nemorosa type*, *Anemone nemorosa* type/*Hepatica nobilis*, *Anemone nemorosa/Anemone ranunculoides*, *Anemone* type, *Hepatica*, *Pulsatilla*, Ranunculaceae
Genus	*Ranunculus*	*Ranunculus*, *Ranunculus ficaria* type, *Ranunculus flammula* type, *Ranunculus glacialis* type, *Ranunculus montanus* type, *Ranunculus muricatus* type, *Ranunculus nivalis* type, *Ranunculus parviflorus*, *Ranunculus repens* type, *Ranunculus sceleratus* type, *Ranunculus* type, *Ranunculus acer* type, *Ranunculus aconitifolius*, *Ranunculus aconitifolius* type, *Ranunculus acris*, *Ranunculus acris* type, *Ranunculus arvensis*, *Ranunculus arvensis* type, *Ranunculus asiaticus* type
Family	Resedaceae	*Reseda*, *Reseda lutea* type, Resedaceae
Family	Rhamnaceae	Rhamnaceae
Genus	*Rhamnus*	*Rhamnus*, *Rhamnus catharticus*, *Rhamnus* type
Genus	*Rhododendron*	*Rhododendron*, *Rhododendron ferrugineum*, *Rhododendron* type
Genus	*Rhus*	*Rhus*, *Rhus coriaria*
Genus	*Ribes*	*Ribes*, *Ribes* type
Family	Rosaceae	*Agrimonia*, *Fragaria* type, *Geum*, *Geum rivale* type, *Geum* type, *Pirus* type, *Prunus/Rubus* type, *Pyrus/Malus*, *Rosa*, *Rosa canina* type, *Rosa* type, *Agrimonia eupatoria*, *Rosa/Prunus*, Rosaceae, *Spiraea*, *Alchemilla*, *Alchemilla* type, *Filipendula*, *Filipendula* type, *Filipendula ulmaria*, *Filipendula vulgaris*, *Fragaria*
Genus	*Rosmarinus*	*Rosmarinus*, *Rosmarinus* type
Family	Rubiaceae	*Asperula*, *Galium*, *Galium* type, Rubiaceae, *Theligonum*
Genus	*Rubus*	*Rubus*, *Rubus arcticus*, *Rubus arcticus* type, *Rubus chamaemorus*, *Rubus fruticosus* type, *Rubus idaeus* type, *Rubus saxatilis*, *Rubus* type
Genus	*Ruscus*	*Ruscus*
Family	Rutaceae	*Haplophyllum*, *Ruta*, Rutaceae
Genus	*Salix*	*Salix*, *Salix glauca* type, *Salix helvetica* type, *Salix herbacea*, *Salix herbacea* type, *Salix herbacea/Salix reticulata*, *Salix pentandra* type
Genus	*Salvia*	*Salvia*, *Salvia verticillata* type
Genus	*Sambucus*	*Sambucus*, *Sambucus ebulus*, *Sambucus nigra*, *Sambucus nigra* type, *Sambucus nigra/Sambucus racemosa*, *Sambucus racemosa*, *Sambucus* type

Genus	*Sanguisorba group*	*Poterium*, *Sanguisorba*, *Sanguisorba minor*, *Sanguisorba minor ssp minor*, *Sanguisorba minor* type, *Sanguisorba officinalis*, *Sanguisorba* type, *Sarcopoterium*
Family	Santalaceae	*Arceuthobium oxycedri*, *Comandra elegans*, *Osyris alba* type, *Thesium*
Family	Saxifragaceae	*Chrysosplenium*, *Saxifraga oppositifolia*, *Saxifraga oppositifolia* type, *Saxifraga paniculata* type, *Saxifraga stellaris*, *Saxifraga stellaris* type, *Saxifraga tricuspidata*, Saxifragaceae, *Chrysosplenium* type, *Micranthes nivalis* type, *Saxifraga*, *Saxifraga cernua* type, *Saxifraga cespitosa* type, *Saxifraga foliolosa* type, *Saxifraga granulata*, *Saxifraga granulata* type
Family	Scrophulariaceae	*Antirrhinum* type, *Scrophularia/Verbascum*, Scrophulariaceae, *Verbascum*, *Verbascum* type, *Veronica*, *Veronica* type, *Antirrhinum/Linaria*, *Digitalis*, *Digitalis purpurea* type, *Digitalis* type, *Linaria*, *Linaria* type, *Scrophularia*, *Scrophularia* type
Genus	*Smilax*	*Smilax*
Family	Solanaceae	*Capsicum* type, *Lycium*, Solanaceae, *Solanum*, *Solanum dulcamara*, *Solanum nigrum*, *Solanum nigrum* type
Genus	*Sorbus*	*Sorbus*, *Sorbus aria*, *Sorbus aucuparia*, *Sorbus aucuparia* type, *Sorbus* type
Genus	*Styrax*	*Styrax officinalis*
Genus	*Suaeda*	*Suaeda*, *Suaeda* type
Genus	*Syringa*	*Syringa*
Genus	*Tamarix*	*Tamarix*
Genus	*Taxus*	*Taxus*, *Taxus baccata*
Genus	*Teucrium*	*Teucrium*, *Teucrium* type
Genus	*Thalictrum*	*Thalictrum*, *Thalictrum alpinum*, *Thalictrum aquilegiifolium*, *Thalictrum flavum* type, *Thalictrum lucidum*, *Thalictrum* type
Family	Thymelaeaceae	*Thymelaea*, Thymelaeaceae
Genus	*Tilia*	*Tilia*, *Tilia cordata*, *Tilia cordata* type, *Tilia platyphyllos*, *Tilia platyphyllos* type
Genus	*Tofieldia*	*Tofieldia*
Genus	*Trollius*	*Trollius*, *Trollius europaeus*, *Trollius* type
Genus	*Ulmus*	*Ulmus*, *Ulmus glabra*, *Ulmus glabra* type, *Ulmus minor*
Genus	*Ulmus/Zelkova*	*Ulmus/Zelkova*, *Zelkova*, *Zelkova* type

Family	Urticaceae	*Parietaria*, *Parietaria/Urtica*, *Urtica*, *Urtica dioica*, *Urtica dioica* type, *Urtica pilulifera* type, *Urtica* type, *Urtica urens*, Urticaceae
Genus	*Vaccinium*	*Vaccinium*, *Vaccinium myrtillus*, *Vaccinium myrtillus type*, *Vaccinium oxycoccos*, *Vaccinium* type, *Vaccinium uliginosum* type, *Vaccinium/Oxycoccus*
Family	Valerianaceae	*Centranthus*, *Valerianella*, *Valeriana*, *Valeriana dioica* type, *Valeriana officinalis*, *Valeriana officinalis* type, *Valeriana sambucifolia* type, *Valeriana tripteris* type, *Valeriana* type, Valerianaceae
Family	Verbenaceae	*Verbena*, *Verbena officinalis*
Genus	*Viburnum*	*Viburnum*, *Viburnum opulus*, *Viburnum opulus* type, *Viburnum* type
Family	Violaceae	*Viola*, *Viola arvensis* type, *Viola canina* type, *Viola palustris*, *Viola palustris* type, *Viola tricolor*, *Viola tricolor/Viola arvensis*, Violaceae
Genus	*Viscum*	*Viscum*, *Viscum album*, *Viscum album* type, *Viscum* type
Genus	*Vitex*	*Vitex*
Genus	*Ziziphus*	*Ziziphus* type, *Zizyphus*, *Zizyphus lotus*
Family	Zygophyllaceae	*Tribulus*, *Tribulus terrestris*, Zygophyllaceae, *Zygophyllum*

Supplementary Table 4.2. Metadata of the pollen records used in the reconstructions

Latitude position	Entity name	Latitude	Longitude	Elevation	References
1	Kismohos	48.33724	20.42333	315	Willis et al (1997)
2	Preluca	47.8175	23.5358	730	Feurdean (2005); Feurdean & Bennike (2004); Feurdean et al (2008)
3	Steregoiu	47.813	23.5447	790	Björkman et al. (2003); Feurdean & Bennike (2004); Feurdean et al (2008)
4	Iaz Core	47.10833	22.66111	300	Grindean et al. (2014)
5	Kardashinski Swamp	46.51667	32.61667	4	Kremenetski (1995)
6	Capatana core	46.46611	23.13639	1220	Farcas et al. (2003)
7	Mohos1	46.083	25.9167	1050	Tantau (2003); Tantau et al. (2003)
8	Avrig 1	45.716	24.383	400	Tantau (2003); Tantau et al. (2006)
9	Pesteana peat bog	45.5433	22.8061	480	Farcas & Tantau (2012)
10	Taul Zanogutii core	45.32778	22.80278	1840	Farcas et al. (1999)
11	Semenic 1	45.18	22.0594	1400	Roesch & Fischer (2000)
12	Chernaya NG-2	44.57	33.6	2	Cordova & Lehman (2005)
13	Yaila	44.49	34.06	1205	Cordova & Lehman (2003); Cordova & Lehman (2005)
14	Lake Srebarna Lazarova94 Core	44.10914	27.06915	20	Lazarova (1995)
15	Mire Garvan Lazarova94 Core	44.10825	26.98818	20	Lazarova (1995)
16	Luganskoe	43.72	40.68	2428	Kvavadze et al. (1994)
17	Quartzevoe	43.67	41.17	2726	Kvavadze & Efremov (1996)
18	Serni Core	43.66667	40.480556	2485	Kvavadze & Efremov (1994)
19	Lake Durankulak 3	43.66667	28.55	4	Marinova (2003)
20	Adange core 1	43.31	41.33	1750	Kvavadze & Rukhadze (1989)
21	Amtkel core 1	43.27	41.31	1830	Kvavadze & Rukhadze (1989)
22	Sibista	43.23333	41.43056	2160	Kvavadze & Rukhadze (1989)

23	Lake Varna - 3	43.2	27.83333	0	Filipova-Marinova et al. (2014)
24	Khodzal Kvavadze89 Core	42.95417	41.91111	2030	Kvavadze & Rukhadze (1989)
24	Khodzal Kvavadze89 Core	42.95417	41.91111	2030	Kvavadze & Rukhadze (1989)
25	Sredna Gora Mountains	42.83333	24.83333	1300	Filipovitch (1977); Filipovitch (1992); Filipovitch et al. (1998); Petrov and Filipovitch (1987)
26	Straldza	42.6308	26.7728	137	Tonkov et al. (2008); Tonkov et al. (2009)
27	Straldzha mire CANAL	42.6308	26.7728	137	Connor et al. (2013)
28	Kumata Core	42.59028	23.25167	1770	Tonkov & Possnert (2016)
29	Vitosha Mountain Filipovitch81 Core	42.56809	23.26895	2000	Filipovitch (1975); Filipovitch (1985)
30	Beg Bunar peat bog	42.1525	22.535	1750	Lazarova et al. (2009)
31	Dry Lake 2	42.038	23.533	1900	Bozilova & Smit (1979); Bozilova et al. (1986)
32	Kupena-3	41.98333	24.3333	1356	Tonkov et al. (2013); Tonkov et al. (2014)
33	Besbog-2 Stefanova87	41.75	23.66667	2240	Stefanova et al. (2006)
34	Popovo Ezero Stefanova86	41.71667	23.66667	2185	Stefanova & Bozilova (1995)
35	Didachara core	41.68389	42.49694	2000	Connor et al. (2017)
36	Imera core 1	41.65	44.22	1610	Connor & Sagona (2007); Connor et al. (2004)
37	Aligol core 1	41.63	44.02	1550	Connor & Sagona (2007); Connor et al. (2004)
38	Lake Blatisto	41.62139	24.67806	1540	van Huis et al. (2013a); van Huis et al. (2013b)
39	Kumisi core 1	41.58	44.83	469	Connor et al (2004)
40	Sakhare core 1	41.58	45.32	800	Connor et al (2004)
41	Mutorog Bozilova93 Core	41.52432	23.61661	1700	Panovska et al. (1995)
42	Elatia-Rhodopes	41.47972	24.32583	1520	Athanasiadis et al. (1993)

42	Elatia-Rhodopes	41.47972	24.32583	1520	Gerasimidis & Athanasiadis (1995)
43	Beles Mountain	41.31944	23.01611	1400	Athanasiadis et al. (2003)
44	Lailias_core	41.26778	23.59944	1420	Gerasimidis (2000); Gerasimidis & Athanasiadis (1995)
45	Paiko	41.05167	22.27472	1080	Gerasimidis & Athanasiadis (1995); Gerasimidis et al. (2008)
46	Voras	41.0179	21.9122	1640	Gerasimidis & Athanasiadis (1995); Gerasimidis et al. (2009)
47	Lake Ohrid	40.938	20.759	693	Wagner et al. (2009)
48	Edessa1	40.81806	21.9525	350	Bottema (1974)
49	Vegoritis 8 Bottema Core	40.75	21.75	570	Bottema (1982)
50	Sapanca long core SA03R6	40.71806	30.25833	30	Leroy et al. (2010)
51	Khimaditis Ib Bottema65 Core	40.61667	21.58333	560	Bottema (1974)
52	Orestias G25	40.5117	21.2578	630	Kouli & Dermitzakis (2010)
53	Kaz Gölü	40.28333	36.15		Bottema et al. (1993)
54	Flambouro mire	40.25944	22.17083	1645	Gerasimidis & Athanasiadis (1995)
54	Flambouro mire	40.25944	22.17083	1645	Gerasimidis & Panajiotidis (2010)
55	Litochoro_core	40.13889	22.54611	25	Athanasiadis (1975)
56	Rezina	39.98778	20.77556	1760	Willis (1992)
57	Demiryurt Gölü Bottema Core	39.73333	37.383333		Bottema et al. (1993)
58	Pertouli core	39.52417	21.4775	1440	Athanasiadis (1975)
59	Trikhonis 5 Bottema Core	38.6	21.5	20	Bottema(1982)
60	Lake Almalou	37.66528	46.63194	2410	Djamali et al. (2009); Djamali et al. (2010)
61	Lake Lerna	37.58083	22.73	0	Jahns (1993)

62	HCGA05-core	37.46944	47.3525	-27	Leroy et al. (2011); Amini et al. (2012)
63	Köycegiz Gölü Bottema70 Core	36.875	28.641667	1491.76	Bottema & Woldring (1984)
64	EIG	36.55	51.4833	550	Ramezani et al. (2013)
65	Asi Gonia 1	35.24861	24.27778	780	Atherden & Hall (1999)
66	Asi Gonia 2	35.24861	24.2778	780	Atherden & Hall (1999)
67	Bouara Bottema84 core	35.23333	41.18333		Gremmen & Bottema (1991)
68	Chamsine	33.75278	35.948056	856	Hajar et al. (2010); Cheddadi & Khater (2016)
69	Wadi Shallalah	32.6	35.9	385	Cordova (2007)
70	Dead Sea DS7-1SC core	31.493	35.4361	-402	Leroy (2010)
71	Ein Gedi	31.46528	35.39417	-413	Litt et al. (2012)

References for pollen records

Amini, A., Harami, R.M., Lahijani, H., and Mahboubi, A.(2012) Holocene sedimentation rate in Gorgan Bay and adjacent coast in Southeast of Caspian Sea. Journal of Basic and Applied Scientific Research 2: 289-297.

Athanasiadis, N. (1975) Zur postglazialen Vegetationsentwicklung von Litochoro Katerinis und Pertouli Trikalon (Griechenland). Flora 164: 99-132.

Athanasiadis, N., Gerasimidis, A., and Panajiotidis, S. (2003) A palynological study in the Beles Mountains, Northern Greece. In: Aspects of Palynology and Palaeoecology. Festschrift in Honour of Elissaveta Bozilova, pp. 185-197. PENSOFT, Sofia-Moscow.

Athanasiadis, N., Gerasimidis, A., Eleftheriadou, E., and Theodoropoulos. K. (1993) Zur postglazialen Vegetationsentwicklung des Rhodopi-Gebirges (Elatia Dramas - Griechenland). Dissertationes botanicae, 196: 427-437.

Atherden, M.A., and Hall, J.A. (1999) Human impact on vegetation in the White Mountains of Crete since AD 500. The Holocene, 9:183-193.

Björkman, L., Feurdean, A., and Wohlfarth, B., (2003) Late-Glacial and Holocene forest dynamics at Steregoiu in the Gutaiului Mountains, Northwest Romania. Review of Palaeobotany and Palynology 124: 79-111.

Bottema, S. (1974) Late Quaternary Vegetation History of Northwestern Greece. Ph.D. Dissertation. University of Groningen, Groningen, The Netherlands

Bottema, S., (1982) Palynological investigations in Greece with special reference to pollen as indicator of human activity. Palaeohistoria, 24: 257-289.

Bottema, S., and Woldring, H. (1984) Late Quaternary vegetation and climate of southwestern Turkey. Part II. Palaeohistoria 26: 123-149.

Bottema,S., Woldring, H. and Aytug, B. (1993) Late Quaternary vegetation history of northern Turkey. Palaeohistoria 35/36: 13-72

Bozilova, E., and Smit, A.G. (1979) Palynology of lake Sucho Ezero from South Rila Mountain (Bulgaria). Phytologia 11: 54-67.

Bozilova, E., Tonkov, S., and Pavloa, D. (1986) Pollen and plant macrofossil analyses of the Lake Sucho Ezero in the south Rila mountains. Annual Journal of Sofia University, Faculty of Biology 80: 48-57.

Cheddadi, R., and Khater, C. (2016) Climate change since the last glacial period in Lebanon and the persistence of Mediterranean species. Quaternary Science Reviews 150: 146-157.

Connor, SE, and Sagona, A, (2007) Environment and society in the late prehistory of southern Georgia, Caucasus. In B. Lyonnet (ed.) Les cultures du Caucase (VI-IIIeme millenaires av. notrere). Leurs relations avec le Proche-Orient Ancien, Peeters Press, pp. 21-26.

Connor, S.E., D. Colombaroli, F. Confortini, E. Gobet, B.P. Ilyashuk, E.A. Ilyashuk, J.F.N. van Leeuwen, M. Lamentowicz, W.O. van der Knaap, E. Malysheva, A. Marchetto, N. Margalitadze, Y. Mazei, E.A.D. Mitchell, R.J. Payne, and B. Ammann (2017) Long-term population dynamics – theory and reality in a peatland ecosystem. Journal of Ecology DOI: 10.1111/1365-2745.12865

Connor, S.E., Ross, S.A., Sobotkova, A., Herries, A.I.R., Mooney, S.D., Longford, C. and Iliev, I. (2013) Environmental conditions in the SE Balkans since the Last Glacial Maximum and their influence on the spread of agriculture into Europe. Quaternary Science Reviews, 68: 200-215.

Connor, S.E., Thomas, I., Kvavadze, E.V., Arabuli, G.J., Avakov, G.S., & Sagona, A. (2004) A survey of modern pollen and vegetation along an altitudinal transect in southern Georgia, Caucasus region. Review of Palaeobotany and Palynology 129: 229-250.

Cordova, C.E. (2007). Millenial Landscape Change in Jordan: Geoarchaeology and Cultural Ecology. Tucson: University of Arizona Pres 272 p.

Cordova, C.E., and Lehman, P.H. (2003) Archaeopalynology of synanthropic vegetation in the chora of Chersonesos, Crimea, Ukraine. Journal of Archaeological Science 30:1483-1501.

Cordova, C.E., and Lehman, P.H. (20050 Holocene environmental change in southwestern Crimea (Ukraine) in pollen and soil records. The Holocene 15:263-277.

Djamali, M., de Beaulieu, J.L., Andrieu-Ponel, V., Berberian, M., Miller, N.F., Gandouin, E., Lahijani, H.A.K., Shah-Hosseini, M., Ponel, P., Salimian, M., and Guiter, F. (2009) A late Holocene pollen record from Lake Almalou in NW Iran: evidence for changing land-use in relation to some historical events during the last 3700 years. Journal of Archaeological Science, 36: 1363-1375.

Djamali, M., Miller, N.F., Ramezani, E., Andrieu-Ponel, V., de Beaulieu, J.L., Berberian, M., Guibal, F., Lahijani, H.A.K., Lak, R., and Ponel, P. (2010) Notes on arboricultural and agricultural practices in Ancient Iran based on new pollen evidence. Paléorient 36: 175-188.

Farcas, S., and Tantau, I. (2012) Contribution to the European Pollen Database. 16. Poiana Rusca Mountains (Romania): Pesteana peat bog. Grana 51: 249-251.

Farcas, S., de Beaulieu, J.L., Reille, M., Coldea, G., Diaconeasa, B., Goeury, C., Goslar, T., and Jull, T. (1999) First ^{14}C dating of Late Glacial and Holocene pollen sequences from Romanian Carpathes. Compte Rendu de l'Académie des Sciences Paris, Série III, Sciences de la Vie 322: 799-807.

Farcas, S., Lupsa, V., Tantau, I., and Bodnariuc, A. (2003) Reflectarea procesului de antropizare in diagramele sporo-polinice din Muntii Apuseni. In: Environment and Progress, Cluj-Napoca, pp. 231-236.

Feurdean, A. (2005) Holocene forest dynamics in northwestern Romania. The Holocene 15: 435-446.

Feurdean, A., and Bennike, O. (2004) Late Quaternary palaeoecological and palaeoclimatological reconstruction in the Gutaiului Mountains, northwest Romania. Journal of Quaternary Science 19: 808-827.

Feurdean, A., Klotz, S., Mosbrugger, V., and Wohlfarth, B. (2008) Pollen-based quantitative reconstructions of Holocene climate variability in NW Romania. Palaeogeography, Palaeoclimatology, Palaeoecology 260: 494-504.

Filipova-Marinova M., Pavlov, D., Vergiev, S., Slavchev, V., and Giosan. L. (2014) Contributions to the European Pollen Database. 24. Varna Lake (north-eastern Bulgaria): vegetation history and human impact during the last 8000 years. Grana 53: 309-311.

Filipovitch, L. (1975) Vegetation history of the high parts of Vitosha mountain during the Late Postglacial times. Fitologija 34: 3-27

Filipovitch, L. (1977). Palynological data for the postglacial distribution of Juglans in the composition of Bulgarian flora. Phytology 6: 32-37.

Filipovitch, L. (1985) Palynological studies of peat bogs on the southern slopes of Vitosha mountain. Forest Science 2: 3-16.

Filipovitch, L. (1992 Anthropogenic activity as a factor for the formation of contemporary plant communities in the central Sredna Gora mountain. Fitologija 43: 30-35.

Filipovitch, L., Lazarova, M., Stefanova, I., and Petrova, M. (1998) Development of vegetation in Mt Sredna Gora during theHolocene. Phytologia Balcanica 4: 13-29.

Gerasimidis, A. (2000) Palynological evidence for human influence on the vegetation of mountain regions in northern Greece: the case of Lailias, Serres. Sheffield Studies in Aegian Archaeology. Sheffield Academic Press, Sheffield England.

Gerasimidis, A., and Athanasiadis, N. (1995) Woodland history of northern Greece from the mid Holocene to recent time based on evidence from peat polln profiles. Vegetation History and Archaeobotany 4:109-116.

Gerasimidis, A., and Panajiotidis, S. (2010) Contributions to the European Pollen Database. 9. Flambouro, Pieria Mountains (northern Greece). Grana 49: 76-78

Gerasimidis, A., Athanasiadis, N., and Panajiotidis, S. (2008) Contributions to the European Pollen Database. 4. Mount Paiko (northern Greece). Grana 47: 316-318.

Gerasimidis, A., Athanasiadis, N., and Panajiotidis, S. (2009) Contributions to the European Pollen Database. 8. Mount Voras (north-west Greece). Grana 48: 316-318.

Gremmen, W.H.E., and Bottema, S. (1991). Palynological investigations in the Syrian Gazira. In H. Kühne (Ed.), Die rezente Umwelt von Tall Seh Hamad und Daten zur

Umweltrekonstruktion der assyrischen Stadt Dur-Katlimmu. Dietrich Reimer Verlag, Berlin, Germany, pp 105-116.

Grindean, R., Tantau, I., Farcas, S., and Panait, A. (2014) Middle to Late Holocene vegetation shifts in the NW Transylvanian lowlands (Romania). Studia UBB Geologia 59: 29-37.

Hajar, L., Haïdar-Boustani, M., Khater, C., and Cheddadi, R. (2010) Environmental changes in Lebanon during the Holocene: Man vs. climate impacts. Journal of Arid Environments 74: 746-755.

Jahns, S. (1993) On the Holocene vegetation history of the Argive plain (Peloponnese, southern Greece). Vegetation History and Archaeobotany 2: 187-203.

Kouli, K., and Dermitzakis, M.D. (2010) Contributions to the European Pollen Database. 11. Lake Orestiás (Kastoria, northern Greece). Grana 49:154-156.

Kremenetski, C. (1995) Holocene vegetation and climate history of southwestern Ukraine. Review of Paleobotany and Palynology 85: 289-301

Kvavadze, E.V., and Efremov, Y.V. (1994) Palynological studies of Holocene lake sediments in the headwaters of the river Bezymianka (West Caucasus). Acta Palaeobotanica 34: 205-214.

Kvavadze, E. V, and Efremov, Y.V. (1996): Palynological studies of lake and lake-swamp sediments of the Holocene in the high mountains of Arkhys (Western Caucasus). Acta Palaeobotanica 36: 107-119.

Kvavadze, E.V., and Rukhadze, L.I. (1989). Rastitel'nost' i klimat golotsena Abkhazii (Vegetation and climate of the Holocene in Abkhazia). Metsniereba, Tbilisi, 137pp

Kvavadze, E.V., Efremov, Y.V., Bukreeva, G.V., and Akatov, V.V. (1994) Palynological characteristic of the series of lacustrine and paludal deposites of the Holocene in the headwaters of the Zakan river (Western Caucsus). Bulletin of the Georgian Academy of Sciences 150: 177-184.

Lazarova, M.A. (1995): Human impact on the natural vegetation in the region of Lake Srebarna and mire Garvan (northeastern Bulgaria). Palynological and palaeoethnobotanical evidence. In: E. Bozilova and Tonkov, S. (Eds.). Advances in Holocene Palaeoecology in Bulgaria, pp. 47-67

Lazarova, M.A., Tonkov, S., Snowball, I., and Marinova, E. (2009) Contribution to the European Pollen Database. 6. Peat-bog Begubar (Osogovo Mountains, south-west Bulgaia): Four millenia of vegetation history. Grana 48: 147-149.

Leroy, S.A.G. (2010) Pollen analysis of core DS7-1SC (Dead Sea) showing intertwined effects of climatic change and human activities in the Late Holocene. Journal of Archaeological Science 37: 306-316.

Leroy, S.A.G., Lahijani, H.A.K., Djamali, M., Naqinezhad, A., Moghadam, M.V., Arpe, K., Shah-Hosseini, M., Hosseindoust, M., Miller, C.S., Tavakoli, V., Habibi, P., Naderi Beni. M. (2011) Late Little Ice Age palaeoenvironmental records from the Anzali and Amirkola Lagoons (south Caspian Sea): Vegetation and sea level changes. Palaeogeography, Palaeoclimatology, Palaeoecology 302:415-434.

Leroy, S.A.G., Schwab, M.J., Costa, P.J.M. (2010) Seismic influence on the last 1500-year infill history of Lake Sapanca (North Anatolian Fault, NW Turkey). Tectonophysics 486: 15-27

Litt, T., Ohlwein, C., Neumann, F.H., Hense, A., Stein, M. (2012): Holocene climate variability in the Levant from the Dead Sea pollen record. Quaternary Science Reviews 49: 95-105.

Marinova, E. (2003) The new pollen core Lake Durankulak-3: a contribution to the vegetation history and human impact in Northeastern Bulgaria. In Tonkov, S. (Ed.) Aspects of Palynology and Palaeoecology: Festschrift in Honour of Elissaveta Bozilova, pp. 279-288.

Panovska, H., Bozilova, E., Tonkov, S. (1995) A palaeoecological investigation on the vegetaion history in the Southern Pirin Mts. (SW. Bulgaria). In: Advances in Holocene Palaeoecology in Bulgaria. Bozilova, E. and Tonkov, S. (Eds.) Pensoft Publications, Sofia-Moscow, pp. 32-46.

Ramezani, E., Marvie Mohadjer, M.R., Knapp, H.D., Theuerkauf, M., Manthey, M., and Joosten, H. (2013) Pollen-vegetation relationships in the central Caspian (Hyrcanian) forests of northern Iran. Review of Palaeobotany and Palynology 189: 38-49.

Roesch, M., and Fischer, E. (2000) A radiocarbon dated Holocene pollen profile from the Banat mountains (Southwestern Carpathians, Romania). Flora 195: 277-286.

Stefanova, I., Bozilova, E. (1995) Studies on the Holocene history of vegetation in the Northern Pirin Mts., southwestern Bulgaria. In: Advances in Holocene Palaeoecology in Bulgaria, Bozilova, E. and Tonkov, S. (Eds.) Pensoft Publications, Sofia-Moscow, 9-31.

Stefanova, I., Atanassova, J., Delcheva, M., Wright, H.E. (2006) Chronological framework for the Lateglacial pollen and macrofossil sequence in the Pirin Mountains, Bulgaria: Lake Besbog and Lake Kremensko-5. The Holocene 16: 877-892.

Tantau, I. (2003) Pollen Analytic Researches in the Eastern Romanian Carpathians. History of Vegetation and Human Impact. PhD thesis Aix-Marseille III University and Babes-Bolyai of Cluj-Napoca University.

Tantau, I., Reille, M., De Beaulieu, J.-L., Farcas, S., Goslar, T., and Paterne, M. (2003) Vegetation history in the Eastern Romanian Carparthians: pollen analysis of the two sequences from the Mohos crater. Vegetation History and Archaeobotany 12: 113-125.

Tantau, I., Reille, M., De Beaulieu, J.-L., and Farcas, S. (2006) Late Glacial and Holocene vegetation history in the southern part of Transylvania (Romania): pollen analysis of two sequences from Avrig. Journal of Quaternary Science 21: 49-61.

Tonkov, S., and Possnert, G. (2016) Contributions to the European Pollen Database. 30. Peat bog Kumata-1, Vitosha Mountain (Bulgaria). Grana 55: 250-252.

Tonkov, S., Bozilova, E., Marinova, E., and Jungner, H. (2008) History of vegetation and landscape during the last 4000 years in the area of Straldzha mire (southeastern Bulgaria). Phytologia Balcanica 14: 185-191.

Tonkov, S., Bozilova, E., and Jungner, H. (2009) Contributions to the European Pollen Database. 7. Mire Staldza (Southeastern Bulgaria): Late Holocene vegetation history. Grana 48: 235-237.

Tonkov, S., Lazarova, M.A., Bozilova, E., Ivanov, D., and Snowball, I. (2013) Contributions to the European Pollen Database. 19. Mire Kupena, Westren Rhodopes Mountains (South Bulgaria). Grana 52: 238-240.

Tonkov, S., Lazarova, M.A., Bozilova, E., Ivanov, D., and Snowball, I. (2014) A 30,000-year pollen record from Mire Kupena, Western Rhodopes Mountains (south Bulgaria). Review of Palaeobotany and Palynology 209: 41-51.

van Huis, J., Tonkov, S., and Bozilova, E. (2013a). Contributions to the European Pollen Database. 18. Lake Blatisto, Rhodopes Mountains (South Bulgaria). Grana 52:78-80.

van Huis, J., Tonkov, S., and Bozilova, E. (2013b) Two millennia of vegetation history in the Smolyan lake area, Central Rhodopes Mountains (Bulgaria). Phytologia Balcanica 19: 169-178.

Wagner, B., Lotter, A.F., Nowaczyk, N.R., Reed, J.M., Schwalb, A., Sulpizio, R., Valsecchi, V., Wessels, M., and Zanchetta, G. (2009): A 40,000-year record of environmental change from ancient Lake Ohrid (Albania and Macedonia). Journal of Paleolimnology, 41, 407-430.

Willis, K.J. (1992) The late Quaternary vegetational history of northwest Greece. II. Rezina marsh. New Phytologist 121: 119-138.

Willis, K.J., Braun, M., Sumegi, P., and Toth, A. (1997) Does soil change cause vegetation change or vice versa? A temporal perspective from Hungary. Ecology 73: 740-750.

Supplementary Table 4.3. Details of the models used for the transient climate simulations.

Model	Model code	Time frame (yr BP)	Horizontal resolution (lat x long)	Vegetation	References
Institut Pierre Simon Laplace Earth System Model	IPSL-CMIP5	6000-0	1.875 x 3.75	prescribed	Dufresne et al., 2013; Sepulcre et al., 2020; Braconnot et al., 2019a, b
Institut Pierre Simon Laplace Earth System Model	IPSL-CMIP5	6000-0	1.25 x 2.5	dynamic	Dufresne et al., 2013; Braconnot et al., 2019a, b
Max Planck Institute Earth System Model version 1.2	MPI	7950-100	T63	dynamic	Bader et al., 2020; Dallmeyer et al., 2021
Alfred Wegener Institute Earth System Model version 2	AWI	6000-0	T63	dynamic	Sidorenko et al., 2019; Lamping et al., 2021; Shi et al., 2022
LOVECLIM	LOVECLIM	11500-0	T21	dynamic	Goosse et al., 2010; Zhang et al., 2016
Community Climate System Model, version 3	TRACE-21k-I	22000-0	T31	dynamic	Collins et al., 2006; Otto-Bleisner et al., 2006; Liu et al., 2009
Community Climate System Model, version 3	TRACE-21k-II	22000-0	T31	dynamic	He and Clark, 2022

References for model simulations

Bader, J., Jungclaus, J., Krivova, N., Lorenz, S., Maycock, A., Raddatz, T., Schmidt, H., Toohey, M., Wu, C.-J., and Claussen, M.: Global temperature modes shed light on the Holocene temperature conundrum. Nat. Commun. 11, 4726, https:// doi.org/10.1038/s41467-020-18478-6, 2020.

Braconnot, P., Cretat, J., Marti, O., Balkanski, Y., Caubel, A., Cozic, A., Foujols, M.-A., and Sanogo, S.: Impact of multiscale variability on last 6,000 Years Indian and West african monsoon rain. Geophys. Res. Lett. 46, 14021e14029, https:// doi.org/10.1029/2019GL084797, 2019a.

Braconnot, P., Zhu, D., Marti, O., and Servonnat, J.: Strengths and challenges for transient Mid- to Late Holocene simulations with dynamical vegetation. Clim. Past 15, 997e1024, 2019b.

Dallmeyer, A., Claussen, M., Lorenz, S.J., and Shanahan, T.: The end of the African humid period as seen by a transient comprehensive Earth system model simulation of the last 8000-years. Clim. Past, 16, 117–140, https://doi.org/10.5194/cp-16-117-2020, 2020.

Dufresne, J.-L., Foujols, M.-A., Denvil, S., Caubel, A., Marti, O., Aumont, O., Balkanski, Y., Bekki, S., Bellenger, H., Benshila, R., Bony, S., Bopp, L., Braconnot, P., Brockmann, P., Cadule, P., Cheruy, F., Codron, F., Cozic, A., Cugnet, D., de Noblet, N., Duvel, J.-P., Ethe, C., Fairhead, L., Fichefet, T., Flavoni, S., Friedlingstein, P., Grandpeix, J.-Y., Guez, L., Guilyardi, E., Hauglustaine, D., Hourdin, F., Idelkadi, A., Ghattas, J., Joussaume, S., Kageyama, M., Krinner, G., Labetoulle, S., Lahellec, A.,

Lefebvre, M.-P., Lefevre, F., Levy, C., Li, Z.X., Lloyd, J., Lott, F., Madec, G., Mancip, M., Marchand, M., Masson, S., Meurdesoif, Y., Mignot, J., Musat, I., Parouty, S., Polcher, J., Rio, C., Schulz, M., Swingedouw, D., Szopa, S., Talandier, C., Terray, P., Viovy, N., and Vuichard, N.: Climate change projections using the IPSL-CM5 earth system model: from CMIP3 to CMIP5. Clim. Dynam. 40, 2123e2165, https://doi.org/10.1007/s00382-012-1636-1, 2013.

Goosse, H., Brovkin, V., Fichefet, T., Haarsma, R., Huybrechts, P., Jongma, J., Mouchet, A., Selten, F., Barriat, P.-Y., Campin, J.-M., Deleersnijder, E., Driesschaert, E., Goelzer, H., Janssens, I., Loutre, M.-F., Morales Maqueda, M. A., Opsteegh, T., Mathieu, P.-P., Munhoven, G., Pettersson, E. J., Renssen, H., Roche, D. M., Schaeffer, M., Tartinville, B., Timmermann, A., and Weber, S. L.: Description of the Earth system model of intermediate complexity LOVECLIM version 1.2, Geosci. Model Dev., 3, 603–633, https://doi.org/10.5194/gmd-3-603-2010, 2010.

He, F., and Clark, P.U.: Freshwater forcing of the Atlantic Meridional Overturning Circulation revisited. Nat. Clim. Change, 12, 449-454, https://doi.org/10.1038/s41558-022-01328-2, 2022

Lamping, N., Müller, J., Hefter, J., Mollenhauer, G., Haas, C., Shi, X., Vorrath, M.-E., Lohmann, G., and Hillenbrand, C.-D.: Evaluation of lipid biomarkers as proxies for sea ice and ocean temperatures along the Antarctic continental margin. Clim. Past, 17, 2305–2326, https://doi.org/10.5194/cp-17-2305-2021, 2021.

Liu, Z., Otto-Bliesner, B. L., He, F., Brady, E. C., Tomas, R.. Clark, P. U., Carlson, A. E., Lynch-Stieglitz, J., Curry, W., Brook, E., Erickson, D., Jacob, R., Kutzbach, J., and Cheng, J.: Transient Simulation of Last Deglaciation with a New Mechanism for Bolling-Allerod Warming. Science, 325, 310-314, doi:10.1126/science.1171041, 2009.

Otto-Bliesner, B.L., Hewitt, C.D., Marchitto, T.M., Brady, E., Abe-Ouchi, A., Crucifix, M., Murakami, S., and Weber, S.L.: Last Glacial Maximum ocean thermohaline circulation: PMIP2 model intercomparisons and data constraints, Geophys. Res. Lett., 34, L12706, doi:10.1029/2007GL029475, 2007

Sepulchre, P., Caubel, A., Ladant, J.-B., Bopp, L., Boucher, O., Braconnot, P., Brockmann, P., Cozic, A., Donnadieu, Y., Dufresne, J.-L., Estella-Perez, V., Ethe, C., Fluteau, F., Foujols, M.-A., Gastineau, G., Ghattas, J., Hauglustaine, D., Hourdin, F., Kageyama, M., Khodri, M., Marti, O., Meurdesoif, Y., Mignot, J., Sarr, A.-C., Servonnat, J., Swingedouw, D., Szopa, S., and Tardif, D.: IPSL-CM5A2 e an Earth system model designed for multi-millennial climate simulations. Geosci. Model Dev., 13, 3011e3053. https://doi.org/10.5194/gmd-13-3011-2020, 2020.

Sidorenko, D., Goessling, H. f., von Koldunov, N., Scholz, P., Danilov, S., Barbi, D., Cabos, W., Gurses, O., Harig, S., Hinrichs, C., Juricke, S., Lohmann, G., Losch, M., Mu, L., Rackow, T., Rakowsky, N., Sein, D., Semmler, T., Shi, X., … and Jung, T.: Evaluation of FESOM2.0 coupled to ECHAM6.3: Preindustrial and HighResMIP simulations. J. Adv. Model. Earth Syst., 11, 3794–3815. https://doi.org/10.1029/2019MS001696, 2019.

Zhang, Y., Renssen, H., and Seppä, H.: Effects of melting ice sheets and orbital forcing on the early Holocene warming in the extratropical Northern Hemisphere. Clim. Past, 12, 1119–1135. https://doi.org/10.5194/cp-12-1119-2016, 2016.

Supplementary Table 4.4. Leave-out cross-validation fitness of fxTWA-PLSv2 for mean temperature of the coldest month (MTCO), mean temperature of the warmest month (MTWA), growing degree days above base level 0°C (GDD0) and plant-available moisture (α) with p-spline smoothed fx estimation, using bins of 0.02, 0.02 and 0.002, showing results for all the components. RMSEP is the root-mean-square error of prediction. p assesses whether using the current number of components is significantly different from using one component less; the last significant number of components is indicated in bold. The degree of overall compression is assessed by linear regression of the cross-validated reconstructions onto the climate variable, where b1 and b1.se are the slope and the standard error of the slope, respectively. The overall compression is reduced as the slope approaches 1.

Variable	Compo-nent	R2	Average bias	Max absolute bias	Min absolute bias	RMSEP	p	b1	b1.se
MTCO	1	0.67	-0.41	19.78	0.00	4.08	0.001	0.82	0.01
MTCO	2	0.70	-0.37	16.47	0.00	3.85	0.001	0.84	0.01
MTCO	3	0.72	-0.20	22.75	0.00	3.72	0.001	0.86	0.01
MTCO	**4**	**0.73**	**-0.22**	**26.35**	**0.00**	**3.67**	**0.001**	**0.86**	**0.01**
MTCO	5	0.73	-0.22	30.22	0.00	3.70	0.948	0.87	0.01
MTWA	1	0.61	-0.19	15.33	0.00	3.36	0.001	0.76	0.01
MTWA	**2**	**0.63**	**-0.10**	**14.05**	**0.00**	**3.22**	**0.001**	**0.78**	**0.01**
MTWA	3	0.63	-0.08	13.90	0.00	3.22	0.699	0.78	0.01
MTWA	4	0.64	-0.13	15.07	0.00	3.20	0.027	0.78	0.01
MTWA	5	0.64	-0.11	13.87	0.00	3.20	0.405	0.79	0.01
GDD0	1	0.67	67.56	3907.85	0.56	916.31	0.001	0.78	0.01
GDD0	**2**	**0.69**	**56.46**	**3702.27**	**0.24**	**880.33**	**0.001**	**0.79**	**0.01**
GDD0	3	0.70	57.82	3740.39	0.02	877.97	0.155	0.79	0.01
GDD0	4	0.70	34.31	4231.43	0.65	871.31	0.069	0.79	0.01
GDD0	5	0.70	36.70	4961.93	0.00	872.04	0.654	0.80	0.01
α	1	0.71	-0.01	0.64	0.00	0.16	0.001	0.79	0.01
α	**2**	**0.73**	**-0.01**	**0.65**	**0.00**	**0.15**	**0.001**	**0.80**	**0.01**
α	3	0.73	-0.01	0.65	0.00	0.15	0.593	0.80	0.01
α	4	0.74	-0.01	0.65	0.00	0.15	0.001	0.82	0.01
α	5	0.74	-0.01	0.68	0.00	0.15	0.431	0.83	0.01

Supplementary Figure 4.1. Map of distribution of the modern pollen samples the SPECIAL Modern Pollen Data Set (SMPDS) (Harrison, 2019) used to train the model.

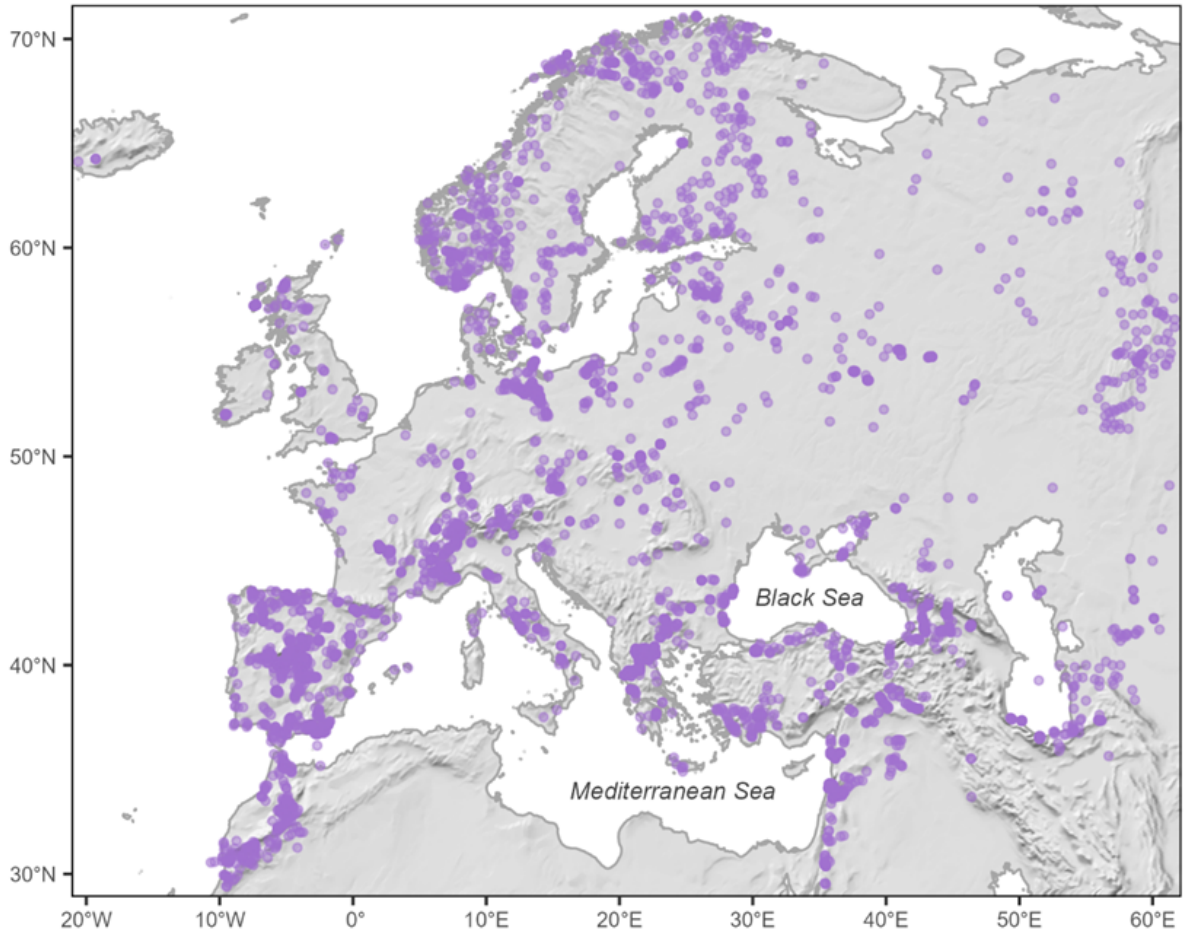

Supplementary Figure 4.2. Distribution of Hill N2 values of the fossil pollen samples. Samples with an N2 value of <2 (indicated by the red dotted line) were excluded from the analysis.

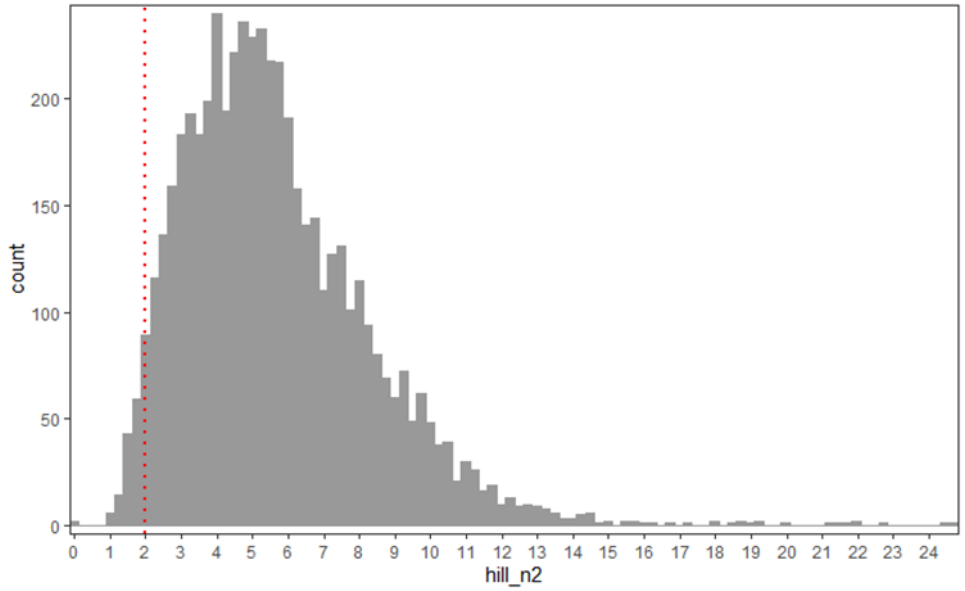

Supplementary Figure 4.3. Impact of correcting for the direct effect of changing CO2 levels following Prentice et al. (2022) on the reconstruction of α. The original reconstruction is shown in blue and the corrected reconstruction in red.

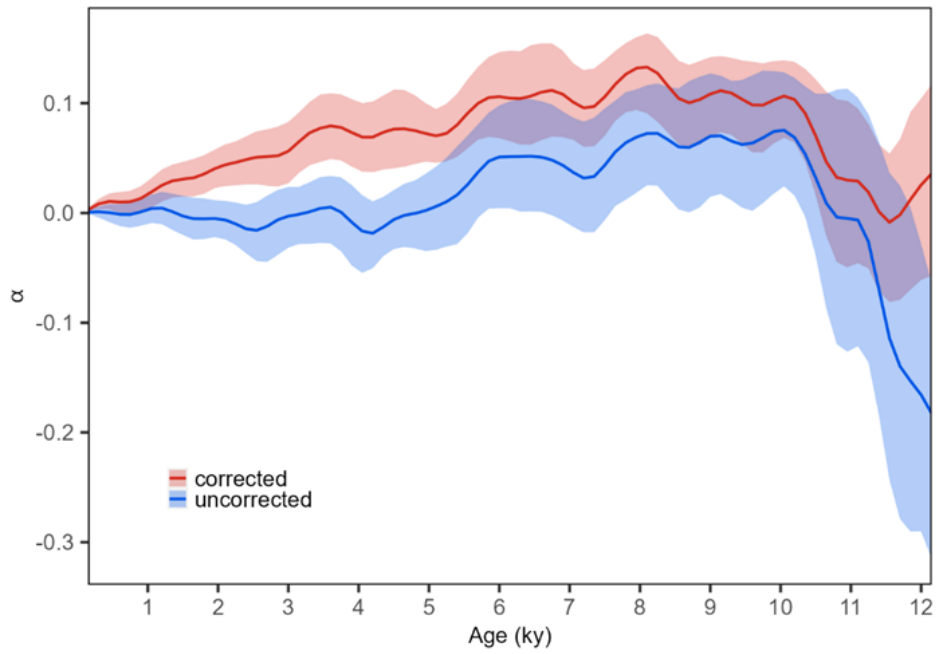

Supplementary Figure 4.4. Comparison of mean temperature of the coldest month (MTCO) and mean temperature of the warmest month (MTWA) in the EMBSeCBIO domain from the TRACE-21K-I simulation, showing both the calendar adjusted version (green) and non-calendar adjusted version (orange), and compared to the non-calendar adjusted outputs from the TRACE-21K-II (red) simulation.

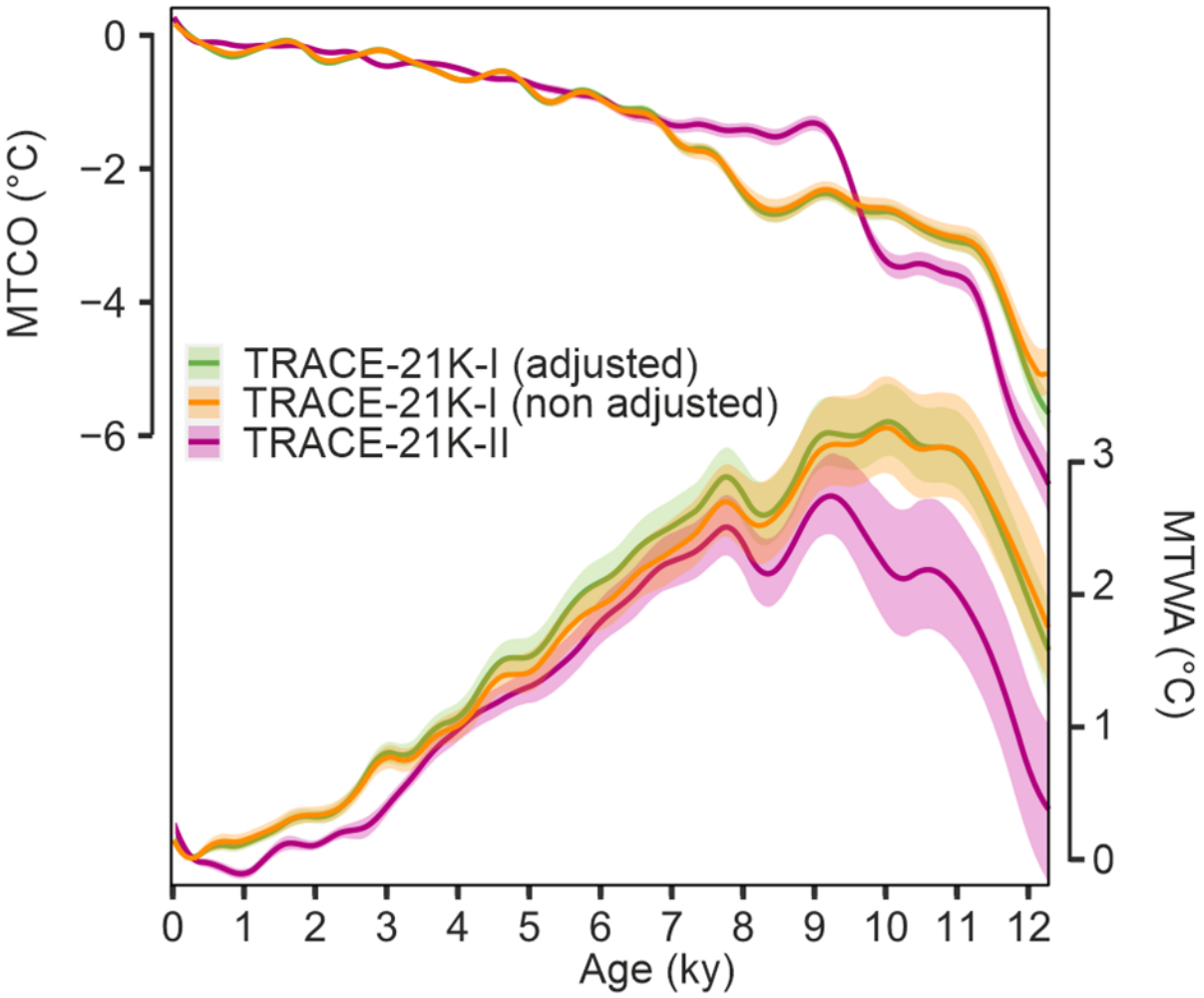

Supplementary Figure 5.5. Geopotential height, expressed as anomalies compared to present, from the LOVECLIM simulations for four key times during the Holocene: 11+0.15, 9+0.15, 6+0.15 and 3+0.15 ka.

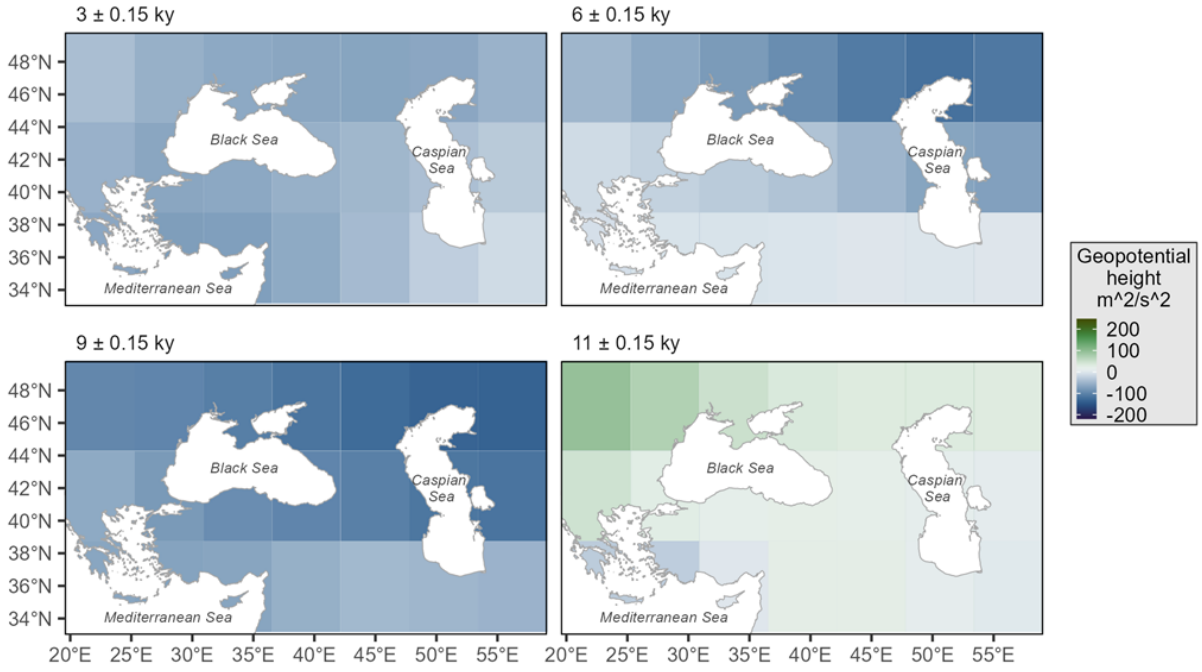

Chapter 5. Discussion

This chapter discusses the overall implications of my research on reconstructing vegetation and climate changes during the Holocene in the Eastern Mediterranean. The study comprised three individual papers, each focusing on specific aspects of the topic. Three integrative themes emerge from these papers: (1) the use of large-scale pollen data syntheses for climate and vegetation reconstructions, (2) the wide applicability of the approaches to other regions and their potential to address questions about the impact of environmental change on ancient civilizations, and (3) the insights gained from comparing reconstructions, which contribute to the understanding of the environmental history of the Eastern Mediterranean. The chapter concludes by identifying some future directions for moving forward from this research.

5.1 The use of large-scale pollen data syntheses for addressing uncertainties in the reconstruction of vegetation and climate

One of the key aspects of this research is the use of large-scale pollen data synthesis in reconstructing climate and vegetation changes. Through analysis of pollen datasets from multiple locations across the Eastern Mediterranean, the study was able to provide a regional perspective of past environmental dynamics.Relying on the interpretation of individual sites to obtain a regional picture is challenging because of the potential for idiosyncrasies between individual records due to site-specific differences, for example in basin size or sensitivity to changes in the local environment. Individual records can also have hiatuses which can cause significant data gaps. Comparing individual records is also difficult because of differences in the level of pollen taxonomic identification, age modelling, and in the case of climate reconstructions differences in the reconstruction methods (Sadori et al., 2011; Bini et al., 2019). Creating and using a regional database helps to overcome these challenges because it implies an effort to standardize the taxonomy, the chronologies, and the metadata to create a uniform dataset that can be analysed in a consistent manner. Regional data syntheses make it possible to benefit from the advantages of big data analysis (Harrison, 2017). This thesis explored how to use big data analysis to tackle uncertainties in reconstructing climate and vegetation from pollen data by developing or using predictive models and applying different statistical methods.

In this project, I used pollen data synthesized in two databases from two different efforts. The first is the Special Modern Pollen Data Set (SMPDS) version 1 (Villegas-Diaz & Harrison, 2022), which consists of over 6000 modern pollen samples collected from Europe and Western Asia. The second data set, made as part of the EMBSeCBIO project (Cordova et al., 2009; Marinova et al., 2018), focused on compiling fossil pollen data from the eastern Mediterranean region. It included data from various sources, including previously unpublished records. Alternative pollen databases exist for other regions, for example, the European Pollen Database (Davis et al., 2003, 2013), but although some sites from the eastern Mediterranean region are included in these other

databases, there was no specific database for this region until the EMBSeCBIO project was created. For this thesis, I further improved the EMBSeCBIO database (Harrison, Marinova, et al., 2021) by adding missing data and metadata and correcting errors. Ten new records were included in the database. Additionally, new age models were constructed for all of the records where there was sufficient information, 120 out of the total 180 records. These models were made using the latest version of the northern hemisphere Radiocarbon Age Calibration Curve, Intcal IntCal20 (Reimer et al., 2020) and the Bayesian ACcumulatiON histories for deposits software (BACON: Blaauw et al., 2021) coupled to the Supervised Age Models software (ageR: Villegas-Diaz et al., 2021) to concurrently execute multiple models and enhance the efficiency of the process. The updated age models allowed the establishment of a common chronological framework among the records, facilitating cross-comparison. The modern pollen data were used for the development and calibration of the new technique for the reconstruction of vegetation presented in Chapter 2 and the calibration of the technique for reconstructing climate presented in Chapter 4. Both methods rely on a training dataset that characterises the modern environmental gradients as a way to avoid dependency on expert knowledge. Particularly Chapter 2 introduced a method for reconstructing Natural Potential Vegetation types or biomes, that is vegetation in equilibrium with natural abiotic (e.g. climate, geology, lithology, hydrology) and biotic factors (e.g. competitors, dispersal vectors) while excluding anthropogenic influences (e.g. land use or water abstraction). The method relies on having a large modern dataset filtered to exclude pollen taxa linked to human activities (e.g. species of Poaceae explicitly identified as cultivars) and focuses on characterizing changes in pollen abundances within a broader climate-driven pattern rather than on local variations. The method assumes that local or interannual variability in pollen production is relatively minor compared to the more substantial variation present across climate gradients. The method is uniformitarian in that it assumes that the relationship between pollen abundances and climate factors has been constant through time.

The fossil data were used to make regional reconstructions of changes in vegetation (Chapter 3) and climate (Chapter 4) over the past 12,000 years. The creation of a large fossil data set allowed the application of techniques such as time-series compositing to extract a coherent regional signal of vegetation changes (Chapter 3) and climate changes (Chapter 4). Time-series compositing is advantageous because it highlights common features and trends across multiple records in a region and also helps minimize the impact of site-specific processes on the target signals. Compositing has been previously used in paleoenvironmental reconstruction with other types of data, such as with charcoal records (Power et al., 2008; Daniau et al., 2012) and speleothem isotope data (Parker, Harrison, Comas-Bru, et al., 2021; Parker, Harrison, & Braconnot, 2021) to obtain regional reconstructions in the form of time series. Compositing of individual charcoal records, for example, has allowed the identification of trends in wildfires since the Last Glacial Maximum both at global and regional scales (Power et al., 2008; Daniau et al., 2012; Marlon et al., 2013) as well as the response of wildfires to abrupt events during the glacial (Daniau et al., 2010). Compositing of speleothem oxygen isotopes has been used both to detect regional changes in climate (Parker, Harrison, Comas-Bru, et al., 2021) and also to identify the global nature of the 8.2 ka event in the Holocene (Parker & Harrison, 2022).

While time-series compositing has been used with some types of palaeodata, it has been less commonly exploited to reconstruct vegetation patterns at a regional scale. In this study, the compositing approach went beyond the traditional averaging of the abundance of arboreal/non-arboreal pollen, specific functional groups or indicative taxa (e.g. Morellón et al., 2018; Roberts et al., 2019) based on a limited number of selected sites. Instead, compositing was based on classifying pollen samples into vegetation types at the finest scale by accounting for all taxa in the pollen samples and then re-grouping them at coarser scales, e.g. of specific biomes or into closed and open vegetation types. This followed the approach of modern ecology for classifying modern vegetation patterns at different levels of resolution (e.g. Table 5.1). This approach is advantageous because it does not rely on only one or a few indicator taxa or functional groups and benefits from using a large number of sites, thus providing a more comprehensive understanding of vegetation changes in the region. Moreover, the construction of a single vegetation time series made it possible to compare the reconstructions with composite records from other types of data, including climate reconstructions or population estimates (Chapter 3).

Coarsest level	**Intermediate level**	**Finest level**
Open biomes	Savannas	C4 savannas with broad-leaved trees Coniferous woodlands Eucalypt woodlands
	Shrublands	Sclerophyllous shrublands Heathlands Low shrublands
	Grasslands	C3-dominated grasslands/steppes C4-dominated grasslands
Closed biomes	Forest	Needle-leaved forests Broad-leaved winter deciduous forests Broad-leaved summer deciduous forests Broad-leaved evergreen forests Sclerophyllous forests

Table 5.1 Examples of structurally based (climate-independent) biomes at different resolution levels (the coarsest on the left) based on modern ecological classifications (Woodward et al., 2004). After Pausas & Bond (2021).

Climate reconstructions have traditionally been presented as maps for specific time windows (COHMAP Members, 1988; Bartlein et al., 2011) for the evaluation of climate model simulations made in time-slice mode (Timm & Timmermann, 2007; Renssen et al., 2012; Smith & Gregory, 2012; Zhang et al., 2016; Braconnot, Zhu, et al., 2019; Braconnot, Crétat, et al., 2019; Crétat et al., 2020; Dallmeyer et al., 2022; Kapsch et al., 2022). However, with increasing computational power, transient climate simulations are becoming more common and this trend necessitates the

creation of observational time series for comparison (Carré et al., 2021; Parker, Harrison, Comas-Bru, et al., 2021; Marsicek et al., 2018). While there have been a few time-series composites of climate reconstructions (Davis et al., 2003; Marcott et al., 2013; Kaufman et al., 2020; Zhang et al., 2022), they have not focused on comparisons with transient climate simulations to explore forcing mechanisms or evaluate the models. Additionally, these composites have mostly focused on global or sub-continental scale patterns, which can blur smaller-scale patterns. In Chapter 3, I produced a composite specifically for the Eastern Mediterranean where I quantify the uncertainty in the reconstructed climate through bootstrap resampling of the records. This composite was then compared with transient climate simulations of the response to known changes in forcing, specifically changes in insolation and in the decay of the northern hemisphere ice sheets, in order to examine the degree to which the reconstructed climate changes could be related to these changes in forcing.

In Chapter 2, I used breakpoint analysis to identify the inception of reforestation after the Younger Dryas in the eastern Mediterranean region in the individual records from the regional composite. Previous studies identified the timing of reforestation by visually assessing the abundance of arboreal pollen (Wick et al., 2003; Joannin et al., 2014; Messager et al., 2017, 2013). However, this approach is highly subjective and may identify changes that are not statistically significant above the noise of the records. Furthermore, different analysts may use different thresholds to mark the start of a change in vegetation, leading to inconsistencies in the conclusions about the timing of an event. The use of statistical techniques to identify changes is important. Ön et al. (2021), for example, based on Bayesian analyses, have demonstrated that many records previously cited as evidence for the 4.2 ka event did not show statistically significant excursions using a Bayesian structural time series analysis. A similar conclusion was reached by Parker and Harrison (2022) showing through a global analysis that the 4.2 ka event was not registered in speleothem as a statistically significant excursion although, in contrast, the 8.2 ka event was a statistically significant excursion. The use of breakpoint analysis (Chapter 3) provided a strong and objective basis for demonstrating that the timing of reafforestation after the Younger Dryas varied across sites but showed no systematic delay from the east to the west of the region as had been previously claimed (Wick et al., 2003; Djamali et al., 2010; Messager et al., 2017).

Overall, this research highlights the importance of regional data synthesis combined with the advantages of statistical analysis to minimise uncertainties in the reconstruction of past climate and vegetation dynamics. Although the combination of an improved fossil database and the application of rigorous statistical approaches allowed me to shed light on a number of debates about the vegetation history of the region during the Holocene (Chapter 3), nevertheless some aspects of the research were constrained by limitations in the spatial and temporal distribution of the data. For example, the analysis of the archaeological radiocarbon data showed distinct patterns of changes in population across the region. However, certain culturally important areas with distinct trends in population compared to other regions, such as the Zagros Mountains in Mesopotamia and Anatolia, had too few pollen records or high-resolution records to make a comparison with the vegetation trends possible at this sub-regional scale. The Zagros Mountains

present a challenge when it comes to detailed analysis, as the only available record with a radiocarbon-based chronology covering the latter half of the Holocene (reaching back to 8200 years BP) is from Lake Zeribar. Similarly, despite having more than 10 records, the data from Anatolia is generally of very low resolution (averaging 500 years throughout the Holocene) precluding detailed analysis of the vegetation changes. These regions are not only culturally significant but also occupy a climate convergence zone and serve as meeting points for three major biodiversity hotspots (the Mediterranean, Caucasian, and Iranian-Anatolian). Additionally, they host exceptional levels of plant diversity and endemism (Noroozi et al., 2019). Given the importance of these regions, additional fieldwork to collect high-quality, high-resolution paleoenvironmental data would be beneficial and allow more comprehensive analyses of the impact of changes in human populations on vegetation in these culturally and ecologically significant areas.

Even in other regions of the eastern Mediterranean, additional data collection to generate higher-resolution records would be useful. The coarse resolution of some records in the EMBSeCBIO database, particularly older records, limited the application of statistical approaches. For example, the break-point analysis used to identify the timing of reafforestation (Chapter 3) was restricted to 19 records with at least 13 samples in the interval between 11600 and 7000 years BP. There were 121 records that could not be used in this analysis because they did not have sufficient resolution during this interval. Although various smoothing techniques or aggregating the data over larger time intervals can be applied to reduce noise and increase the signal-to-noise ratio, this can result in minimizing the apparent variability. The difficulty of obtaining a regional picture of vegetation changes was further aggravated because most of the high-resolution records are from the western part of the region. More high-resolution data is needed from the eastern part of the region to improve the accuracy of the analysis. However, despite the uncertainties of the breakpoint analysis, our results align with the palynological evidence. The pollen diagrams from the Didachara record, a high-resolution pollen record from the east of the Black Sea, indicate reforestation starting from the early Holocene (between ca. 10 and 11 ky), based on a chronology established with eleven radiocarbon samples (Connor et al., 2017)

Lack of data also underpins the focus on the Holocene in this thesis, as there are only 38 records that extend back beyond 11700 ca. years BP with an acceptable chronology. It would have been useful to have pre-Holocene records to address the debate about the suitability of environmental conditions for agriculture. The hypothesis that agriculture was not feasible before the Holocene due to low CO2 levels (Sage, 1995; Richerson et al., 2009), for example, could be empirically tested with more records from the deglaciation. Fourthermore, although the Holocene provides evidence of the vegetation response in climates warmer than today, and thus can provide insights into the response to future warming, the changes occurred slowly compared to projected 21st-century changes. There is a growing argument for studying rapid climate changes such as Dansgaard-Oeschger (D-O) events during the last glacial (e.g. Malmierca-Vallet et al., 2023) as a way of understanding the potential impacts of rapid climate changes in the future. Expanding the database to include records from the glacial period would provide solid reasons to study

pre-Holocene topics, aiding the understanding of past climate variability, the suitability of environmental conditions for agriculture, and potential implications of vegetation changes to past climate changes for future environmental changes.

Regardless of the gaps in data coverage, my research has demonstrated that a large-scale synthesis of pollen data analysed using statistical methods is highly valuable to provide climate and vegetation reconstructions at the regional scale and allows the identification and quantification of trends or significant deviations from a baseline (e.g. time-series of forest abundance or of climate anomalies), making it possible to examine the driving mechanisms behind these changes.

5.2 Widely applicable approaches

Another important theme that emerges from my research is the potential for climate and vegetation reconstruction techniques to be used more widely. The climate reconstructions (Chapter 4) were made using frequency-weighted Weighted Average Partial Least Squares regression (fxTWA-PLS2) (Liu et al., 2020, 2023), a modification of the Weighted Average Partial Least Squares regression (WA-PLS) approach (ter Braak & Juggins, 1993). fxTWA-PLS was developed (and has been shown) to minimise the tendency for regression-based methods to compress reconstructions towards the middle of the sampled climate range, a feature that would tend to minimise the temporal variability in climate reconstructions. The improved method has until now only been applied to reconstruct Holocene climate changes in the Iberian Peninsula (Liu et al., 2023). The application of this technique to the Eastern Mediterranean (Chapter 4) produced plausible reconstructions of changes in summer and winter temperature, as well as moisture availability, changes that are consistent with other evidence and the consequences of known changes in climate forcing. In the case of winter temperature, for example, the trends are consistent with insolation changes. In the case of summer temperature, the trends are broadly consistent with model simulations of the response to the combined effects of orbital and ice sheet forcing. Thus, the analyses in Chapter 4 suggest that fxTWA-PLS is a useful tool. Given that it produces more realistic reconstructions of climate variability through minimising compression, it would be valuable to apply this technique in other regions. The method relies on the existence of an extensive modern training data set, but such data sets are now available for most regions of the world.

A new method for reconstructing past vegetation changes has been developed and presented in this thesis. It produces more realistic reconstructions than the biomisation approach in the eastern Mediterranean region (Marinova et al., 2018). Furthermore, it reduced the tendency for small variations in pollen abundance to cause shifts between biomes, often referred to as the "flickering switch" problem, that was characteristic of the application of biomisation to make down-core reconstructions (Allen et al., 2000; Allen & Huntley, 2009). A further advantage of the new method is that it allows the explicit identification of non-analogue vegetation types, which

was not possible using the biomisation technique. Biomisation was originally designed to reconstruct vegetation in cases where there was only limited or no modern pollen data that could be used for calibration. The new method requires a large modern training dataset for calibration but, as pointed out above, these are now available for most regions of the world. Thus, this new technique could be usefully applied to reconstruct vegetation changes in other regions and, in particular, to update the global maps of vegetation produced by BIOME 6000 (Prentice et al., 2000; Prentice & Webb, 1998) and still routinely used for model evaluation. Given that most climate models now simulate vegetation dynamically (Fisher & Koven, 2020; Blyth et al., 2021; Argles et al., 2022) the creation of new global reconstructions would be useful. Furthermore, since the method minimizes the flickering switch problem, it can be used to create time series of vegetation changes. These time series, along with confidence intervals (Chapter 4), can be directly compared with transient simulations made with Earth System Models (Braconnot, Zhu, et al., 2019; Dallmeyer et al., 2022).

The techniques employed in this thesis have broad applicability and could be used for climate and vegetation reconstructions in other regions of the world. The availability of extensive modern training datasets and the ability to address common challenges in reconstruction methodologies make these approaches valuable tools for studying past environmental changes and evaluating climate models.

5.3 Insights into the Environmental History of the Eastern Mediterranean from comparing reconstructions

The third integrative theme in the study focuses on comparing vegetation and climate reconstructions with alternative reconstructions derived from different data sources or model simulations. Systematic comparison of multiple sources of climate information provides a better understanding of the dynamics of the system than relying on a single source because many types of records can be influenced by multiple factors. The oxygen-isotope record from speleothems, for example, is often interpreted in terms of changes in moisture availability, particularly in the eastern Mediterranean region (e.g. Burstyn et al., 2019), but these records could be affected by changes in moisture source or in temperature (Fleitmann et al., 2009; Göktürk, 2010; Göktürk et al., 2011; M. J. Jacobson et al., 2021; Bar-Matthews & Ayalon, 2004). The comparison with reconstructed plant available moisture (Chapter 4) showed that the speleothem records from the eastern Mediterranean were broadly coherent with the pollen-based reconstructions thus confirming that they are indeed indicators of moisture availability, at least in this region.

Climate changes have caused the major changes in regional vegetation through the Holocene (Huntley & Prentice, 1988; Sadori et al., 2011; Peyron et al., 2017; Joannin et al., 2014). However, debates exist regarding the extent to which changes in regional vegetation represent human influence on landscapes (Roberts et al., 2001; Connor & Sagona, 2007; Connor & Kvavadze, 2009; Roberts et al., 2011). Chapter 3 explored human influence over time by comparing pollen-based

reconstructions with population changes derived from archaeological radiocarbon dates summed probability distributions (SPD curves). The utilization of archaeological radiocarbon dating in studying prehistoric populations was pioneered by Rick (1987). This method assumes that greater population sizes result in more cultural carbon, evident in radiocarbon age frequency distributions (Rick, 1987; Surovell & Brantingham, 2007).

Radiocarbon dating offers a more accurate chronological structure compared to other methods like the molecular clock or cultural phases (Gamble et al., 2005; Wang et al., 2014). Despite its wide application, challenges persist (Surovell et al., 2009; Williams, 2012; Mithen & Wicks, 2021). Mithen & Wicks (2021) have identified seven main sources of bias: (a) Cultural Variation Bias, where different societies produce varying amounts of material suitable for radiocarbon dating; sedentary societies, for example, may generate more organic waste than mobile hunter-gatherers; (b) Methodology Bias, where certain archaeological periods are overrepresented in the radiocarbon record due to targeted research projects; (c) Single Site Dating Bias, characterized by variation in the number of radiocarbon dates from single sites, influenced by the historical trajectory of research; (d) Region Size and Diversity Bias, arising from uneven distribution of hunter-gatherers across the landscapes that affects the representativeness of archaeological coverage. Small study areas may not secure a representative sample, while continental-scale models risk blurring signals; (e) Calibration Curve Bias, stemming from natural variations in atmospheric carbon concentration over time, resulting in plateaus in the calibration curve which affects the precision of calibrated date ranges such that the dating precession of individual records varies through time; (f) Landscape Change Bias, where environmental changes, such as sea level rise, can induce biased preservation and discovery of archaeological sites, thereby influencing the distribution of radiocarbon dates; (g) Mobility and Settlement Pattern Bias, where hunter-gatherer mobility and settlement patterns shape the creation and preservation of archaeological sites, yielding diverse archaeological records based on the distribution of resources in the environment.

Efforts for correcting these biases, including comparisons with independent proxies of prehistoric population growth enhance the reliability of population estimates using radiocarbon data (Williams, 2012; Robinson et al., 2019; Mithen & Wicks, 2021). SPD curves from the eastern Mediterranean have proved valuable in examining relationships among vegetation, climate, and population changes at a subregional level. The SPD curve for Greece, for example, aligns with the archaeological narrative as documented by (Weiberg et al., 2019). However, in other subregions such as Anatolia, the validity of the SPD curve may be less reliable because of the limited number of dates (Roberts et al., 2019). While our vegetation reconstructions exhibit greater similarity to climate patterns than to the SPDs, suggesting that human activities had a limited impact on vegetation history, it would be useful to re-examine this when more archaeological data is available, either in the form of more systematic collections of radiocarbon dates from which SPDs could be created on a sub-regional scale or through combining this information with other sources of data such as archaeological demographies (see e.g. Timmermann et al., 2022).

There have been previous studies in the eastern Mediterranean that have explored potential causes of observed changes by comparing vegetation, climate, and population density indicators, but they have used vegetation reconstructions based on the abundance of specific taxonomic groups, vegetation clusters based on dominant taxa (e.g. Fyfe et al., 2019) or of arboreal/non-arboreal pollen (e.g. Roberts et al., 2019) and climate reconstructions from existing sources based on different indicators or methodologies (Palmisano et al., 2021; Flohr et al., 2016). The approach taken in Chapter 3 is more systematic in that it uses vegetation and climate reconstructions from sites across the eastern Mediterranean region made using consistent methodologies. By combining two dominant forest biomes, temperate deciduous malacophyll broadleaf forest (TEDE) and cool mixed evergreen needleleaf and deciduous broadleaf forest (CMIX), we aimed to comprehensively identify and quantify forested sites across the landscape, rather than focusing on individual biomes. This approach enabled the construction of forest time-series, shedding light on the prevalence of tree-dominated landscapes in the region. This method provides insights into the environmental history of the area. For instance, the systematic comparison of climate, reconstructed from pollen and as inferred from speleothem records, pollen-based vegetation changes, and archaeological indicators of population changes showed that climate was the major driver of vegetation changes during the second half of the Holocene (Chapter 3). This is contrary to the hypothesis that anthropogenic activities were the primary driver of vegetation changes during this period (Pons & Quézel, 1998; Reille & Pons, 1992; Roberts, Brayshaw, et al., 2011; Roberts, Eastwood, et al., 2011) but supports the alternative interpretation that has been put forward that, despite the substantial influence exerted by human activities on the region, climate was the strongest driver shaping vegetation patterns for the Holocene as a whole (Huntley & Prentice, 1988; Sadori et al., 2011; Pérez-Obiol et al., 2011; Marquer et al, 2017).

The debate about climate versus human influence on vegetation has largely relied on investigations at individual sites, and indeed my analysis does not rule out an anthropogenic influence at the local scale. However, the ability to examine patterns across a region is crucial to understanding the drivers of environmental change. Regional scale analysis is greatly facilitated by the efforts that have been made to compile data from various sources, such as the SISAL database for speleothem data (Comas-Bru et al., 2020) and the p3k14c global database for archaeological radiocarbon dates (Bird et al., 2022). These databases facilitate the comparison of reconstructions from different sources, enabling a more comprehensive exploration of reconstructed vegetation patterns and their potential drivers.

The comparison of pollen-based climate and vegetation reconstructions with model simulations is a valuable method for understanding past climate changes, since the observations provide information about the large-scale patterns of change and the underlying causes and mechanisms can be investigated through models. The Cooperative Holocene Mapping Project (COHMAP) utilized this approach by comparing reconstructions of global climate at 3000-year intervals from the Last Glacial Maximum to the present based on pollen and lake records with model simulations driven by known changes in climate forcing (COHMAP Members, 1988; Wright et al., 1993). One key result from these comparisons was the attribution of the waxing and waning of the

African monsoon since the Last Glacial Maximum to changes in orbital forcing (Kutzbach & Street-Perrott, 1985). This approach of explaining observations using model simulations has been expanded to include a wider range of paleoclimate records, such as snowline reconstructions (e.g. Kageyama et al., 2005) and charcoal (Daniau et al., 2012), as well as to explore vegetation changes (Ni et al., 2006). The use of transient model simulations to explain observed changes is a more recent phenomenon (e.g. Parker et al., 2021). However, as the analyses in Chapter 4 show, they provide a powerful tool to explain observed changes, in particular where these changes are not straightforward responses to external forcing but involve interactions between different forcings.

Climate reconstructions based on sites in the eastern Mediterranean have been included in larger-scale continental or hemispheric reconstructions (Mauri et al., 2015; Herzschuh et al., 2022), but these studies did not focus on the climate evolution of the eastern Mediterranean itself. Nor did they use data-model comparison to explore the mechanisms driving the observed regional changes. The comparison of pollen-based quantitative climate reconstruction with different transient simulations (Chapter 4) shows that the inclusion of ice sheets and meltwater forcing, in addition to changes in orbital forcing and greenhouse gases, was necessary to match the patterns of the reconstructed climate variables in the early and middle Holocene. This argues that the apparently delayed response of summer temperature to changes in summer insolation is likely a reflection of the persistence of the Laurentide and Fennoscandian ice sheets.

Comparing reconstructed and simulated climates also offers insights into the origins of agriculture in the region. Our climate reconstructions show drier conditions at the Holocene beginning, followed by a rapid increase in plant-available moisture from ca. 10.5 to 9 ka (ka: calibrated thousand years before present), potentially influencing the establishment of agricultural economies in the Eastern Mediterranean, dated ca. 10.6 ky (during the Pre-Pottery Neolithic B: ca.10.6 – 8.8 ky) (Goring-Morris et al., 2009; Dietrich et al., 2019). The nature and timing of this transition are still debated, with evidence at the Levant suggesting "pre-domestication cultivation" involving deliberate use of wild cereals and pulses well before clear domestication, complicating the identification and full understanding of this shift. For instance, sites like Göbekli Tepe and Dhra', in the Levant, display evidence of labour-intensive practices similar to those related to developed agricultural systems, supporting signs of pre-domestication cultivation (Colledge et al., 2018; Dietrich et al., 2019). Contemporary southern sites share technology, materials, and symbolisms (e.g., WF16: Mithen et al., 2023). A new ecological model challenges the traditional view, proposing that pre-domestication cultivation in the Levant did not rely on regular tillage but rather on low-input exploitation practices that aligned with the ecological strategies of competitive large-seeded grasses (Weide et al., 2022). Our climate reconstructions suggest optimal agricultural conditions in the Eastern Mediterranean were not achieved until around 10.5 ky due to rising CO_2 and warming. This likely facilitated the transition from long-term pre-domestication cereal use to an agricultural economy capitalizing on increased productivity.

These findings highlight the significance of considering multiple lines of evidence, including pollen-based reconstructions and model simulations, to gain a comprehensive understanding of past climate variability and its impact on vegetation and human activities. By combining different data sources and approaches, it is possible to explore the mechanisms behind climatic evolution and its implications for environmental and societal changes in specific regions, such as the eastern Mediterranean.

5.4 Future research directions

There are several avenues for future research, particularly in the field of human-environment interactions, that would build upon the findings of the three papers in this thesis.

The timing of the transition to agriculture in the eastern Mediterranean is still debated (E.G. Weide et al., 2021). Crop models offer a methodological approach (Qiao et al., 2020, 2021, 2023; Harrison, Cramer, et al., 2021) to investigate the cereal yields during the Late Pleistocene and the "pre-domestication cultivation period". These models determine plant productivity and seed yield as a function of environmental conditions, including climate and atmospheric CO2 levels. The regional climate reconstructions presented in Chapter 4, would be an essential input for crop modelling. Comparisons with archaeological data on crop yields could be used to evaluate the model's performance. The vegetation reconstructions presented in Chapter 3 provide another source of data to test the accuracy of these models since they provide constraints on estimates of gross primary production. Integrating these reconstructions of climate and vegetation with modelling techniques could provide insights into the constraints on food supplies and thus the timing of the transition to agricultural economies.

Another potential research area using the new methodology presented in Chapter 2 is to predict human-related vegetation features, such as crops, human-disturbed forests, or anthropogenic biomes, from pollen samples. The model could be trained using existing maps of modern vegetation types related to human activities, such as the maps of Anthropogenic Biomes (Anthromes: Ellis et al., 2010; Ellis & Ramankutty, 2008), Global Human Modification (Kennedy et al., 2018; Theobald et al., 2020), Human Footprint Index (Sanderson et al., 2002) and Low Impact Areas (Jacobson et al., 2019). One potential challenge of this approach would be the correct selection of the map of modern vegetation types related to human activities, as each one relies on different stressors to define a human impacted landscape, and as a consequence, such maps show limited agreement for limited regions (Riggio et al. 2019). Alternatively, the model could be trained with specific factors of interest, including cropland or grazing land, available in the History Database of the Global Environment (HYDE version 3.2: Klein Goldewijk et al., 2017). It could then be applied to reconstruct anthropogenically impacted vegetation types through time. This data-driven approach would provide a quantitative and objective assessment of human impacts on vegetation, helping to resolve controversies regarding the relative importance of climate change and human activities in shaping landscapes over time.

Understanding the extent and timing of human impacts on vegetation is crucial because land cover changes resulting from anthropogenic activities can have significant implications for climate and the carbon cycle (Harrison et al., 2020; Myhre et al., 2013; Perugini et al., 2017; Pongratz et al., 2010). By utilizing data-driven reconstructions of anthropogenic vegetation, it would be possible to evaluate the outputs of anthropogenic land use models and assess their accuracy (Harrison et al., 2020). Evaluations of such models currently rely on vegetation cover estimates based on the REVEALS pollen-source area model (Sugita, 2007), the geographic coverage of which is limited by the availability of pollen productivity estimates (RPPs). By employing my new methodology for reconstructing vegetation to mapping anthropogenic vegetation types would provide an alternative approach to reconstruct anthropogenic land use scenarios. Existing reconstructions of the extent of anthropogenic impacts on the landscape during the Holocene (e.g. Ramankutty & Foley, 1999; Pongratz et al., 2008; Kaplan et al., 2017; Klein Goldewijk, Beusen, et al., 2017b; Klein Goldewijk, Dekker, et al., 2017) differ considerably from one another because, although they all assume that the extent of anthropogenic influence is a function of population density, they make different assumptions in order to extrapolate this influence (Gaillard et al., 2010; Kaplan et al., 2017; Harrison et al., 2020). This is responsible for considerably different estimates of the climate impact of anthropogenic land use and land cover changes (Vavrus et al., 2008; Pongratz et al., 2010; He et al., 2014; Smith et al., 2016) . Using an alternative data-driven reconstruction of anthropogenic vegetation as input to climate models could provide a more accurate estimate of human influence on past climates.

These two research directions offer opportunities to improve our understanding of human-environment interactions at different spatial and temporal scales. Employing improved methodologies for reconstructing past environmental changes, and integrating them with modelling would contribute to a deeper understanding of our past and help to inform how we might adapt to future climate changes.

5.5 References

Allen, J. R. M., & Huntley, B. (2009). Last Interglacial palaeovegetation, palaeoenvironments and chronology: A new record from Lago Grande di Monticchio, southern Italy. Quaternary Science Reviews, 28(15), Article 15. https://doi.org/10.1016/j.quascirev.2009.02.013

Allen, J. R. M., Watts, W. A., & Huntley, B. (2000). Weichselian palynostratigraphy, palaeovegetation and palaeoenvironment; the record from Lago Grande di Monticchio, southern Italy. Quaternary International, 73–74, 91–110. https://doi.org/10.1016/S1040-6182(00)00067-7

Argles, A. P. K., Moore, J. R., & Cox, P. M. (2022). Dynamic Global Vegetation Models: Searching for the balance between demographic process representation and computational tractability. PLOS Climate, 1(9), e0000068. https://doi.org/10.1371/journal.pclm.0000068

Asouti, E., & Fuller, D. Q. (2012). From foraging to farming in the southern Levant: The development of Epipalaeolithic and Pre-pottery Neolithic plant management strategies. Vegetation History and Archaeobotany, 21(2), 149–162. https://doi.org/10.1007/s00334-011-0332-0

Bar-Matthews, M., & Ayalon, A. (2004). Speleothems as palaeoclimate indicators, a case study from Soreq Cave located in the Eastern Mediterranean Region, Israel. In R. W. Battarbee, F. Gasse, & C. E. Stickley (Eds.), Past Climate Variability through Europe and Africa (pp. 363–391). Springer Netherlands. https://doi.org/10.1007/978-1-4020-2121-3_18

Bartlein, P. J., Harrison, S. P., Brewer, S., Connor, S., Davis, B. A. S., Gajewski, K., Guiot, J., Harrison-Prentice, T. I., Henderson, A., Peyron, O., Prentice, I. C., Scholze, M., Seppä, H., Shuman, B., Sugita, S., Thompson, R. S., Viau, A. E., Williams, J., & Wu, H. (2011). Pollen-based continental climate reconstructions at 6 and 21 ka: A global synthesis. Climate Dynamics, 37(3), Article 3. https://doi.org/10.1007/s00382-010-0904-1

Bar-Yosef, O., Bar-Matthews, M., & Ayalon, A. (2017). 12,000–11,700 cal BP: The Collapse of Foraging and Origins of Cultivation in Western Asia. In H. Weiss (Ed.), Megadrought and Collapse: From Early Agriculture to Angkor (p. 0). Oxford University Press. https://doi.org/10.1093/oso/9780199329199.003.0002

Bevan, A., Colledge, S., Fuller, D., Fyfe, R., Shennan, S., & Stevens, C. (2017). Holocene fluctuations in human population demonstrate repeated links to food production and climate. Proceedings of the National Academy of Sciences of the United States of America, 114(49), E10524–E10531. https://doi.org/10.1073/pnas.1709190114

Bini, M., Zanchetta, G., Perşoiu, A., Cartier, R., Català, A., Cacho, I., Dean, J. R., Di Rita, F., Drysdale, R. N., Finnè, M., Isola, I., Jalali, B., Lirer, F., Magri, D., Masi, A., Marks, L., Mercuri, A. M., Peyron, O., Sadori, L., … Brisset, E. (2019). The 4.2 ka BP Event in the Mediterranean region: An overview. Climate of the Past, 15(2), 555–577. https://doi.org/10.5194/cp-15-555-2019

Bird, D., Miranda, L., Vander Linden, M., Robinson, E., Bocinsky, R. K., Nicholson, C., Capriles, J. M., Finley, J. B., Gayo, E. M., Gil, A., d'Alpoim Guedes, J., Hoggarth, J. A., Kay, A., Loftus, E., Lombardo, U., Mackie, M., Palmisano, A., Solheim, S., Kelly, R. L., & Freeman, J. (2022). P3k14c, a synthetic global database of archaeological radiocarbon dates. Scientific Data, 9(1), 27. https://doi.org/10.1038/s41597-022-01118-7

Blaauw, M., Christen, J. A., Lopez, M. A. A., Vazquez, J. E., V, O. M. G., Belding, T., Theiler, J., Gough, B., & Karney, C. (2021). rbacon: Age-Depth Modelling using Bayesian Statistics (2.5.6) [R]. https://CRAN.R-project.org/package=rbacon

Blyth, E. M., Arora, V. K., Clark, D. B., Dadson, S. J., De Kauwe, M. G., Lawrence, D. M., Melton, J. R., Pongratz, J., Turton, R. H., Yoshimura, K., & Yuan, H. (2021). Advances in Land Surface Modelling. Current Climate Change Reports, 7(2), 45–71. https://doi.org/10.1007/s40641-021-00171-5

Braconnot, P., Crétat, J., Marti, O., Balkanski, Y., Caubel, A., Cozic, A., Foujols, M.-A., & Sanogo, S. (2019). Impact of Multiscale Variability on Last 6,000 Years Indian and West African Monsoon Rain. Geophysical Research Letters, 46(23), 14021–14029. https://doi.org/10.1029/2019GL084797

Braconnot, P., Zhu, D., Marti, O., & Servonnat, J. (2019). Strengths and challenges for transient Mid- to Late Holocene simulations with dynamical vegetation. Climate of the Past, 15(3), 997–1024. https://doi.org/10.5194/cp-15-997-2019

Burstyn, Y., Martrat, B., Lopez, J. F., Iriarte, E., Jacobson, M. J., Lone, M. A., & Deininger, M. (2019). Speleothems from the Middle East: An example of water limited environments in the SISAL database. Quaternary, 2(2), 16. https://doi.org/10.3390/quat2020016

Carré, M., Braconnot, P., Elliot, M., d'Agostino, R., Schurer, A., Shi, X., Marti, O., Lohmann, G., Jungclaus, J., Cheddadi, R., Abdelkader di Carlo, I., Cardich, J., Ochoa, D., Salas Gismondi, R., Pérez, A., Romero, P. E., Turcq, B., Corrège, T., & Harrison, S. P. (2021). High-resolution marine data and transient simulations support orbital forcing of ENSO amplitude since the mid-Holocene. Quaternary Science Reviews, 268, 107125. https://doi.org/10.1016/j.quascirev.2021.107125

Chaput, M. A., & Gajewski, K. (2016). Radiocarbon dates as estimates of ancient human population size. Anthropocene, 15, 3–12. https://doi.org/10.1016/j.ancene.2015.10.002

COHMAP Members. (1988). Climatic Changes of the Last 18,000 Years: Observations and Model Simulations. Science, 241(4869), Article 4869. https://doi.org/10.1126/science.241.4869.1043

Colledge, S., Conolly, J., Finlayson, B., & Kuijt, I. (2018). New insights on plant domestication, production intensification, and food storage: The archaeobotanical evidence from PPNA Dhra'. Levant, 50(1), 14–31. https://doi.org/10.1080/00758914.2018.1424746

Comas-Bru, L., Rehfeld, K., Roesch, C., Amirnezhad-Mozhdehi, S., Harrison, S. P., Atsawawaranunt, K., Ahmad, S. M., Brahim, Y. A., Baker, A., Bosomworth, M., Breitenbach, S. F. M., Burstyn, Y., Columbu, A., Deininger, M., Demény, A., Dixon, B., Fohlmeister, J., Hatvani, I. G., Hu, J., … SISAL Working Group members. (2020). SISALv2: A comprehensive speleothem isotope database with multiple age-depth models. Earth System Science Data, 12(4), 2579–2606. https://doi.org/10.5194/essd-12-2579-2020

Connor, S., & Kvavadze, E. V. (2009). Modelling late Quaternary changes in plant distribution, vegetation and climate using pollen data from Georgia, Caucasus. Journal of Biogeography, 36(3), 529–545. https://doi.org/10.1111/j.1365-2699.2008.02019.x

Connor, S., & Sagona, A. (2007). Environment and society in the late prehistory of southern Georgia, Caucasus. In B. Lyonnet (Ed.), The Cultures of the Caucasus (6th to 3rd centuries B.C.E): Their Relations with the Near East (Vol. 3, pp. 21–36). CNRS Editions.

Connor, S., Colombaroli, D., Confortini, F., Gobet, E., Ilyashuk, B. P., Ilyashuk, E. A., van Leeuwen, J. F. N., Lamentowicz, M., van der Knaap, W. O., Malysheva, E., Marchetto, A., Margalitadze, N., Mazei, Y., Mitchell, E. A. D., Payne, R. J., & Ammann, B. (2017). Long-term population dynamics: Theory

and reality in a peatland ecosystem. The Journal of Ecology, 106(1), Article 1. https://doi.org/10.1111/1365-2745.12865

Cordova, C. E., Harrison, S. P., Mudie, P. J., Riehl, S., Leroy, S. A. G., & Ortiz, N. (2009). Pollen, plant macrofossil and charcoal records for palaeovegetation reconstruction in the Mediterranean-Black Sea Corridor since the Last Glacial Maximum. Quaternary International, 197(1–2), 12–26. https://doi.org/10.1016/j.quaint.2007.06.015

Crétat, J., Braconnot, P., Terray, P., Marti, O., & Falasca, F. (2020). Mid-Holocene to present-day evolution of the Indian monsoon in transient global simulations. Climate Dynamics, 55(9), 2761–2784. https://doi.org/10.1007/s00382-020-05418-9

Dallmeyer, A., Kleinen, T., Claussen, M., Weitzel, N., Cao, X., & Herzschuh, U. (2022). The deglacial forest conundrum. Nature Communications, 13(1), Article 1. https://doi.org/10.1038/s41467-022-33646-6

Daniau, A.-L., Bartlein, P. J., Harrison, S. P., Prentice, I. C., Brewer, S., Friedlingstein, P., Harrison-Prentice, T. I., Inoue, J., Izumi, K., Marlon, J. R., Mooney, S., Power, M. J., Stevenson, J., Tinner, W., Andrič, M., Atanassova, J., Behling, H., Black, M., Blarquez, O., … Zhang, Y. (2012). Predictability of biomass burning in response to climate changes. Global Biogeochemical Cycles, 26(4). https://doi.org/10.1029/2011GB004249

Daniau, A.-L., Harrison, S. P., & Bartlein, P. J. (2010). Fire regimes during the Last Glacial. Quaternary Science Reviews, 29(21), 2918–2930. https://doi.org/10.1016/j.quascirev.2009.11.008

Davis, B. A. S., Brewer, S., Stevenson, A. C., & Guiot, J. (2003). The temperature of Europe during the Holocene reconstructed from pollen data. Quaternary Science Reviews, 22(15), Article 15. https://doi.org/10.1016/S0277-3791(03)00173-2

Davis, B. A. S., Zanon, M., Collins, P., Mauri, A., Bakker, J., Barboni, D., Barthelmes, A., Beaudouin, C., Bjune, A. E., Bozilova, E., Bradshaw, R. H. W., Brayshay, B. A., Brewer, S., Brugiapaglia, E., Bunting, J., Connor, S., de Beaulieu, J.-L., Edwards, K., Ejarque, A., … Kaplan, J. O. (2013). The European Modern Pollen Database (EMPD) project. Vegetation History and Archaeobotany, 22(6), Article 6. https://doi.org/10.1007/s00334-012-0388-5

Dietrich, L., Meister, J., Dietrich, O., Notroff, J., Kiep, J., Heeb, J., Beuger, A., & Schütt, B. (2019). Cereal processing at Early Neolithic Göbekli Tepe, southeastern Turkey. PLOS ONE, 14(5), e0215214. https://doi.org/10.1371/journal.pone.0215214

Djamali, M., Akhani, H., Andrieu-Ponel, V., Braconnot, P., Brewer, S., de Beaulieu, J.-L., Fleitmann, D., Fleury, J., Gasse, F., Guibal, F., Jackson, S. T., Lézine, A.-M., Médail, F., Ponel, P., Roberts, N., & Stevens, L. (2010). Indian summer monsoon variations could have affected the early-Holocene woodland expansion in the Near East. The Holocene, 20(5), 813–820. https://doi.org/10.1177/0959683610362813

Ellis, E. C., Klein Goldewijk, K., Siebert, S., Lightman, D., & Ramankutty, N. (2010). Anthropogenic transformation of the biomes, 1700 to 2000. Global Ecology and Biogeography, 19(5), 589–606. https://doi.org/10.1111/j.1466-8238.2010.00540.x

Ellis, E. C., & Ramankutty, N. (2008). Putting people in the map: Anthropogenic biomes of the world. Frontiers in Ecology and the Environment, 6(8), 439–447. https://doi.org/10.1890/070062

Fisher, R. A., & Koven, C. D. (2020). Perspectives on the Future of Land Surface Models and the Challenges of Representing Complex Terrestrial Systems. Journal of Advances in Modeling Earth Systems, 12(4), e2018MS001453. https://doi.org/10.1029/2018MS001453

Fleitmann, D., Cheng, H., Badertscher, S., Edwards, R. L., Mudelsee, M., Göktürk, O. M., Fankhauser, A., Pickering, R., Raible, C. C., Matter, A., Kramers, J., & Tüysüz, O. (2009). Timing and climatic impact of Greenland interstadials recorded in stalagmites from northern Turkey. Geophysical Research Letters, 36(19), L19707. https://doi.org/10.1029/2009GL040050

Flohr, P., Fleitmann, D., Matthews, R., Matthews, W., & Black, S. (2016). Evidence of resilience to past climate change in Southwest Asia: Early farming communities and the 9.2 and 8.2 ka events. Quaternary Science Reviews, 136, 23–39. https://doi.org/10.1016/j.quascirev.2015.06.022

Fyfe, R. M., Woodbridge, J., Palmisano, A., Bevan, A., Shennan, S., Burjachs, F., Legarra Herrero, B., García Puchol, O., Carrión, J.-S., Revelles, J., & Roberts, C. N. (2019). Prehistoric palaeodemographics and regional land cover change in eastern Iberia. The Holocene, 29(5), 799–815. https://doi.org/10.1177/0959683619826643

Gaillard, M.-J., Sugita, S., Mazier, F., Trondman, A.-K., Broström, A., Hickler, T., Kaplan, J. O., Kjellström, E., Kokfelt, U., Kuneš, P., Lemmen, C., Miller, P., Olofsson, J., Poska, A., Rundgren, M., Smith, B., Strandberg, G., Fyfe, R., Nielsen, A. B., … Seppä, H. (2010). Holocene land-cover reconstructions for studies on land cover-climate feedbacks. Climate of the Past, 6(4), 483–499. https://doi.org/10.5194/cp-6-483-2010

Gamble, C., Davies, W., Pettitt, P., Hazelwood, L., & Richards, M. (2005). The Archaeological and Genetic Foundations of the European Population during the Late Glacial: Implications for 'Agricultural Thinking'. Cambridge Archaeological Journal, 15(2), 193–223. https://doi.org/10.1017/S0959774305000107

Goring-Morris, A., Hovers, E., & Belfer-Cohen, A. (2009). The dynamics of Pleistocene and early Holocene settlement patterns and human adaptations in the Levant: An overview. In J. Shea & D. Lieberman (Eds.), Transitions in Prehistory. Essays in Honour of Ofer Bar-Yosef. (pp. 185–252). Oxford and Oakville: Oxbow Books.

Göktürk, O. M. (2010). Climate in the Eastern Mediterranean through the Holocene inferred from Turkish stalagmites [Ph.D., University of Bern]. https://occrdata.unibe.ch/students/theses/phd/68.pdf

Göktürk, O. M., Fleitmann, D., Badertscher, S., Cheng, H., Edwards, R. L., Leuenberger, M., Fankhauser, A., Tüysüz, O., & Kramers, J. (2011). Climate on the southern Black Sea coast during the Holocene: Implications from the Sofular Cave record. Quaternary Science Reviews, 30(19), 2433–2445. https://doi.org/10.1016/j.quascirev.2011.05.007

Harrison, S. P. (2017). The big data revolution and paleoecology. Past Global Changes Magazine, 25(2), 96–97. https://doi.org/10.22498/pages.25.2.96

Harrison, S. P., Cramer, W., Franklin, O., Prentice, I. C., Wang, H., Brännström, Å., de Boer, H., Dieckmann, U., Joshi, J., Keenan, T. F., Lavergne, A., Manzoni, S., Mengoli, G., Morfopoulos, C., Peñuelas, J., Pietsch, S., Rebel, K. T., Ryu, Y., Smith, N. G., … Wright, I. J. (2021). Eco-evolutionary optimality as a means to improve vegetation and land-surface models. New Phytologist, 231(6), 2125–2141. https://doi.org/10.1111/nph.17558

Harrison, S. P., Gaillard, M.-J., Stocker, B. D., Vander Linden, M., Klein Goldewijk, K., Boles, O., Braconnot, P., Dawson, A., Fluet-Chouinard, E., Kaplan, J. O., Kastner, T., Pausata, F. S. R., Robinson, E., Whitehouse, N. J., Madella, M., & Morrison, K. D. (2020). Development and testing scenarios for implementing land use and land cover changes during the Holocene in Earth system model experiments. Geoscientific Model Development, 13(2), Article 2. https://doi.org/10.5194/gmd-13-805-2020

Harrison, S. P., Marinova, E., & Cruz-Silva, E. (2021). EMBSeCBIO pollen database [Data set]. University of Reading. https://doi.org/10.17864/1947.309

He, F., Vavrus, S. J., Kutzbach, J. E., Ruddiman, W. F., Kaplan, J. O., & Krumhardt, K. M. (2014). Simulating global and local surface temperature changes due to Holocene anthropogenic land cover change. Geophysical Research Letters, 41(2), 623–631. https://doi.org/10.1002/2013GL058085

Herzschuh, U., Böhmer, T., Li, C., Cao, X., Hébert, R., Dallmeyer, A., Telford, R. J., & Kruse, S. (2022). Reversals in Temperature-Precipitation Correlations in the Northern Hemisphere Extratropics During the Holocene. Geophysical Research Letters, 49(22), e2022GL099730. https://doi.org/10.1029/2022GL099730

Huntley, B., & Prentice, I. C. (1988). July Temperatures in Europe from Pollen Data, 6000 Years Before Present. Science, 241(4866), 687–690. https://doi.org/10.1126/science.241.4866.687

Jacobson, A. P., Riggio, J., M. Tait, A., & E. M. Baillie, J. (2019). Global areas of low human impact ('Low Impact Areas') and fragmentation of the natural world. Scientific Reports, 9(1), Article 1. https://doi.org/10.1038/s41598-019-50558-6

Jacobson, M. J., Flohr, P., Gascoigne, A., Leng, M. J., Sadekov, A., Cheng, H., Edwards, R. L., Tüysüz, O., & Fleitmann, D. (2021). Heterogenous Late Holocene Climate in the Eastern Mediterranean—The Kocain Cave Record From SW Turkey. Geophysical Research Letters, 48(20), e2021GL094733. https://doi.org/10.1029/2021GL094733

Joannin, S., Ali, A. A., Ollivier, V., Roiron, P., Peyron, O., Chevaux, S., Nahapetyan, S., Tozalakyan, P., Karakhanyan, A., & Chataigner, C. (2014). Vegetation, fire and climate history of the Lesser Caucasus: A new Holocene record from Zarishat fen (Armenia). Journal of Quaternary Science, 29(1), 70–82. https://doi.org/10.1002/jqs.2679

Kageyama, M., Harrison, S. P., & Abe-Ouchi, A. (2005). The depression of tropical snowlines at the last glacial maximum: What can we learn from climate model experiments? Quaternary International, 138–139, 202–219. https://doi.org/10.1016/j.quaint.2005.02.013

Kaplan, J. O., Krumhardt, K. M., Ellis, E. C., Ruddiman, W. F., Lemmen, C., & Goldewijk, C. G. M. K. (2017). Holocene carbon emissions as a result of anthropogenic land cover change—Jed O. Kaplan,

Kristen M. Krumhardt, Erle C. Ellis, William F. Ruddiman, Carsten Lemmen, Kees Klein Goldewijk, 2011. https://journals.sagepub.com/doi/abs/10.1177/0959683610386983

Kapsch, M.-L., Mikolajewicz, U., Ziemen, F., & Schannwell, C. (2022). Ocean Response in Transient Simulations of the Last Deglaciation Dominated by Underlying Ice-Sheet Reconstruction and Method of Meltwater Distribution. Geophysical Research Letters, 49(3), e2021GL096767. https://doi.org/10.1029/2021GL096767

Kaufman, D., McKay, N., Routson, C., Erb, M., Dätwyler, C., Sommer, P. S., Heiri, O., & Davis, B. (2020). Holocene global mean surface temperature, a multi-method reconstruction approach. Scientific Data, 7(1), Article 1. https://doi.org/10.1038/s41597-020-0530-7

Kennedy, C., Oakleaf, J. R., Theobald, D. M., Baruch-Mordo, S., & Kiesecker, J. (2018). Global Human Modification [Data set]. figshare. https://doi.org/10.6084/m9.figshare.7283087.v1

Klein Goldewijk, K., Beusen, A., Doelman, J., & Stehfest, E. (2017a). Anthropogenic land use estimates for the Holocene – HYDE 3.2. Earth System Science Data, 9(2), 927–953. https://doi.org/10.5194/essd-9-927-2017

Klein Goldewijk, K., Beusen, A., Doelman, J., & Stehfest, E. (2017b). Anthropogenic land use estimates for the Holocene – HYDE 3.2. Earth System Science Data, 9(2), 927–953. https://doi.org/10.5194/essd-9-927-2017

Klein Goldewijk, K., Dekker, S. C., & van Zanden, J. L. (2017). Per-capita estimations of long-term historical land use and the consequences for global change research. Journal of Land Use Science, 12(5), 313–337. https://doi.org/10.1080/1747423X.2017.1354938

Kutzbach, J. E., & Street-Perrott, F. A. (1985). Milankovitch forcing of fluctuations in the level of tropical lakes from 18 to 0 kyr BP. Nature, 317(6033), Article 6033. https://doi.org/10.1038/317130a0

Liu, M., Prentice, I. C., ter Braak, C. J. F., & Harrison, S. P. (2020). An improved statistical approach for reconstructing past climates from biotic assemblages. Proceedings of the Royal Society A: Mathematical, Physical and Engineering Sciences, 476(2243), 20200346. https://doi.org/10.1098/rspa.2020.0346

Liu, M., Shen, Y., González-Sampériz, P., Gil-Romera, G., ter Braak, C. J. F., Prentice, I. C., & Harrison, S. P. (2023). Holocene climates of the Iberian Peninsula: Pollen-based reconstructions of changes in the west–east gradient of temperature and moisture. Climate of the Past, 19(4), 803–834. https://doi.org/10.5194/cp-19-803-2023

Malmierca-Vallet, I., Sime, L. C., & the D–O community members. (2023). Dansgaard–Oeschger events in climate models: Review and baseline Marine Isotope Stage 3 (MIS3) protocol. Climate of the Past, 19(5), 915–942. https://doi.org/10.5194/cp-19-915-2023

Marcott, S. A., Shakun, J. D., Clark, P. U., & Mix, A. C. (2013). A Reconstruction of Regional and Global Temperature for the Past 11,300 Years. Science, 339(6124), 1198–1201. https://doi.org/10.1126/science.1228026

Marinova, E., Harrison, S. P., Bragg, F., Connor, S., Laet, V. de, Leroy, S. A. G., Mudie, P., Atanassova, J., Bozilova, E., Caner, H., Cordova, C., Djamali, M., Filipova-Marinova, M., Gerasimenko, N., Jahns, S., Kouli, K., Kotthoff, U., Kvavadze, E., Lazarova, M., … Tonkov, S. (2018). Pollen-derived biomes in the Eastern Mediterranean–Black Sea–Caspian-Corridor. Journal of Biogeography, 45(2), 484–499. https://doi.org/10.1111/jbi.13128

Marlon, J. R., Bartlein, P. J., Daniau, A.-L., Harrison, S. P., Maezumi, S. Y., Power, M. J., Tinner, W., & Vanniére, B. (2013). Global biomass burning: A synthesis and review of Holocene paleofire records and their controls. Quaternary Science Reviews, 65, 5–25. https://doi.org/10.1016/j.quascirev.2012.11.029

Marsicek, J., Shuman, B. N., Bartlein, P. J., Shafer, S. L., & Brewer, S. (2018). Reconciling divergent trends and millennial variations in Holocene temperatures. Nature, 554(7690), Article 7690. https://doi.org/10.1038/nature25464

Marquer, L., Gaillard, M.-J., Sugita, S., Poska, A., Trondman, A.-K., Mazier, F., Nielsen, A. B., Fyfe, R. M., Jönsson, A. M., Smith, B., Kaplan, J. O., Alenius, T., Birks, H. J. B., Bjune, A. E., Christiansen, J., Dodson, J., Edwards, K. J., Giesecke, T., Herzschuh, U., … Seppä, H. (2017). Quantifying the effects of land use and climate on Holocene vegetation in Europe. Quaternary Science Reviews, 171, 20–37. https://doi.org/10.1016/j.quascirev.2017.07.001

Mauri, A., Davis, B. A. S., Collins, P. M., & Kaplan, J. O. (2015). The climate of Europe during the Holocene: A gridded pollen-based reconstruction and its multi-proxy evaluation. Quaternary Science Reviews, 112, 109–127. https://doi.org/10.1016/j.quascirev.2015.01.013

Messager, E., Belmecheri, S., Von Grafenstein, U., Vincent, O., Voinchet, P., Puaud, S., Courtin-nomade, A., Guillou, H., Mgeladze, A., Dumoulin, J.-P., Mazuy, A., & Lordkipanidze, D. (2013). Late Quaternary record of the vegetation and catchment-related changes from Lake Paravani (Javakheti, South Caucasus). Quaternary Science Reviews, 77, 125–140. https://doi.org/10.1016/j.quascirev.2013.07.011

Messager, E., Nomade, S., Wilhelm, B., Joannin, S., Scao, V., Grafenstein, U. von, Martkoplishvili, I., Ollivier, V., Mgeladze, A., Dumoulin, J., Mazuy, A., Belmecheri, S., & Lordkipanidze, D. (2017). New pollen evidence from Nariani (Georgia) for delayed postglacial forest expansion in the South Caucasus. Quaternary Research, 87(1), 121–132. https://doi.org/10.1017/qua.2016.3

Mithen, S., Richardson, A., & Finlayson, B. (2023). The flow of ideas: Shared symbolism during the Neolithic emergence in Southwest Asia: WF16 and Göbekli Tepe. Antiquity, 97(394), 829–849. https://doi.org/10.15184/aqy.2023.67

Mithen, S., & Wicks, K. (2021). Population level models for testing hunter-gatherer resilience and settlement response to the combined impact of abrupt climatic events and sea level change: A case study from the Holocene of northern Britain. Quaternary Science Reviews, 265, 107027. https://doi.org/10.1016/j.quascirev.2021.107027

Morellón, M., Aranbarri, J., Moreno, A., González-Sampériz, P., & Valero-Garcés, B. L. (2018). Early Holocene humidity patterns in the Iberian Peninsula reconstructed from lake, pollen and speleothem records. Quaternary Science Reviews, 181, 1–18. https://doi.org/10.1016/j.quascirev.2017.11.016

Munro, NatalieD. (2004). Zooarchaeological Measures of Hunting Pressure and Occupation Intensity in the Natufian: Implications for Agricultural Origins. Current Anthropology, 45(S4), S5–S34. https://doi.org/10.1086/422084

Myhre, G., Shindell, D., Bréon, F.-M., Collins, W., Fuglestvedt, J., Huang, J., Koch, D., Lamarque, J.-F., Lee, D., Mendoza, B., Nakajima, T., Robock, A., Stephens, G., Zhang, H., Aamaas, B., Boucher, O., Dalsøren, S. B., Daniel, J. S., Forster, P., … Shine, K. (2013). Anthropogenic and Natural Radiative Forcing. In Climate Change 2013: The Physical Science Basis. Contribution of Working Group I to the Fifth Assessment Report of the Intergovernmental Panel on Climate Change. Cambridge University Press.

Nesbitt, M. (2002). When and where did domesticated cereals first occur in southwest Asia? In R. T. J. Cappers & S. Bottema (Eds.), The dawn of farming in the Near East (pp. 113–132). Ex Oriente.

Ni, J., Harrison, S. P., Prentice, I. C., Kutzbach, J. E., & Sitch, S. (2006). Impact of climate variability on present and Holocene vegetation: A model-based study. Ecological Modelling, 191(3–4), Article 3–4.

Noroozi, J., Zare, G., Sherafati, M., Mahmoodi, M., Moser, D., Asgarpour, Z., & Schneeweiss, G. M. (2019). Patterns of Endemism in Turkey, the Meeting Point of Three Global Biodiversity Hotspots, Based on Three Diverse Families of Vascular Plants. Frontiers in Ecology and Evolution, 7. https://www.frontiersin.org/articles/10.3389/fevo.2019.00159

Ön, Z. B., Greaves, A. M., Akçer-Ön, S., & Özeren, M. S. (2021). A Bayesian test for the 4.2 ka BP abrupt climatic change event in southeast Europe and southwest Asia using structural time series

analysis of paleoclimate data. Climatic Change, 165(1), 7. https://doi.org/10.1007/s10584-021-03010-6

Palmisano, A., Bevan, A., Kabelindde, A., Roberts, N., & Shennan, S. (2021). Long-term demographic trends in prehistoric Italy: Climate impacts and regionalised socio-ecological trajectories. Journal of World Prehistory, 34(3), 381–432. https://doi.org/10.1007/s10963-021-09159-3

Parker, S. E., & Harrison, S. P. (2022). The timing, duration and magnitude of the 8.2 ka event in global speleothem records. Scientific Reports, 12(1), Article 1. https://doi.org/10.1038/s41598-022-14684-y

Parker, S. E., Harrison, S. P., & Braconnot, P. (2021). Speleothem records of monsoon interannual-interdecadal variability through the Holocene. Environmental Research Communications, 3(12), 121002. https://doi.org/10.1088/2515-7620/ac3eaa

Parker, S. E., Harrison, S. P., Comas-Bru, L., Kaushal, N., LeGrande, A. N., & Werner, M. (2021). A data–model approach to interpreting speleothem oxygen isotope records from monsoon regions. Climate of the Past, 17(3), 1119–1138. https://doi.org/10.5194/cp-17-1119-2021

Pausas, J. G., & Bond, W. J. (2021). Alternative biome states challenge the modelling of species' niche shifts under climate change. Journal of Ecology, 109(12), 3962–3971. https://doi.org/10.1111/1365-2745.13781

Pérez-Obiol, R., Jalut, G., Julià, R., Pèlachs, A., Iriarte, M. J., Otto, T., & Hernández-Beloqui, B. (2011). Mid-Holocene vegetation and climatic history of the Iberian Peninsula. The Holocene, 21(1), Article 1. https://doi.org/10.1177/0959683610384161

Perugini, L., Caporaso, L., Marconi, S., Cescatti, A., Quesada, B., Noblet-Ducoudré, N. de, House, J. I., & Arneth, A. (2017). Biophysical effects on temperature and precipitation due to land cover change. Environmental Research Letters, 12(5), 053002. https://doi.org/10.1088/1748-9326/aa6b3f

Peyron, O., Combourieu-Nebout, N., Brayshaw, D., Goring, S., Andrieu-Ponel, V., Desprat, S., Fletcher, W., Gambin, B., Ioakim, C., Joannin, S., Kotthoff, U., Kouli, K., Montade, V., Pross, J., Sadori, L., & Magny, M. (2017). Precipitation changes in the Mediterranean basin during the Holocene from terrestrial and marine pollen records: A model–data comparison. Climate of the Past, 13(3), 249–265. https://doi.org/10.5194/cp-13-249-2017

Pongratz, J., Reick, C. H., Raddatz, T., & Claussen, M. (2010). Biogeophysical versus biogeochemical climate response to historical anthropogenic land cover change. Geophysical Research Letters, 37(8). https://doi.org/10.1029/2010GL043010

Pongratz, J., Reick, C., Raddatz, T., & Claussen, M. (2008). A reconstruction of global agricultural areas and land cover for the last millennium. Global Biogeochemical Cycles, 22(3). https://doi.org/10.1029/2007GB003153

Pons, A., & Quézel, P. (1998). À propos de la mise en place du climat méditerranéen. Comptes Rendus de l'Académie des Sciences - Series IIA - Earth and Planetary Science, 327(11), 755–760. https://doi.org/10.1016/S1251-8050(99)80047-0

Power, M. J., Marlon, J., Ortiz, N., Bartlein, P. J., Harrison, S. P., Mayle, F. E., Ballouche, A., Bradshaw, R. H. W., Carcaillet, C., Cordova, C., Mooney, S., Moreno, P. I., Prentice, I. C., Thonicke, K., Tinner, W., Whitlock, C., Zhang, Y., Zhao, Y., Ali, A. A., … Zhang, J. H. (2008). Changes in fire regimes since the Last Glacial Maximum: An assessment based on a global synthesis and analysis of charcoal data. Climate Dynamics, 30(7), 887–907. https://doi.org/10.1007/s00382-007-0334-x

Prentice, I. C., Jolly, D., & BIOME 6000 Participants. (2000). Mid-Holocene and glacial-maximum vegetation geography of the northern continents and Africa. Journal of Biogeography, 27(3), Article 3. https://doi.org/10.1046/j.1365-2699.2000.00425.x

Prentice, I. C., & Webb, T. (1998). BIOME 6000: Reconstructing global mid-Holocene vegetation patterns from palaeoecological records. Journal of Biogeography, 25(6), Article 6.

Qiao, S., Harrison, S. P., Prentice, I. C., & Wang, H. (2023). Optimality-based modelling of wheat sowing dates globally. Agricultural Systems, 206, 103608. https://doi.org/10.1016/j.agsy.2023.103608

Qiao, S., Wang, H., Prentice, I. C., & Harrison, S. P. (2020). Extending a first-principles primary production model to predict wheat yields. Agricultural and Forest Meteorology, 287, 107932. https://doi.org/10.1016/j.agrformet.2020.107932

Qiao, S., Wang, H., Prentice, I. C., & Harrison, S. P. (2021). Optimality-based modelling of climate impacts on global potential wheat yield. Environmental Research Letters, 16(11), 114013. https://doi.org/10.1088/1748-9326/ac2e38

Ramankutty, N., & Foley, J. A. (1999). Estimating historical changes in global land cover: Croplands from 1700 to 1992. Global Biogeochemical Cycles, 13(4), 997–1027. https://doi.org/10.1029/1999GB900046

Reille, M., & Pons, A. (1992). The Ecological Significance of Sclerophyllous Oak Forests in the Western Part of the Mediterranean Basin: A Note on Pollen Analytical Data. Vegetatio, 99/100, 13–17.

Reimer, P., Austin, W. E. N., Bard, E., Bayliss, A., Blackwell, P. G., Ramsey, C. B., Butzin, M., Cheng, H., Edwards, R. L., Friedrich, M., Grootes, P. M., Guilderson, T. P., Hajdas, I., Heaton, T. J., Hogg, A. G., Hughen, K. A., Kromer, B., Manning, S. W., Muscheler, R., … Talamo, S. (2020). The IntCal20 Northern Hemisphere radiocarbon age calibration curve (0-55 cal kBP). Radiocarbon, 62(4). https://doi.org/10.1017/RDC.2020.41

Renssen, H., Seppä, H., Crosta, X., Goosse, H., & Roche, D. M. (2012). Global characterization of the Holocene Thermal Maximum. Quaternary Science Reviews, 48, 7–19. https://doi.org/10.1016/j.quascirev.2012.05.022

Richerson, P. J., Boyd, R., & Bettinger, R. L. (2009). Was Agriculture Impossible during the Pleistocene but Mandatory during the Holocene? A Climate Change Hypothesis. American Antiquity, 66(3), 387–411. https://doi.org/10.2307/2694241

Rick, J. W. (1987). Dates as data: An examination of the Peruvian preceramic radiocarbon record. American Antiquity, 52(1), 55–73. https://doi.org/10.2307/281060

Riggio, J., Baillie, J. E. M., Brumby, S., Ellis, E., Kennedy, C. M., Oakleaf, J. R., Tait, A., Tepe, T., Theobald, D. M., Venter, O., Watson, J. E. M., & Jacobson, A. P. (2020). Global human influence maps reveal clear opportunities in conserving Earth's remaining intact terrestrial ecosystems. Global Change Biology, 26(8), 4344–4356. https://doi.org/10.1111/gcb.15109

Roberts, N., Brayshaw, D., Kuzucuoğlu, C., Perez, R., & Sadori, L. (2011). The mid-Holocene climatic transition in the Mediterranean: Causes and consequences. The Holocene, 21(1), 3–13. https://doi.org/10.1177/0959683610388058

Roberts, N., Eastwood, W. J., Kuzucuoglu, C., Fiorentino, G., & Caracuta, V. (2011). Climatic, vegetation and cultural change in the eastern Mediterranean during the mid-Holocene environmental transition. The Holocene, 21(1), 147–162. https://doi.org/10.1177/0959683610386819

Roberts, N., Palmisano, A., Bevan, A., Fyfe, R., & Shennan, S. (2019). Mediterranean landscape change during the Holocene: Synthesis, comparison and regional trends in population, land cover and climate. The Holocene, 29(5), 923–937. https://doi.org/10.1177/0959683619826697

Roberts, N., Reed, J. M., Leng, M. J., Kuzucuoğlu, C., Fontugne, M., Bertaux, J., Woldring, H., Bottema, S., Black, S., Hunt, E., & Karabiyikoglu, M. (2001). The tempo of Holocene climatic change in the eastern Mediterranean region: New high-resolution crater-lake sediment data from central Turkey. The Holocene, 11(6), 721–736. https://doi.org/10.1191/09596830195744

Robinson, E., Zahid, H. J., Codding, B. F., Haas, R., & Kelly, R. L. (2019). Spatiotemporal dynamics of prehistoric human population growth: Radiocarbon 'dates as data' and population ecology models. Journal of Archaeological Science, 101, 63–71. https://doi.org/10.1016/j.jas.2018.11.006

Rosen, A. M., & Rivera-Collazo, I. (2012). Climate change, adaptive cycles, and the persistence of foraging economies during the late Pleistocene/Holocene transition in the Levant. Proceedings of the National Academy of Sciences, 109(10), 3640–3645. https://doi.org/10.1073/pnas.1113931109

Sadori, L., Jahns, S., & Peyron, O. (2011). Mid-Holocene vegetation history of the central Mediterranean. The Holocene, 21(1), Article 1. https://doi.org/10.1177/0959683610377530

Sage, R. F. (1995). Was low atmospheric CO2 during the Pleistocene a limiting factor for the origin of agriculture? Global Change Biology, 1(2), 93–106. https://doi.org/10.1111/j.1365-2486.1995.tb00009.x

Sanderson, E. W., Jaiteh, M., Levy, M. A., Redford, K. H., Wannebo, A. V., & Woolmer, G. (2002). The Human Footprint and the Last of the Wild: The human footprint is a global map of human

influence on the land surface, which suggests that human beings are stewards of nature, whether we like it or not. BioScience, 52(10), 891–904. https://doi.org/10.1641/0006-3568(2002)052[0891:THFATL]2.0.CO;2

Smith, B. D. (2001). Low-Level Food Production. Journal of Archaeological Research, 9(1), 1–43. https://doi.org/10.1023/A:1009436110049

Smith, M. C., Singarayer, J. S., Valdes, P. J., Kaplan, J. O., & Branch, N. P. (2016). The biogeophysical climatic impacts of anthropogenic land use change during the Holocene. Climate of the Past, 12(4), 923–941. https://doi.org/10.5194/cp-12-923-2016

Smith, R. S., & Gregory, J. (2012). The last glacial cycle: Transient simulations with an AOGCM. Climate Dynamics, 38(7), 1545–1559. https://doi.org/10.1007/s00382-011-1283-y

Surovell, T. A., & Brantingham, P. J. (2007). A note on the use of temporal frequency distributions in studies of prehistoric demography. Journal of Archaeological Science, 34(11), 1868–1877. https://doi.org/10.1016/j.jas.2007.01.003

Surovell, T. A., Byrd Finley, J., Smith, G. M., Brantingham, P. J., & Kelly, R. (2009). Correcting temporal frequency distributions for taphonomic bias. Journal of Archaeological Science, 36(8), 1715–1724. https://doi.org/10.1016/j.jas.2009.03.029

ter Braak, C. J. F., & Juggins, S. (1993). Weighted averaging partial least squares regression (WA-PLS): An improved method for reconstructing environmental variables from species assemblages. Hydrobiologia, 269(1), 485–502. https://doi.org/10.1007/BF00028046

Theobald, D. M., Kennedy, C., Chen, B., Oakleaf, J., Baruch-Mordo, S., & Kiesecker, J. (2020). Earth transformed: Detailed mapping of global human modification from 1990 to 2017. Earth System Science Data, 12(3), 1953–1972. https://doi.org/10.5194/essd-12-1953-2020

Timm, O., & Timmermann, A. (2007). Simulation of the Last 21 000 Years Using Accelerated Transient Boundary Conditions. Journal of Climate, 20(17), 4377–4401. https://doi.org/10.1175/JCLI4237.1

Timmermann, A., Yun, K.-S., Raia, P., Ruan, J., Mondanaro, A., Zeller, E., Zollikofer, C., Ponce de León, M., Lemmon, D., Willeit, M., & Ganopolski, A. (2022). Climate effects on archaic human habitats and species successions. Nature, 604(7906), Article 7906. https://doi.org/10.1038/s41586-022-04600-9

Vavrus, S., Ruddiman, W. F., & Kutzbach, J. E. (2008). Climate model tests of the anthropogenic influence on greenhouse-induced climate change: The role of early human agriculture, industrialization, and vegetation feedbacks. Quaternary Science Reviews, 27(13), 1410–1425. https://doi.org/10.1016/j.quascirev.2008.04.011

Villegas-Diaz, R., Cruz-Silva, E., & Harrison, S. P. (2021). ageR: Supervised Age Models [R]. Zenodo. https://doi.org/10.5281/zenodo.4636716

Villegas-Diaz, R., & Harrison, S. P. (2022). The SPECIAL Modern Pollen Data Set for Climate Reconstructions, version 2 (SMPDSv2) [Data set]. University of Reading. https://doi.org/10.17864/1947.000389

Wang, C., Lu, H., Zhang, J., Gu, Z., & He, K. (2014). Prehistoric demographic fluctuations in China inferred from radiocarbon data and their linkage with climate change over the past 50,000 years. Quaternary Science Reviews, 98, 45–59. https://doi.org/10.1016/j.quascirev.2014.05.015

Weiberg, E., Bevan, A., Kouli, K., Katsianis, M., Woodbridge, J., Bonnier, A., Engel, M., Finné, M., Fyfe, R., Maniatis, Y., Palmisano, A., Panajiotidis, S., Roberts, C. N., & Shennan, S. (2019). Long-term trends of land use and demography in Greece: A comparative study. The Holocene, 29(5), 742–760. https://doi.org/10.1177/0959683619826641

Weide, A., Green, L., Hodgson, J. G., Douché, C., Tengberg, M., Whitlam, J., Dovrat, G., Osem, Y., & Bogaard, A. (2022). A new functional ecological model reveals the nature of early plant management in southwest Asia. Nature Plants, 8(6), Article 6. https://doi.org/10.1038/s41477-022-01161-7

Weiss, H., & Bradley, R. S. (2001). What Drives Societal Collapse? Science, 291(5504), 609–610. https://doi.org/10.1126/science.1058775

Wick, L., Lemcke, G., & Sturm, M. (2003). Evidence of Lateglacial and Holocene climatic change and human impact in eastern Anatolia: High-resolution pollen, charcoal, isotopic and geochemical records from the laminated sediments of Lake Van, Turkey. The Holocene, 13(5), Article 5. https://doi.org/10.1191/0959683603hl653rp

Willcox, G. (2012). Searching for the origins of arable weeds in the Near East. Vegetation History and Archaeobotany, 21(2), 163–167. https://doi.org/10.1007/s00334-011-0307-1

Williams, A. N. (2012). The use of summed radiocarbon probability distributions in archaeology: A review of methods. Journal of Archaeological Science, 39(3), 578–589. https://doi.org/10.1016/j.jas.2011.07.014

Woodward, F. I., Lomas, M. R., & Kelly, C. K. (2004). Global climate and the distribution of plant biomes. Philosophical Transactions of the Royal Society of London. Series B: Biological Sciences, 359(1450), 1465–1476. https://doi.org/10.1098/rstb.2004.1525

Wright, H. E., Kutzbach, J. E., Webb, T., Ruddiman, W. F., Street-Perrott, F. A., & Bartlein, P. J. (1993). Global Climates since the Last Glacial Maximum (NED-New edition). University of Minnesota Press. https://www.jstor.org/stable/10.5749/j.ctttsqhb

Zeder, M. A. (2011). The Origins of Agriculture in the Near East. Current Anthropology, 52(S4), S221–S235. https://doi.org/10.1086/659307

Zhang, W., Wu, H., Cheng, J., Geng, J., Li, Q., Sun, Y., Yu, Y., Lu, H., & Guo, Z. (2022). Holocene seasonal temperature evolution and spatial variability over the Northern Hemisphere landmass. Nature Communications, 13(1), Article 1. https://doi.org/10.1038/s41467-022-33107-0

Zhang, Y., Renssen, H., & Seppä, H. (2016). Effects of melting ice sheets and orbital forcing on the early Holocene warming in the extratropical Northern Hemisphere. Climate of the Past, 12(5), 1119–1135. https://doi.org/10.5194/cp-12-1119-2016